UNIVERSITY OF CALIFORNIA,
IRVINE

Chemically Modified Viruses for Prostate Cancer Detection

DISSERTATION

submitted in partial satisfaction of the requirements
for the degree of

DOCTOR OF PHILOSOPHY

in Chemistry

by

Kritika Mohan

Dissertation Committee:

Professor Gregory A. Weiss, Chair

Professor James S. Nowick

Assistant Professor Jennifer A. Prescher

2016

DEDICATION

To my parents,

Uma and Rakesh Mohan,

in recognition of their immense love and support.

TABLE OF CONTENTS

LIST OF FIGURES

LIST OF TABLES

LIST OF SCHEMES

ACKNOWLEDGEMENTS

I would like to begin by expressing my sincerest appreciation to my advisor and committee chair, Professor Gregory A. Weiss. He has been a phenomenal mentor and guide at every step. Greg is an exceptional advisor who focuses on not just the project and experiments at hand, but on the overall growth and development of his students. And, most importantly, his own personal enthusiasm for science leads to motivation of his students on an everyday basis. Thank you!

In addition, I would like to express my gratitude to my co-advisor and collaborating PI, Professor Reginald M. Penner. Your ability to scan through all those million fleeting ideas, to catch the potential ones is commendable and inspiring. The depth of your knowledge, grasp of science, and down-to-earth attitude are admirable. I am very thankful to have been able to collaborate with your lab, and for the opportunity to learn so much from you. I would also like to thank you for treating me like any other member of your lab, and not just a collaborator.

I would like to thank my committee members, Professors James S. Nowick and Jennifer A. Prescher. You both have guided me from the beginning; starting from my first quarter at UCI, through the advancement process, and the rest of my Ph.D. James, I have always enjoyed my discussions with you, and it has always amazed me how you seem to know something about everything. Jenn, your commitment and dedication to science are prodigious and inspiring.

A heartfelt thanks to all the Weiss lab members, past and present. Every single person has been a delightful fellow lab member. I had the pleasure and the unique opportunity of learning from most of the senior and junior members of the lab, when I joined. I would like to thank Dr. Jessica Arter, Dr. Agnes Hajduczki, Dr. Issa Moody, Dr. Glenn Eldridge, Dr. Rosemarie Vithayathil, Dr. Tivoli Olsen, and Dr. Cathie Overstreet for all their help and guidance. I would especially like to thank Johnny Rodriguez, though an undergraduate in the lab at the time, proved to be a great teacher and friend. I would also like to thank Dr. Tom Yuan for years worth of helpful discussions, and for being an amazing pseudo bench mate. And last but not the least, a big thank you to the current set of graduate students, we dealt with the ups and downs (somehow, tend to prevail and occur rather more frequently than desired) of graduate life together, and you all provided the biggest and the best support system for dealing with everything. From random day-night unceasing 'scientific' discussions to unmentionable traditions, and never-ending text messages, completely random yet perfectly-timed hugs to multi-lingual conversations, a big thank you to Josh Smith, Kaitlin Pugliese, Dr. Amanda Gilliam, Mariam Iftikhar, Andrew Gansmiller, Luz Meneghini, Rebekah Dyer, and Joshua Britton. And, thank you Dr. Mark Richardson for sharing your knowledge and experience with me.

Thank you to the many undergraduates and post-baccalaureates our lab has had over the years. Thank you Will Brown, discussing science and explaining concepts to you sometimes really made me rethink things in a different

way. A big thanks to Stephan Kudlacek, Rebecca Drake, and Sasan Zomorodian for being great undergraduates, it was a lot of fun training you guys. Stephan and Rebecca, I finally give you both the much talked about and rather long overdue acknowledgement, which unfortunately could not be a part of the journal article; thank you very much for keeping me entertained through some really grueling experiments! And, last but not the least, Josh Edgar, Johnathon Truong, Shae Schlegel, Jeffrey Briggs, Andrew Nguyen, Marcus Woodworth, and Kevin Johnston, you guys were the heart and soul of the lab. I am sure you all will have extraordinary careers.

I also thank my amazing collaborators Crystin Eggers and Alana Ogata. You both have been an absolute delight to work with. Crystin, thank you for your support, scientific and otherwise, throughout these past few years. Your perseverance is commendable. Alana, I really admire your dedication and optimism. I also thank Dr. Keith Donavan for training me to be an electrochemist. In addition, I thank all the Penner lab members who always made me feel like a part of their lab, and were extremely helpful with everything.

Thank you to the many graduate and undergraduate friends who made me feel welcome here. What started out with a couple of names grew to be a rather long list to provide individual acknowledgements. All I can say is, thank you for being there with me through these past five years, and thank you for therapeutic shopping, chats, and dinners, random outings, window shopping and then some, movies, calls, texts and everything else that graduate school needs besides

research to keep us going. And, alongside I wish to thank the love and support of my friends from back home who never gave up on our friendship or me, despite me being unreachable and unresponsive at times. With friends like you, I can pick up from wherever we left off irrespective of how much time has elapsed. Thank you for being there at all times, day or night, you all were literally always just a phone call or a text message away, as you all had promised you would be years ago.

And, finally, most importantly, thank you to my parents. I don't think words can ever describe how thankful I am for your unending love and support. As you both like to say, between the two of you, you had every subject covered except for one, and you know how much I like making things difficult. You always had the time and patience to listen to my problems, and offer suggestions and solutions, and if nothing else, you always had something encouraging to say. I would also like to take this opportunity to thank them for one of the best and most thoughtful presents ever, a Canon DSLR camera with a set of wide angle and telephoto zoom lenses. It gave me a hobby and a passion that I cherish beyond words. Thank you! You have always encouraged me to be better than who I was yesterday. And, I hope to have made you proud, and will never stop trying to do that. Lots of love and admiration!

KRITIKA MOHAN

Kritikamohan@gmail.com • (949) 214-8955

EDUCATION

University of California, Irvine, Irvine, CA 2010-2016
Ph.D. Chemistry
GPA: 3.9 (out of 4)

Indian Institute of Technology, Delhi, India 2007-2009
Master of Science, Chemistry
CGPA: 8.4 (out of 10)

St. Stephen's College, University of Delhi, Delhi, India 2004-2007
Bachelor of Science, Chemistry (Honors)
Absolute percentage 85%

RESEARCH AND WORK EXPERIENCE

University of California, Irvine, Irvine, CA March 2011-January 2016
Advisor: Professor Gregory A. Weiss
Co-Advisor: Professor Reginald M. Penner

Developed chemically and genetically modified viruses for the early detection of prostate cancer. These viruses were then incorporated as the biological recognition element in Virus-PEDOT film-based biosensors. A 100 pM limit of detection was obtained for the electrochemical detection of prostate cancer-associated biomarker in synthetic urine. Furthermore, viruses non-genetically modified with PEGylated-ligands were used for the detection of cell-surface biomarkers towards detection of metastasizing cells.

Reliance Life Sciences, Mumbai, India 2009-2010
Research assistant
Advisor: Dr. Dhananjay Saranath
Research Director, Molecular Medicine

Studied the BRAF (V-raf murine sarcoma viral oncogene homolog B1) gene mutation found in colorectal cancer, and also designed and validated a diagnostic test for the same. Also, analyzed patient blood samples for HIV infection as part of the training process.

Akums Drugs and Pharmaceuticals Ltd., Haridwar, India Summer, 2009
Summer research assistant
Advisor: M. D. Sahu
Technical Director

Analyzed the stability and dissolution parameters of Azithromycin and Glimepiride-Metformin hydrochloride, sustained release drug formulations, during drug manufacturing.

Indian Institute of Technology, New Delhi, India 2008- 2009
Advisor: Professor B. Jayaram

***Master's thesis project**: Implemented a supervised learning method, Support Vector Machine (SVM) in conjunction with Chemgenome software for genome annotation at the supercomputing facility for bioinformatics and computational biology (SCFBIO). The open reading frames (ORFs) of a genome of any prokaryotic organism were represented as vectors in three dimensional space. Next, SVM, which constructs hyperplanes was applied for the classification and annotation of these ORFs as genes and non-genes.*

Indian Institute of Technology, New Delhi, India 2007- 2008
Master's student research
Advisor: Professor B. Jayaram

Analyzed the minimalist genome for an organism in order to find the essential gene set required for the sustenance of the minimalist organism at SCFBIO.

TEACHING EXPERIENCE

Teaching Assistant, University of California, Irvine

- Chemical Biology — Winter 2013
  Supervisor: Professor Gregory A. Weiss
- Organic Chemistry Laboratory — Fall and Winter 2011
  Supervisor: Dr. Renee D. Link
- General Chemistry Laboratory — Spring 2011
  Supervisor: Dr. Kimberly D. Edwards
- Organic Chemistry Laboratory — Fall 2010
  Supervisor: Dr. Renee D. Link

PUBLICATIONS AND PATENTS

5. **Kritika Mohan**, Gregory A. Weiss. Chemically modifying viruses for diverse applications (Review). *Submitted*, **2016**.
4. **Kritika Mohan**, Gregory A. Weiss. Engineering chemically modified viruses for prostate cancer cell recognition. *Mol BioSys*, **2015**, 11, 3264-3272. (This article is part of themed collection: Chemical Biology in Mol BioSys and 2015 Hot Articles in Mol BioSys.)
3. **Kritika Mohan**, Reginald M. Penner, Gregory A. Weiss. Biosensing with virus electrode hybrids. *Current Protocols,* **2015**, 7(2), 53-72. (Invited Article)
2. **Kritika Mohan**, Gregory A. Weiss. Dual genetically encoded phage-displayed ligands. *Anal Biochem,* **2014**, 453, 1-3.
1. **Kritika Mohan**, Keith C. Donavan, Jessica A. Arter, Reginald M. Penner, and Gregory A. Weiss. Sub-nanomolar Detection of Prostate-Specific Membrane Antigen in Synthetic Urine by Synergistic, Dual-Ligand Phage. *J. Am. Chem. Soc.*, **2013**, 135(20), 7761-7767.

Patents

2. **Kritika Mohan**, Gregory A. Weiss (**2015**). PEGylated phage for specific molecular recognition of heterogeneous surfaces including cancer cells. U.S. Provisional Patent Application Serial No. 62/237,781.
1. **Kritika Mohan**, Gregory A. Weiss, Reginald M. Penner, Lindsay Kindra (**2014**). Phage wrapping. U.S. Provisional Patent Application Serial No. 61/944,425.

HONORS AND AWARDS

- American Chemical Society Division of Analytical Chemistry Graduate fellowship 2015
- Regent's dissertation fellowship 2015
  University of California, Irvine – awarded for distinguished academic achievement
- ACS travel award from the division of biological chemistry 2014
- Taihi Hong Memorial Graduate Student Education award 2013
- Allergan Graduate Fellowship in Synthetic Organic Chemistry 2013
  University of California, Irvine – awarded for demonstrating excellence in research and examinations and shows unusual future promise
- Poster presentation competition – first position 2012
  Chao Family Comprehensive Cancer Center Scientific Retreat, Palm Springs, CA.
- Prof. A.C. Jain Merit Scholarship 2006
  St. Stephens College, Delhi – awarded for obtaining the highest marks in the University Examination
- Science Meritorious Award 2006
  University of Delhi – awarded for performance of special merit in University exams
- Prof. A.C. Jain Merit Scholarship, St. Stephen's College, Delhi 2005
- Science Meritorious Award, University of Delhi 2005
- Virendra Kumar Memorial prize, St. Stephen's College, Delhi 2005
  Awarded for displaying great proficiency in Laboratory Work (Chemistry)
- Certificate of Merit 2003
  Central Board of Secondary Education, Delhi – awarded for outstanding academic performance and for being among the top 0.1% of successful candidates in Physics
- First position, AISSCE, Central Board of Secondary Education, North zone 2003
- Special Certificate of Merit, Bharitya Vidya Bhavan, Chandigarh 2003

RESEARCH PRESENTATIONS

Systematic Engineering and Synergistic Binding of PEGylated Ligands on Phage for the Detection of Prostate Cancer Cells. UCI Cancer Research Institute Symposium on Basic Cancer Research, Irvine, CA, poster presentation; Spring **2015**.

Systematic Engineering and Synergistic Binding of PEGylated Ligands on Phage for the Detection of Prostate Cancer Cells. 249th ACS National meeting, Denver, CO, poster presentation; Spring **2015**.

Viruses and electronics for early prostate cancer detection. Cancer Biology Research in Progress Series, Irvine, CA, invited talk; Spring **2014**.

Viruses and electronics for early prostate cancer detection. AGS Symposium, Irvine, CA, A 10 min talk designed for common public; Spring **2014**.

Sub-nanomolar Detection of Prostate-Specific Membrane Antigen in Synthetic Urine by Synergistic, Dual-Ligand Phage. 247th ACS National meeting, Dallas, TX, oral presentation; Spring **2014**.

Chemically Synthesized and Genetically Encoded Ligands for Synergistic Binding and Detection of Prostate Specific Membrane Antigen. Chao Family Comprehensive Cancer Center Scientific Retreat, Palm Springs, CA, poster presentation; Fall **2013**.

Chemically Synthesized and Genetically Encoded Ligands for Synergistic Binding and Detection of Prostate Specific Membrane Antigen. UCI Cancer Research Institute Symposium on Basic Cancer Research, Irvine, CA, poster presentation; Spring **2013**.

Chemically Synthesized and Genetically Encoded Ligands for Synergistic Binding and Detection of Prostate Specific Membrane Antigen. Chao Family Comprehensive Cancer Center Scientific Retreat, Palm Springs, CA, poster presentation; Fall **2012**.

MEDIA COVERAGE

- Press release by UCI: 'UCI Chemists devise inexpensive, accurate way to detect prostate cancer.' http://news.uci.edu/press-releases/uci-chemists-devise-inexpensive-accurate-way-to-detect-prostate-cancer/
- Guest for the 'Prostate cancer detection testing' telecasted on *Real Orange,* PBS Socal. http://video.pbssocal.org/video/2365016479
- Interviewed by KPCC on 'New prostate cancer test designed to use urine instead of blood.' http://www.scpr.org/news/2013/05/22/37363/new-prostate-cancer-test-designed-to-use-urine-ins/

SKILLS

Laboratory: Molecular biology, bacterial over-expression of recombinant proteins, protein purification, tissue culture, enzyme and cell-based assays, phage-display of peptides and proteins, phage-displayed peptide library design and mutagenesis, solid-phase peptide synthesis and purification, bioconjugation, quantitative PCR, UV/Vis spectroscopy, mass spectrometry, high-pressure liquid chromatography (HPLC), dynamic light scattering (DLS), gel permeation chromatography (GPC), confocal microscopy, device fabrication of virus-PEDOT film-based biosensors, cyclic voltammetry and electrochemical impedance spectroscopy (EIS), sequencing and genotyping.

Additional laboratory skills include training undergraduate and graduate students, ordering and managing chemical and laboratory supplies, organizing journal club, and managing chemical and biomedical waste.

Computer: Programming languages FoxPro, Basic, Elementary C++ and Linux. Additional computer related skills include proficiency in MS Excel, MS Word, MS PowerPoint, Adobe Photoshop, Adobe Illustrator, ChemDraw, Pymol.

REFERENCES

Professor Gregory A. Weiss
University of California Irvine
Department of Chemistry
Irvine, CA 92607
(949) 824-5566
gweiss@uci.edu

Professor Reginald M. Penner
University of California Irvine
Department of Chemistry
Irvine, CA 92697
(949) 824-8572
rmpenner@uci.edu

Professor James S. Nowick
University of California Irvine
Department of Chemistry
Irvine, CA 92607
(949) 824-6091
jsnowick@uci.edu

Professor Jennifer A. Prescher
University of California Irvine
Department of Chemistry
Irvine, CA 92697
(949) 824-1706
jprescher@uci.edu

ABSTRACT OF THE DISSERTATION

Chemically Modified Viruses for Prostate Cancer Detection

By

Kritika Mohan

Doctor of Philosophy in Chemistry

University of California, Irvine, 2016

Professor Gregory A. Weiss, Chair

The sensitive detection of cancer biomarkers in urine could revolutionize cancer diagnostics and treatment. Such detectors must be inexpensive, easy to interpret, and sensitive. M13 bacteriophage provides one such highly inexpensive, and easily functionalizable platform for the development of such detectors. My work focuses on genetically and chemically modifying M13 viruses towards biological recognition of prostate-specific membrane antigen (PSMA), a prostate cancer biomarker. Elevated PSMA levels have been observed in prostate cancer patients' urine, and also found on the surface of prostate cancer cells. For early diagnosis of prostate cancer, I have developed the chemistry necessary for the detection of clinically relevant concentrations of PSMA (<0.25 nM) in synthetic urine for direct application to patients' samples. High sensitivity to PSMA results from the synergistic binding by two different ligands to PSMA on the same phage particle. The primary ligand is genetically encoded, and the secondary recognition ligand is chemically synthesized to electrostatically wrap

around the phage surface. The concept of 'phage wrapping' utilizes the electrostatic attraction between the negatively charged phage surface and the positively charged oligolysine peptide 'wrapper.' Furthermore, the dual ligands result in bidentate binding with high copy, dense ligand display for enhanced PSMA detection through a chelate-based, avidity effect. Such dual modified viruses integrated into electrically conductive poly(3,4-ethylenedioxythiophene (PEDOT) films, act as the bioaffinity matrix for the electrochemical sensing of PSMA. The capture and binding of PSMA results in a change in the virus-PEDOT film's resistance, which is also proportional to the PSMA concentration. Biosensing with films provides a 100 pM limit of detection for PSMA in synthetic urine without requiring enzymatic or other amplification. I further utilized this concept to reduce the non-specific adhesion between viruses and prostate cancer cells through wrapping the phage surface with polyethylene glycol. Additionally, I developed orthogonal wrapping techniques to selectively attach ligands and polyethylene glycol on the phage surface in desired ratios and architectures for the capture of PSMA-positive prostate cancer cells for metastasis detection. The combination of orthogonal chemically-modified viruses and biosensors holds the potential for the development of a real-time and reagent-free point-of-care device for prostate cancer detection.

CHAPTER 1

Beyond Infectious Diseases: Applying Modified Viruses in the 21st Century

INTRODUCTION

Beyond causing infectious diseases, viruses provide a useful benchtop for chemical experiments and building complex biomedical reagents. Filamentous bacteriophages, such as the closely homologous M13 and fd phage, infect bacteria, and propagate in a non-lytic manner. Furthermore, the lack of mammalian promoter sequences prevents them from causing human diseases.[1–3] Such properties make M13 and fd phage nearly ubiquitous tools for a wide-range of biotechnology applications.

These members of the Ff class of phage have highly uniform structures. The phage (approximately 1 μm by 6 nm) encapsulates a ssDNA genome encapsulated in a flexible, long, rod-like protein coat formed entirely from multiple copies of five individual proteins. Along the entire length of the virion, ≈2700 copies of the amphiphilic P8 protein are closely packed with a five-fold symmetry axis, and a free, unstructured *N*-terminus; the proteins' *C*-termini interact with the phage genome. Each phage end is capped by five copies each of minor coat proteins P3 and P6 at one end, and, P7 and P9 at the other end.[1]

Viruses offer a nanometer-scale benchtop for chemical biologists to build molecular-scale devices and materials for a wide variety of applications. Major

attributes for the ease of phage-based applications include the low cost of production, and wide temperature and pH stability.[3,4] Additionally, phage are easy to propagate and handle at all scales of production. Furthermore, the relatively monodispersed phage self-assemble into liquid crystalline structures. The virus capsid presents a huge surface with easily modifiable residues to attach genetically non-encoded moieties with dense display. Here, the focus is on these widely versatile viruses, highlighting their tremendous potential as 'nano-benchtops.'

GENETIC MODIFICATION OF VIRUSES

Phage display features a peptide or protein of interest fused to the outer terminus of the coat proteins. This approach provides a link between the genotype and the phenotype, with the gene of interest fused to the gene encoding the coat protein.[1] The close packed structure of the phage capsid prevents the display of most proteins (>6 residues) on every copy of the major coat protein.[5] To solve this problem, a phagemid system allows a mixture of unmodified and protein of interest-fused coat proteins to be expressed in bacterial cells. The phagemid display of short peptides on P8 provides ≈10% incorporation levels without affecting the packing of the phage capsid.[6]

The conventional usage of phage has been towards selections and biopanning.[7,8] Peptide ligands have been reported for a variety of targets from

protein biomarkers to small molecules such as TNT[9] and organic crystals,[10] and the scope of selections has even been extended to screening for catalysts.[11] Furthermore, a combination of different display methods can provide dual-displayed phage particles. This can either be achieved through combining modified genes, or through modified phage propagation protocols utilizing double virus infection,[12] as reviewed by Bratkovič and coworkers.[13]

CHEMICAL MODIFICATION OF VIRUSES

Though molecular display dominates conventional applications of viruses, non-genetic manipulation of the virus surface expands their repertoires and applications. Both covalent and non-covalent modifications, some in conjunction with genetic modifications, offer improvements on nature's functionalities. The modifications can be categorized into four broad classes, described below.

First, attachment to the functionalities inherent to amino acid sidechains (Figure 1-1), is the most commonly used strategy, typically employing the reactive amino acid sidechains present on P8. Wang and coworkers compared the reactivities of the three prominent functionalities open to modification: carboxylates on Asp and Glu, phenol functionalities of Tyr, and the amines of Lys.[14] The carboxylate groups can be activated through carbodiimide (such as EDC) treatment for coupling to amine-functionalized moieties, whereas the Tyr sidechains can be coupled to diazonium salts. The amine groups, including the *N*-termini and Lys sidechains could be coupled to NHS (N-hydroxysuccinimide)

esters or other activated carboxylates (e.g., tetrafluorophenyl esters).[15] Amine functionalities proved most reactive and efficient at such coupling reactions.[14] Preincorporation of the azide on the diazonium salt further enhances the scope of chemical modification through the use of copper-catalyzed azide-alkyne cycloaddition 'click' reaction.

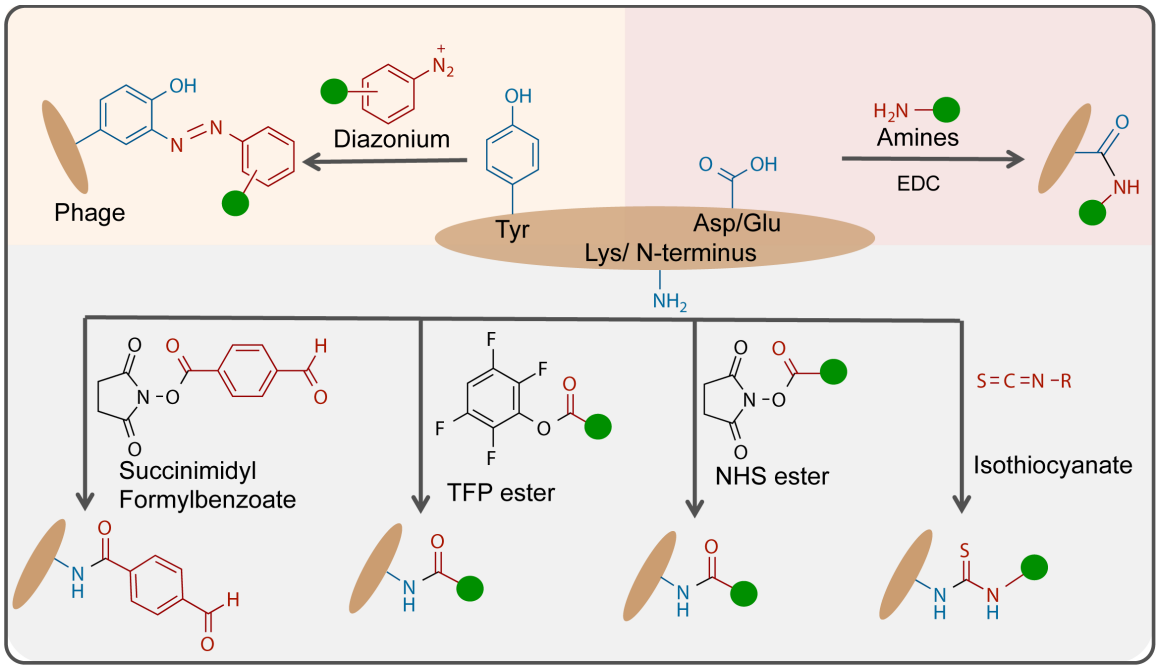

Figure 1-1. A compendium of the inherent functionalities present on the phage coat protein, and the most commonly applied modification techniques. The green circle indicates the appended handle or the probe.

Though the extent of modification reported was relatively lower for carboxylic acid groups and Tyr, it could still be applied for the generation of dual modified phage especially in conjunction with amine modifications or genetic display. The amine groups, including the *N*-terminal amine and Lys side chains could be coupled to NHS (N-hydroxysuccinimide) esters.[14] Alternately, other activated esters such as tetrafluorophenyl esters could also be used for amine coupling.[15]

The next classes of modifications include the chemically and genetically imparted functionalities, which provide the desired handle for further modifications. In the second classification, modification of *N*-terminal amines into aldehydes introduces a range of bioorthogonal reactions,[16] Figure 1-2. The third class of chemical modifications begins with the genetic incorporation of either Cys or unnatural amino acids with desirable new functionalities, Figure 1-3. For example, genetically-displayed *N*-terminal Cys can be modified in a variety of ways including native chemical ligation.[17] Naturally occurring selenocysteine, which offers high nucleophilicity, has also been genetically displayed using an opal stop codon suppressing tRNA, and provides a reactive handle for further chemical modifications.[18] Schultz and coworkers extended their approach to phage display, leading to the incorporation of p-azidophenylalanine, which provides one of the most easily modifiable azide handles on the phage surface.[19,20]

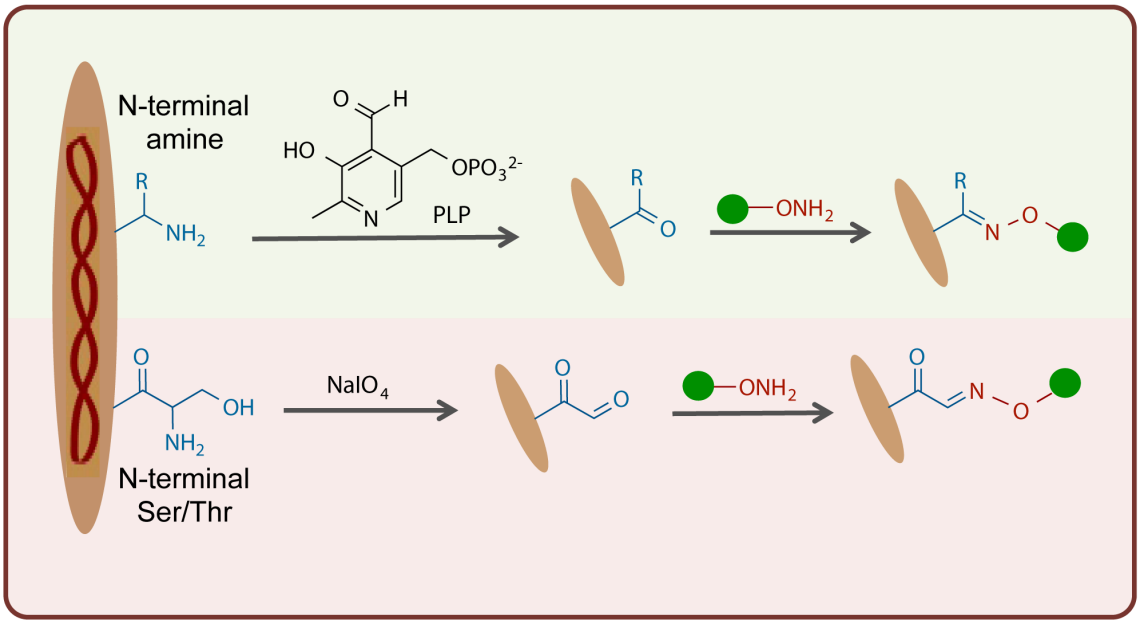

Figure 1-2. The set of chemically imparted functionalities providing an orthogonal aldehyde handle on the *N*-terminus of coat proteins.

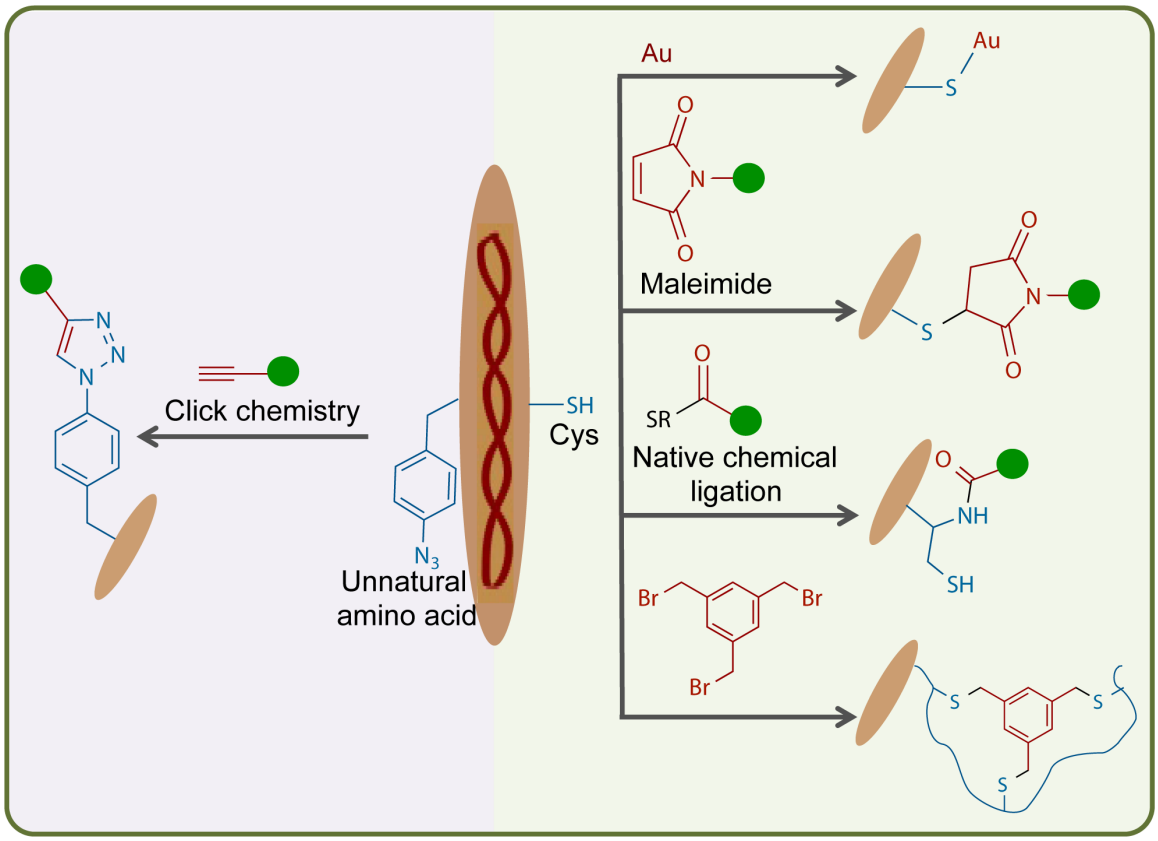

Figure 1-3. A compendium of functionalities genetically incorporated onto the phage surface, and the most commonly applied modification techniques.

Though phage particles are stable to a wide variety of covalent bond forming conditions, the limited solvent accessibility of some residues can limit modification efficiency. To circumvent this limitation, non-covalent modifications to the phage coat have also been employed, Figure 1-4, forming the fourth set of classifications. Such modifications either utilize the high negative charge on the phage surface arising from the presence of Glu and Asp acid residues in the *N*-terminal region, or build upon the amphiphilic character of the P8 coat protein.[21] Here, the chemical approaches to equip the viruses with such capabilities and functionalities are discussed.

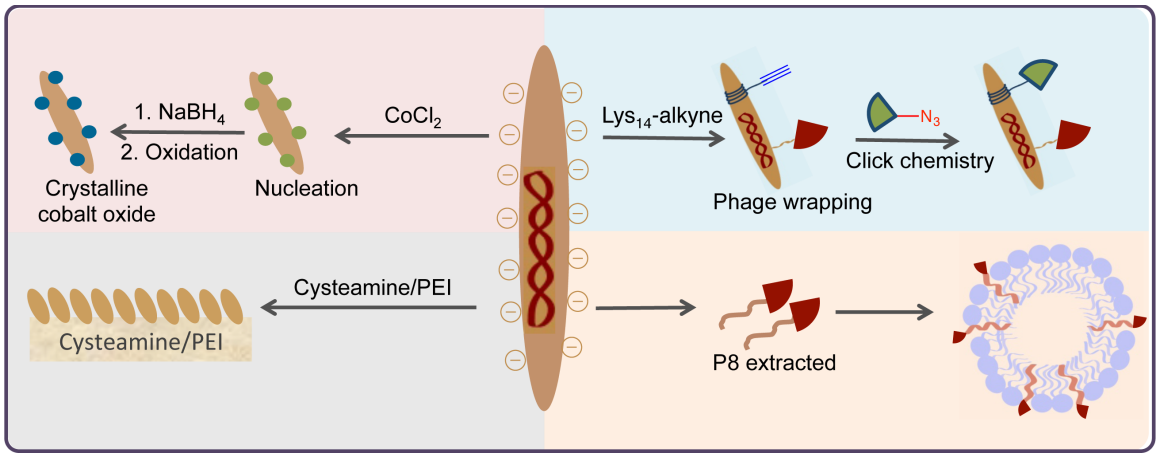

Figure 1-4. The set of non-covalent phage modifications, which utilize the surface charge or the amphiphilic character of the P8 coat protein.

APPLICATIONS OF MODIFIED PHAGE

1.1 Modified Phage for Enhanced Imaging

In recent years, improvements to in-vivo imaging have started to address the key issues hindering the broader adoption of this powerful technology. First, the chosen wavelengths of light must have minimal tissue autofluorescence and optical transparency, for example near-IR wavelengths. Second, the imaging agents must exhibit suitability for bioconjugation, and water solubility. Low solubility results in aggregation, which leads to intermolecular quenching of fluorescence emission. The high solubility of viruses and their versatility for surface modifications enables their applications as imaging scaffolds.

One of the earlier chemical modifications of phage leveraged free amines on the phage surface to conjugate a near-IR dye. This approach takes advantage of the large number of free amines on P8 and the phage surface. The alkyl-thioether Cyanine dyes were activated with NHS to provide the corresponding succinimidyl ester for bioconjugation. Cyanine dyes exhibit strong emission in the near-IR wavelengths allowing deep tissue penetration. Additionally, the phage used in this example displayed a peptide targeting the cell surface receptor VCAM-1 to allow binding and internalization into MCEC cells for imaging.[22] Building on these results, *in vivo* screening tool was also developed for selectants from a phage-displayed library of peptides targeting SPARC (Secreted Protein, Acidic and Rich in Cysteine). In this example, FITC-modified phage

selectants were examined for binding to SPARC in mice injected with Lewis lung carcinoma cells. These results allowed relative ranking and elimination of initial leads, and could identify unfavorable pharmacokinetics or non-specific binding. The use of phage as a scaffold allowed attachment of up to 800 fluorophores/phage for higher sensitivity, without losses from proximity-based quenching.[23]

This straightforward approach to phage surface modification was applied to ratiometrically detect pH homeostasis and its disruptions, which are associated with cancer and other diseases. The ratios of pH-sensitive to pH-insensitive Cyanine dyes allowed normalization and intracellular pH measurements. Again, the use of phage allowed dye conjugation of 400-500 copies per phage, thereby increasing the overall brightness and signal to noise ratios. The differences in the tissue penetration of light at the emitted wavelengths still posed a challenge for ratiometric determination of pH. Nevertheless, the method allowed imaging and pH determination with >95% accuracy.[24] In a variation of this approach, a FRET pair was immobilized on the phage surface modified with NHS-activated cyclodextrin through EDC coupling.[25] Adamantyl-functionalized FITC and rhodamine were complexed with cyclodextrin-phage. The emission intensity of FITC varies linearly with protonation thereby allowing pH analysis in the range of 5-8.5.[26] Whereas, direct conjugation of the FRET pair through isothiocyanate functionalization on each fluorophore provided linear pH analysis in a narrow range from 6.4-7.4.[27]

Further extension of IR imaging employed probes such as single-walled carbon nanotubes (SWNTs), which fluoresce in the second NIR window (950-1400 nm). This imaging moiety allows deep tissue penetration and low tissue autofluorescence. Despite their favorable properties, the hydrophobicity of SWNT poses a challenge for *in vivo* use. Belcher and coworkers solved this challenge by binding SWNTs to the highly soluble M13 phage with phage-displaying a SWNT-binding peptide on P8. This allowed imaging at low concentrations of 2 μg/mL with penetration of up to 2.5 cm in matrigel-based tissue samples. Phage served as an ideal scaffold, as P3 displayed a SPARC-binding peptide for tumor targeting, thus, combining both the imaging and tumor homing moieties.[28] The system could be used as probes for image-guided surgery of sub-millimeter tumors.[29] In a related study, the bacterial enzyme sortase was used to chemoenzymatically attach fluorophores to P8 amines. Sortase recognizes its substrate, LPXTG peptide tagged on the fluorophore, and cleaves between the T and G residues leading to the generation of an acyl enzyme intermediate. Next, nucleophilic attack by the phage amines results in conjugation to the fluorophore. By introducing an orthogonal reaction, sortases increase the versatility of phage surface modifications.[30]

Imaging techniques such as MRI and radiolabeling have also incorporated phage as scaffolds. For example, magnetic iron-oxide nanoparticles, bearing a positive charge, were assembled on the surface of triglutamate-displaying phage vector by electrostatic interactions, resulting in ≈26 nanoparticles/phage targeted

to SPARC receptors using a P3-displayed peptide. This approach allows increased delivery to the target site and consequently improves image contrast. Phage, again proved efficient as the scaffold bearing multiple nanoparticle copies, compared to conventional technique, which would deliver single nanoparticles.[31] Additionally, electrostatic interactions can drive phage to form biomimetic structures with noble metals such as Au and Ag for tumor imaging and photodynamic therapy.[32]

Due to the inherent specificity of phage for F^+ bacteria, radiolabeled phage provide additional opportunities for selective imaging and distinguishing bacterial infections from inflammation. In this example, phage were functionalized with the activated NHS ester of mercaptoacetyltriglycine, which can coordinate ^{99m}Tc.[33] In a follow-up study, the approach was extended to four different types of phage allowing detection of host bacteria specific to each phage, though in vivo specificity remains a concern.[34]

Phage can also deliver hyper-polarized ^{129}Xe-MRI contrast agents termed 'Xe biosensors' for MRI and NMR. Xe has a natural affinity for hydrophobic cavities such as cryptophane A (CryA), but these molecular cages often need a solubilizing, targeting domain and multiple copies for improved sensitivity and specificity. The surface of phage provides the ideal benchtop for implanting such additional functionality. First, *N*-terminal amines of P8 were transaminated in a novel reaction with pyridoxal phosphate, Figure 1-2.[16] This reaction site specifically introduces ketone groups. In the next step, ketone-functionalized

phage react with aminoxy-functionalized CryA. Additional solubility for the phage-CryA complex was provided by step-wise attachment with aminoxy-PEG followed by CryA (1:10 PEG: CryA). Next, Xe bound to CryA is in continuous exchange with solvated Xe in the surrounding aqueous environment termed CEST (chemical exchange saturation transfer), with distinct resonance frequencies for each. ^{129}Xe spins provide remarkable detection limits of sub-pM (230 fM) concentration without much optimization.[35] In a following study, cell targeting ability was provided by P3 proteins displaying scFv, which binds to EGFR on MDA-MB-231 cells, with hyperpolarization of Xe providing a 10,000 fold signal enhancement.[36] Furthermore, Xe is completely abiotic and inert, and this approach should have broad biocompatibility and essentially negligible background signal. The key issue of scFv specificity and affinity remains inherent to essentially all biosensors. Further developments of this element in phage-based devices could impact the field, as the sub-pM sensitivities exceed the capabilities of the best molecular recognition scaffolds.

Desired handles can also be introduced on the phage surface through a combination of genetic and chemical modifications. Another approach to introduce the bio-orthogonal aldehyde chemistry employed sodium periodate, Figure 1-2. This phage scaffold included P3 *N*-terminal Ser or Thr residues for conversion to *N*-terminal glyoxal functionality through the periodate oxidation.[37] Such moieties can then be selectively modified with aminooxy-functionalized glycans or derivatized-aminobenzamidoxime. The conjugation provides long term

stability in comparison to conventional hydrazone formation, and holds the potential for future development into fluorogenic probes.[38]

1.2 Phage as a Drug Delivery Vehicle

Systemic delivery of disease therapeutics can lead to side effects in addition to the drug's desired activity. Toxic side effects arise from the indiscriminate delivery of the drug to non-tumor sites, where the compound can be modified, or bind inappropriately. Targeted drug delivery can solve this problem by more precisely dosing the disease site, and thereby decreasing the required drug dosage. Antibody-drug conjugates, the most successful targeted drug delivery approach requires expensive development and manufacturing. Phage offer a highly amenable platform for development, and also inexpensive production costs. Though a key consideration towards the use of phage as a drug delivery vehicle is the presence of toxic lipopolysachharides, which need to be carefully eliminated during phage purification.

The tremendous hydrophilicity and solubility of phage particles has been demonstrated in the display of highly aggregation-prone membrane proteins.[39] Conjugation of hydrophobic drugs (e.g. Doxorubicin, Dox) can reduce clearance by the mononuclear phagocyte system (MPS). Phage-displaying DFK, a cathepsin B cleavage site, were conjugated to Dox through EDC coupling for drug loading levels of ≈3500 Dox/phage, to allow reduced dosage and administration frequency. Furthermore, P3 of the modified phage displayed IgG

binding domain for binding to target specific antibody allowing cell targeting and internalization. A limitation of this cathepsin linkage is the release of the drug as an Asp adduct, which can render some drugs inactive.[40] Building on this method, Belcher and coworkers modified the P3 to SPARC-binding peptide, and reduced Dox loading to ≈257 Dox/phage. The phage-drug conjugate exhibited a 100-fold more potent response, with a 20-fold higher selectivity for SPARC-positive cells and reduced non-specificity resulting from hydrophobic adhesion to cell membranes.[41]

Delivery vehicles have been built using phage fragments, amphiphilic P8 proteins embedded in vesicles, Figure 1-4. The hydrophobic helix of P8 spontaneously inserts into the lipid bilayer of the liposomes, and orients with the *N*-terminus exposed on the vesicle surface for cell targeting by fused peptides. Tumor targeting of Dox-loaded PEGylated-liposomes enhanced drug cytotoxicity.[42–46] In addition, Petrenko and coworkers attributed enhanced cytotoxicity to endosomal membrane disruption, as provided by P8.[47] In a variation of this approach, P8-targeting peptides were incorporated into PEGylated-polymeric micelles for targeted delivery of the encapsulated hydrophobic and bulky-structured drug, paclitaxel. Again, the use of PEG reduces non-specificity while increasing the blood circulation time.[43,48]

Encapsulation of hydrophobic drugs has also been achieved through self-assembly of phage and block-copolymers. Here again, phage provides solubilization and a large surface for target-specific modification. In this example,

low pH biodegradable PCL-P2VP copolymer forms a core encapsulating Dox, and phage form a shell for these spherical nanoassemblies of ≈200 nm diameter. The phage were premodified with folic acid through the EDC and sulfo-NHS bioconjugation, allowing folate receptor-mediated endocytosis at the target cells. In addition, protonation of the pyridine units in the polymer leads to deformation of the assembly and pH-dependent release of Dox. The method however results in very large sized particles, which could render them susceptible to clearance by MPS.[49]

Multi-stage delivery vectors comprising Si, Au nanoparticles (NPs) and phage have been designed to improve loading efficiency, and target site accumulation and delivery. In this method, the components self-assemble due to electrostatic interactions. For example, assemblies of Au-NP and phage-displaying RGD with an overall negative zeta potential,[50] were attached to Si-NP bearing a net positive charge. Additionally, the pores of Si mesoporous disc-shaped nanoparticles included secondary payload-carrying NPs such as carboxylated quantum dots or amine-functionalized super-paramagnetic iron oxide NPs.[51]

Additionally, progress has been made towards the use of phage-displayed peptides for eliciting the desired immune response, and as a vaccine carrier. This approach is especially useful for the display of poorly immunogenic peptides, which benefit form the multi-copy dense display of the peptide. For a detailed account of this topic, we refer the reader to the review by Scott and co-workers.[52]

1.2.1 Nucleotide Delivery

Delivery of siRNA for cancer treatment can be challenging due to this biopolymer's instability in physiological fluids, and its inability to internalize into cells. Consequently, targeted liposomes were modified to electrostatically encapsulate siRNA, and phage P8.[53] The positively charged *C*-terminus of P8 electrostatically complexes with the negatively charged siRNA providing complexes termed 'nanophages.' For targeted delivery, the *N*-terminus was again conjugated to a cell homing peptide.[54] Specific delivery to the nuclei was achieved through the use of liposome-transposon complex, which also incorporated nuclear localization peptide. The various components used electrostatic interactions for assembly.[55] Along similar lines, DNA was incorporated into porous, glutathione-degradable clusters of silica NPs and paramagnetic iron oxide, coated with PEI covalently linked to P8 through NHS-EDC reaction. Targeted delivery is achieved through magnetically guiding iron oxide, in addition to P8-displayed peptide.[56] This approach holds the potential to combine drug delivery with tissue regeneration. An early report also described the use of phagemid infective particles to target and express the gene of interest inside the cell.[57] Furthermore, elimination of the P3 expression cassette reduced the phagemid size, improving the efficiency of gene delivery.[58] Phage containing a eukaryotic transgene cassette have also been electrostatically complexed with cationic polymers such poly-D-Lysine, PEI for efficient gene delivery.[59]

1.3 Phage as an Intrinsic and Extrinsic Antimicrobial Agent

The constant rise of multi-drug resistant bacteria drive the need for alternative antimicrobial therapies. Bacteriophage especially lytic ones, can kill bacterial cells with high specificity and potency. But, bacterial cell lysis leads to the release of large amounts of endotoxins with undesirable side-effects. In light of these facts, non-lytic phage serve as a promising alternative. Removal of the restriction endonuclease gene renders the phage incapable of replication, a useful property for 'therapeutic' phage. Furthermore, chemical modifications of the phage surface with currently existing drugs allow higher drug loading combined with targeted delivery. Thus, a high concentration of the drug results in the bacterial cell environment, increasing the drug potency.

In earlier studies, P8 amines were conjugated to NHS-activated chloramphenicol-prodrug on phage-displaying an *S. aureus* targeting peptide on P3. Chloramphenicol prodrug was achieved by coupling with glutaric anhydride, which was active off-phage as a result of serum-based proteases.[60] In a further modification, neomycin was inserted as a hydrophilic aminoglycoside solubility enhancing linker, countering the hydrophobicity of the drug, which can disrupt phage stability at high concentrations. The NHS-activated chloramphenicol was first conjugated to amine group on neomycin. Next, the chloramphenicol-neomycin adduct was conjugated to P8 carboxyl groups through EDC coupling, improving the drug loading to almost 10,000 chloramphenicol molecules/phage. The phage-drug complex was also found to be 20,000 fold more potent than free

drug, as opposed to the 20-fold improvement obtained without the linker.[61] In mice-based studies, chloramphenicol-phage complex was found to be non-toxic with low clearance rate from blood, and also generated a reduced immunogenic response compared to unconjugated phage.[62] These results expand on the now-classic phage infectivity approaches to antibiotics, leveraging the high density workbench on the phage surface for drug delivery to cells.

Silverized materials offer another interesting anti-bacterial approach that minimizes the risk of developing resistance. Glutaraldehyde enables phage crosslinking to generate micrometer-scale diameter phage fibers. The phage used were genetically modified to display a tri-Glu peptide to enhance the negative charge on the phage surface. This highly anionic surface bound silver ions due to electrostatic interactions. These silverized phage demonstrate rapid bactericidal action within 300 μm of the fiber. Such silverized phage coatings retained their anti-microbial activity even on Kevlar fibers, for use in future material development.[63]

1.4 Phage as a Biomimetic Matrix for Tissue Regeneration

Regeneration scaffolds focus on mimicking the inherent relationship between the cell and its extracellular matrix (ECM). Phage can provide both the ECM structure and chemical cues. For example, liquid crystalline films comprised of self-assembled phage can serve as a scaffold providing a number of desirable properties, including long rod shape, nanometer-scale size, monodispersity,

topographical features such as indentations and grooves, and the ability to attach ligands for cell-adhesion and growth. One early application applied aligned and self-assembled thin films of phage. Next, the phage amines were modified through reaction with alkyne-functionalized NHS ester, which was further conjugated to azide-functionalized RGD peptides. The RGD peptides are implicated in cellular recognition and attachment mediated through integrins. The click chemistry bioconjugation proceeds in aqueous media, at room temperatures, with typically high efficiencies, and can readily attach a variety azide-derivatized moieties. The approach enables high density display with some control over RGD peptide levels through the bioconjugation conditions. The approach enhances cell adhesion and growth on the surface of these phage films, as observed for NIH3T3 cells.[64]

In a related study, high density display of cell adhesion peptides applied selection for peptide linkers to either RGD or IKVAV sequences. These selectants displayed the cell adhesion peptides on every copy of P8, and were used to compose a 3D phage-based fibrilar matrix for neural progenitor cell growth.[65] In a subsequent study, two-dimensional films were obtained by subjecting the RGD-modified phage to a shearing force providing long-range orientation for cell growth.[66] In addition to the chemical cues for tissue adhesion provided by RGD-displaying phage, display of the streptavidin binder HPQ (biotin-like peptide) sequence allows dense conjugation of large growth factors

such as FGFb and NGF, which provide biochemical cues for neural progenitor cell differentiation.[67]

Charge-based binding to the phage surface is a straightforward modification requiring little additional processing or reagents, Figure 1-4. Lee and coworkers deposited phage films on gold-coated glass slides to further characterize cell proliferation. As a lab-on-a-chip platform, the slides were first coated with positively charged cysteamine allowing charged layer stacking of negatively charged phage. Next, the growth of NIH3T3 cells was monitored using SPR spectroscopy. Cell proliferation directly correlated with growth factor concentration demonstrating the importance of dense bioconjugation on the phage surface. The phage uniquely allow such density, which will also be exploited in drug delivery applications.[68] In a further extension of this approach, microfabrication techniques on gold substrates allowed patterning with phage on cysteamine films.[69] Furthermore, the generation of three-dimensional phage matrices was achieved through electrostatic stabilization with cationic polymers. Poly-L-lysine and chitosan stabilized matrices showed >90% cell survival.[70]

Bone regeneration therapy has also advanced through the application of modified phage. Both biochemical and topographical features of the artificially generated matrix affect cell proliferation and differentiation. A collagen-derived, DGEA peptide displayed on phage served to induce the desired cellular response. The MC3T3 cells exhibited a significant outgrowth morphology, in addition to DGEA-caused expression of cytoskeleton proteins such as actin,

collagen.[71] Similarly, Mao and co-workers generated a two-dimensional artificial ECM through layer-by-layer (LBL) self-assembly of the phage and poly-L-lysine. The inherently high anionicity of phage allowed the formation of these films without requiring additional modifications, and also assembled as parallel ridges. A mixture of phage displaying RGD or PHSRN (synergy site of RGD), which promotes RGD-based cell adhesion was used to induce differentiation of mesenchymal stem cells,[72] and induced pluripotent stem cells (iPSCs).[73]

In a crucial development and follow-up paper, Mao and co-workers generated a virus-activated matrix for bone repair, which requires both angiogenesis and osteogenesis. The pores in a 3D-printed bone scaffold were filled with a matrix comprising of phage. Yet again, the negative charge on the phage was utilized for matrix formation through chitosan-stabilization. The matrix was then implanted in a bone defect, where the RGD-phage induced new bone formation through angiogenesis and mesenchymal stem cell differentiation.[74]

1.5 Modified Phage for Detection

Early and efficient detection of disease-related markers, either proteins or whole cells, is key to favorable prognosis and patient outcomes. In addition to the parameters required for successful detection, the method should have a quick turnaround time and very little sample preparation, for successful development into a clinical test or a point-of-care diagnostic system. Phage provide scaffolds for both ligand display and highly versatile surfaces for further modification with

two or more different moieties. Furthermore, enhanced readouts are achieved through multi-copy functionalization of the large number of P8 coat proteins.

Lateral flow assays (LFA) are rapid, easily commercializable form of point-of-care (POC) diagnostics, provided key issues are addressed. For example, LFAs are notably poor at detecting viruses due to their limit of detection (LOD) falling outside the clinically relevant range. Dual-modified phage particles are being employed to increase the sensitivity of LFAs. The P3 coat proteins were genetically modified with SamAvi peptide tag, which could be biotinylated using birA enzyme. Next, the biotinylated detection antibody, which binds to the target was conjugated to phage-biotin through neutravidin. Additionally, the P8 coat proteins were modified to enhance visualization of the LFA readout. First Traut's reagent functionalized the P8 amines with a free thiol. Next, the thiol was conjugated to maleimide-functionalized horseradish peroxidase (HRP) enzyme. This approach requires addition of TMB as a substrate for HRP, thus detection is not reagent-free. Nevertheless, the study provided a detection limit of 10^4 pfu/mL for MS2 viruses.[75] Subsequently, a 100-fold lower LOD directly compared to conventional Au nanoparticles was observed for noroviruses, specifically Norwalk virus like particles.[76] In a subsequent study, the detection antibody was replaced with an aptamer linked to P3 through a biotinylated PEG linker and neutravidin, as before.[77] The combination of aptamers and phage-displayed peptides could allow more diverse libraries and novel selections.

Fluorescence combined with diffraction-limited objects such as phage addresses the lack of quantitativeness associated with LFAs. For example, Willson and Conrad research teams designed phage labeled with fluorescent dyes, allowing the use of automated image processing and direct counting, assisting quantification.[78] As described above, P3 were functionalized with detection antibodies, whereas the P8 amines were conjugated to the succinimidyl ester of Alexa Fluor 555. This approach eliminates the need for addition of HRP substrates. The system provided a 10^4 pfu/mL LOD. However, the limited dynamic range resulted in saturation at 100 pfu/strip. Setting aside the need for sophisticated optics, stability and photobleaching of fluorogenic dyes, the approach illustrates dual conjugation to phage for sensitive detection of viruses.

Tests for circulating tumor cells (CTCs) promise to identify metastasizing cells for distinguishing cancer aggressiveness and monitoring the course of the disease. In particular, sensitivity, specificity and cell viability for tumor heterogeneity analysis, remain key unsolved challenges. M13 phage could solve such issues because they offer multipoint functionalization. However, the non-specific binding between viruses and the multitude of cell surface receptors must be eliminated. Towards this goal, we have generated viruses modified with various architectures of PEG and PEGylated ligands for prostate cancer cell detection.[79] PEG or PEGylated ligands were functionalized with azides or maleimides and conjugated to on-phage oligolysine (Lys_{14}) peptide 'wrappers' functionalized with alkyne or thiol functionalities, Figure 1-4. In these

experiments, PEG contributes multiple essential functions. First, PEG disrupts non-specific adhesion, a conventional role for PEG. Second, PEG spaces the multiple ligands to control the relative spatial configuration for optimal avidity-based binding. Third, PEG was used to anchor non-genetically encoded ligands on the phage. The flexibility and versatility of PEG was required in these roles, but the two step attachment through wrappers was necessary to avoid encapsulation of the oligolysine peptide by PEG. The oligolysine wrappers utilize the high negative charge present on the phage surface to electrostatically bind to the phage. PEG polymers provide an ≈80% reduction in non-specific binding, and the ligands selectively bind to and capture from solution, PSMA-positive LNCaP cells.[79] We plan to incorporate these PEGylated viruses in film-based biosensors for the sensitive detection of cells.

In another study utilizing PEGylated phage, anti-Her2 antibodies were conjugated to P8 amines using a 6-arm-PEG15K-NHS linker. The technique allowed placement of ≈150 antibodies per phage particle. Phage were also linked to magnetic particles conjugated to anti-P3 antibody. With 250 target cells mixed with leukocytes (4×10^6 cells/mL), the group achieved an unprecedented >90% capture efficiency, with 80% purity and >85% cell viability. The capture purity dropped to 40% when the number of target cells dropped to 25 in the mixture. Notably, non-specific capture was unobserved.[80]

Towards detection of analytes at low concentrations, SERS provides a sensitive technique acquiring raman scattering signals from surface-adsorbed

molecules. The enhancement in signal is obtained through the incorporation of Au or Ag noble metal nanoparticles. Pasqualini, Arap and coworkers ascribe the assembly of phage into a hydrogel from a Au colloidal solution, through the net positive charge of P8 coat protein (pI 9.4).[50] However, under their conditions (pH 7.0 and imidazole), the thiols of cysteine side chains are likely to form Au-S bonds in the hydrogel. Such cysteines are present through misincorporation .[81] In the hydrogel, phage displayed peptides target α_v integrins on melanoma cells. The levels of imidazole used for hydrogel formation governed internalization or cell surface localization of the material. The approach was advanced by designing Ag nanoparticle-phage assemblies based on electrostatic interactions without imidazole. P8-displayed peptide was selected for affinity to lymphoma U937 cells, and bioconjugation to fluorescein isothiocyanate allowed in vitro imaging. Phage binding to the cells generated a distinct shift in raman peaks, which benefits from Ag nanoparticles providing a much higher signal to noise ratio. In this assay, cells were immobilized for detection, thus, capture efficiency and sensitivity require further development.[82]

In another interesting approach, Cha and coworkers phosphine-stabilized Au nanoparticles aggregated on thiolated-phage to provide an optical indicator of antigen binding. Phage displaying a peptide ligand for IgG were thiolated by covalent conjugation to cysteamine using the amide forming EDC reagent. Next, biotin-IgG bound phage were concentrated on a streptavidin-modified surface. The addition of Au-nanoparticles leading to their aggregation on the phage

surface generated a red shift, which was visually detectable at 100 fmol biotin-IgG concentrations.[83] To quantify biotin-IgG concentration, thiolated-phage were next conjugated to maleimide-functionalized DNA with the sequence of A_{30}. Thiols were introduced by reaction with N-succinimidyl 3-[2-pyridyldithio]-propionate (SPDP). Next, captured phage were detected using complementary T_{15}-modified Au nanoparticles. Subsequently, DNA-Au NPs were eluted with T_{30}-DNA to produce a quantitative result with 25 fmole LOD.[84] Within the long phage, inter- and intramolecular crosslinking presents challenges to this approach.

To further improve the selectivity of conjugation, Cha and coworkers derivatized the IgG-binding phage with aldehyde groups. P8 amines were first reacted with succinimidyl 4-formylbenzoate to introduce an aldehyde functionality. This functionality can provide more reliable conjugation to hydrazine-derivatized DNA. In parallel, Au NPs were modified to not just bind to phage but also generate a SERS signal. Ag-modified Au NP with complementary DNA, also carried Cy3. A further enhancement in SERS signal was achieved through introduction of additional layers of these SERS-active NPs on the same IgG-bound phage. In these applications, phage provides an ideal benchtop for conjugation to multiple entities, which lead to an enhanced signal to noise ratio.[85]

Fluorophores such as Alexa Fluor, conjugated to P8 amines have also been employed by Belcher and coworkers for bacterial cell detection and imaging. The P3 proteins were genetically modified to display BAP (Biotin Acceptor Peptide), which after biotinylation bound to a streptavidin modified

antibody for *S. aureus*. As expected, phage due to their inherent binding for F-positive cells, detected such *E. coli* strains without the need for further modification with antibody. The detection and imaging was also performed in vivo, though for efficient treatment with antibiotics, the specificity of bacterial strain detection would be crucial.[86]

1.5.1 Phage as a Biological Recognition Unit in Biosensors

Traditionally, antibodies have been used for biological recognition in biosensors. But antibodies have limitations such as the high cost of production, and require an antigenic target. Phage can serve as a cost-effective, easily modifiable alternative to antibodies, and also hold the potential for label free detection. A large number of approaches for phage incorporation into biosensors have been described. Broadly classifying the approaches as either covalent or non-covalent phage incorporation, reveals key trends.

For example, covalently modified silicon nitride chip surfaces for light addressable potentiometric sensing of the MDAMB231 cancer cell line. The chip surface was first treated with APTES to generate free amines, which were then converted to aldehydes using glutaraldehyde. Next, P8-amines reacted with the surface to form imines. Like most such approaches, the chip surface required blocking with bovine serum albumin to prevent non-specific signal generation. This method proved useful for the detection of bigger moieties such as cells, but

ineffective at detecting smaller biomolecules. Again, P8 amines serve as a easily modifiable handle for phage incorporation and immobilization.[87]

Similarly, we have developed biosensors with phage covalently attached to the gold surface. First, the gold surface was modified with NHS-thioctic ester leading to a thiol-gold bonded self-assembled monolayer (SAM). Next, P8 amines reacted with the activated NHS ester providing the virus electrodes. Upon analyte binding, electrochemical impedance spectroscopy provided a corresponding readout as an increase in the impedance.[88,89] A 120 nM LOD was obtained for prostate-specific membrane antigen (PSMA) through recognition by phage-displayed peptide ligands. Despite the ease of detection, low signal to noise and sensitivity of detection remained key issues, and also required passivation of the unmodified gold surface through blocking with additional proteins such as BSA.[88] In a subsequent study, the approach was used in conjunction with quartz crystal microbalance providing a 7 nM LOD for anti-M13 antibody.[90]

Non-covalent incorporation of phage into biosensors invariably relies on the surface charge of phage. The biggest advantage of using this method, besides the need for little or no other chemical reagents required, is the tunability of the resulting film. In general, the surface charge and thickness can be easily modified. Mao and coworkers modified the phage surface charge to generate a polycationic surface through display of four arginine residues. Next, LBL assembly was used to generate alternate films of such viruses and negatively

charged Au-nanoparticles, simply by immersion in the solution. The resulting nanocomposite films displayed a unique SPR spectra, which was responsive to environmental humidity due to its effect on inter-nanoparticle spacing.[91]

To improve the sensitivity of the device, we switched to non-covalent immobilization of phage in electrically conducting films. Composite films are deposited on the surface of a planar gold electrode consisting of a conducting organic polymer PEDOT (poly-3,4 ethylenedioxythiophene) into which virus particles are incorporated during polymerization. PEDOT in perchlorate solution undergoes an oxidation reaction resulting in a p-doped positively charged polymer. These PEDOT units associate with the negatively charged phage as the counter ion during deposition on gold. PEDOT-nanowires synthesized via lithographically patterned nanowire electrodeposition obtained a ≈20 nM LOD for anti-M13 antibody.[92] The method was extended to the detection of PSMA and provided a 66 nM LOD in synthetic urine.[93] This detection approach doesn't require the addition of redox reporter species, or gold surface passivation to prevent non-specificity, though priming of the gold surface with PEDOT was necessary before plating of virus-PEDOT. This technique appears to block non-specific binding due to complete coverage of the gold surface with PEDOT.

The architecture of the devices likely plays a crucial role in the device sensitivity. For example, a modified approach deposited virus-PEDOT composite as films on the surface of a planar gold electrode, without the need for priming the gold electrode with PEDOT, unlike previous nanowire virus-PEDOT

synthesis.[94,95] In contrast to the above mentioned studies, virus-PEDOT films can be generated and the analyte detected in about an hour, compared to >24h working time for SAM-based approaches. Furthermore, without optimizing this approach provided a 6 nM LOD for anti-M13 antibody. This method provides a lower LOD for the antibody as each phage presents ≈2700 epitopes for antibody binding. The remaining challenge at this stage was the sensitivity required for cancer biomarker detection.[94]

In a subsequent study, we developed the concept of 'phage wrapping' to increase the density of ligands present on the surface of the phage for increased sensitivity through avidity and bidentate binding mode. One ligand to PSMA was genetically displayed through the phagemid system, whereas the second peptide ligand was conjugated to an oligolysine (Lys_{14}) peptide. Phage wrapping maximizes the number of ligands on phage for bidentate synergistic binding to PSMA, Figure 1-4. As the negative charge on the phage is required for both incorporation into PEDOT and wrapping, the phage-PEDOT films were first synthesized and then wrapped with additional ligands. This strategy allowed us to detect PSMA at 100 pM concentrations in synthetic urine with an osmolality of 516.2 mOsm/kg.[96,97] The technique is currently being developed into a point-of-care detection device.

Phage-based electrochemical immunosensors have also been applied towards the detection of small molecules such as the herbicide atrizine, which are conventionally detected through competitive assays with low sensitivity. In

this report, phage-displaying peptide specifically recognizes the atrazine-capture antibody complex on magnetic beads. Then, HRP-conjugated anti-M13 antibody bound to the phage catalyzes the conversion of pyrocatechol to benzoquinone, which can be analyzed by chronoamperometry.[98] In this example, phage provides the ideal scaffold for immobilization of the various moieties involved in the assay.

Besides the standard applications of phage-displayed peptides in biosensors, colorimetric sensors termed 'phage litmus' have also been designed towards the sensitive detection of chemicals. Lee and coworkers demonstrate the use of self-templated assembly of trinitrotoluene-binding peptides displayed on phage, to generate bundles that undergo structural changes on analyte binding providing a 300 ppb LOD.[99] This example thus leverages the self-templated assembly of phage, and the resultant structure for a novel detection modality.

1.6 Phage as a Biological Template for Material Design

The precise assembly of nanoscale building blocks for the generation of complex structures in optical, electronic, magnetic devices or materials is often critical to the resultant functions of the smart materials. Key characteristics of such materials include monodispersed size and shapes, with desired composition and structure, in addition to economical and scalable manufacturing. More recently, efforts have been directed towards the use of organic and biological molecules for structured assembly. Phage, anisotropic in nature, with

relatively monodispersed size and shape, provide an easily functionalizable surface for such material generation. Phage also feature a five-fold symmetry axis along their length, and peptides displayed on phage with 20% incorporation rates will be ≈3 nm apart.[100] Furthermore, the tendency of phage to self-organize into long-range order, such as liquid crystalline structures can provide additional advantages for some applications.

1D-Micro and nano-sized phage fibers with high surface-to-volume ratios can be generated through electrospinning with glutaraldehyde cross-linking. Belcher and coworkers showed the generation of virus-PVP (polyvinyl pyrolidone, a highly water soluble material) composite fibers with nematic ordered morphologies.[101] Phage-based functional fibers were achieved through conjugation of P8 carboxylates to amine-functionalized cadmium selenide quantum dots prior to electrospinning.[102] Silverized phage fibers, and coatings on Kevlar fibers have also been developed through electrostatic interactions and crosslinking.[63] The surface charge on phage can also be achieved by reacting the P8 amines with glutaric anhydride, providing multiple carboxylic acid residues. This highly anionic surface adheres to polyaniline, in the presence of poly-sulfonated styrene to generate highly conductive composite fibers.[103]

Hybridization of DNA strands attached to the phage can dictate specific geometries and therefore properties of the resultant materials. The versatility of the phage surface can provide specific attachment sites at either termini for DNA modification, which, in turn, allows reversible ligation. Thiolated-DNA strands

were conjugated to P3 or P9 through maleimide-functionalized substrates for sortase-mediated bioconjugation reactions. The method allowed sequential linking of three different phage types in the desired order.[104]

Two-dimensional assembly of viruses has also been achieved for NP nucleation and other purposes. Multilayers of oppositely charged polyelectrolytes, linear-polyethyleneimine (LPEI) and polyacrylic acid (PAA) display characteristic interdiffusion between layers. A dropcast phage layer competes with PAA for binding to LPEI. The stronger affinity of PAA for LPEI forces the phage towards the surface, and results in the formation of a highly ordered phage monolayer.[105] These sandwiched stacks of LBL assembled LEPI-PAA can be patterned using a capillary-assisted molding approach.[106] Such LBL assemblies of phage have also been generated on carboxylate-functionalized graphene-oxide sheets. P3-displayed peptide with affinity for the carboxylate functionalities of graphene oxide orients the phage, and external shear force provides alignment. Stacking of such layers generates ultrathin nanomesh membranes with highly selective pore sizes suitable for water-treatment applications.[107]

1.6.1 Inorganic Nucleation

In earlier studies, peptides binding to semiconductors with the selectivity to recognize crystal composition and crystalline faces were obtained through phage-displayed libraries. This work lays the foundation for organic materials to be used for the structural assembly of inorganic materials.[108] Similarly, phage-

displayed peptides selected to recognize ZnS crystals, direct alignment and nucleation into 3D smectic layered structures,[109] and quantum dot and highly conductive nanowires,[110,111] and also superparamagnetic nanoparticles.[112]

Multicomposite materials have also been generated through utilization of the polyanionic phage surface. Metals such as Rh, Pd, Ru complex to form cationic species in aqueous solutions. Such materials can nucleate on the phage surface. These aggregated nanoparticles remain anchored on the surface after sodium borohydride reduction. For bifunctional materials, P3 proteins were genetically modified to bind Fe_3O_4 for magnetic separation. A key limitation of this approach is the failure to nucleate metals such as Au and Pt, which typically form anionic species in solutions.[113]

The polyanionic phage surface has also been utilized to biomimic the composition and orientation of crystallized minerals for bone-like material fabrication. The biggest challenge in this area is the lack of precise control over 1D organization. Mao and coworkers loaded Ca^{2+} onto phage to generate phage bundles held together by electrostatic interactions. Furthermore, the helically chiral phage surface allows precise alignment of Ca^{2+} for nucleation and crystallization of hydroxyapatite.[114] Hierarchical fibril architecture resembling bone ECM was further achieved through the combination of collagen with increased phage anionicity through Glu_8 phagemid display.[115] The development of such biomaterials mimicking bone ECM could allow bone regeneration therapy especially in combination with bone repair as discussed in section 1.4 above. In

another example, phage films treated with apatite precursor solution provided a template for biomineralization leading to the formation of tooth enamel-like composites.[116]

Mesoporous Si structures have widely varied applications including catalysis, adsorbents, and drug delivery agents. However, the generation of highly ordered structures is a major challenge. In addition, the shape, size and morphology of the pores can govern the incorporation of functional materials such as Au acting as a heterogeneous catalyst. Monodispersed phage serve as an ideal template providing ordered pore lattices, and a benchtop for introducing a variety of chemical handles for further modification or nucleation of metals. Mao and coworkers utilized the surface charge on phage for anchoring APTES, which acts as a nuclei for polycondensation of TEOS leading to SiO_2 formation. They authors further examined the effect on pore structures with varying charges on the phage surface.[117] Campero and coworkers applied phage reacted with N-succinimidyl S-acetylthioacetate or N-succinimidyl S-acetylthiopropionate to display thiols providing nucleation sites for metal NP formation. The Au NPs thus incorporated were catalytically active, and allowed free flow of molecules due to encrustation in the walls after calcination.[118] The phage, thus, can act as temporary spacers removed through high temperature treatment.

Catalytic nanowires composed entirely of noble metals increase the cost of preparation. As a result, noble metal nanowires have been synthesized with composite materials. Again, phage-displaying a peptide with affinity for Au

provide powerful approaches to nanowire fabrication. The nanowires were extended to develop Au-Pt core-shell nanowires. The composite noble metal system provided enhanced catalytic activity.[119]

1.6.2 Virus Batteries

In a rather non-intuitive application, viruses have been used to design nanostructures for energy storage and conversion. A variety of materials and techniques have been employed for constructing dimensionally small batteries. Nanostructured materials hold the potential to improve secondary (rechargeable) batteries due to their monodispersed size and hierarchical organization. In an early study, dual-modified viruses allowed the generation of crystalline and uniformly packed Co_3O_4-phage nanowires, dispersed with Au. Such an electrode provided greater reversible storage in comparison to the conventional graphite anode used in Li-ion batteries.[120] Furthermore, placement of these virus-templated Co_3O_4-phage layers in the LBL assembly of solid-state polyelectrolyte LPEI-PAA system further improved electrochemical performance.[121] Again, the ability of phage to form highly organized structures and nucleate materials on its surface allows such applications.

Enhanced electronic conductivity of active materials such as iron phosphate has indirectly been achieved through phage conjugation. Phage nucleating iron phosphate and conjugated to SWNT serve as cathodes with no apparent affect on capacity retention up to 50 cycles.[122] Replacing 1D-SWNT

with 2D-graphene in phage-based cathodes increases the battery's specific capacity.[123] Additionally, SWNTs coated with polyaniline provide materials with high electrical conductivity. First, phage binding to SWNTs through a displayed peptide were cross-linked using glutaraldehyde to generate a hydrogel scaffold. A porous film of polyaniline was next synthesized on the hydrogel. Phage provides the ideal benchtop for uniform and dense contact area between SWNTs and polyaniline leading to high specific capacity. In addition, phage eliminates the requirement for solubilizing agents for otherwise aggregation-prone materials.[124] In another variation, phage nucleating different compositions of transition metal (Co, Mn) oxides provided over two-fold increased specific capacities.[125]

Methanol fuel cells offer multiple advantages but the cost of noble metal electrodes deters their commercialization. Phage selectively modified to nucleate or conjugate Au/Ag/Pt NPs can considerably reduce the cost with electroactivities in a range similar to conventional materials. First, the P8 amines were reacted with NHS-acetylthiopropionate followed by hydroxylamine hydrochloride to generate thiolated phage. Next, the thiols allowed both selective conjugation of pre-formed NPs, and nucleation of metals from solution leading to NP formation.[126]

Phage, in addition to the characteristics detailed above, also exhibits piezoelectric properties due to the lack of an inversion center. The P8 coat proteins have an inherent dipole from the *N*- to *C*-terminus, with a five-fold axis of symmetry allowing polarization and generation of piezoelectricity.[127] The energy-

harvesting capabilities were further enhanced with the nanocrystal formation of perovskite-structured piezoelectric material, $BaTiO_3$ on phage through charge-based nucleation of barium.[128]

1.6.3 Photosensitive Materials

The development of light harvesting systems requires efficient electron and energy transfer to the reaction center. The subnanometer-scale phage have been applied to allow precision nanoscale structuring to increase exciton flux, the transfer of energy without charge transfer. Furthermore, modification of the *N*-terminal and Lys sidechain amines on the P8 coat protein results in formation of FRET pairs with average distances of <2.5 nm. For artificial photosynthesis, these P8 amines were coupled to the carboxylate-modified Zn-porphyrin complexes through the use of NHS-EDC. This Zn-porphyrin phage showed an intense but broad Soret band at 406 nm; the broadness could result from altered P8 structure due to Trp-porphyrin aromatic stacking interactions, which lead to different excited states. Furthermore, the exciton migration through FRET was verified through pump-probe transient absorption spectroscopy.[129] This exciton migration ability of covalently modified phage was applied to formation of nanowire-based photoanode for dye-sensitized solar cells. For this material, anatase was used to efficiently transport electrons. This method leveraged the nucleation ability of phage films allowing deposition of $TiCl_4$ before conversion to anatase. Phage were first cross-linked by glutarldehyde or EDC to provide a

stable hydrogel-like material. Hydrolysis at 80 °C and high temperature annealing at 450 °C of these films converts the amorphous $TiCl_4$ to form crystalline TiO_2 (anatase), which improves electron collection. Additionally, phage can bind Au NPs prior to anatase coating for efficient optical absorption.[130,131]

The conjugation of azo compounds to biomolecules can impart photoresponsivity with reversibility. But, such modifications have largely not been extended to materials in higher dimensional architecture. Phage forming higher ordered self-assembled structures could potentially solve this challenge. Towards this goal, phage were genetically modified to display Tyr on P8, which were then converted to azo compounds by diazotization with p-substituted anilines. The resultant azo-phage complex retains the photoswitchable cis-trans isomerization of the azo functionality.[132] This photoswitchable isomerization has also been used to develop light-responsive ligands using a disulphide-constrained library. The azo functionality was introduced through disulphide reduction followed by reaction with 3,3'-bis(sulfonato)-4,4'-bis(chloroacetamido)azobenzene.[133]

Phage-based photosensitizers have also been developed for photodynamic therapy. Phage terminal amines were conjugated to the photosensitizer, 9-ethenyl-14-ethyl-4,6,13,18-tetramethyl-20-oxo-3-phorbine-propanoic acid. Also, to achieve selective localization, P8 displayed peptides with affinity to the target cancer cells. Illumination with light at 658 nm generated cytotoxic singlet oxygen species.[134]

1.7 Beyond the Traditional Selections

Chemical modifications have also been applied to increase the scope of phage-display based selections. For example, glycopeptide ligands to lectins such as concanavalin A have also been achieved using phage with both genetic and chemical modifications. Derda and coworkers conjugated a P3-displayed library with mannose. The *N*-terminal Ser was first converted to aldehyde (Figure 1-2), and subsequently reacted with aminooxy-functionalized mannose.[135,136] In another approach, a P3 displayed library containing a free Cys was conjugated to mannose through the formation of a disulphide bond through the use of 2-(3-nitropyridyl disulfide ethyl)-mannopyranoside.[137] Such methods present an alternative form of synergistic binding mode obtained through the use of phage. Furthermore, synergistic binding based selections have also been performed with a phage-displayed Cys containing peptide library, conjugated to a pre-determined maleimide-functionalized ligand. The approach provided a much higher affinity extended ligand system.[138] Cyclic peptide libraries have also been generated on phage P3 proteins. First, peptide library containing three reactive Cys is genetically displayed. Next, cyclization is achieved through reaction with tris-(bromomethyl)benzene, providing two peptide loops (Figure 1-3).[139]

CONCLUSIONS

As summarized here, phage provide an exceedingly flexible benchtop for the inclusion of a wide-range of useful functionalities. Such functionalities and multiple modalities on the phage surface result from a combination of chemical and genetic modifications. Moving forward, future examples will combine and extend such modifications in synergistic, novel ways. For example, we imagine applications with flotillas of modified viruses providing targeting, imaging, cell killing, gene delivery, and tissue regenerating functionalities for patient-specific diagnosis and treatment. To date, examples described here report cooperativity for up to two such functions, but multifunctional viruses could improve healthcare in a dramatic way. We hope, the widespread yet field-of-application specific modifications of the phage surface, which currently limit the viruses to up to two functions can be extended through the utilization of cross approaches. To accomplish such multi-functionality, the orthogonal reactions described above could be combined. For example, the materials nucleation offers fascinating new properties for implantable sensors. Similarly, a combination of covalent and non-covalent modifications on the same phage particle could further broaden the scope of phage-based applications. The work described in this thesis utilizes genetic and non-covalent modifications on phage towards sensitive and specific detection of prostate cancer.

REFERENCES

(1) Smith, G. P. Filamentous Fusion Phage: Novel Expression Vectors That Display Cloned Antigens on the Virion Surface. *Science* **1985**, *228*, 1315–1317.

(2) Russel, M.; Lowman, H. B.; Tim, C. *Phage Display: Practical Approach*; Lowman, H. B.; Clackson, T., Eds.; Oxford University Press: New York, 2004.

(3) Sidhu, S. S.; Weiss, G. A. *Phage Display: A Practical Approach*; Lowman, H. B.; Clackson, T., Eds.; Oxford University Press: New York, 2004.

(4) Wan, J.; Shu, H.; Huang, S.; Fiebor, B.; Chen, I.-H.; Petrenko, V. A.; Chin, B. A. Phage-Based Magnetoelastic Wireless Biosensors for Detecting Bacillus Anthracis Spores. *IEEE Sens. J.* **2007**, *7*, 470–477.

(5) Iannolo, G.; Minenkova, O.; Petruzzelli, R.; Cesareni, G. Modifying Filamentous Phage Capsid: Limits in the Size of the Major Capsid Protein. *J. Mol. Biol.* **1995**, *248*, 835–844.

(6) Sidhu, S. S.; Weiss, G. A.; Wells, J. A. High Copy Display of Large Proteins on Phage for Functional Selections. *J. Mol. Biol.* **2000**, *296*, 487–495.

(7) Kehoe, J. W.; Kay, B. K. Filamentous Phage Display in the New Millennium. *Chem. Rev.* **2005**, *105*, 4056–4072.

(8) Levin, A. M.; Weiss, G. A. Optimizing the Affinity and Specificity of Proteins with Molecular Display. *Mol. Biosyst.* **2006**, *2*, 49–57.

(9) Jaworski, J. W.; Raorane, D.; Huh, J. H.; Majumdar, A.; Lee, S.-W. Evolutionary Screening of Biomimetic Coatings for Selective Detection of Explosives. *Langmuir* **2008**, *24*, 4938–4943.

(10) Cho, W.; Fowler, J. D.; Furst, E. M. Targeted Binding of the M13 Bacteriophage to Thiamethoxam Organic Crystals. *Langmuir* **2012**, *28*, 6013–6020.

(11) Maeda, Y.; Javid, N.; Duncan, K.; Birchall, L.; Gibson, K. F.; Cannon, D.; Kanetsuki, Y.; Knapp, C.; Tuttle, T.; Ulijn, R. V; *et al.* Discovery of Catalytic Phages by Biocatalytic Self-Assembly. *J. Am. Chem. Soc.* **2014**, *136*,

15893–15896.

(12) Mohan, K.; Weiss, G. A. Dual Genetically Encoded Phage-Displayed Ligands. *Anal. Biochem.* **2014**, *453*, 1–3.

(13) Molek, P.; Bratkovič, T. Bacteriophages as Scaffolds for Bipartite Display: Designing Swiss Army Knives on a Nanoscale. *Bioconjug. Chem.* **2015**, *26*, 367–378.

(14) Li, K.; Chen, Y.; Li, S.; Nguyen, H. G.; Niu, Z.; You, S.; Mello, C. M.; Lu, X.; Wang, Q. Chemical Modification of M13 Bacteriophage and Its Application in Cancer Cell Imaging. *Bioconjug. Chem.* **2010**, *21*, 1369–1377.

(15) Jayanna, P. K.; Bedi, D.; Deinnocentes, P.; Bird, R. C.; Petrenko, V. A. Landscape Phage Ligands for PC3 Prostate Carcinoma Cells. *Protein Eng. Des. Sel.* **2010**, *23*, 423–430.

(16) Carrico, Z. M.; Farkas, M. E.; Zhou, Y.; Hsiao, S. C.; Marks, J. D.; Chokhawala, H.; Clark, D. S.; Francis, M. B. N-Terminal Labeling of Filamentous Phage to Create Cancer Marker Imaging Agents. *ACS Nano* **2012**, *6*, 6675–6680.

(17) Dwyer, M. a; Lu, W.; Dwyer, J. J.; Kossiakoff, a a. Biosynthetic Phage Display: A Novel Protein Engineering Tool Combining Chemical and Genetic Diversity. *Chem. Biol.* **2000**, *7*, 263–274.

(18) Sandman, K. E.; Benner, J. S.; Noren, C. J. Phage Display of Selenopeptides. *J. Am. Chem. Soc.* **2000**, *122*, 960–961.

(19) Tian, F.; Tsao, M.-L.; Schultz, P. G. A Phage Display System with Unnatural Amino Acids. *J. Am. Chem. Soc.* **2004**, *126*, 15962–15963.

(20) Liu, C. C.; Mack, A. V; Tsao, M.-L.; Mills, J. H.; Lee, H. S.; Choe, H.; Farzan, M.; Schultz, P. G.; Smider, V. V. Protein Evolution with an Expanded Genetic Code. *Proc. Natl. Acad. Sci. USA* **2008**, *105*, 17688–17693.

(21) Welsh, L. C.; Symmons, M. F.; Sturtevant, J. M.; Marvin, D. A.; Perham, R. N. Structure of the Capsid of Pf3 Filamentous Phage Determined from X-Ray Fibre Diffraction Data at 3.1 A Resolution. *J. Mol. Biol.* **1998**, *283*, 155–177.

(22) Hilderbrand, S. A.; Kelly, K. A.; Weissleder, R.; Tung, C.-H. Monofunctional near-Infrared Fluorochromes for Imaging Applications. *Bioconjug. Chem.* **2005**, *16*, 1275–1281.

(23) Kelly, K. A.; Waterman, P.; Weissleder, R. In Vivo Imaging of Molecularly Targeted Phage. *Neoplasia* **2006**, *8*, 1011–1018.

(24) Hilderbrand, S. A.; Kelly, K. A.; Niedre, M.; Weissleder, R. Near Infrared Fluorescence-Based Bacteriophage Particles for Ratiometric pH Imaging. *Bioconjug. Chem.* **2008**, *19*, 1635–1639.

(25) Chen, L.; Zhao, X.; Lin, Y.; Su, Z.; Wang, Q. Dual Stimuli-Responsive Supramolecular Hydrogel of Bionanoparticles and Hyaluronan. *Polym. Chem.* **2014**, *5*, 6754–6760.

(26) Chen, L.; Wu, Y.; Lin, Y.; Wang, Q. Virus-Templated FRET Platform for the Rational Design of Ratiometric Fluorescent Nanosensors. *Chem. Comm.* **2015**, *51*, 10190–10193.

(27) Tian, Y.; Wu, M.; Liu, X.; Liu, Z.; Zhou, Q.; Niu, Z.; Huang, Y. Probing the Endocytic Pathways of the Filamentous Bacteriophage in Live Cells Using Ratiometric pH Fluorescent Indicator. *Adv. Heal. Mater.* **2015**, *4*, 413–419.

(28) Yi, H.; Ghosh, D.; Ham, M.-H.; Qi, J.; Barone, P. W.; Strano, M. S.; Belcher, A. M. M13 Phage-Functionalized Single-Walled Carbon Nanotubes as Nanoprobes for Second near-Infrared Window Fluorescence Imaging of Targeted Tumors. *Nano Lett.* **2012**, *12*, 1176–1183.

(29) Ghosh, D.; Bagley, A. F.; Na, Y. J.; Birrer, M. J.; Bhatia, S. N.; Belcher, A. M. Deep, Noninvasive Imaging and Surgical Guidance of Submillimeter Tumors Using Targeted M13-Stabilized Single-Walled Carbon Nanotubes. *Proc. Natl. Acad. Sci. USA* **2014**, *111*, 13948–13953.

(30) Hess, G. T.; Cragnolini, J. J.; Popp, M. W.; Allen, M. A.; Dougan, S. K.; Spooner, E.; Ploegh, H. L.; Belcher, A. M.; Guimaraes, C. P. M13 Bacteriophage Display Framework That Allows Sortase-Mediated Modification of Surface-Accessible Phage Proteins. *Bioconjug. Chem.* **2012**, *23*, 1478–1487.

(31) Ghosh, D.; Lee, Y.; Thomas, S.; Kohli, A. G.; Yun, D. S.; Belcher, A. M.; Kelly, K. A. M13-Templated Magnetic Nanoparticles for Targeted in Vivo Imaging of Prostate Cancer. *Nat. Nanotechnol.* **2012**, *7*, 677–682.

(32) Wang, F.; Liu, P.; Sun, L.; Li, C.; Petrenko, V. A.; Liu, A. Bio-Mimetic Nanostructure Self-Assembled from Au@Ag Heterogeneous Nanorods and Phage Fusion Proteins for Targeted Tumor Optical Detection and Photothermal Therapy. *Sci. Rep.* **2014**, *4*, 6808.

(33) Rusckowski, M.; Gupta, S.; Liu, G.; Dou, S.; Hnatowich, D. J. Investigations of a 99mTc-Labeled Bacteriophage as a Potential Infection-Specific Imaging Agent. *J. Nucl. Med.* **2004**, *45*, 1201–1208.

(34) Rusckowski, M.; Gupta, S.; Liu, G.; Dou, S.; Hnatowich, D. J. Investigation of Four (99m)Tc-Labeled Bacteriophages for Infection-Specific Imaging. *Nucl. Med. Biol.* **2008**, *35*, 433–440.

(35) Stevens, T. K.; Palaniappan, K. K.; Ramirez, R. M.; Francis, M. B.; Wemmer, D. E.; Pines, A. HyperCEST Detection of a 129Xe-Based Contrast Agent Composed of Cryptophane-A Molecular Cages on a Bacteriophage Scaffold. *Magnet. Reson. Med.* **2013**, *69*, 1245–1252.

(36) Palaniappan, K. K.; Ramirez, R. M.; Bajaj, V. S.; Wemmer, D. E.; Pines, A.; Francis, M. B. Molecular Imaging of Cancer Cells Using a Bacteriophage-Based 129Xe NMR Biosensor. *Angew. Chem., Int. Ed.* **2013**, *52*, 4849–4853.

(37) Ng, S.; Jafari, M. R.; Matochko, W. L.; Derda, R. Quantitative Synthesis of Genetically Encoded Glycopeptide Libraries Displayed on M13 Phage. *ACS Chem. Biol.* **2012**, *7*, 1482–1487.

(38) Kitov, P. I.; Vinals, D. F.; Ng, S.; Tjhung, K. F.; Derda, R. Rapid, Hydrolytically Stable Modification of Aldehyde-Terminated Proteins and Phage Libraries. *J. Am. Chem. Soc.* **2014**, *136*, 8149–8152.

(39) Vithayathil, R.; Hooy, R. M.; Cocco, M. J.; Weiss, G. A. The Scope of Phage Display for Membrane Proteins. *J. Mol. Biol.* **2011**, *414*, 499–510.

(40) Bar, H.; Yacoby, I.; Benhar, I. Killing Cancer Cells by Targeted Drug-Carrying Phage Nanomedicines. *BMC Biotechnol.* **2008**, *8*, 37.

(41) Ghosh, D.; Kohli, A. G.; Moser, F.; Endy, D.; Belcher, A. M. Refactored M13 Bacteriophage as a Platform for Tumor Cell Imaging and Drug Delivery. *ACS Synth. Biol.* **2012**, *1*, 576–582.

(42) Jayanna, P. K.; Bedi, D.; Gillespie, J. W.; DeInnocentes, P.; Wang, T.;

Torchilin, V. P.; Bird, R. C.; Petrenko, V. A. Landscape Phage Fusion Protein-Mediated Targeting of Nanomedicines Enhances Their Prostate Tumor Cell Association and Cytotoxic Efficiency. *Nanomedicine* **2010**, *6*, 538–546.

(43) Wang, T.; Petrenko, V. A.; Torchilin, V. P. Paclitaxel-Loaded Polymeric Micelles Modified with MCF-7 Cell-Specific Phage Protein: Enhanced Binding to Target Cancer Cells and Increased Cytotoxicity. *Mol. Pharm.* **2010**, *7*, 1007–1014.

(44) Bedi, D.; Gillespie, J. W.; Petrenko, V. A. Selection of Pancreatic Cancer Cell-Binding Landscape Phages and Their Use in Development of Anticancer Nanomedicines. *Protein Eng. Des. Sel.* **2014**, *27*, 235–243.

(45) Wang, T.; Hartner, W. C.; Gillespie, J. W.; Praveen, K. P.; Yang, S.; Mei, L. A.; Petrenko, V. A.; Torchilin, V. P. Enhanced Tumor Delivery and Antitumor Activity in Vivo of Liposomal Doxorubicin Modified with MCF-7-Specific Phage Fusion Protein. *Nanomedicine* **2014**, *10*, 421–430.

(46) Gillespie, J. W.; Gross, A. L.; Puzyrev, A. T.; Bedi, D.; Petrenko, V. A. Combinatorial Synthesis and Screening of Cancer Cell-Specific Nanomedicines Targeted via Phage Fusion Proteins. *Front Microbiol.* **2015**, *6*, 628.

(47) Wang, T.; Yang, S.; Petrenko, V. A.; Torchilin, V. P. Cytoplasmic Delivery of Liposomes into MCF-7 Breast Cancer Cells Mediated by Cell-Specific Phage Fusion Coat Protein. *Mol. Pharm.* **2010**, *7*, 1149–1158.

(48) Wang, T.; Petrenko, V. A.; Torchilin, V. P. Optimization of Landscape Phage Fusion Protein-Modified Polymeric PEG-PE Micelles for Improved Breast Cancer Cell Targeting. *J. Nanomed. Nanotechnol.* **2012**, *Suppl 4*, 008.

(49) Suthiwangcharoen, N.; Li, T.; Li, K.; Thompson, P.; You, S.; Wang, Q. M13 Bacteriophage-Polymer Nanoassemblies as Drug Delivery Vehicles. *Nano Res.* **2011**, *4*, 483–493.

(50) Souza, G. R.; Christianson, D. R.; Staquicini, F. I.; Ozawa, M. G.; Snyder, E. Y.; Sidman, R. L.; Miller, J. H.; Arap, W.; Pasqualini, R. Networks of Gold Nanoparticles and Bacteriophage as Biological Sensors and Cell-Targeting Agents. *Proc. Natl. Acad. Sci. USA* **2006**, *103*, 1215–1220.

(51) Srinivasan, S.; Alexander, J. F.; Driessen, W. H.; Leonard, F.; Ye, H.; Liu, X.; Arap, W.; Pasqualini, R.; Ferrari, M.; Godin, B. Bacteriophage Associated Silicon Particles: Design and Characterization of a Novel Theranostic Vector with Improved Payload Carrying Potential. *J. Mater. Chem. B* **2013**, *1*, 5218–5229.

(52) Henry, K. A.; Arbabi-Ghahroudi, M.; Scott, J. K. Beyond Phage Display: Non-Traditional Applications of the Filamentous Bacteriophage as a Vaccine Carrier, Therapeutic Biologic, and Bioconjugation Scaffold. *Front Microbiol.* **2015**, *6*, 755.

(53) Bedi, D.; Musacchio, T.; Fagbohun, O. A.; Gillespie, J. W.; Deinnocentes, P.; Bird, R. C.; Bookbinder, L.; Torchilin, V. P.; Petrenko, V. A. Delivery of siRNA into Breast Cancer Cells via Phage Fusion Protein-Targeted Liposomes. *Nanomedicine* **2011**, *7*, 315–323.

(54) Bedi, D.; Gillespie, J. W.; Petrenko, V. A.; Ebner, A.; Leitner, M.; Hinterdorfer, P.; Petrenko, V. A. Targeted Delivery of siRNA into Breast Cancer Cells via Phage Fusion Proteins. *Mol. Pharm.* **2013**, *10*, 551–559.

(55) Ma, K.; Wang, D.-D.; Lin, Y.; Wang, J.; Petrenko, V.; Mao, C. Synergetic Targeted Delivery of Sleeping-Beauty Transposon System to Mesenchymal Stem Cells Using LPD Nanoparticles Modified with a Phage-Displayed Targeting Peptide. *Adv. Funct. Mater.* **2013**, *23*, 1172–1181.

(56) Gandra, N.; Wang, D.-D.; Zhu, Y.; Mao, C. Virus-Mimetic Cytoplasm-Cleavable Magnetic/Silica Nanoclusters for Enhanced Gene Delivery to Mesenchymal Stem Cells. *Angew. Chem., Int. Ed.* **2013**, *52*, 11278–11281.

(57) Mount, J. D.; Samoylova, T. I.; Morrison, N. E.; Cox, N. R.; Baker, H. J.; Petrenko, V. A. Cell Targeted Phagemid Rescued by Preselected Landscape Phage. *Gene* **2004**, *341*, 59–65.

(58) Li, Z.; Zhang, J.; Zhao, R.; Xu, Y.; Gu, J. Preparation of Peptide-Targeted Phagemid Particles Using a Protein III-Modified Helper Phage. *Biotechniques* **2005**, *39*, 493–497.

(59) Yata, T.; Lee, K.-Y.; Dharakul, T.; Songsivilai, S.; Bismarck, A.; Mintz, P. J.; Hajitou, A. Hybrid Nanomaterial Complexes for Advanced Phage-Guided Gene Delivery. *Mol. Ther. Nucleic Acids* **2014**, *3*, e185.

(60) Yacoby, I.; Shamis, M.; Bar, H.; Shabat, D.; Benhar, I. Targeting

Antibacterial Agents by Using Drug-Carrying Filamentous Bacteriophages. *Antimicrob Agents Chemother.* **2006**, *50*, 2087–2097.

(61) Yacoby, I.; Bar, H.; Benhar, I. Targeted Drug-Carrying Bacteriophages as Antibacterial Nanomedicines. *Antimicrob Agents Chemother.* **2007**, *51*, 2156–2163.

(62) Vaks, L.; Benhar, I. In Vivo Characteristics of Targeted Drug-Carrying Filamentous Bacteriophage Nanomedicines. *J. Nanobiotechnology* **2011**, *9*, 58.

(63) Mao, J. Y.; Belcher, A. M.; Van Vliet, K. J. Genetically Engineered Phage Fibers and Coatings for Antibacterial Applications. *Adv. Funct. Mater.* **2010**, *20*, 209–214.

(64) Rong, J.; Lee, L. A.; Li, K.; Harp, B.; Mello, C. M.; Niu, Z.; Wang, Q. Oriented Cell Growth on Self-Assembled Bacteriophage M13 Thin Films. *Chem. Comm.* **2008**, 5185–5187.

(65) Merzlyak, A.; Indrakanti, S.; Lee, S.-W. Genetically Engineered Nanofiber-like Viruses for Tissue Regenerating Materials. *Nano Lett.* **2009**, *9*, 846–852.

(66) Chung, W.-J.; Merzlyak, A.; Yoo, S. Y.; Lee, S.-W. Genetically Engineered Liquid-Crystalline Viral Films for Directing Neural Cell Growth. *Langmuir* **2010**, *26*, 9885–9890.

(67) Yoo, S. Y.; Merzlyak, A.; Lee, S.-W. Facile Growth Factor Immobilization Platform Based on Engineered Phage Matrices. *Soft Matter* **2011**, *7*, 1660.

(68) Yoo, S. Y.; Oh, J.-W.; Lee, S.-W. Phage-Chips for Novel Optically Readable Tissue Engineering Assays. *Langmuir* **2012**, *28*, 2166–2172.

(69) Yoo, S. Y.; Chung, W.-J.; Kim, T. H.; Le, M.; Lee, S.-W. Facile Patterning of Genetically Engineered M13 Bacteriophage for Directional Growth of Human Fibroblast Cells. *Soft Matter* **2011**, *7*, 363–368.

(70) Chung, W.-J.; Merzlyak, A.; Lee, S.-W. Fabrication of Engineered M13 Bacteriophages into Liquid Crystalline Films and Fibers for Directional Growth and Encapsulation of Fibroblasts. *Soft Matter* **2010**, *6*, 4454.

(71) Yoo, S. Y.; Kobayashi, M.; Lee, P. P.; Lee, S.-W. Early Osteogenic

Differentiation of Mouse Preosteoblasts Induced by Collagen-Derived DGEA-Peptide on Nanofibrous Phage Tissue Matrices. *Biomacromolecules* **2011**, *12*, 987–996.

(72) Wang, W.; Chen, X.; Li, T.; Li, Y.; Wang, R.; He, D.; Luo, W.; Li, X.; Wu, X. Screening a Phage Display Library for a Novel FGF8b-Binding Peptide with Anti-Tumor Effect on Prostate Cancer. *Exp. Cell Res.* **2013**, *319*, 1156–1164.

(73) Wang, J.; Wang, L.; Yang, M.; Zhu, Y.; Tomsia, A.; Mao, C. Untangling the Effects of Peptide Sequences and Nanotopographies in a Biomimetic Niche for Directed Differentiation of iPSCs by Assemblies of Genetically Engineered Viral Nanofibers. *Nano Lett.* **2014**, *14*, 6850–6856.

(74) Wang, J.; Yang, M.; Zhu, Y.; Wang, L.; Tomsia, A. P.; Mao, C. Phage Nanofibers Induce Vascularized Osteogenesis in 3D Printed Bone Scaffolds. *Adv. Mater.* **2014**, *26*, 4961–4966.

(75) Adhikari, M.; Dhamane, S.; Hagström, A. E. V; Garvey, G.; Chen, W.-H.; Kourentzi, K.; Strych, U.; Willson, R. C. Functionalized Viral Nanoparticles as Ultrasensitive Reporters in Lateral-Flow Assays. *Analyst* **2013**, *138*, 5584–5587.

(76) Hagström, A. E. V; Garvey, G.; Paterson, A. S.; Dhamane, S.; Adhikari, M.; Estes, M. K.; Strych, U.; Kourentzi, K.; Atmar, R. L.; Willson, R. C. Sensitive Detection of Norovirus Using Phage Nanoparticle Reporters in Lateral-Flow Assay. *PLoS One* **2015**, *10*, e0126571.

(77) Adhikari, M.; Strych, U.; Kim, J.; Goux, H.; Dhamane, S.; Poongavanam, M.-V.; Hagström, A. E. V; Kourentzi, K.; Conrad, J. C.; Willson, R. C. Aptamer-Phage Reporters for Ultrasensitive Lateral Flow Assays. *Anal. Chem.* **2015**, *87*, 11660–11665.

(78) Kim, J.; Adhikari, M.; Dhamane, S.; Hagström, A. E. V; Kourentzi, K.; Strych, U.; Willson, R. C.; Conrad, J. C. Detection of Viruses by Counting Single Fluorescent Genetically Biotinylated Reporter Immunophage Using a Lateral Flow Assay. *ACS Appl. Mater. Interfaces* **2015**, *7*, 2891–2898.

(79) Mohan, K.; Weiss, G. A. Engineering Chemically Modified Viruses for Prostate Cancer Cell Recognition. *Mol. Biosyst.* **2015**, *11*, 3264–3272.

(80) Jo, S.-M.; Lee, J.; Heu, W.; Kim, H.-S. Nanotentacle-Structured Magnetic

Particles for Efficient Capture of Circulating Tumor Cells. *Small* **2015**, *11*, 1975–1982.

(81) Pedersen, H.; Holder, S.; Sutherlin, D. P.; Schwitter, U.; King, D. S.; Schultz, P. G. A Method for Directed Evolution and Functional Cloning of Enzymes. *Proc. Natl. Acad. Sci. USA* **1998**, *95*, 10523–10528.

(82) Lentini, G.; Fazio, E.; Calabrese, F.; De Plano, L. M.; Puliafico, M.; Franco, D.; Nicolò, M. S.; Carnazza, S.; Trusso, S.; Allegra, A.; *et al.* Phage-AgNPs Complex as SERS Probe for U937 Cell Identification. *Biosens. Bioelectron.* **2015**, *74*, 398–405.

(83) Lee, J. H.; Cha, J. N. Amplified Protein Detection through Visible Plasmon Shifts in Gold Nanocrystal Solutions from Bacteriophage Platforms. *Anal. Chem.* **2011**, *83*, 3516–3519.

(84) Lee, J. H.; Domaille, D. W.; Cha, J. N. Amplified Protein Detection and Identification through DNA-Conjugated M13 Bacteriophage. *ACS Nano* **2012**, *6*, 5621–5626.

(85) Lee, J. H.; Xu, P. F.; Domaille, D. W.; Choi, C.; Jin, S.; Cha, J. N. M13 Bacteriophage as Materials for Amplified Surface Enhanced Raman Scattering Protein Sensing. *Adv. Funct. Mater.* **2014**, *24*, 2079–2084.

(86) Bardhan, N. M.; Ghosh, D.; Belcher, A. M. M13 Virus Based Detection of Bacterial Infections in Living Hosts. *J. Biophotonics* **2014**, *7*, 617–623.

(87) Jia, Y.; Qin, M.; Zhang, H.; Niu, W.; Li, X.; Wang, L.; Li, X.; Bai, Y.; Cao, Y.; Feng, X. Label-Free Biosensor: A Novel Phage-Modified Light Addressable Potentiometric Sensor System for Cancer Cell Monitoring. *Biosens. Bioelectron.* **2007**, *22*, 3261–3266.

(88) Yang, L.-M. C.; Tam, P. Y.; Murray, B. J.; McIntire, T. M.; Overstreet, C. M.; Weiss, G. A.; Penner, R. M. Virus Electrodes for Universal Biodetection. *Anal. Chem.* **2006**, *78*, 3265–3270.

(89) Yang, L.-M. C.; Diaz, J. E.; McIntire, T. M.; Weiss, G. A.; Penner, R. M. Direct Electrical Transduction of Antibody Binding to a Covalent Virus Layer Using Electrochemical Impedance. *Anal. Chem.* **2008**, *80*, 5695–5705.

(90) Yang, L.-M. C.; Diaz, J. E.; McIntire, T. M.; Weiss, G. A.; Penner, R. M.

Covalent Virus Layer for Mass-Based Biosensing. *Anal. Chem.* **2008**, *80*, 933–943.

(91) Liu, A.; Abbineni, G.; Mao, C. Nanocomposite Films Assembled from Genetically Engineered Filamentous Viruses and Gold Nanoparticles: Nanoarchitecture- and Humidity-Tunable Surface Plasmon Resonance Spectra. *Adv. Mater.* **2009**, *21*, 1001–1005.

(92) Arter, J. A.; Taggart, D. K.; McIntire, T. M.; Penner, R. M.; Weiss, G. A. Virus-PEDOT Nanowires for Biosensing. *Nano Lett.* **2010**, *10*, 4858–4862.

(93) Arter, J. A.; Diaz, J. E.; Donavan, K. C.; Yuan, T.; Penner, R. M.; Weiss, G. A. Virus-Polymer Hybrid Nanowires Tailored to Detect Prostate-Specific Membrane Antigen. *Anal. Chem.* **2012**, *84*, 2776–2783.

(94) Donavan, K. C.; Arter, J. A.; Pilolli, R.; Cioffi, N.; Weiss, G. A.; Penner, R. M. Virus-poly(3,4-Ethylenedioxythiophene) Composite Films for Impedance-Based Biosensing. *Anal. Chem.* **2011**, *83*, 2420–2424.

(95) Donavan, K. C.; Arter, J. A.; Weiss, G. A.; Penner, R. M. Virus-Poly(3,4-Ethylenedioxythiophene) Biocomposite Films. *Langmuir* **2012**, *28*, 12581–12587.

(96) Mohan, K.; Donavan, K. C.; Arter, J. A.; Penner, R. M.; Weiss, G. A. Sub-Nanomolar Detection of Prostate-Specific Membrane Antigen in Synthetic Urine by Synergistic, Dual-Ligand Phage. *J. Am. Chem. Soc.* **2013**, *135*, 7761–7767.

(97) Mohan, K.; Penner, R. M.; Weiss, G. A. Biosensing with Virus Electrode Hybrids. *Curr. Protoc. Chem. Biol.* **2015**, *7*, 53–72.

(98) González-Techera, A.; Zon, M. A.; Molina, P. G.; Fernández, H.; González-Sapienza, G.; Arévalo, F. J. Development of a Highly Sensitive Noncompetitive Electrochemical Immunosensor for the Detection of Atrazine by Phage Anti-Immunocomplex Assay. *Biosens. Bioelectron.* **2015**, *64*, 650–656.

(99) Oh, J.-W.; Chung, W.-J.; Heo, K.; Jin, H.-E.; Lee, B. Y.; Wang, E.; Zueger, C.; Wong, W.; Meyer, J.; Kim, C.; *et al.* Biomimetic Virus-Based Colourimetric Sensors. *Nat. Commun.* **2014**, *5*, 3043.

(100) Mao, C.; Solis, D. J.; Reiss, B. D.; Kottmann, S. T.; Sweeney, R. Y.;

Hayhurst, A.; Georgiou, G.; Iverson, B.; Belcher, A. M. Virus-Based Toolkit for the Directed Synthesis of Magnetic and Semiconducting Nanowires. *Science* **2004**, *303*, 213–217.

(101) Lee, S.-W.; Belcher, A. M. Virus-Based Fabrication of Micro- and Nanofibers Using Electrospinning. *Nano Lett.* **2004**, *4*, 387–390.

(102) Chiang, C.-Y.; Mello, C. M.; Gu, J.; Silva, E. C. C. M.; Van Vliet, K. J.; Belcher, A. M. Weaving Genetically Engineered Functionality into Mechanically Robust Virus Fibers. *Adv. Mater.* **2007**, *19*, 826–832.

(103) Niu, Z.; Bruckman, M. A.; Harp, B.; Mello, C. M.; Wang, Q. Bacteriophage M13 as a Scaffold for Preparing Conductive Polymeric Composite Fibers. *Nano Res.* **2008**, *1*, 235–241.

(104) Hess, G. T.; Guimaraes, C. P.; Spooner, E.; Ploegh, H. L.; Belcher, A. M. Orthogonal Labeling of M13 Minor Capsid Proteins with DNA to Self-Assemble End-to-End Multiphage Structures. *ACS Synth. Biol.* **2013**, *2*, 490–496.

(105) Yoo, P. J.; Nam, K. T.; Qi, J.; Lee, S.-K.; Park, J.; Belcher, A. M.; Hammond, P. T. Spontaneous Assembly of Viruses on Multilayered Polymer Surfaces. *Nat. Mater.* **2006**, *5*, 234–240.

(106) Yoo, P. J.; Nam, K. T.; Belcher, A. M.; Hammond, P. T. Solvent-Assisted Patterning of Polyelectrolyte Multilayers and Selective Deposition of Virus Assemblies. *Nano Lett.* **2008**, *8*, 1081–1089.

(107) Lee, Y. M.; Jung, B.; Kim, Y. H.; Park, A. R.; Han, S.; Choe, W.-S.; Yoo, P. J. Nanomesh-Structured Ultrathin Membranes Harnessing the Unidirectional Alignment of Viruses on a Graphene-Oxide Film. *Adv. Mater.* **2014**, *26*, 3899–3904.

(108) Whaley, S. R.; English, D. S.; Hu, E. L.; Barbara, P. F.; Belcher, A. M. Selection of Peptides with Semiconductor Binding Specificity for Directed Nanocrystal Assembly. *Nature* **2000**, *405*, 665–668.

(109) Lee, S.-W. Ordering of Quantum Dots Using Genetically Engineered Viruses. *Science* **2002**, *296*, 892–895.

(110) Mao, C.; Flynn, C. E.; Hayhurst, A.; Sweeney, R.; Qi, J.; Georgiou, G.; Iverson, B.; Belcher, A. M. Viral Assembly of Oriented Quantum Dot

Nanowires. *Proc. Natl. Acad. Sci. USA* **2003**, *100*, 6946–69451.

(111) Huang, Y.; Chiang, C.-Y.; Lee, S. K.; Gao, Y.; Hu, E. L.; Yoreo, J. De; Belcher, A. M. Programmable Assembly of Nanoarchitectures Using Genetically Engineered Viruses. *Nano Lett.* **2005**, *5*, 1429–1434.

(112) Lee, S.-K.; Yun, D. S.; Belcher, A. M. Cobalt Ion Mediated Self-Assembly of Genetically Engineered Bacteriophage for Biomimetic Co-Pt Hybrid Material. *Biomacromolecules* **2006**, *7*, 14–17.

(113) Avery, K. N.; Schaak, J. E.; Schaak, R. E. M13 Bacteriophage as a Biological Scaffold for Magnetically-Recoverable Metal Nanowire Catalysts: Combining Specific and Nonspecific Interactions To Design Multifunctional Nanocomposites. *Chem. Mater.* **2009**, *21*, 2176–2178.

(114) Wang, F.; Cao, B.; Mao, C. Bacteriophage Bundles with Pre-Aligned Ca Initiate the Oriented Nucleation and Growth of Hydroxylapatite. *Chem. Mater.* **2010**, *22*, 3630–3636.

(115) He, T.; Abbineni, G.; Cao, B.; Mao, C. Nanofibrous Bio-Inorganic Hybrid Structures Formed through Self-Assembly and Oriented Mineralization of Genetically Engineered Phage Nanofibers. *Small* **2010**, *6*, 2230–2235.

(116) Chung, W.-J.; Oh, J.-W.; Kwak, K.; Lee, B. Y.; Meyer, J.; Wang, E.; Hexemer, A.; Lee, S.-W. Biomimetic Self-Templating Supramolecular Structures. *Nature* **2011**, *478*, 364–368.

(117) Mao, C.; Wang, F.; Cao, B. Controlling Nanostructures of Mesoporous Silica Fibers by Supramolecular Assembly of Genetically Modifiable Bacteriophages. *Angew. Chem., Int. Ed.* **2012**, *51*, 6411–6415.

(118) Vera-Robles, L. I.; González-Gracida, J.; Hernández-Gordillo, A.; Campero, A. Using the M13 Phage as a Biotemplate to Create Mesoporous Structures Decorated with Gold and Platinum Nanoparticles. *Langmuir* **2015**, *31*, 9188–9197.

(119) Lee, Y.; Kim, J.; Yun, D. S.; Nam, Y. S.; Shao-Horn, Y.; Belcher, A. M. Virus-Templated Au and Au–Pt Core–shell Nanowires and Their Electrocatalytic Activities for Fuel Cell Applications. *Energy Environ. Sci.* **2012**, *5*, 8328–8334.

(120) Nam, K. T.; Kim, D.-W.; Yoo, P. J.; Chiang, C.-Y.; Meethong, N.;

Hammond, P. T.; Chiang, Y.-M.; Belcher, A. M. Virus-Enabled Synthesis and Assembly of Nanowires for Lithium Ion Battery Electrodes. *Science* **2006**, *312*, 885–888.

(121) Nam, K. T.; Wartena, R.; Yoo, P. J.; Liau, F. W.; Lee, Y. J.; Chiang, Y.-M.; Hammond, P. T.; Belcher, A. M. Stamped Microbattery Electrodes Based on Self-Assembled M13 Viruses. *Proc. Natl. Acad. Sci. USA* **2008**, *105*, 17227–17231.

(122) Lee, Y. J.; Yi, H.; Kim, W.-J.; Kang, K.; Yun, D. S.; Strano, M. S.; Ceder, G.; Belcher, A. M. Fabricating Genetically Engineered High-Power Lithium-Ion Batteries Using Multiple Virus Genes. *Science* **2009**, *324*, 1051–1055.

(123) Oh, D.; Dang, X.; Yi, H.; Allen, M. A.; Xu, K.; Lee, Y. J.; Belcher, A. M. Graphene Sheets Stabilized on Genetically Engineered M13 Viral Templates as Conducting Frameworks for Hybrid Energy-Storage Materials. *Small* **2012**, *8*, 1006–1011.

(124) Chen, P.-Y.; Hyder, M. N.; Mackanic, D.; Courchesne, N.-M. D.; Qi, J.; Klug, M. T.; Belcher, A. M.; Hammond, P. T. Hydrogels: Assembly of Viral Hydrogels for Three-Dimensional Conducting Nanocomposites *Adv. Mater.* **2014**, *26*, 5069–5069.

(125) Oh, D.; Qi, J.; Han, B.; Zhang, G.; Carney, T. J.; Ohmura, J.; Zhang, Y.; Shao-Horn, Y.; Belcher, A. M. M13 Virus-Directed Synthesis of Nanostructured Metal Oxides for Lithium-Oxygen Batteries. *Nano Lett.* **2014**, *14*, 4837–4845.

(126) Vera-Robles, L. I.; Van Tran Nhieu, G.; Laberty-Robert, C.; Livage, J.; Sanchez, C. Flexible Electroactive Nanomaterials Biotemplated with Versatile M13 Phage Platforms. *Adv. Eng. Mater.* **2013**, *15*, 954–961.

(127) Lee, B. Y.; Zhang, J.; Zueger, C.; Chung, W.-J.; Yoo, S. Y.; Wang, E.; Meyer, J.; Ramesh, R.; Lee, S.-W. Virus-Based Piezoelectric Energy Generation. *Nat. Nanotechnol.* **2012**, *7*, 351–356.

(128) Jeong, C. K.; Kim, I.; Park, K.-I.; Oh, M. H.; Paik, H.; Hwang, G.-T.; No, K.; Nam, Y. S.; Lee, K. J. Virus-Directed Design of a Flexible $BaTiO_3$ Nanogenerator. *ACS Nano* **2013**, *7*, 11016–11025.

(129) Nam, Y. S.; Shin, T.; Park, H.; Magyar, A. P.; Choi, K.; Fantner, G.; Nelson, K. A.; Belcher, A. M. Virus-Templated Assembly of Porphyrins into Light-

Harvesting Nanoantennae. *J. Am. Chem. Soc.* **2010**, *132*, 1462–1463.

(130) Chen, P.-Y.; Dang, X.; Klug, M. T.; Qi, J.; Dorval Courchesne, N.-M.; Burpo, F. J.; Fang, N.; Hammond, P. T.; Belcher, A. M. Versatile Three-Dimensional Virus-Based Template for Dye-Sensitized Solar Cells with Improved Electron Transport and Light Harvesting. *ACS Nano* **2013**, *7*, 6563–6574.

(131) Courchesne, N.-M. D.; Klug, M. T.; Chen, P.-Y.; Kooi, S. E.; Yun, D. S.; Hong, N.; Fang, N. X.; Belcher, A. M.; Hammond, P. T. Assembly of a Bacteriophage-Based Template for the Organization of Materials into Nanoporous Networks. *Adv. Mater.* **2014**, *26*, 3398–3404.

(132) Murugesan, M.; Abbineni, G.; Nimmo, S. L.; Cao, B.; Mao, C. Virus-Based Photo-Responsive Nanowires Formed by Linking Site-Directed Mutagenesis and Chemical Reaction. *Sci. Rep.* **2013**, *3*, 1820.

(133) Jafari, M. R.; Deng, L.; Kitov, P. I.; Ng, S.; Matochko, W. L.; Tjhung, K. F.; Zeberoff, A.; Elias, A.; Klassen, J. S.; Derda, R. Discovery of Light-Responsive Ligands through Screening of a Light-Responsive Genetically Encoded Library. *ACS Chem. Biol.* **2014**, *9*, 443–450.

(134) Gandra, N.; Abbineni, G.; Qu, X.; Huai, Y.; Wang, L.; Mao, C. Bacteriophage Bionanowire as a Carrier for Both Cancer-Targeting Peptides and Photosensitizers and Its Use in Selective Cancer Cell Killing by Photodynamic Therapy. *Small* **2013**, *9*, 215–221.

(135) Ng, S.; Lin, E.; Kitov, P. I.; Tjhung, K. F.; Gerlits, O. O.; Deng, L.; Kasper, B.; Sood, A.; Paschal, B. M.; Zhang, P.; *et al.* Genetically Encoded Fragment-Based Discovery of Glycopeptide Ligands for Carbohydrate-Binding Proteins. *J. Am. Chem. Soc.* **2015**, *137*, 5248–5251.

(136) Tjhung, K. F.; Kitov, P. I.; Ng, S.; Kitova, E. N.; Deng, L.; Klassen, J. S.; Derda, R. Silent Encoding of Chemical Post-Translational Modifications in Phage-Displayed Libraries. *J. Am. Chem. Soc.* **2015**.

(137) Arai, K.; Tsutsumi, H.; Mihara, H. A Monosaccharide-Modified Peptide Phage Library for Screening of Ligands to Carbohydrate-Binding Proteins. *Bioorgan. Med. Chem. Lett.* **2013**, *23*, 4940–4943.

(138) Santoso, B.; Lam, S.; Murray, B. W.; Chen, G. A Simple and Efficient Maleimide-Based Approach for Peptide Extension with a Cysteine-

Containing Peptide Phage Library. *Bioorgan. Med. Chem.* **2013**, *23*, 5680–5683.

(139) Heinis, C.; Rutherford, T.; Freund, S.; Winter, G. Phage-Encoded Combinatorial Chemical Libraries Based on Bicyclic Peptides. *Nat. Chem. Biol.* **2009**, *5*, 502–507.

CHAPTER 2

Sub-nanomolar Detection of Prostate-Specific Membrane Antigen in Synthetic Urine by Synergistic, Dual Ligand Phage

ABSTRACT

The sensitive detection of cancer biomarkers in urine could revolutionize cancer diagnosis and treatment. Such detectors must be inexpensive, easy to interpret, and sensitive. This report describes a bioaffinity matrix of viruses integrated into PEDOT films for electrochemical sensing of prostate specific membrane antigen (PSMA), a prostate cancer biomarker. High sensitivity to PSMA resulted from synergistic action by two different ligands to PSMA on the same phage particle. One ligand was genetically encoded, and the secondary recognition ligand was chemically synthesized to wrap around the phage. The dual ligands result in a bidentate binder with high copy, dense ligand display for enhanced PSMA detection through a chelate-based, avidity effect. Biosensing with virus-PEDOT films provides a 100 pM limit of detection for PSMA in synthetic urine without requiring enzymatic or other amplification.

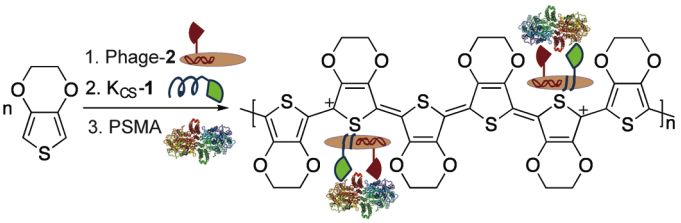

Key reference: Kritika Mohan, Keith C. Donavan, Jessica A. Arter, Reginald M. Penner, and Gregory A. Weiss. Sub-nanomolar Detection of Prostate-Specific Membrane Antigen in Synthetic Urine by Synergistic, Dual-Ligand Phage. *J. Am. Chem. Soc.*, **2013**, 135(20), 7761-7767.

INTRODUCTION

More effective biosensors could address a critical need for detecting cancer-associated biomarkers. An estimated 29,000 men in the US will succumb to prostate cancer in 2013.[1] Unfortunately, the lack of validated clinical diagnostic markers complicates efforts to develop tests for early prostate cancer detection. For example, a recent report concludes that the Prostate Specific Antigen (PSA) test used for prostate cancer diagnostics is more harmful than beneficial.[2] Despite this caveat, PSA remains an important biomarker for detecting recurrent prostate cancer. However, early detection of the disease could enable more effective treatment and prognosis.[3] Thus, issues addressable by bioanalytical chemistry include the development of more sensitive measurements of protein concentration and then applying such measurements to identify and validate more effective biomarkers.

Unlike PSA, Prostate Specific Membrane Antigen (PSMA) concentrations in biological fluids appear to offer a more useful metric for prostate cancer diagnosis and prognosis.[4] For example, elevated PSMA levels have been observed in prostate cancer patients' urine.[5] The PSMA concentration increases from 0.25 nM to approximately 3.5 nM in prostate cancer patients' biological fluids including urine.[6] PSMA, a 750-residue, 90 kD glycoprotein, is overexpressed on the surface of tumor cells as a non-covalent homodimer in >94.3 and >57.7% of primary and metastatic prostate cancers respectively.[7,8] Elevated PSMA levels also correlate with the aggressiveness of tumor growth.[9] Thus, PSMA offers an important

biomarker for the development of biosensor-based diagnostic devices. This report describes the development of a biosensor capable of detecting clinically relevant concentrations of PSMA (<0.25 nM) in synthetic urine.

In 2003, Petrenko and Vodyanoy demonstrated the use of whole virus particles as a bioaffinity matrix for biosensors.[10,11] In an improved generation of biosensors, T7 virus particles with a peptide antigen from the West Nile virus on their surfaces have been incorporated into conducting polymers by Cosnier and coworkers to allow detection of antibodies to the West Nile virus.[12] This strategy can offer higher density ligands for biomarker binding, as T7 phage have a high density of peptides displayed on their surface. Improving biosensor sensitivity through increasing the density of ligands on the phage surface inspired in part the approach reported here.

M13 bacteriophage, or more commonly 'phage,' serve as receptors for biosensors reported by our laboratories. Viruses that infect only bacteria, the M13 bacteriophage have a readily customized protein coat, which can be tailored to bind to cancer biomarkers.[13] The M13 viruses have ssDNA encapsulated by approximately 2700 copies of the major coat protein (P8) and five copies each of the four minor coat proteins. Manipulating the encapsulated DNA can provide peptides and proteins fused to the phage coat proteins, which are displayed on the phage surface.[13] Combinatorial engineering of such polypeptides allows molecular evolution to obtain displayed ligands with specific binding affinities and specificities.[14,15]

For direct electrical detection of biomarkers, M13 bacteriophage have been incorporated into films of an electronically conductive polymer, PEDOT (poly-3,4-ethylenedioxythiophene).[16–20] Synthesis of the biosensor film is accomplished by electropolymerizing EDOT on the surface of a planar gold electrode from a solution that contains virus particles. During biosensor measurements, the electrochemical impedance of the virus-PEDOT film increases upon exposure to the biomarker, providing a quantifiable readout for analyte binding.[21]

Modifications to the biosensing films could further improve the device's limit of detection (LOD) for translational relevance. In a previous report, we have described phage-incorporated into PEDOT nanowires, which resulted in biosensors with a >66 nM LOD for PSMA in synthetic urine.[22] Conventional phage display results in a low density of genetically encoded ligands displayed on the surface of the phage. Here, we focus on increasing the density of such ligands, as a strategy for more sensitive measurements with higher signal-to-noise ratios. The concept of "phage wrapping" to improve ligand density builds upon our previous reports of wrapping the negatively charged phage surface with positively charged polymers to prevent non-specific binding to the phage.[23,24] The approach takes advantage of the presence of negatively charged residues, one Glu and two Asp, on the *N*-terminus of each P8. Since each phage includes 2700 copies of P8, such carboxylate-bearing residues result in a high negative charge on the outer surface of the virus particle.[25] As reported here, additional ligands wrapped onto the phage surface due to this electrostatic interaction, lead to enhanced affinity and selectivity for PSMA.

RESULTS AND DISCUSSION

2.1 Genetically-Encoded, Phage-Displayed Ligands Targeting PSMA

The two forms of PSMA, monomeric and dimeric, offer different targets for ligand binding; the dimeric form is overexpressed by prostate cancer cells, and the monomeric form offers a closely matched negative control for non-specificity, as a protein only found in healthy prostate cells.[9] The relative binding affinities of two previously reported phage-displayed ligands,[22] phage-**1** and phage-**2**, (sequences and nomenclature in Table 2-1) for the PSMA isoforms were first examined by ELISA (Figure 2-1). Phage-**2** binds with higher affinity to the PSMA dimer, than phage-**1**. Neither phage-displayed ligand binds with significant affinity to the PSMA monomer. Thus, the peptide ligands selectively bind the dimeric form of PSMA. The specificity of phage-displayed ligands for the dimeric PSMA is critical for potential clinical applications. Additional negative controls include phage-displayed peptides targeting the blocking agent (bovine serum albumin, BSA) and Stop-4 phage targeting PSMA; the latter phage includes an analogous phagemid packaged into phage without ligands displayed on their surfaces. As expected, the negative controls failed to show any significant binding.

X	Amino acid sequence	Genetically encoded	Chemically synthesized	Structure of the chemically synthesized peptide
1	CALCEFLG	phage – **1**	K_{cs} –**1**	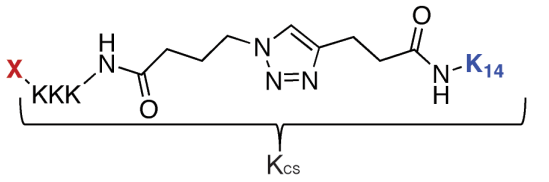
2	SECVEVFQNSCDW	phage – **2**	K_{cs} –**2**	

Table 2-1. PSMA ligands, sequence and nomenclature. PSMA ligands, sequence and nomenclature nomenclature. The "X" in the structure describes the entries in the first column, and is the PSMA binding ligand; K_{14} is defined as a peptide composed of 14 lysines.

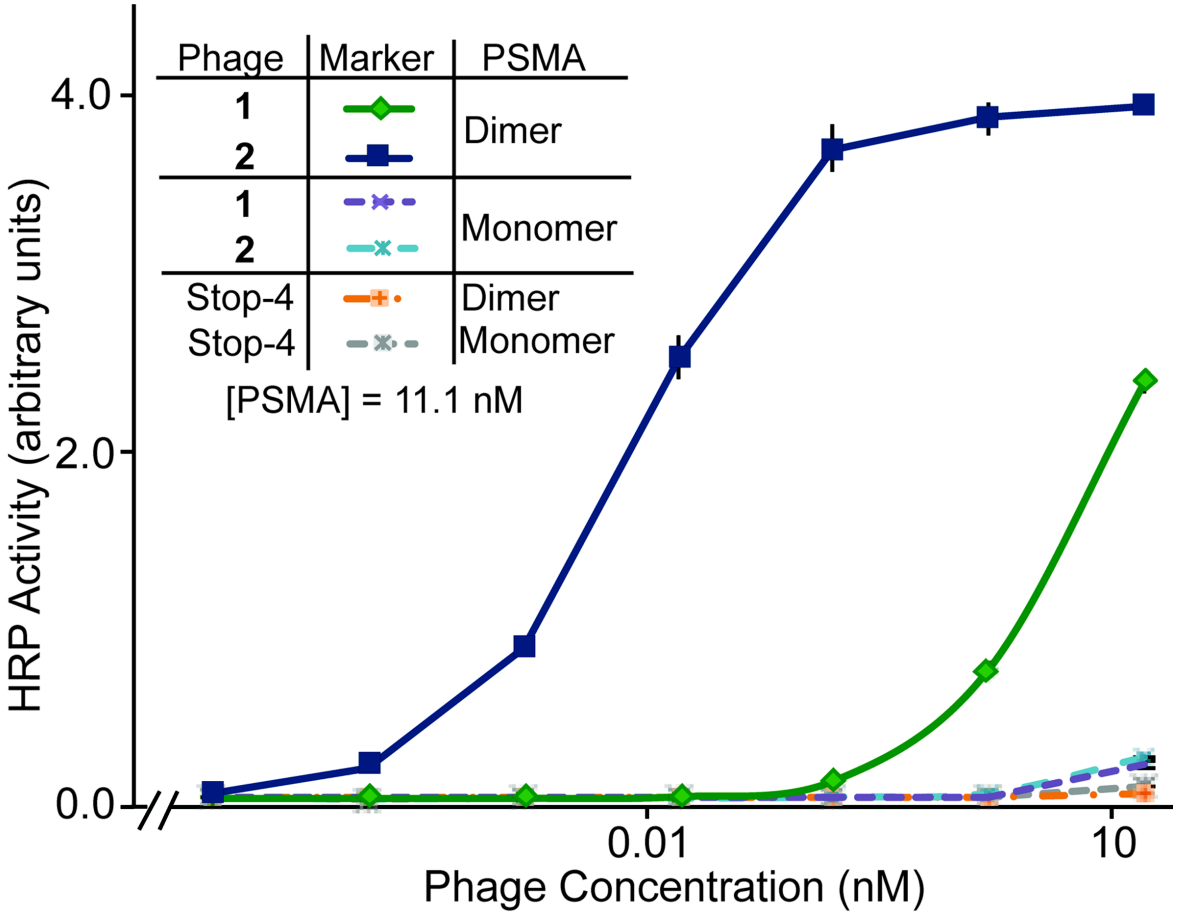

Figure 2-1. Phage-based ELISA comparing ligand binding to monomeric and dimeric forms of PSMA. This ELISA includes PSMA monomer; all other reported experiments with PSMA apply the cancer-relevant PSMA dimer. Stop-4 provides a negative control with helper phage packaging the phagemid DNA. Throughout this report, error bars for ELISA data represent standard error (n = 3). All experimental data points with the exception of the negative controls (n = 1) include such error bars, though often these are quite small.

The two PSMA ligands, **1** and **2**, provide a starting point for the development of biosensors. For translational relevance, the LOD of the resultant biosensor must be <0.25 nM, and a high-signal-to-noise ratio is essential for definitive diagnosis. In theory, the affinity of the ligands for their target analyte should correlate with their usefulness in biosensor applications. For example, a higher affinity ligand could enhance sensitivity for the analyte. In a previous report, we described using phage-displayed homolog shotgun scanning to improve phage-displayed ligand affinity for PSMA by >100 fold.[22] However, this approach requires extensive mutagenesis and selections.

Nature applies evolution-guided affinity maturation, but also relies on another approach for more rapid affinity maturation. The immune system, for example, applies the principle of avidity to boost the apparent affinity of a weaker initial lead. During the initial immune response, the IgM protein presents receptors in a decavalent format, allowing weak initial binders to attain higher apparent affinity through proximity- and chelate-based avidity.[26] The large, phage surface with repeatitive structural motifs appears well-suited to this approach, and, indeed avidity effects are often present during phage-based selections and screens.[27] This concept could provide a generalized method for expedient improvement of ligand affinity and biosensor sensitivity.

2.2 Cycloaddition to Generate the Secondary Recognition Ligand

To exploit this avidity effect, phage wrapping was used to boost ligand density, subsequent affinity, and the resultant sensitivity and the signal-to-noise of phage-based biosensors. Each 'wrapper' consists of two parts linked together by the Cu^{I}-catalyzed azide-alkyne cycloaddition ('click') reaction (Scheme 2-1).[28] The first component, an oligolysine (K_{14}) peptide provides affinity to the phage surface. For the click reaction, an alkyne (4-pentynoic acid) was coupled to the *N*-terminus of the K_{14} peptide. The second component of the wrapper is the peptide ligand to PSMA. In previous studies, the PSMA-binding peptides, **1** and **2,** exhibited limited solubility in water. The peptides were therefore synthesized as fusions to the solubilizing peptide sequence K_3 on their *N*-termini. For the click reaction, the *N*-termini of the peptide ligands were coupled to an azide (4-azidobutanoic acid).

The two parts of each wrapper were chemically synthesized using solid phase peptide synthesis and purified by reversed-phase HPLC before the cycloaddition reaction. Here, click chemistry offers a convergent synthesis, and the reaction takes place at room temperature and in aqueous solution.[28] The resultant secondary recognition ligands thus provide an oligolysine half to wrap the phage (termed K_{CS} for "lysine, chemically synthesized"), and a second component, the PSMA ligand (**1** or **2**), to bind to the analyte**,** Figure 2-2. The products formed by the click reaction (K_{CS}-**1** or K_{CS}-**2**) were characterized by MALDI-TOF MS (Figure 2-3), and purified by reverse-phase HPLC to an estimated 90% purity.

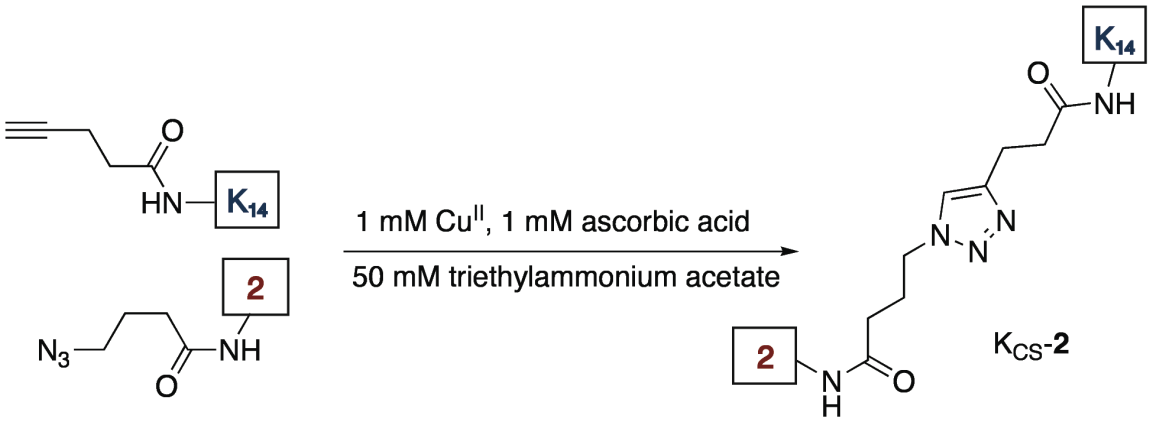

Scheme 2-1. The Cu^{I}-catalyzed azide-alkyne cycloaddition reaction to generate the secondary recognition ligand, K_{CS}-**2**. The boxed **2** and $\mathbf{K_{14}}$ indicate the ligand **2** and oligolysine peptides, respectively.

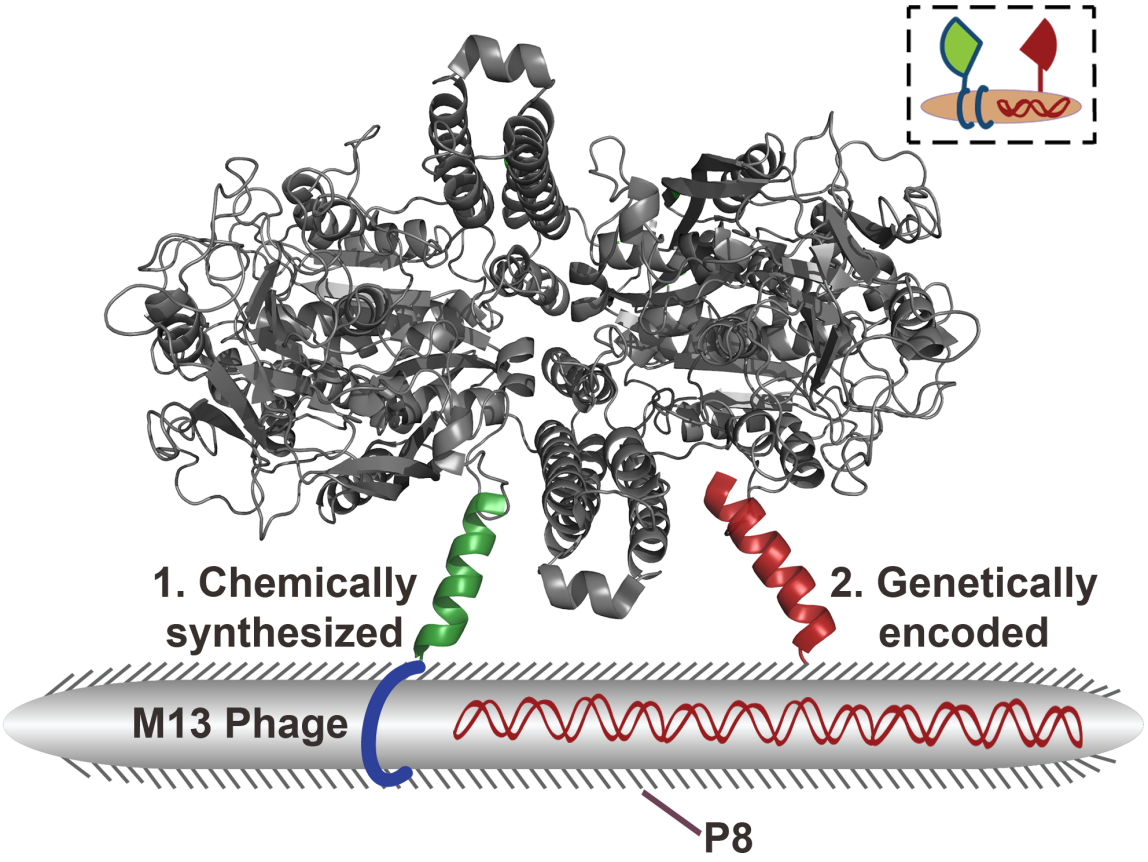

Figure 2-2. Schematic diagram of bidentate binding to PSMA by chemically synthesized (K_{CS}-**1**, green) and genetically encoded (peptide **2**, red) ligands to PSMA (PDB: 1Z8L). The former ligand wraps non-covalently onto the negatively charged P8 proteins found on the phage surface due to conjugation with a positively charged K_{14} peptide (blue). Simultaneous binding by the two ligands provides higher apparent affinity to PSMA. The inset depicts a simplified version of the schematic appearing in the subsequent figures shown here.

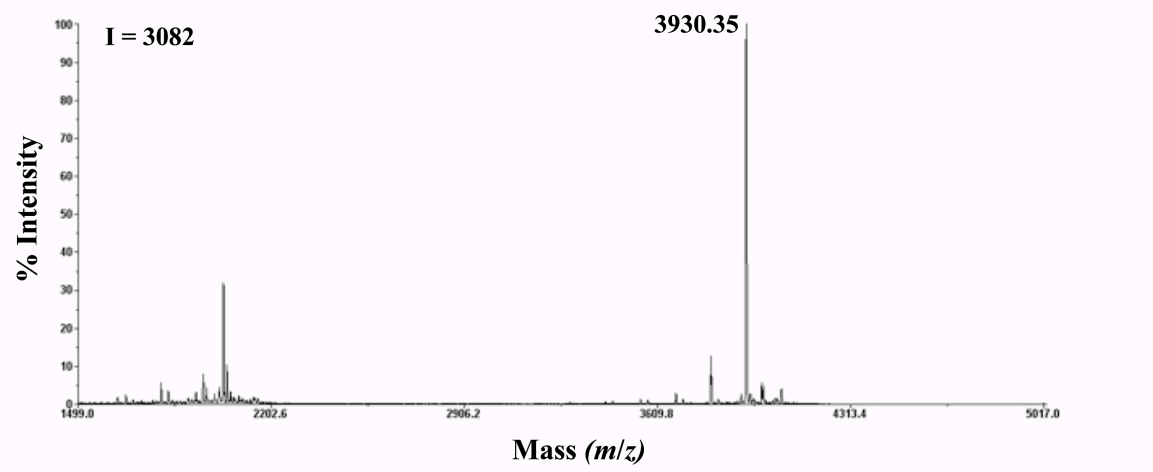

Figure 2-3. A representative MALDI-TOF spectra of the purified product from the azide-alkyne cycloaddtion reaction. The azide-functionalized peptide-**2** and alkyne-functionalized oligolysine yields K_{CS}-**2**. The calculated *m*/*z* for K_{CS}-**2** [M^+] 3930.31, found 3930.35.

2.3 Phage Wrapping to Maximize Ligand Density

Wrapping the phage with chemically synthesized PSMA ligands described above clearly enhances binding affinity to PSMA (Figure 2-4). The phage-displayed ligand (phage-**2**) was wrapped with the secondary recognition ligands (K_{CS}-**1**, K_{CS}-**2** or a mixture of the two) to generate a phage surface displaying two PSMA ligands. The wrapped phage were then assayed for binding to the PSMA dimer. Negative controls, which resulted in no detectable binding, included the PSMA ligands targeting BSA and Stop-4 targeting PSMA. Phage-**2** wrapped with K_{CS}-**2** exhibits ≈50 times higher affinity for PSMA than phage-**2** without the ligand wrapper, Figure 2-4. Additional optimization examined the concentration of the wrapper, Figure 2-5. As a result, the wrapper concentration can maximize the ligand density on the phage surface. The effectiveness of wrapping for improved apparent binding affinity is dramatically demonstrated by comparing the binding affinities of the helper phage (KO7) versus KO7 wrapped with K_{CS}-**2**, Figure 2-6. Lacking a displayed ligand, KO7 phage displays no significant binding to PSMA, but KO7 phage wrapped with K_{CS}-**2** binds with significant affinity to PSMA. Taken together, the results demonstrate that the wrapping strategy achieves much higher affinity for the target and the wrapped ligands remain functional. Additional negative control, Stop-4 phage wrapped with $\mathbf{K_{14}}$ targeting PSMA resuled in no detectable binding, as expected, Figure 2-7.

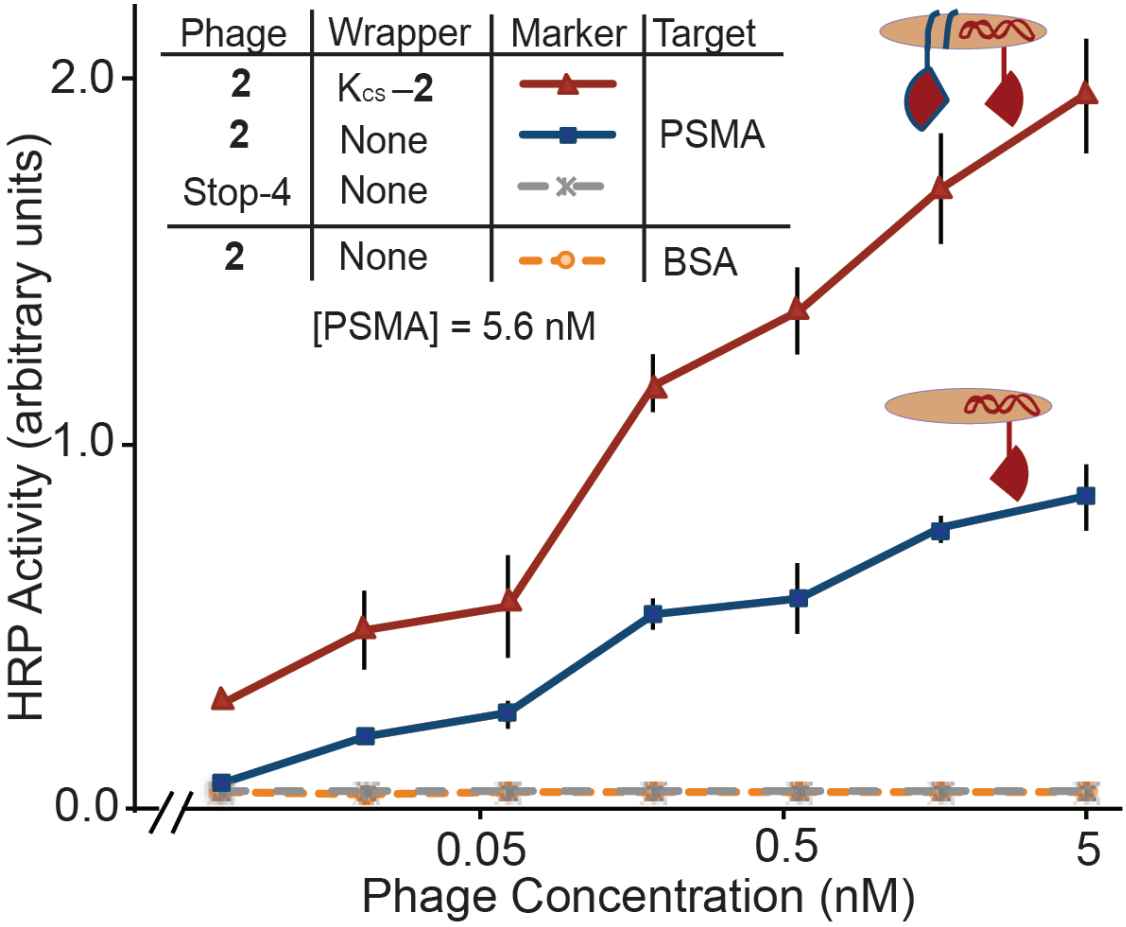

Figure 2-4. Phage-based ELISAs demonstrating the effectiveness of ligand wrapping. Phage with chemically and genetically encoded ligands bind with much higher apparent affinity to the targeted PSMA.

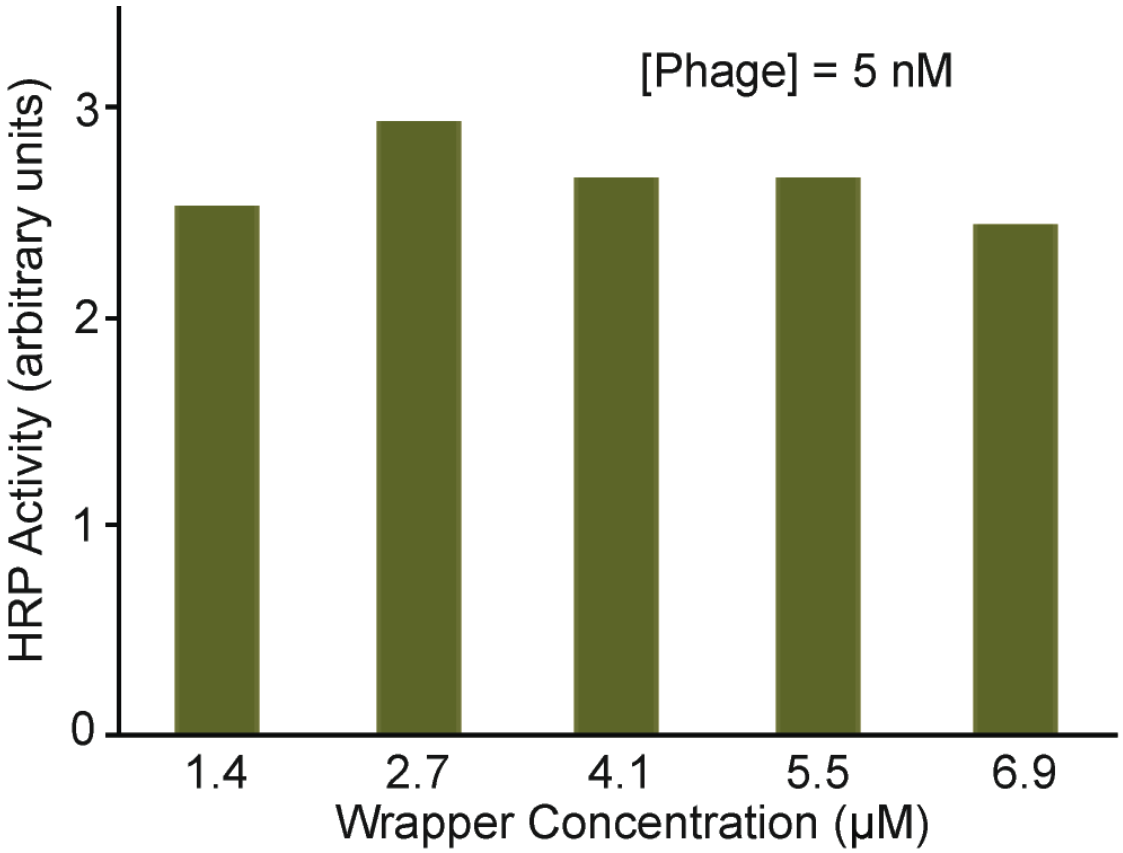

Figure 2-5. Phage-based ELISA illustrating optimization of K_{CS}-**1** levels. A concentration of 2.7 μM for K_{CS}-**1**, offers an approximate 15% increase in apparent affinity to PSMA, versus other concentrations.

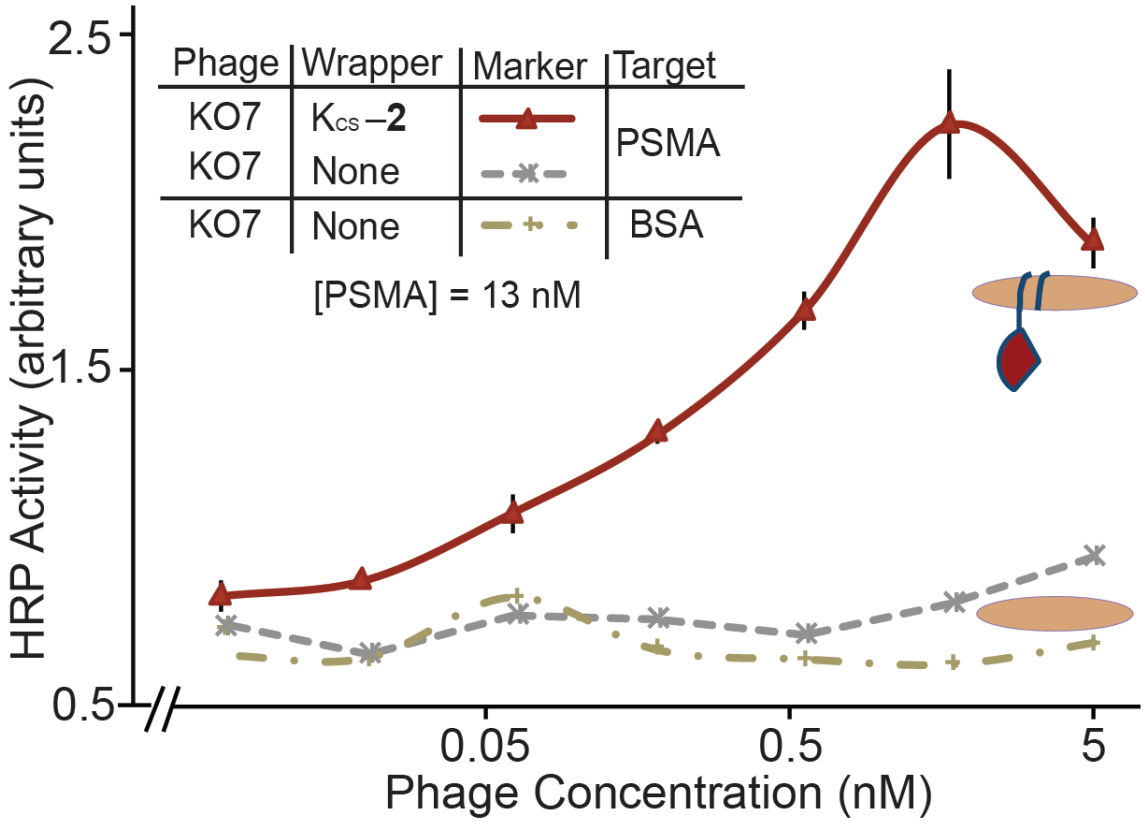

Figure 2-6. Phage-based ELISAs demonstrating the effectiveness of ligand wrapping. The chemically synthesized K_{CS}-**2** wrapper converts helper phage, KO7, lacking a genetically encoded PSMA ligand, into a high affinity binding partner to PSMA. The decrease in apparent binding affinity at the highest phage concentration could be attributed to steric effects.

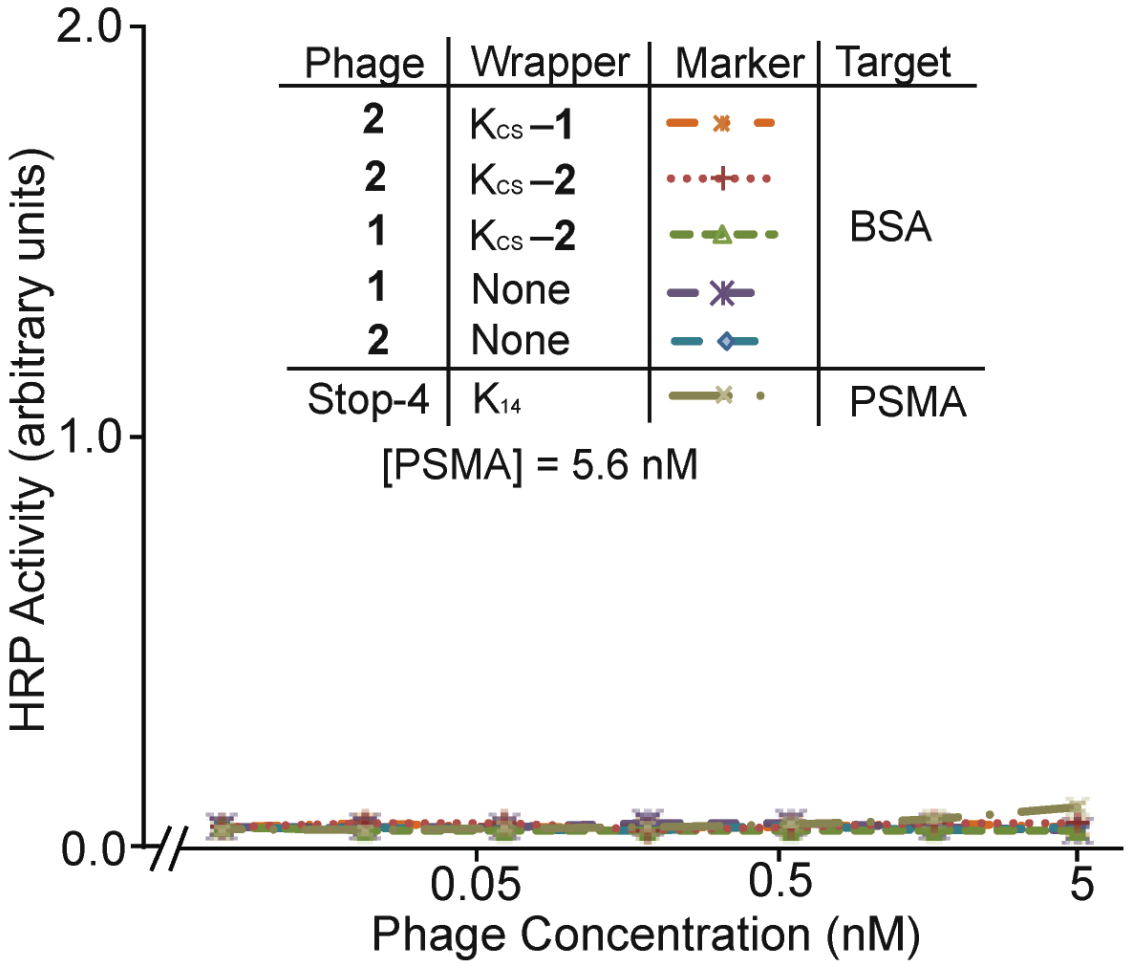

Figure 2-7. Phage-based ELISA illustrating additional negative controls, the PSMA binding ligands targeting BSA and Stop-4 phage wrapped with $\mathbf{K_{14}}$ targeting PSMA.

2.4 Primary and Secondary Recognition Ligands on Phage for Bidentate Binding

The arrangement and density of the primary, genetically encoded ligand and the secondary, chemically synthesized ligand determines the affinity of the wrapped phage for PSMA. For example, wrapping phage-**2** with K_{CS}-**1** results in phage with an apparent 4-fold higher affinity for PSMA than phage-**2** wrapped with K_{CS}-**2** (Figure 2-8). Peptide **1**, however, has a much lower apparent affinity for PSMA than peptide **2**, as shown in Figure 2-1. Thus, the increased binding affinity of phage-**2** wrapped with K_{CS}-**1**, suggests that the two ligands target different sites on the surface of PSMA. Furthermore, a 1:1 mixture of K_{CS}-**1** and K_{CS}-**2** wrapped on the surface of phage-**2**, offers intermediate affinity between neat K_{CS}-**1** and neat K_{CS}-**2**. The results demonstrate that phage-**2** wrapped with K_{CS}-**1** results in improved affinity due to a bidentate binding interaction. Conversely, phage-**2** wrapped with K_{CS}-**2** fails to access this bidentate binding mode. Thus, the two ligands displayed on phage, for phage-**2** wrapped with K_{CS}-**1**, can result in a chelate-based avidity effect, which enhances binding affinity beyond the gains achieved purely by maximization of ligand density.

In practice, chelate-based avidity effects can be challenging to design, as geometry and sterics must be satisfied to allow both ligands to reach an optimal interaction with the receptor. In fragment-based drug discovery efforts, for example, development of linkers with appropriate configuration is a non-trivial problem.[29]

Phage wrapping provides a more expedient solution to this problem. The second ligand, presented by a non-covalently bound wrapper, can equilibrate on the phage surface until finding a satisfactory geometry to allow simultaneous binding for synergistic effect.

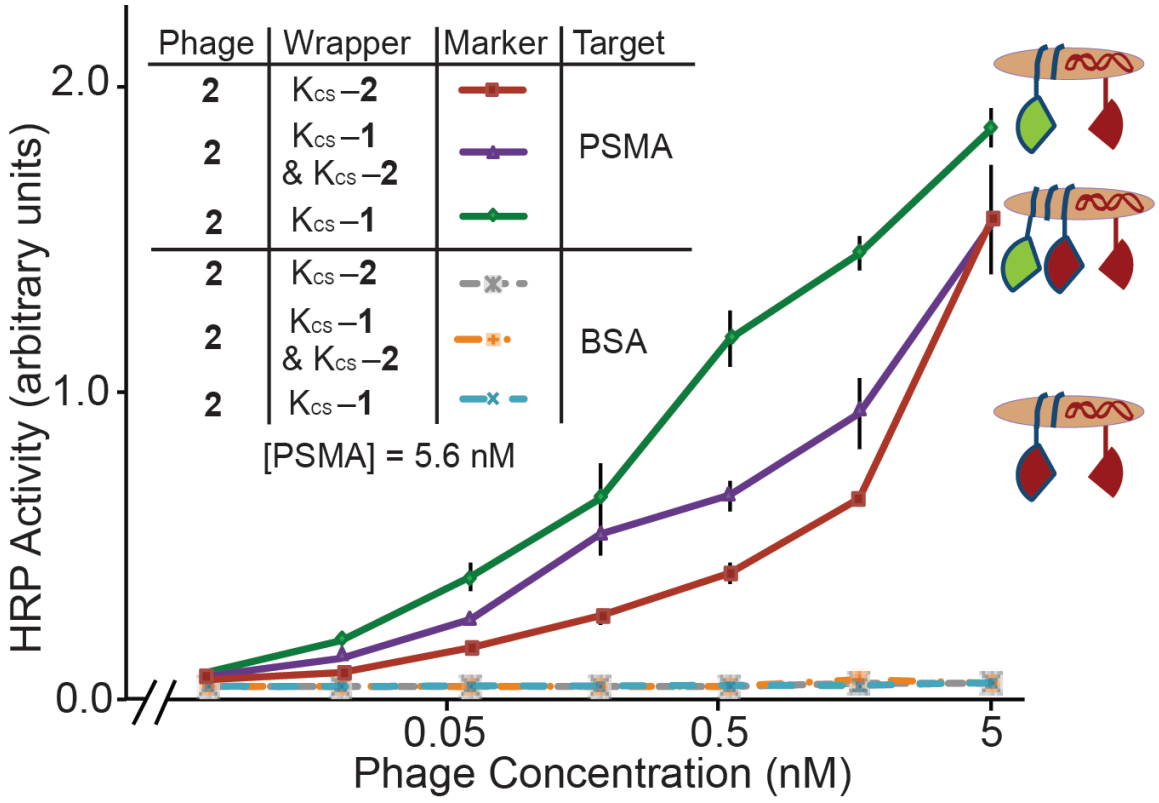

Figure 2-8. Phage-based ELISA comparing different ligand wrappers. The wrapper combination of K_{CS}-**2** & K_{CS}-**1** indicates a 1:1 (w/w) ratio of ligand wrappers.

2.5 Biosensing with Virus-PEDOT Films

Can these wrapped virus particles be exploited to create virus-electrode biosensors with a higher sensitivity for PSMA? To explore this question, films of PEDOT were prepared on gold electrodes by electropolymerization in the presence of phage-**2** (Scheme 2-2). The PEDOT formed in solution during electropolymerization, associate with the negatively charged perchlorate ions from the electrolyte solution as it is deposited onto the gold electrode.[30] Polymerization of EDOT in the presence of negatively charged phage particles leads to incorporation of virus particles into the polymeric film as counter-ion dopants due to electrostatic interactions.[21] The cyclic voltammogram acquired during electrodeposition of the virus-PEDOT bioaffinity matrix indicates that the maximum current increases with every deposition cycle, consistent with the expected increase in the surface area of the film during growth (Figure 2-9A). SEM imaging confirms incorporation of phage into the bioaffinity matrix; we observe both filament-like and less-extended features having dimensions consistent with phage integrated as rope-like bundles into the polymer at various angles to the film, Figure 2-10. The K_{CS}-**1** wrapper was then applied in vitro simply by exposing the resultant phage-**2** film for a short time to an aqueous solution of the wrapper. For the biosensing measurements, only the highest affinity ligand combination of phage-**2** wrapped with K_{CS}-**1** was used, and studied in comparison to phage-**2** films.

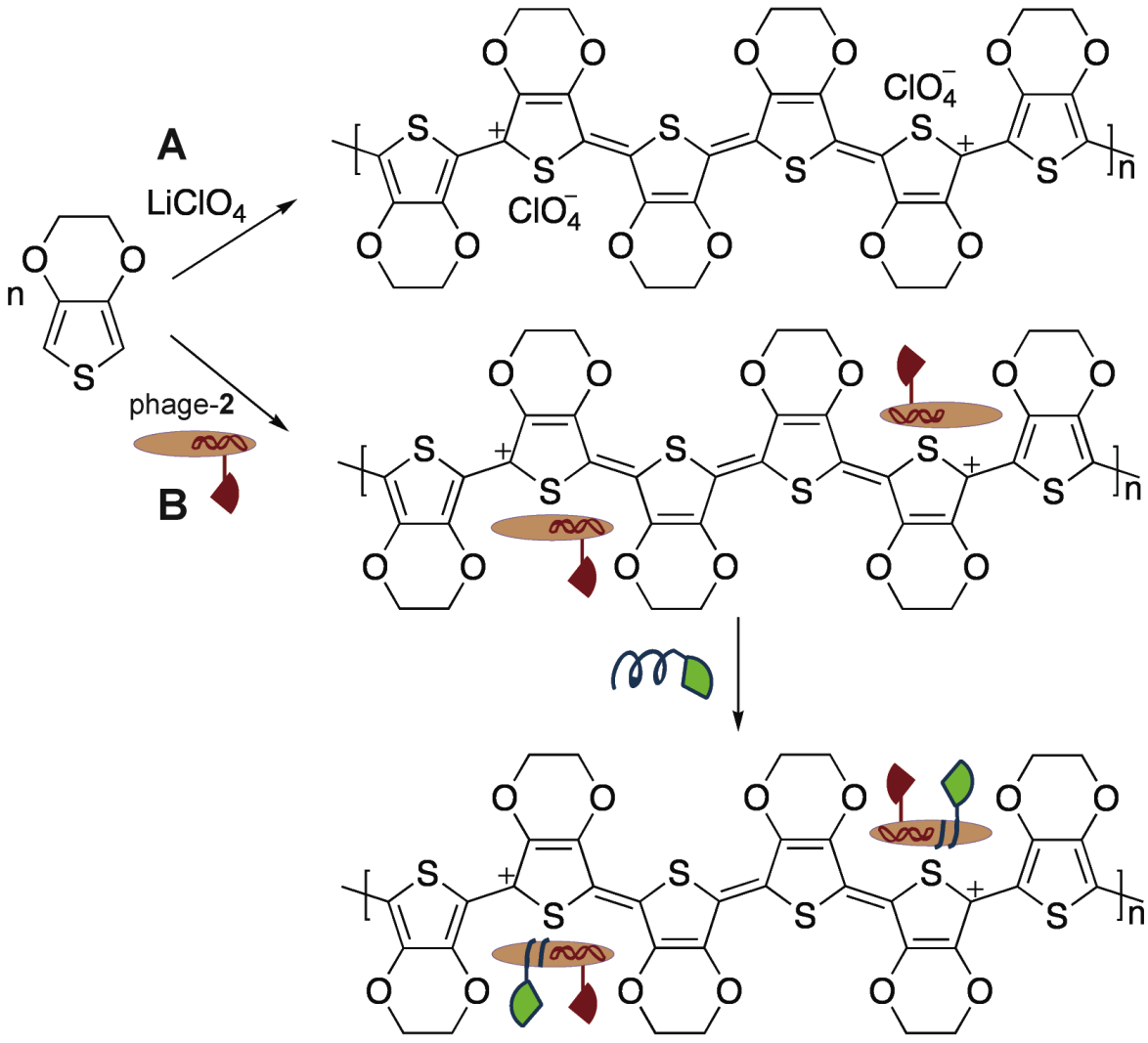

Scheme 2-2. Polymerization of EDOT in the presence of (A) $LiClO_4$ or (B) phage-**2**, followed by wrapping with K_{CS}-**1** (green and blue).

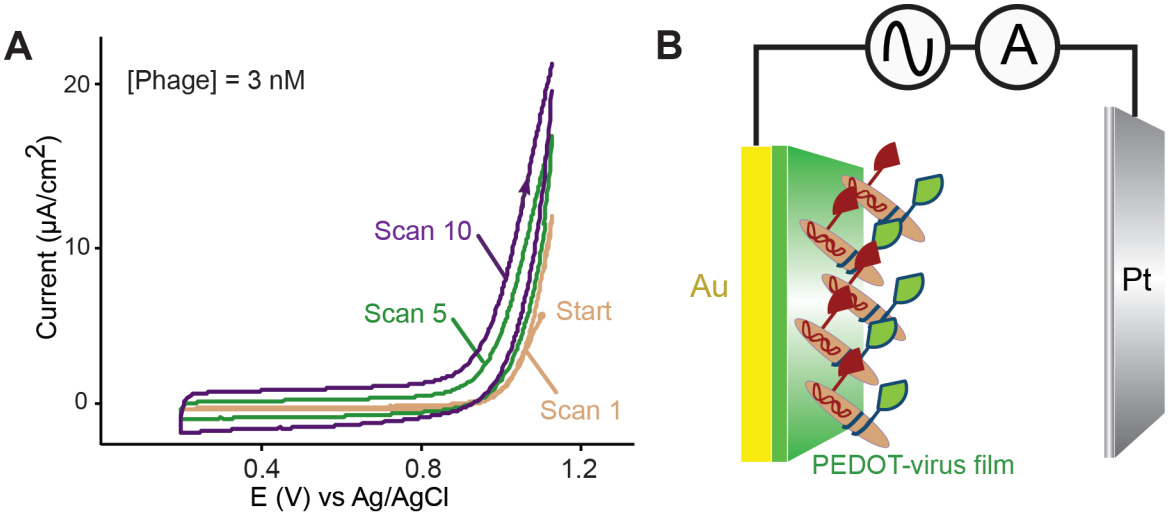

Figure 2-9. (A) Cyclic voltammogram for the electrodeposition of virus-PEDOT films on the surface of a planar gold electrode. (B) Binding of the analyte to the phage-displayed peptides in the bioaffinity layer produces a quantifiable resistance change.

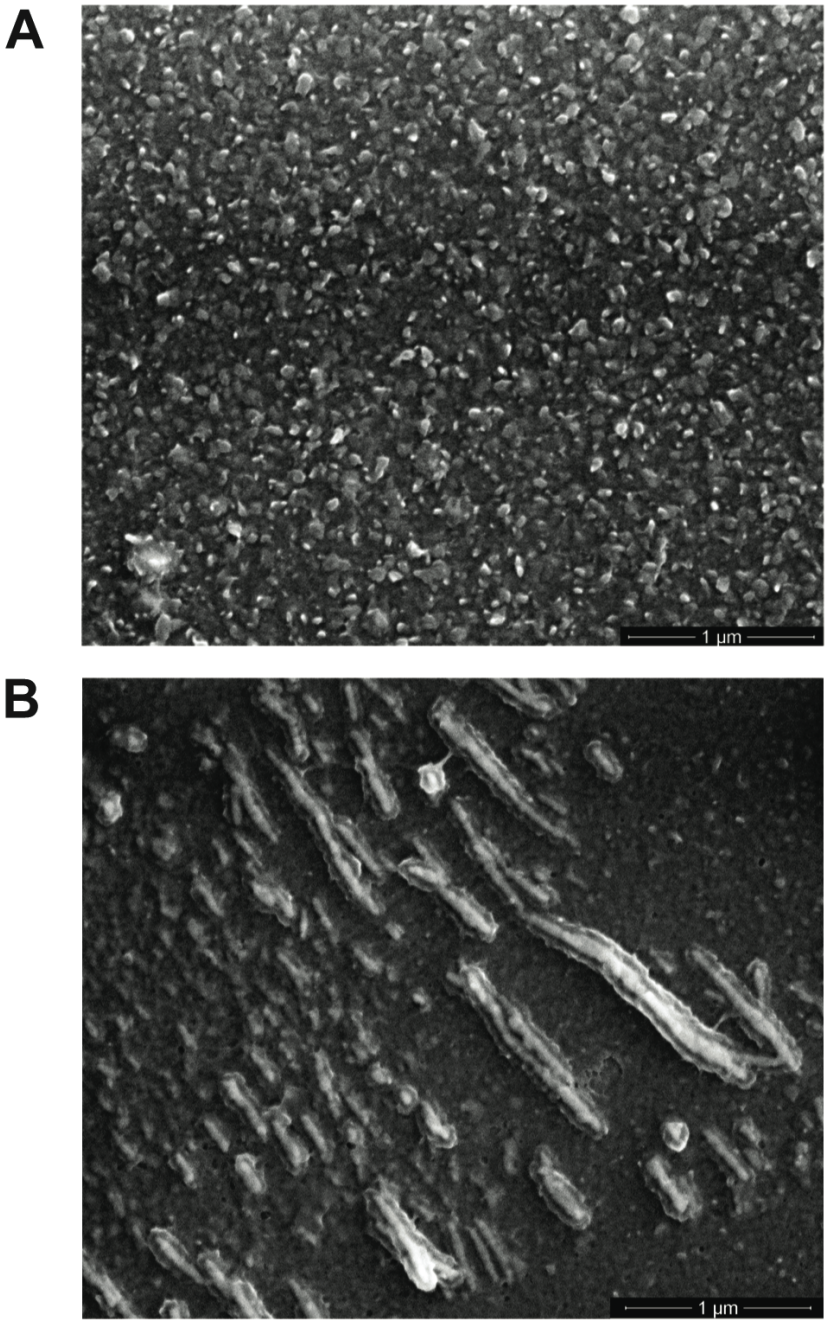

Figure 2-10. SEM image of a (A) PEDOT film and a (B) virus-PEDOT film prepared under the same conditions.

2.6 EIS to Quantify PSMA Binding

As we have observed in our prior work,[21] the electrochemical impedance of the virus-PEDOT film increases as PSMA selectively binds to the phage-displayed peptide ligands (Figure 2-11). The real component of the impedance, R, in particular, increases upon PSMA binding. In previous work, we demonstrated that the increase in R, ΔR, normalized by the initial resistance, R_o, ($\Delta R/R_o$) can be correlated with the concentration of a target molecule.[21] Here, impedance data were acquired in PBF (phosphate buffered fluoride)-Tween buffer, spanning a frequency range from 0.1 Hz to 1 MHz in an electrochemical cell with a Pt counter electrode, and virus-PEDOT film electroplated on a planar gold working electrode (Figure 2-9B). The films incorporating phage-**2** wrapped with K_{CS}-**1** provide higher sensitivity for PSMA detection than films incorporating phage-**2** (Figure 2-12). For example, the relative impedance change, $\Delta R/R_o$, at each concentration of PSMA is three-fold higher. The noise present in this measurement (estimated as the standard deviation for five impedance measurements) is unchanged resulting in a much higher signal-to-noise ratio for phage-**2** wrapped with K_{CS}-**1** relative to unwrapped phage-**2**. A series of negative controls validate the data obtained. The PEDOT films incorporating Stop-4 phage, PEDOT films lacking PSMA binding ligands, and PEDOT films incubated with K_{CS}-**1** result in no significant binding to PSMA, as expected. The specificity of PSMA binding was investigated by using an alternative target, transferrin receptor (TfR), which has 54% sequence similarity to PSMA. No significant binding affinity to TfR was observed, as expected. This experiment

illustrates the negligible change in impedance caused by the wrapper due to the small size of the wrapper.

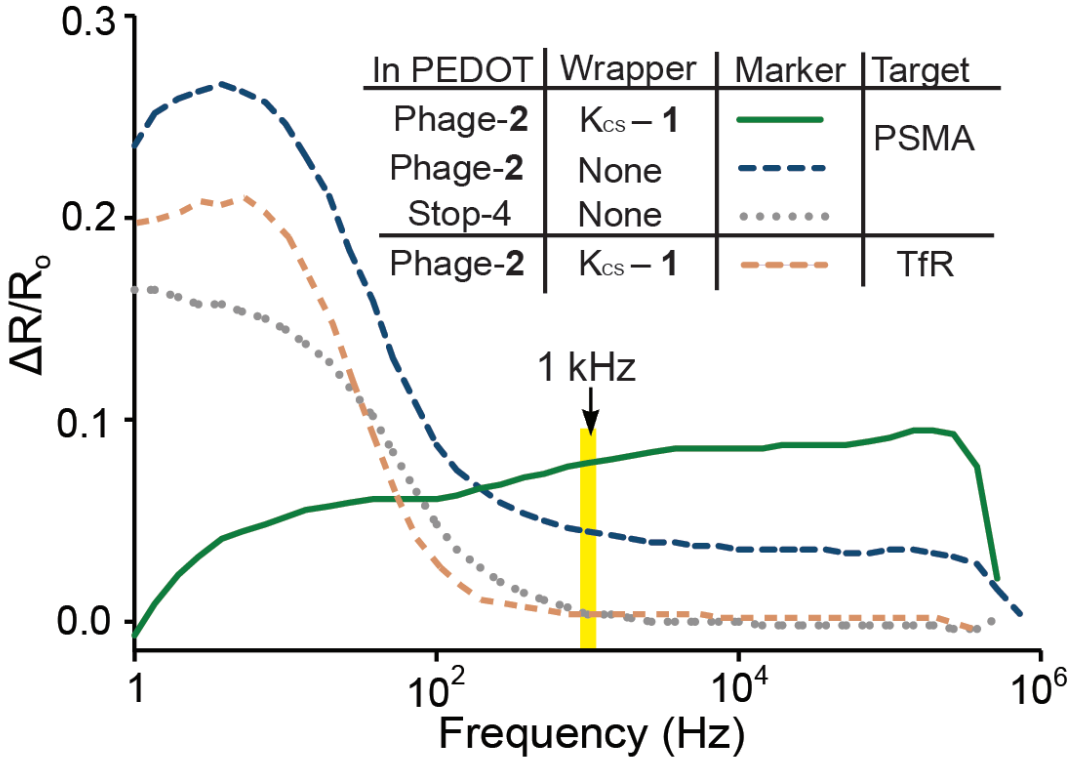

Figure 2-11. Biosensing with virus-PEDOT films. Relative change in resistance obtained, $\Delta R/R_o$, plotted as a function of frequency for phage-displayed ligands targeting PSMA. Data collected at 1 kHz (highlighted), were used for the analysis of PSMA binding.

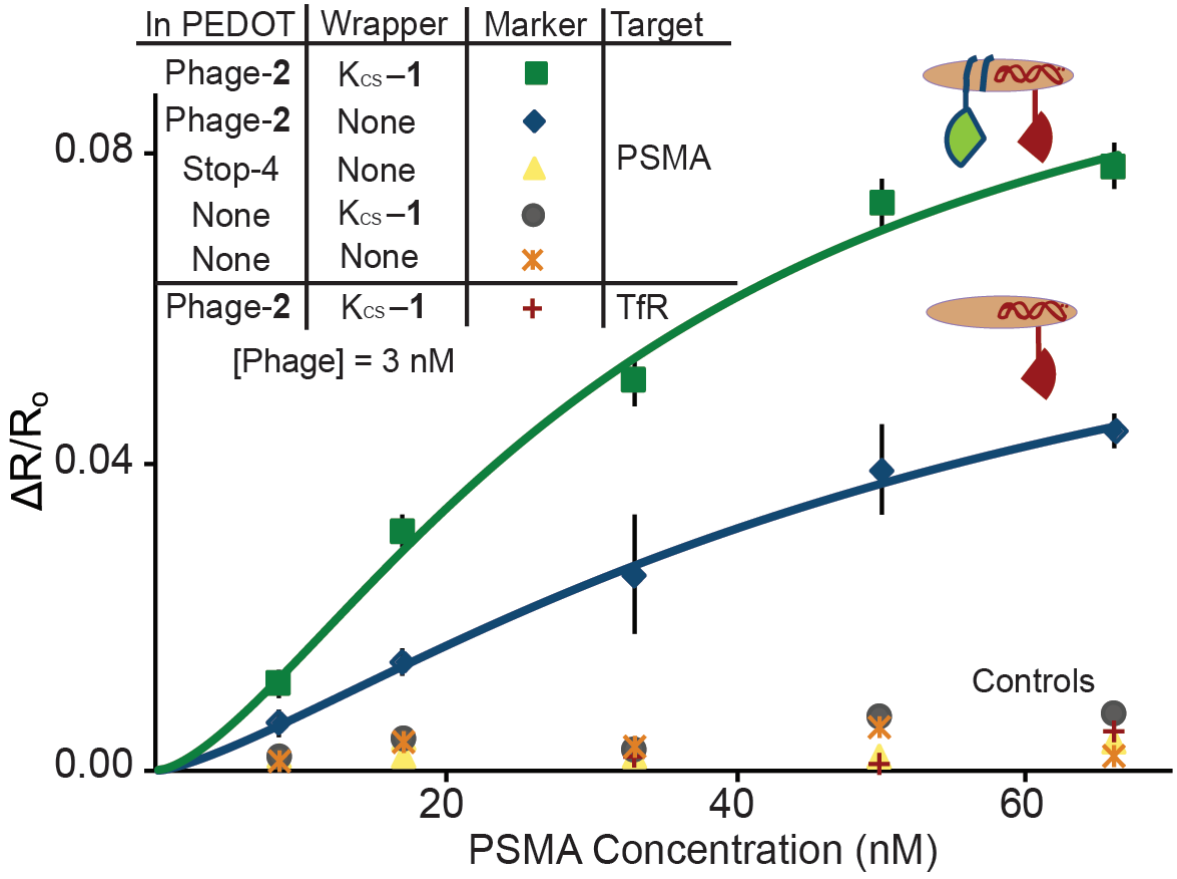

Figure 2-12. Biosensing with virus-PEDOT films. $\Delta R/R_o$ of the film increases with the PSMA concentration. Throughout this report, error bars for the biosensing data represent standard error (n = 5). Data was fit to the indicated lines using the Hill equation, resulting in an R^2 value of >0.99.

2.7 Calculating the Hill Coefficient

The biosensing data acquired for phage-**2**, and phage-**2** wrapped with K_{CS}-**1** targeting PSMA, follows a Langmurian adsorption model. The data acquired was fit to the following Hill equation:

$$Y = \frac{Y_{max} * [L]^n}{[K_d]^n + [L]^n}$$

where Y is $\Delta R/R_o$, L is the ligand concentration, and n is the Hill coefficient.[31] Consequently, the dissociation constant, K_d and n were determined for phage-**2** (K_d = 54 nM, n = 1.3, LOD = 6 nM), and phage-**2** wrapped with K_{CS}-**1** (K_d = 33 nM, n = 1.5, LOD = 3.1 nM). Here, the two LODs, defined as 3x over background signal, were calculated from line fits to the data shown in Figure 2-12. The response obtained for phage-**2** wrapped with K_{CS}-**1** displays a much higher signal-to-noise ratio, compared to films incorporating only phage-**2**. Such sensitivity can play a crucial role in low concentration analyte detection. The n-values obtained are >1, indicating the presence of multiple binding sites and a cooperative binding effect. Phage-**2** can access cooperative binding due to the avidity effect of multi-copy phage-displayed ligands. Wrapping phage with additional ligands leads to a further increase in cooperativity for phage-**2** wrapped with K_{CS}-**1**. Again, the synergism of the two ligands leads to higher PSMA binding affinity for phage-**2** wrapped with K_{CS}-**1**.

2.8 PSMA Detection in Synthetic Urine

To further demonstrate the usefulness of the approach for potential clinical applications, biosensing data was next acquired in synthetic urine. This complex solution includes water, nitric acid, urea, sodium sulfate, potassium chloride, sodium dihydrogen phosphate, sodium chloride, ammonium chloride and 10 other components; the resultant solution has a high salt concentration (a calculated osmolality of 516.2 mOsm/kg and a pH of 5.8).[32,33] The solution provides a good model for the clinical challenge of identifying cancer biomarkers found in urine samples. Substituting synthetic urine for PBF, impedance measurements with virus-PEDOT films were acquired as before (Figure 2-13). Having already established phage-**2** wrapped with K_{CS}-**1** as the most effective ligand combination for detecting PSMA in terms of sensitivity, specificity and signal-to-noise ratio, our experiments focused on this ligand combination for synthetic urine-based biosensing. In the presence of PSMA, the impedance scans for virus-PEDOT films of phage-**2** wrapped with K_{CS}-**1** follow similar trends in both PBF and synthetic urine. However, the lower frequency ranges differ dramatically for the negative controls. For example, the negative control with Stop-4 phage in PBF displayed a much higher $\Delta R/R_o$; this response at low frequencies was suppressed in synthetic urine. Thus, the measurements in synthetic urine resulted in higher specificity for the PSMA-ligand interaction.

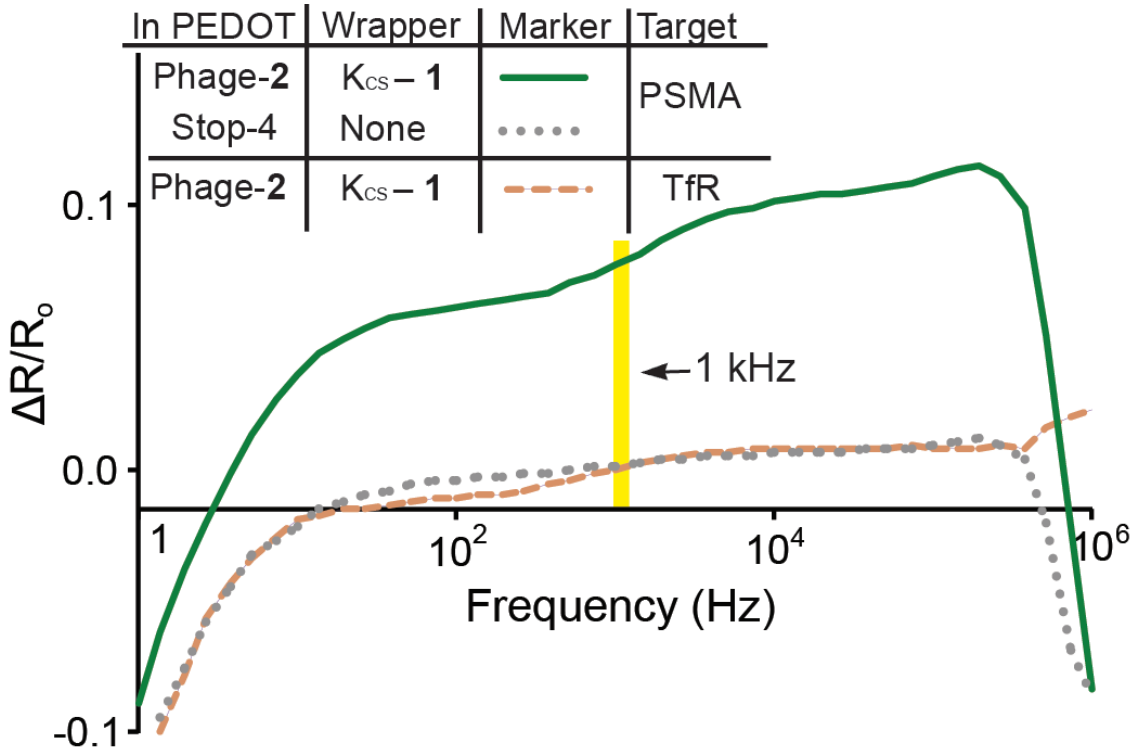

Figure 2-13. Detection of PSMA in synthetic urine using virus-PEDOT film biosensors. $\Delta R/R_o$ versus frequency for the detection, in synthetic urine, of PSMA.

Turning next to the measurement of PSMA concentration, the synthetic urine solution also appeared to enhance measurement sensitivity. The calibration curves in PBF and synthetic urine were overlaid for comparison (Figure 2-14, green and purple, respectively). At high analyte concentrations, measurements in PBF and synthetic urine are superimposable. Both conditions reach saturation at high PSMA concentrations, hence the overlap in device response. At the lowest PSMA concentrations, the higher $\Delta R/R_o$ response in synthetic urine can be attributed to higher sensitivity and selectivity for PSMA under the high-salt conditions. Phage-**2** films wrapped with K_{CS}-**1** targeting PSMA in synthetic urine, yields a 100 pM experimentally observed LOD. Applying the calculation to determine LOD described above yields a 10 pM LOD for the detection of PSMA in synthetic urine. Furthermore, this sensitivity requires no signal or enzymatic amplification. As before no significant change in impedance was observed for the negative controls.

The high salt concentration in synthetic urine appears to prevent non-specific charge-charge interactions. Binding of the biomarker to the virus-PEDOT film generates a positive $\Delta R/R_o$, whereas a negligible $\Delta R/R_o$ for the negative controls indicates a non-significant extent of non-specific binding by the analyte. The resultant specificity increase in synthetic urine boosts the apparent sensitivity of the device by decreasing background binding. This effect also enhances the sensitivity by unmasking a higher concentration of ligands for analyte detection, which would otherwise be occluded through non-specific binding. Thus, a dramatic improvement in specificity and sensitivity can be obtained through the decreased non-specific

interactions. The results suggest a general strategy for improving biosensor performance through focusing on decreased non-specific binding.

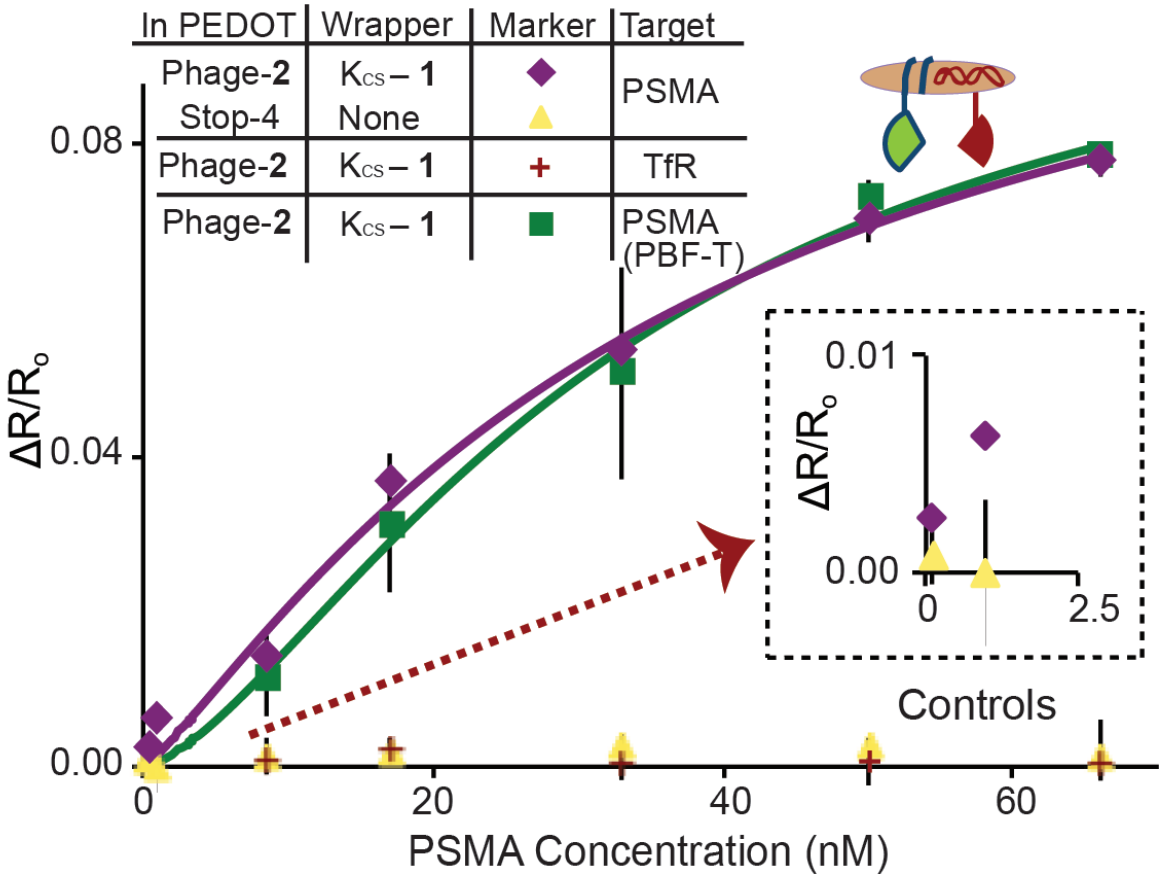

Figure 2-14. Detection of PSMA in synthetic urine using virus-PEDOT film biosensors. $\Delta R/R_o$ versus PSMA concentration. The inset expands the low PSMA concentration region. Data was fit to the indicated lines using the Hill equation, resulting in an R^2 value of >0.99.

2.9 PSMA Detection in Human Urine Samples *(unpublished work)*

The work described in this chapter, so far, was further extended towards the detection of PSMA in human urine samples obtained from patients. The samples assayed could be broadly classified as prostate-specific antigen (PSA) positive or negative, based on the results of the PSA test, which is the current clinical test used for prostate cancer diagnosis. The PSA test results were provided with the samples, Table 2-2. In general, a PSA value of <4 ng/mL is considered normal, implying non-cancerous.[34] The relative capture and detection of PSMA from urine samples was first examined by ELISA, Figure 2-15. For this assay, the wells of the microtiter plate were first immobilized with a capture antibody, anti-PSMA (YPSMA-1) antibody. Next, 100 µL of urine samples were added to the appropriate wells. The relative levels of captured PSMA were then quantified using a detection antibody, anti-PSMA (EP3254) antibody. All the samples assayed showed the expected readouts; the samples from PSA-positive patients displayed high levels of PSMA, and vice-versa. The two PSA-positive samples exhibited high HRP activity, indicating significant amounts of PSMA was captured from 100 µL of the urine samples. Additionally, a 5.6 nM PSMA solution was simultaneously assayed to provide a reference for the readouts. And, both the PSA-positive samples indicated the presence of at least two-fold levels of PSMA compared to the PSMA reference. Furthermore, the four PSA-negative urine samples were also assayed to test the specificity of PSMA detection. As expected, the PSA-negative samples showed readouts below the 5.6 nM PSMA control assayed.

The ability to detect PSMA through ELISAs in human urine samples from cancer patients is a significant step towards the development of a PSMA-detecting urine sample-based diagnostic test. It should be further noted that these results were obtained from only 100 μL of the urine samples. Also, the urine samples assayed had not been concentrated to increase the apparent PSMA concentration. Furthermore, the samples tested in this assay are from 2006-08, and PSMA could have undergone a certain level of degradation. Consequently, it might be possible to achieve a much higher signal to noise ratio with freshly collected urine samples and virus-PEDOT impedance measurements utilizing wrapped viruses. The ability to detect PSMA specifically in patient urine samples demonstrates the potential in PSMA testing for clinical applications. In the future, a wide variety of urine samples will be analyzed to test for sensitivity and specificity of PSMA detection.

Sample number	Study Identification number	Date	PSA Value (ng/mL)
1	A00000304	1/30/08	45.3
2	A00000047	12/7/06	23.7
3	A00000043	1/30/07	0.8
4	A00000076	8/18/06	0.65
5	A00000215	8/20/07	0.47
6	A00000202	3/30/07	0.4

Table 2-2. Details of the urine samples. The study identification numbers, collection dates, and the corresponding PSA values for the urine samples assayed. The samples were provided by Dr. Dan Mercola, Cancer Research Institute, UCI.

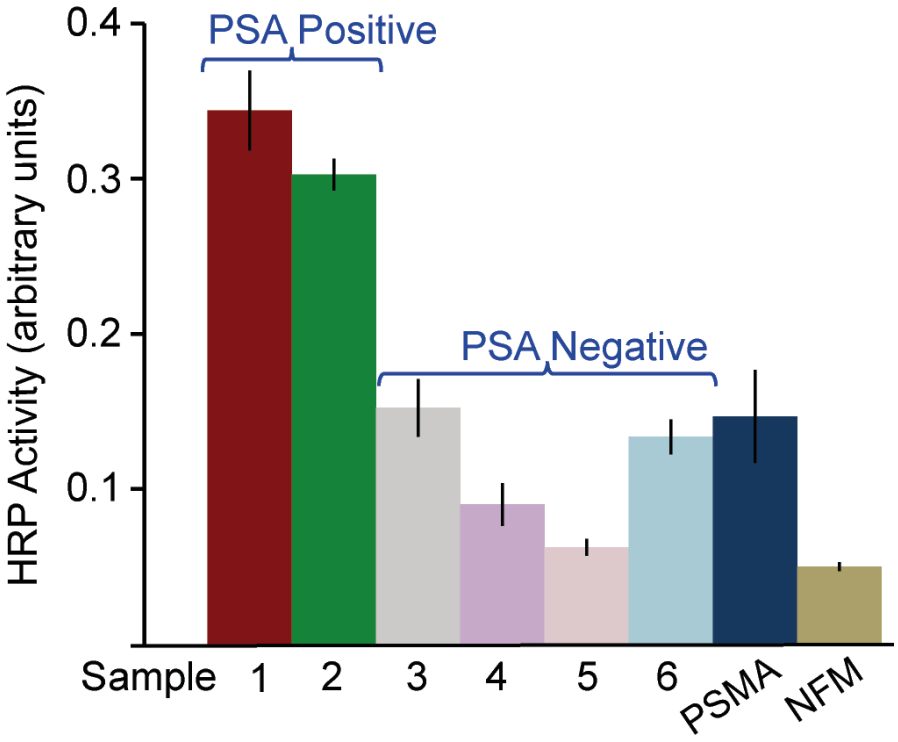

Figure 2-15. Detection of PSMA in human urine samples using PSMA-specific capture and detection antibodies through a sandwich-ELISA. The sample details are included in Table 2-2. A 5.6 nM PSMA solution provides a positive reference. The PSA-negative samples and a 0.2% non-fat milk solution in PBS serve as the negative controls.

CONCLUSIONS

The 100 pM experimentally measured LOD obtained for phage-**2** wrapped with K_{CS}-**1** is a significant improvement over our previous effort, which had a >66 nM LOD[22] for PSMA. This detection sensitivity satisfies a key requirement for clinical applications. The chelate-based avidity effect and high specificity obtained due to the bidentate binding mode distinguishes this work from our previous efforts, and also accounts for the greatly improved signal-to-noise ratio and LOD obtained without enzymatic amplification. Furthermore, inclusion of synthetic urine as an analyte solution expands the applicability of the technique. However, the reported biosensing films have not been optimized. Further improvements could be made to achieve an increased response, without amplification, for lower PSMA concentrations, as demonstrated by earlier experiments with similar biosensing films.[35]

In conclusion, wrapping phage with additional ligands can increase the target affinity due to a chelate-based synergistic effect. Phage-**2** wrapped with K_{CS}-**1** binds to PSMA with a 33 nM K_d and a 3.1 nM LOD in PBF, and a 100 pM experimentally measured LOD in synthetic urine. Furthermore, the ability to detect PSMA from 100 µL of prostate cancer patient urine sample illustrates the potential in PSMA being used as a clinical marker for early diagnostics, and biosensing-based measurements. In the future, the biosensors will be optimized for improved PSMA detection, and will be used for assaying human urine samples.

MATERIALS AND METHODS

All chemicals and reagents were purchased from Sigma-Aldrich, and used as received unless otherwise noted. KO7 helper phage, horseradish peroxidase conjugated to α-M13 monoclonal antibody were purchased from GE Healthcare Life Sciences. PSMA was a generous gift from Drs. William Ernst and Gary Fuji (Molecular Express). 4-Azido butanoic acid was a generous gift from Dr. Ting-Bin Yu and Professor Zhibin Guan (UC, Irvine). 4-Pentynoic acid (GFS Chemicals, Inc.), O-benzotriazole-N,N,N',N'-tetramethyluronium hexafluorophosphate, HBTU (GL Biochem Ltd.), Tris-(benzyltriazolylmethyl)amine (Anaspec Inc.), triethyammonium acetate buffer (Fluka Biochemika) and sorbitan monolaurate, Tween-20 (EMD Science) were used as received. Milli-Q UV water was used for the preparation of solutions.

M13 bacteriophage propagation

The M13 phage display vectors (phagemids) containing the genes encoding P8 fused to either peptide **1** or **2** were used to transform $CaCl_2$ competent *E. coli* XL-1 Blue cells, before plating onto LB agar plates supplemented with 50 μg/mL carbenicilin. The cells were grown at 37 °C in 2 mL 2YT media supplemented with carbenicilin (50 μg/mL) until the culture reached log-phase growth. The culture was then infected with KO7 helper phage (10^{10} phage/mL) and shaken at 250 rpm for 1 h at 37 °C. The starting culture was then transferred to 75 mL 2YT/carbenicilin media supplemented with kanamycin (10 μg/mL). The culture was shaken at 250

rpm for 16-18 h at 37 °C. To isolate the phage from the cells, the culture was centrifuged for 10 min at 10 krpm at 4 °C. The supernatant was decanted into separate tubes, and the phage was precipitated by addition of 1/5th volume of PEG-NaCl (2.5 M NaCl, 20% PEG-8000). The solution was incubated on ice for 1 h. Next, the phage were recovered by centrifugation for 20 min at 10 krpm. The supernatant was discarded, and the phage pellet was resuspended in phosphate-buffered saline (PBS, 135 mM NaCl, 2.50 mM KCl, 8.00 mM Na_2HPO_4, 30.0 mM KH_2PO_4, pH 7.2) with added 0.05% Tween-20. After additional centrifugation for 10 min at 15 krpm, the phage precipitation step was repeated as described above. Phage concentration was determined by UV absorbance at 268 nm (OD_{268} = 8.31 nM).

For incorporation of phage in the virus-PEDOT films, the phage pellet obtained after the above protocol was re-suspended in aqueous $LiClO_4$ (12 mM) solution.

Solid Phase Peptide Synthesis

The peptides were synthesized at 0.40 mmol scale following the standard procedures for solid-phase peptide synthesis with Fmoc-protected amino acids on Rink-amide resin (Novabiochem). The last coupling step was performed with 4-azidobutanoic acid or 4-pentynoic acid to yield the azide- or alkyne-functionalized peptides respectively. The synthesized peptides with a carboxamide C-terminus were cleaved from the resin by treatment with 9.5 mL trifluoroacetic acid, 250 µL

triisopropylsilane and 250 μL of water in a N_2 atmosphere for 3 h. The cleavage mixture was filtered from the resin, and the peptides were precipitated by addition of ice-cold diethyl ether. The peptides were recovered by centrifugation at 3 krpm for 20 min at 4 °C, and resuspended in water before lyophilization. The peptides were characterized by MALDI-TOF mass spectrometry, followed by reverse phase HPLC purification with a C_{18} column. Fractions containing the purified peptides were combined and concentrated using rotary evaporation, followed by lyophilization. The purified peptides were further characterized by MALDI-TOF mass spectrometry. The calculated *m*/*z* for peptide-**1** $[M^+]$ 1349.67, found 1350.1. The calculated *m*/*z* for peptide-**2** $[M^+]$ 2040.28, found 2040.23. The calculated *m*/*z* for alkyne-functionalized K_{14} peptide $[M+Na]^+$ 1914.37, found 1914.18 .

Click chemistry reaction for the synthesis of K_{CS}-2

As a representative protocol for the click chemistry reaction, the synthesis of K_{CS}-**2** was adapted from Lumiprobe Corporation's protocol for application to peptides with the following exceptions.[36] First, the reaction was performed at 200 μM azide-derivatized peptide concentration in 75% acetonitrile and 25% water. Second, water was used as the solvent, in place of DMSO. Third, a final concentration of 1 mM $CuSO_4$ was used, and the acetone precipitation step was skipped. Product formation was confirmed by MALDI-TOF mass spectrometry before purification. For purification, the reaction mixture was first concentrated using 2 kD MW cut-off micro concentrators, and then further concentrated under high

vacuum to approximately 100 µL. The concentrated reaction mixture was purified using reverse-phase analytical HPLC. Purified product was then subjected to reverse-phase analytical HPLC and MALDI-TOF, to verify purity and confirm identity, respectively. The calculated *m*/*z* for K_{CS}-**1** [M^+] 3240.05, found 3240.08. The calculated *m*/*z* for K_{CS}-**2** [M^+] 3930.31, found 3930.35.

PSMA Targeting Enzyme-Linked Immunosorbent Assay (ELISA)

In a phage-based ELISA, specific wells of a 96-well microtiter plate (Nunc Maxisorp) were coated with 100 µL/well of a solution of PSMA (5.56 or 11.1 nM) monomer or dimer protein diluted in PBS. The plate was incubated for 1 h on a shaker at room temperature. The coating solution was removed, and the wells were blocked with 320 µL/well of 0.2% w/v solution of BSA in PBS for 30 min, and washed three times with 300 µL/well of wash buffer PT (0.05% Tween-20 in PBS). Separately, phage-displayed PSMA-binding peptides were serially diluted along with a negative control (KO7) in phage dilution buffer, PBT (0.1% w/v BSA, 0.1% Tween-20 in PBS). The wells on the ELISA plate were then incubated with the phage samples (100 µL/well) for 1 h. The wells were washed five times with PT and then incubated with horseradish-peroxidase-conjugated anti-M13 antibody (100 µL/well, 1:5000 dilution in PBT) for 30 min. The wells were washed three times with PT, and two times with PBS. The plate was then developed by incubating with HRP substrate solution (100 µL/well; 1 mg/mL *o*-phenylenediamine dihydrochloride and 0.02% w/v H_2O_2) in citric acid buffer (50 mM citric acid, 50 mM Na_2HPO_4, pH 5.0).

Following an appropriate incubation time, HRP activity was measured spectrophotometrically at 450 nm using a microtiter plate reader (Bio-Tek).

Phage-based wrapping ELISA: Phage (5 nM in 225 µL) and 2 µL of the purified cycloaddition reaction product, K_{CS}-**1/2** (308.7 µM) in water: acetonitrile (60:40), were mixed and serially diluted in PBT. The solution were shaken at room temperature for 15 min on an orbital shaker. After blocking the ELISA plate, the wells were washed three times with PT and once with 300 µL/well of PBS-NaCl (PBS supplemented with 0.2 M NaCl). The wrapped-phage solutions (100 µL/well) were then transferred to the appropriate wells of an ELISA plate, prepared as described above. The wells were washed four times with PT and two times with PBS, followed by incubation with horseradish-peroxidase-conjugated anti-M13 antibody (1:15000 dilution). The wells were then washed six times with wash buffer PT, and two times with PBS. Levels of phage binding were quantified as described above.

ELISA for PSMA Detection in Urine Samples

For PSMA capture, specific wells of an ELISA plate were coated with 100 µL/well of a solution of anti-PSMA (YPSMA-1, Abcam) capture antibody (1:2000 dilution in PBS). The plate was incubated for 1 h on a shaker at room temperature. The coating solution was removed, and the wells were blocked with 320 µL/well of 0.2% w/v solution of non-fat milk in PBS for 45 min. The blocking solution was

prepared by shaking at room temperature for 30 min, followed by incubation on ice for 30 min. Next, the plate was washed three times with 300 µL/well of PT, and once with 300 µL/well of PBS-NaCl. The wells on the ELISA plate were then incubated with the 100 µL/well of urine samples, or 5.6 nM PSMA solution, or non-fat milk solution (negative control) for 1 h. The wells were washed three times with 300 µL/well of PT, and once with 300 µL/well of PBS-NaCl, and then incubated with 100 µL/well of a solution of rabbit monoclonal anti-PSMA (EP3254, Abcam) detection antibody (1:1000 dilution in PBS) for 1 h. The wells were washed three times with PT, and once with PBS, and then incubated with horseradish-peroxidase-conjugated anti-rabbit secondary antibody (100 µL/well, 1:2000 dilution in PBS) for 1 h. The wells were washed three times with PT, and once with PBS. The plate was then developed by incubating with HRP substrate solution with 2 mg/mL *o*-phenylenediamine dihydrochloride.

Synthesis of Phage-PEDOT films

A circular gold electrode (CH instruments) was manually polished with three diamond polishing pastes (Ted Pella) having particle sizes of 1, 0.5 and 0.25 µm on a polishing microcloth (Buehler), and sonicated in nanopure water for 10 min. A flame-cleaned platinum film electrode was used as the counter electrode. The electrode was placed in the virus-PEDOT plating solution (12.5 mM $LiClO_4$, 2 mM EDOT and 3 nM phage). Electropolymerization occurred by cycling between 0.2 and 1.15 V vs Ag/AgCl reference electrode for 10 cycles using a PARSTAT 2273

controlled with POWERCV software (Princeton Applied Research, Oak Ridge, TN), at a scan rate of 20 mV/s. Synthesized films were rinsed with Milli-Q water and transferred to the run buffer, 0.1% Tween 20 in phosphate buffered fluoride (PBF, 4.2 mM Na_2HPO_4, 1.5 mM KH_2PO_4 and 140 mM NaF, pH 7.2).

SEM Analysis

Scanning electron microscopy was performed using a Philips XL30 FEG SEM at a 10 kV operating voltage. The samples were coated with a thin layer of Ir by sputter coating prior to SEM analysis.

Impedance Measurements

Freshly synthesized virus-PEDOT films were rinsed with Milli-Q water and then equilibrated in PBF-Tween buffer for 10 min. Then five consecutive EIS scans were acquired using a PARSTAT 2273 potentiostat controlled by POWERSine software (Princeton Applied Research, Oak Ridge, TN), at 50 frequency data points spanning 0.1 Hz to 1 MHz with a 10 mV voltage modulation amplitude. The electrode was then rinsed with water, and incubated with PSMA for 30 min followed by rinsing with water and PBF-Tween. The electrode was returned to the run buffer and equilibrated for 10 min before acquisition of five consecutive EIS scans. The data was fit to the Hill equation using GraphPad Prism.[37]

For biosensing with wrapped-viruses, the synthesized virus-PEDOT films were rinsed with Milli-Q water, and then incubated with K_{CS}-**1** (308.7 μM) for 15 min.

The electrode was then rinsed with water and PBF-Tween, followed by incubation with PSMA. EIS scans were acquired as described above. For synthetic urine runs, the electrode with the bio-affinity matrix was incubated with PSMA in synthetic urine to achieve the desired concentration. The EIS scans were acquired as described above.

REFERENCES

(1) Siegel, R.; Naishadham, D.; Jemal, A. Cancer Statistics, 2013. *CA-Cancer J. Clin.* **2013**, *63*, 11–30.

(2) Moyer, V. A. Screening for Prostate Cancer: U.S. Preventive Services Task Force Recommendation Statement. *Ann. Intern. Med.* **2012**, *157*, 120–134.

(3) Madu, C. O.; Lu, Y. L. Novel Diagnostic Biomarkers for Prostate Cancer. *J. Cancer* **2010**, *1*, 150–177.

(4) Murphy, G. P.; Kenny, G. M.; Ragde, H.; Wolfert, R. L.; Boynton, A. L.; Holmes, E. H.; Misrock, S. L.; Bartsch, G.; Klocker, H.; Pointner, J.; *et al.* Measurement of Serum Prostate-Specific Membrane Antigen, a New Prognostic Marker for Prostate Cancer. *Urology* **1998**, *51*, 89–97.

(5) Sokoloff, R. L.; Norton, K. C.; Gasior, C. L.; Marker, K. M.; Grauer, L. S. A Dual-Monoclonal Sandwich Assay for Prostate-Specific Membrane Antigen: Levels in Tissues, Seminal Fluid and Urine. *Prostate* **2000**, *43*, 150–157.

(6) Xiao, Z.; Adam, B.-L.; Cazares, L. H.; Clements, M. A.; Davis, J. W.; Schellhammer, P. F.; Dalmasso, E. A.; Wright, G. L. Quantitation of Serum Prostate-Specific Membrane Antigen by a Novel Protein Biochip Immunoassay Discriminates Benign from Malignant Prostate Disease. *Cancer Res.* **2001**, *61*, 6029–6033.

(7) Schülke, N.; Varlamova, O. A.; Donovan, G. P.; Ma, D.; Gardner, J. P.; Morrissey, D. M.; Arrigale, R. R.; Zhan, C.; Chodera, A. J.; Surowitz, K. G.; *et al.* The Homodimer of Prostate-Specific Membrane Antigen Is a Functional Target for Cancer Therapy. *Proc. Natl. Acad. Sci. USA* **2003**, *100*, 12590–

12595.

(8) Chuang, A.-Y.; DeMarzo, A. M.; Veltri, R. W.; Sharma, R. B.; Bieberich, C. J.; Epstein, J. I. Immunohistochemical Differentiation of High-Grade Prostate Carcinoma from Urothelial Carcinoma. *Am. J. Surg. Pathol.* **2007**, *31*, 1246–1255.

(9) Su, S. L.; Huang, I. P.; Fair, W. R.; Powell, C. T.; Heston, W. D. Alternatively Spliced Variants of Prostate-Specific Membrane Antigen RNA: Ratio of Expression as a Potential Measurement of Progression. *Cancer Res.* **1995**, *55*, 1441–1443.

(10) Petrenko, V. A.; Vodyanoy, V. J. Phage Display for Detection of Biological Threat Agents. *J. Microbiol. Methods* **2003**, *53*, 253–262.

(11) Nanduri, V.; Sorokulova, I. B.; Samoylov, A. M.; Simonian, A. L.; Petrenko, V. A.; Vodyanoy, V. Phage as a Molecular Recognition Element in Biosensors Immobilized by Physical Adsorption. *Biosens. Bioelectron.* **2007**, *22*, 986–992.

(12) Ionescu, R. E.; Cosnier, S.; Herrmann, S.; Marks, R. S. Amperometric Immunosensor for the Detection of Anti-West Nile Virus IgG. *Anal. Chem.* **2007**, *79*, 8662–8668.

(13) Smith, G. P. Filamentous Fusion Phage: Novel Expression Vectors That Display Cloned Antigens on the Virion Surface. *Science* **1985**, *228*, 1315–1317.

(14) Kehoe, J. W.; Kay, B. K. Filamentous Phage Display in the New Millennium. *Chem. Rev.* **2005**, *105*, 4056–4072.

(15) Levin, A. M.; Weiss, G. A. Optimizing the Affinity and Specificity of Proteins with Molecular Display. *Mol. Biosyst.* **2006**, *2*, 49–57.

(16) Weiss, G. A.; Penner, R. M. The Promise of Phage Display: Customized Affinity and Specificity. *Anal. Chem.* **2008**, *80*, 3082–3089.

(17) Diaz, J. E.; Yang, L.-M. C.; Lamboy, J. A.; Penner, R. M.; Weiss, G. A. Biosensors and Biodetection. *Methods Mol. Biol.* **2008**, *504*, 255–274.

(18) Yang, L.-M. C.; Diaz, J. E.; McIntire, T. M.; Weiss, G. A.; Penner, R. M. Direct Electrical Transduction of Antibody Binding to a Covalent Virus Layer Using

Electrochemical Impedance. *Anal. Chem.* **2008**, *80*, 5695–5705.

(19) Yang, L.-M. C.; Tam, P. Y.; Murray, B. J.; McIntire, T. M.; Overstreet, C. M.; Weiss, G. A.; Penner, R. M. Virus Electrodes for Universal Biodetection. *Anal. Chem.* **2006**, *78*, 3265–3270.

(20) Arter, J. A.; Taggart, D. K.; McIntire, T. M.; Penner, R. M.; Weiss, G. A. Virus-PEDOT Nanowires for Biosensing. *Nano Lett.* **2010**, *10*, 4858–4862.

(21) Donavan, K. C.; Arter, J. A.; Pilolli, R.; Cioffi, N.; Weiss, G. A.; Penner, R. M. Virus-poly(3,4-Ethylenedioxythiophene) Composite Films for Impedance-Based Biosensing. *Anal. Chem.* **2011**, *83*, 2420–2424.

(22) Arter, J. A.; Diaz, J. E.; Donavan, K. C.; Yuan, T.; Penner, R. M.; Weiss, G. A. Virus-Polymer Hybrid Nanowires Tailored to Detect Prostate-Specific Membrane Antigen. *Anal. Chem.* **2012**, *84*, 2776–2783.

(23) Lamboy, J. A.; Arter, J. A.; Knopp, K. A.; Der, D.; Overstreet, C. M.; Palermo, E. F.; Urakami, H.; Yu, T.-B.; Tezgel, O.; Tew, G. N.; *et al.* Phage Wrapping with Cationic Polymers Eliminates Nonspecific Binding between M13 Phage and High pI Target Proteins. *J. Am. Chem. Soc.* **2009**, *131*, 16454–16460.

(24) Lamboy, J. A.; Tam, P. Y.; Lee, L. S.; Jackson, P. J.; Avrantinis, S. K.; Lee, H. J.; Corn, R. M.; Weiss, G. A. Chemical and Genetic Wrappers for Improved Phage and RNA Display. *ChemBioChem* **2008**, *9*, 2846–2852.

(25) Welsh, L. C.; Symmons, M. F.; Sturtevant, J. M.; Marvin, D. A.; Perham, R. N. Structure of the Capsid of Pf3 Filamentous Phage Determined from X-Ray Fibre Diffraction Data at 3.1 A Resolution. *J. Mol. Biol.* **1998**, *283*, 155–177.

(26) *Fundamental Immunology*; Paul, W., Ed.; 6th ed.; Lippincott Williams & Wilkins, 2008.

(27) Murase, K.; Morrison, K. L.; Tam, P. Y.; Stafford, R. L.; Jurnak, F.; Weiss, G. A. EF-Tu Binding Peptides Identified, Dissected, and Affinity Optimized by Phage Display. *Chem. Biol.* **2003**, *10*, 161–168.

(28) Rostovtsev, V. V; Green, L. G.; Fokin, V. V; Sharpless, K. B. A Stepwise Huisgen Cycloaddition Process: Copper(I)-Catalyzed Regioselective Ligation of Azides and Terminal Alkynes. *Angew. Chem., Int. Ed.* **2002**, *41*, 2596–2599.

(29) Erlanson, D. A. Introduction to Fragment-Based Drug Discovery. *Top. Curr. Chem.* **2012**, *317*, 1–32.

(30) Sharma, P. S.; Pietrzyk-Le, A.; D'Souza, F.; Kutner, W. Electrochemically Synthesized Polymers in Molecular Imprinting for Chemical Sensing. *Anal. Bioanal. Chem.* **2012**, *402*, 3177–3204.

(31) Hill, A. V. The Possible Effects of the Aggregation of Molecules of Hemoglobin on Its Dissociation Curve. *J. Physiol.* **1910**, *40*, 4–7.

(32) Mccurdy, D.; Lin, Z.; Inn, K. G. W.; Iii, R. B.; Wagner, S.; Efurd, D. W.; Steiner, R.; Duffy, C.; Hamilton, T. F.; Brown, T. A.; *et al.* Second Interlaboratory Comparison Study for the Analysis of 239 Pu in Synthetic Urine at the μ Bq ($\sim$ 100 aCi) Level by Mass Spectrometry. *J. Radioanal. Nucl. Chem.* **2005**, *263*, 447–455.

(33) *Clinical Laboratory Medicine*; McClatchey, K. D., Ed.; 2nd ed.; Lippincott Williams & Wilkins, 2002.

(34) Thompson, I. M.; Pauler, D. K.; Goodman, P. J.; Tangen, C. M.; Lucia, M. S.; Parnes, H. L.; Minasian, L. M.; Ford, L. G.; Lippman, S. M.; Crawford, E. D.; *et al.* Prevalence of Prostate Cancer among Men with a Prostate-Specific Antigen Level < or =4.0 Ng per Milliliter. *N. Engl. J. Med.* **2004**, *350*, 2239–2246.

(35) Donavan, K. C.; Arter, J. A.; Weiss, G. A.; Penner, R. M. Virus-Poly(3,4-Ethylenedioxythiophene) Biocomposite Films. *Langmuir* **2012**, *28*, 12581–12587.

(36) Lumiprobe http://www.lumiprobe.com/protocols/click-chemistry-dna-labeling (accessed Sep 7, 2011).

(37) Motulsky, H. J. Analyzing Data with GraphPad Prism, GraphPad Software Inc., San Diego CA http://www.graphpad.com.

CHAPTER 3

Biosensing with Virus Electrode Hybrids

ABSTRACT

Virus electrodes address two major challenges associated with biosensing. First, the surface of the viruses can be readily tailored for specific, high affinity binding to targeted biomarkers. Second, the viruses are entrapped in a conducting polymer for electrical resistance-based, quantitative measurement of biomarker concentration. To further enhance device sensitivity, two different ligands can be attached to the virus surface, and increase the apparent affinity for the biomarker. In the example presented here, the two ligands bind to the analyte in a bidentate binding mode with a chelate-based avidity effect, and result in an 100 pM experimentally observed limit of detection for the cancer biomarker prostate-specific membrane antigen. The approach does not require enzymatic amplification, and allows reagent-free, real-time measurements. This chapter presents general, in-depth protocols for the development of such biosensors with modified viruses for the enhanced detection of arbitrary target proteins. Building on chapter 2, here I provide an in-depth account of the strategies and protocols adopted, and the associated background information.

Key reference: Kritika Mohan, Reginald M. Penner, Gregory A. Weiss. Biosensing with virus electrode hybrids. *Current Protocols*, **2015**, 7(2), 53-72. (Invited Article)

INTRODUCTION

This chapter describes a general protocol for the development of a biosensor aimed at efficiently detecting cancer biomarkers in patient's biological fluids including blood and urine. The virus electrode biosensors provide highly sensitive, reagent free, real-time detection of the targeted protein.[1] M13 filamentous bacteriophage, the biological recognition element, display peptide ligands to a specific biomarker. These viruses and their phage-displayed ligands are incorporated into the biosensor during electrochemical polymerization with a conducting organic polymer, poly-3,4-ethylenedioxythiophene (PEDOT) onto gold electrodes.[2–6] Upon binding, a perturbation in the electrode's electrical impedance results in a quantitative measurement of the target biomarker. In this article, the target analyte is prostate-specific membrane antigen (PSMA), a prostate cancer biomarker.[7–9]

High sensitivity to PSMA resulted from the synergistic action of two different PSMA ligands on the same virus particle, Figure 2-2. One ligand, termed the primary recognition ligand, was genetically encoded by a phagemid encapsulated within the virus. The second ligand, termed the secondary recognition ligand, was chemically synthesized as a fusion peptide to oligolysine, i.e., K_{CS}-**1** or K_{CS}-**2** (where K_{CS} is defined as "lysine [K], Chemically Synthesized"; see Table 2-1) for electrostatic wrapping around the phage surface. The dual ligands result in a bidentate binder with dense ligand display for enhanced PSMA detection through both a high concentration of ligands and a chelate-based, avidity effect.[10]

Biosensing with virus-PEDOT films provided a 100 pM limit of detection (LOD) for PSMA in synthetic urine without requiring enzymatic or other amplification.[1] The reported approach leverages two ligands with varying target affinities to achieve high sensitivity for the targeted biomarker.

Phage-based biosensors offer a number of key advantages. First, phage and the displayed peptide ligands are extraordinarily stable.[11] For example, the virus-hybrid surfaces are stable for over 14 hours in rapidly flowing, high ionic strength buffer,[4] and the phage retain their binding abilities after 6-weeks at 65 °C.[12] Second, phage form liquid crystals at high concentration, which can maximize the density of packing in the biosensors. We have observed this dense packing, which causes the phage to line-up like match sticks, in atomic force microscopy of our covalent virus surface.[4] Third, the "kelp forest architecture" of the covalent virus surface, which we observed by QCM allows rapid kinetics in binding to biomarkers.[13] Such multi-point, cooperative binding has been observed by SPR for a phage-based surface.[14]

Most importantly, phage readily allow adaptation to arbitrary molecular targets. Phage display has been successfully applied to a wide range of targets, including proteins (as described here), DNA, and small molecules. The architecture described here, for example, can be applied to the detection of different biomarkers for a broad range of diseases simply by modifying the viral DNA to ligands targeting biomarkers associated with each disease.

STRATEGIC PLANNING

Selection of the targeted biomarkers requires careful consideration. For example, PSMA, a prostate cancer biomarker is shed into the urine sample of cancer patients.[15] Thus, it serves as a suitable target for non-invasive testing in urine from patients. Phage-displayed peptide libraries were used to select for ligands that selectively bind to PSMA.[16–18] Theoretically, the ligands displayed on phage could either be peptides or proteins, but for the secondary recognition ligands, peptides are preferred for dense ligand display. In addition, the high copy number of peptide ligands on the phage surfaces increases their effective concentration in the bioaffinity layer.

A wide range of bioorthogonal chemistries could allow attachment of the secondary recognition ligand. A modular approach is preferred rather than the synthesis of a long peptide to obtain higher yields of the synthetic peptide. Additionally, the oligolysine half of the wrapper can remain constant for all wrappers. Thus, it is advantageous to synthesize the two halves separately and substitute different secondary recognition ligands. Copper-catalyzed azide alkyne-cycloaddition, a ‘click’ reaction, can link the two halves of the wrapper, as the reaction offers a convergent synthesis that proceeds at room temperature in aqueous solution.[19]

The generation of the bioaffinity matrix on the gold electrode may be accomplished by adsorption, entrapment, specific interaction, cross-linking and covalent attachment. Biomolecular entrapment of the viruses within a polymer

matrix provides robust attachment and allows the ligands to remain functional.[20] Additionally, the method is expeditious and avoids potential phage-degrading steps.

The protocols in this article describe a general method for the detection of a biomarker using electrochemical biosensors comprising of phage-display ligands wrapped with additional secondary recognition ligands to increase the sensitivity to the target, Figure 2-9B. Three basic procedures will be described. First, the secondary recognition ligands are synthesized from individual peptides. Second, phage-displayed ligands and control phage are propagated and isolated. Third, the virus-PEDOT films are formed before generation of a calibration curve for target protein detection. As a specific example to illustrate the steps mentioned above, the incorporation of peptide ligands into the bio-affinity layer for the detection of PSMA is described here.

PEPTIDE SYNTHESIS OF LIGANDS

Conventional solid phase peptide synthesis was used for the generation of alkyne- and azide-functionalized peptides (Table 2-1). Next, the peptides were purified by reverse-phase HPLC, and the fractions characterized by MALDI. The relevant fractions were then combined, and their purity analyzed by analytical reverse-phase HPLC.

3.1 BASIC PROTOCOL 1: CLICK CHEMISTRY REACTION TO PREPARE K_{CS}-1 AND K_{CS}-2

After the azide- and alkyne-functionalized peptides have been synthesized and purified, the next step is to link them by click reaction, Scheme 2-1, listed as K_{CS}-**1** and K_{CS}-**2** in Table 2-1. The reaction protocol for click reaction is modified from the Lumiprobe protocol for oligonucleotides.[21] While working with Cu(I), the disproportionation of Cu(I) to Cu(II) or Cu(0) leads to the generation of the non-catalytic Cu states. Ligands such as TBTA are commonly used to stabilize the Cu(I) state. Alternatively, if the reaction proceeds at a rapid rate, the addition of ligands can be avoided. Triethylammonium acetate acts as a buffer.

MATERIALS

Alkyne-functionalized peptide stock solution (200 μM in water)

Triethylammonium acetate buffer (1 M, pH 7)

HPLC grade water or Milli-Q water

Azide-functionalized peptide stock solution (200 μM in 1:3 water-acetonitrile mixture)

Ascorbic acid

Copper sulphate

3.1.1 Setting up the Cycloaddition Reaction

1. Prepare a 5 mM ascorbic acid solution in HPLC grade water.

   The solution is unstable and should be discarded after each use. HPLC grade water is recommended, but not required; inconsistent results were observed from reactions performed in Milli-Q water.

2. Aliquot 200 µL of the alkyne-functionalized peptide solution into a 15 mL conical tube.

   The concentration of both azide- and alkyne-functionalized peptides in the final reaction mixture will be 40 µM. Higher concentrations resulted in lower yields. Parallel 40 µM, 1 mL scale reactions should be used to obtain higher yields and more product. The reaction mixtures from the parallel reactions can then be combined before characterization.

3. Add 50 µL triethylammonium acetate buffer solution to a final concentration of 50 mM.

4. Add the required amount of HPLC grade water such that the final reaction volume after the addition of solutions below will be an estimated 1 mL. Vortex the solution.

5. Add 200 µL of the azide-functionalized peptide stock solution. Vortex.

   If necessary, the azide-functionalized peptide may be used in slight excess as suggested in the Lumiprobe protocol. A 1:1 ratio provided the expected results with the peptides used here.

6. Sparge the reaction mixture by bubbling through an inert gas (e.g., nitrogen) for 30 sec.
7. Add 200 µL of the ascorbic acid solution. Briefly vortex.
8. Add 10 µL $CuSO_4$ solution (100 mM).
9. Sparge the reaction mixture again with nitrogen for 10 sec.

    The reaction vessel (conical tube) should be sealed immediately to avoid absorption of oxygen by the solution.

10. Vortex the conical tube, and incubate overnight (≈16 hours) at room temperature.

    A precipitate observed after addition of all reagents likely results from a high concentration of azide-functionalized peptide ligand. In addition to decreased concentrations of the azide-functionalized peptide ligand, the solution can be heated to 80 °C for a few minutes.

3.1.2 Characterization of Product Formation

11. Combine the reactions into one conical tube.
12. Run MALDI-TOF mass spectrometry on a sample of the reaction product to confirm product formation.

    α-Cyano-4-hydroxycinnamic acid was used as the matrix for sample preparation.

3.1.3 Purification of the Cycloaddition Reaction Product

13. Concentrate the reaction mixture using 2 kD molecular weight cut-off micro concentrators.

    In general, ten reactions were run and concentrated down to 500 µL to 1 mL for further purification.

14. Run reverse-phase HPLC for purification.

    The reactions were run at 40 µM, hence the product concentration is insufficient to run preparative HPLC. The product was purified using analytical scale HPLC. Multiple runs were performed. Fractions were analyzed by MALDI-TOF, and appropriate fractions from different runs were combined.

15. Place the fractions under speed vacuum to remove the solvent.

16. Resuspend the product to a final concentration of 1 µg/µL in 60:40 water: acetonitrile mixture.

    HPLC-grade water was used for the final resuspension. The percentage of acetonitrile should be used as needed for solubility.

3.2 BASIC PROTOCOL 2: PHAGE PROPAGATION, ISOLATION, PURIFICATION, AND QUANTIFICATION

M13 bacteriophages infect gram negative bacteria (e.g., *E. coli*), and can be readily isolated from bacterial culture. The phagemids (plasmid-like vectors) encode the display of peptide ligands as fusions to a periplasmic localization signal sequence (stII leader sequence: MKKNIAFLLASMFVFSI ATNAYA or DsbA: MKKIWLALAGLVLAFSASA) and the *N*-terminus of P8, the major coat protein. The signal peptide directs the resultant protein into the periplasm. Furthermore, the sequence also incorporates a signal peptidase site, which is cleaved off leading to the displayed peptide fused to the N-terminus of the P8 coat protein through the Gly-Ser linker (GGGSGSSSGGGSGGG). The order of the resultant fusion is signal sequence-(*N*-terminus-peptide ligand)-(Gly-Ser linker)-P8-COOH. DNA encoding displayed peptides were introduced by mutagenesis.[22] The phagemid also includes an antibiotic resistance marker to allow selections for its propagation in the presence of carbenicillin as used below. Other proteins required for phage propagation and assembly are separately provided by co-infecting the cultures with helper phage (M13 KO7). The genome of KO7 has a mutated packaging signal, which decreases its efficiency and ensures preferential packaging of the phagemid DNA. The encapsulated viruses are then secreted from the bacteria and can be precipitated from the culture

using PEG-NaCl precipitation. This protocol details all steps necessary to obtain purified phage.

MATERIALS

E. Coli XL1 Blue Cells ($CaCl_2$ competent; e.g. Stratagene)

M13 phage-display vectors(phagemids, Vrisko Limited)

2YT medium (16 g tryptone, 10 g yeast extract, 5 g NaCl; adjust to 1 liter with Milli-Q purified water, pH 7; sterilize by autoclaving)

Carbenicillin stock (50 mg/ml in sterile water, i.e., autoclaved Milli-Q purified water)

Tetracycline stock (5 mg/ml in sterile water, i.e., autoclaved Milli-Q purified water)

Kanamycin stock (40 mg/ml in sterile water, i.e., autoclaved Milli-Q purified water)

Helper phage (GE Healthcare Life Sciences)

PEG-NaCl (2.5 M NaCl, 20% PEG-8000)

PBS-Tween (PBS: 135 mM NaCl, 2.5 mM KCl, 8 mM Na_2HPO_4, 30 mM KH_2PO_4, pH 7.2 with added 0.05% Tween-20)

Lithium perchlorate ($LiClO_4$)

15-mL Flacon tubes

50- and 250-mL centrifuge bottles

UV transparent plates (Corning, cat. No 3635)

Microtiter plate reader (Bio-Tek)

Note: All buffers and solutions used for phage propagation are sterilized prior to use by autoclaving. Solutions such as PBS-Tween are sterile-filtered after addition of Tween to sterile PBS.

1. Transform the M13 phage-display vectors (phagemids) encoding peptide-**2** fused to P8 into $CaCl_2$ competent *E. coli* XL1 Blue cells following Addgene's protocol for heat-shock bacterial transformation.[23]
2. Spread the transformed cells onto LB agar plates supplemented with 50 µg/mL carbenicillin. Incubate overnight at 37 °C.

3.2.1 Starter Cultures for Phage Propagation

3. Aliquot 2 mL of 2YT media into two 15 mL Falcon tubes, and add 2 µL of carbenicillin and 1 µL of tetracycline from the antibiotic stocks to each tube.

   XL1 Blue E. coli encode the tetracycline resistance gene on a plasmid with the gene encoding the F pili, which are required for phage infection.

4. Add a single colony to each of the two cultures.
5. Incubate the cultures with shaking at 37 °C until each culture reaches log-phase growth (OD_{600} of ≈0.45-0.5).

   Shaking the cultures in a slanting position improves growth as it provides increased aeration in the Falcon tubes. Growing the cultures to log phase is crucial to obtain high infection efficiency.[24] *There are only a few F pili present per bacterial cell. But, if a high*

density of cells is achieved by allowing the cells to grow past log phase then the F pili expression is lowered. This results in lower infection efficiency. The shaking incubators are set to 250 rpm.

6. Infect the culture with KO7 helper phage with a multiplicity of infection (MOI) of 4.6.

   MOI can also be calculated as the ratio of the number of phage particles being added, to the number of bacterial cells in the culture. For the phage particles, an OD_{268} *of 1 =* 5×10^{12} *particles/mL. For the bacterial cells,* OD_{600} *of 1 =* 1×10^{9} *cells/mL.*

7. Incubate the cultures with shaking for 1 h at 37 °C.

3.2.2 Grow Overnight Cultures

8. Transfer 150 mL of 2YT media to a 500 mL baffled flask. Add 150 µL carbenicillin and 75 µL of kanamycin.

   The kanamycin resistance gene is present in the KO7 helper phage genome. Thus, the antibiotic is added at half strength to the overnight cultures. For overnight cultures, a desirable ratio of volume of flask to culture is >3:1, for optimal culture aeration.

9. Transfer the two starter cultures to the 150 mL overnight culture prepared in step 8.

   A ratio of ≈1:35 between the volumes of starter and overnight cultures works for most phage. Some phage grow better in larger or

*smaller culture sizes. For Stop-4 phage (phagemid packaged into the phage with no displayed ligands) and phage-**2**, 150 mL and 450 mL overnight culture volumes are recommended, respectively. The specific volumes used here were based on the size of the centrifuge bottles available.*

10. Incubate the cultures overnight with shaking at 37 °C.

    *As with culture size, the duration of overnight cultures can be an important variable, which may require customization. For Stop-4 phage and phage-**2**, 16 and 19 h overnight culture durations respectively were found to be optimal.*

3.2.3 Phage Precipitation

11. Aliquot 30 mL of PEG-NaCl into a 250 mL centrifuge bottle. Place the bottle on ice.

    Precooling of the centrifuge tube is recommended for higher yields. The volume of PEG-NaCl used is ≈1/5th the volume of the overnight culture.

12. Transfer the overnight culture to another 250 mL centrifuge tube. Centrifuge for 15,334 × g for 10 min at 4 °C.

    The centrifuge should be pre-cooled to 4 °C before centrifugation. At this point, the bacterial cells are contained in the pellet, and the virus particles remain suspended in the supernatant.

13. Transfer the supernatant from step 12 to the centrifuge tube containing PEG-NaCl (step 11). Mix by inverting the tube 10 times.

    Care should be taken during transfer such that the cell pellet is not disturbed.

14. Incubate the solution on ice for 1 hour.

    The solution contains phage, and thus the tube should always be completely covered with ice.

15. Centrifuge at 15,334 × g for 20 min at 4 °C. Decant and discard the supernatant.

16. Recentrifuge at 2445 × g for 4 min at 4 °C.

    After step 15, the phage pellet can appear as a smear along the side of the tube. This step helps collect the pellet at the bottom of the centrifuge tube. If the centrifuge tubes are placed in the exact position as before, with the pellet facing away from the center of the rotor, the pellet will be collected at the same spot. Care should be taken not to overdo the centrifugation; otherwise the subsequent resuspension of the phage pellet becomes harder. A 4 min spin is usually sufficient and optimal unless the pellet size is extremely small. If necessary, the centrifugation can be reduced to 2 min.

17. Remove excess supernatant by blotting the centrifuge tubes on paper towels for 1-3 min.

18. Resuspend the phage pellet in 5 mL of PBS-Tween.

Tween helps disaggregation of the phage particles. Resuspension should be largely performed by pipetting. After the addition of PBS-Tween to the pellet, incubation on ice for a few min softens the pellet, and assists the resuspension. The pipetting steps may be alternated with quick vortexing steps. During resuspension, the phage should still be kept on ice as much as possible.

19. Transfer to a 50 mL centrifuge tube and re-centrifuge at 13,776 × g for 10 min at 4°C.

    This step pellets the insoluble debris from the cell culture.

3.2.4 Perform Second Precipitation

20. Transfer the supernatant to a fresh centrifuge tube. Add 1/5th volume of PEG-NaCl and incubate on ice for 1 h.

    Repeating the precipitation steps results in a much cleaner phage stock, largely free of impurities.

21. Centrifuge for 20 min at 30,996 × g at 4 °C. Decant and discard the supernatant.

    Since the volume of the solution is much smaller compared to the initial culture size, smaller centrifuge tubes (50 mL) and higher speeds can be used for precipitating the phage.

22. Recentrifuge for 4 min at 2204 × g at 4 °C. Remove excess supernatant by blotting the centrifuge tubes.

Blotting removes any residual PEG, which might interfere with future experiments. At this step, the phage pellet should have a white color. The appearance of any discoloration indicates the presence of impurities.

23. Resuspend the phage pellet in $LiClO_4$ and re-centrifuge at 13,776 × g for 10 min at 4 °C.

    The amount of 12 mM $LiClO_4$ used should be kept to a minimum to avoid over dilution of the phage stock. The resuspension is done in $LiClO_4$ as the phage-EDOT solution needed for the electrodeposition of the film on the gold electrode uses $LiClO_4$. For other biological assays, the phage resuspension may be performed in phosphate buffer.

3.2.5 Phage Quantification

24. Quantify the phage by measuring the UV absorbance of the solution. An OD_{268} of 1 = 8.31 nM or 5×10^9 phage/mL

    For measuring phage concentration, an 1:10 dilution is preferred over an 1:100 dilution, as this volume avoids small pipetting errors that could occur with the latter dilution. For long term storage, phage stocks should be diluted to 40-65 nM. The stability at 4 °C varies, but most phage are stable for a few days. For prolonged storage, phage stocks can be flash-frozen and stored at -80 °C.

Such phage stocks are stable for 6-12 months. The appearance of phage precipitating from the solution indicates an old and unusable phage stock.

25. Similarly, the experiment can be repeated to propagate the negative control Stop-4 phage.

3.3 BASIC PROTOCOL 3: BIOSENSING: FORMATION OF THE BIOAFFINITY MATRIX AND ELECTROCHEMICAL DETECTION

Next, the bioaffinity matrix of the biosensor is prepared for electrochemical detection of PSMA. Incubation and binding of the target analyte, PSMA, to the biological recognition element produces a change in its electrical properties. Specifically, an increase in biosensor resistance is observed upon PSMA binding. As described above, PEDOT is formed by the electrochemical polymerization of EDOT in the presence of $LiClO_4$ and virus particles. The negative charge on the virus surface allows for its incorporation as counter ions to the positively charged PEDOT polymer depositing onto the gold electrode. The concentration of viruses used in the EDOT-$LiClO_4$ solution is an important parameter. Increased virus concentration leads to higher incorporation of viruses into the virus-PEDOT film.[25] A 3 nM virus solution provided an optimal working concentration. The sensitivity for PSMA detection was further improved by wrapping the incorporated viruses with additional secondary recognition ligands.

PSMA detection applies electrochemical impedance spectroscopy for monitoring the change in resistance upon PSMA binding. Data was collected over a wide frequency range and analyte concentrations. For the calibration curve, all calculations performed and parameters extracted were at 1000 Hz as previously described.[26] As a starting point, target concentrations should not fall below the LOD of the device.

The calibration curve provides the relative change in resistance obtained over a wide range of PSMA concentrations. The negative controls must examine non-specific binding between the target and the components forming the bioaffinity matrix; measurements with target binding to PEDOT films (no virus) provide an important control. Such controls also must test whether wrapping the phage with additional ligands increases resistance and non-specific binding. The data obtained can be analyzed to compute parameters such as the apparent K_d for the interaction between target and the virus-displayed ligands, the LOD, and potential cooperativity.

MATERIALS

Lithium Perchlorate ($LiClO_4$)

Ethylene-3,4-dioxythiophene (EDOT)

Phage stocks (See basic protocol 2)

Phosphate-buffered fluoride (PBF)-Tween (PBF, 4.2 mM Na_2HPO_4, 1.5 mM KH_2PO_4 and 140 mM NaF, pH 7.2, sterile filtered, with added 0.1% Tween 20)

K_{CS}-**1** (see Basic Protocol 1; used as a solution: dissolve K_{CS}-**1** in a 40:60 acetonitrile/HPLC-grade water solution to a final concentration of 1 µg/µl; K_{CS}-**1** stock can be stored indefinitely at –20°C)

Piranha solution (optional; sulfuric acid [H_2SO_4] and 30% H_2O_2)

Circular gold electrode (CH instruments)

Polishing microcloth (Buehler)

Diamond polishing paste (Ted Pella) having particle sizes of 1, 0.5 and 0.25 µm

Platinum counter electrode

Ag/AgCl reference electrode

Parstat 2273 potentiostat

POWERCV and POWERSine software (Princeton Applied Research, Oak Ridge, TN)

Glass vial

Kimwipes

Butane Torch

Faraday cage

3.3.1 Preparing the Phage-EDOT Solution

1. Prepare a 50 mL solution of 12.5 mM $LiClO_4$ in water. Vortex.
2. Transfer the solution prepared in step 1 to a glass vial. Add EDOT via pipette to a final concentration of 2.5 mM in water. Vortex gently.

   EDOT can adhere to plastic surfaces, hence the solution should be prepared in a glass vial or jar.
3. Cool the $LiClO_4$-EDOT solution to 4 °C by incubation in a refrigerator for 2 h.

   The protocol for the preparation of phage-EDOT solution was found to provide best results if prepared with intermediate cooling steps. This solution is stable for up to a week.
4. Transfer 10 to 15 mL, 3 nM phage in ≈2 mM EDOT solution in a clean glass vial. Refrigerate overnight.

   Aliquot the EDOT solution, and then add phage to a 3 nM final concentration. The glass vial should have a mouth wide enough to hold the three electrodes. Care should be taken to eliminate any traces of ethanol remaining from the vial cleaning step, as ethanol degrades phage samples.

3.3.2 Physically Clean the Electrode

5. Polish a single gold 3 mm diameter electrode (reusable). Take a sheet of micropolished cloth and cut it up into smaller pieces approximately 2” × 2”. Take a piece and paste it onto a work bench; the reverse surface has

adhesives on it. Place a small quantity of 1 µm diamond polishing paste on one corner.

To avoid additional variables, the same electrode was used for the reported measurements.

6. With some paste on the electrode surface, move the electrode in circles on the polishing cloth approximately ten times. Then, apply more paste and slightly rotate the electrode before repeating the polishing step at a fresh spot on the cloth. Repeat this process for a total of ten times.

   Physical cleaning involves grinding and polishing the electrode surface. This crucial step requires some patience. Rushing through this step is not advisable, nor recommended. A smooth and clean electrode surface can make the difference between stable and disintegrating films.

7. Wipe away excess polish from the edges using a Kimwipe. Rinse well with deionized (DI) water. Wipe off excess water using a Kimwipe.
8. Repeat steps 6 and 7 with 0.5 µm diamond polishing paste.
9. Repeat steps 6 and 7 with 0.25 µm diamond polishing paste.

   Decreasing the size of the polishing paste smoothens out the surface and improves the deposition of the PEDOT-phage film in the subsequent steps.

10. Place the electrode in a vial containing DI water, and immerse the setup in a water bath sonicator. Sonicate for ten minutes. Rinse with DI water.

Sonication helps in removing any material, which might be physically adhered to the glass electrode.

3.3.3 Chemically Clean the Electrode

11. Optional cleaning with piranha solution: Aliquot 3 mL H_2SO_4 in a glass vial, and carefully add 1 mL of 30% H_2O_2. Gently swirl to mix. Incubate the electrode in the solution for 10 min. Rinse with DI water.

    During the swirling process, the formation of bubbles in the piranha solution should be avoided. H_2O_2 should be added very carefully and slowly to H_2SO_4, and not vice-versa. Piranha solution undergoes self-decomposition, hence the solution should be prepared immediately before usage. This step may or may not be needed. In our experiments, this step proved unnecessary.

3.3.4 Cyclic Voltammetry: the Three Electrode Setup

12. Flame-clean the platinum film electrode with a butane torch. Rinse with water. Clamp the electrode, and immerse it into the phage-EDOT solution.

    A platinum electrode is used as the counter electrode.

13. Rinse the Ag/AgCl reference electrode. Clamp the electrode and immerse it into the phage-EDOT solution.

    The Ag/AgCl electrode serves as the reference electrode.

14. Clamp and immerse the Au working electrode into the phage-EDOT solution, place the setup in a Faraday cage.

    The electrodes should not be in contact with each other.

15. Connect all electrodes to the potentiostat.
16. Begin cycling the potential with the following parameters:

    Initial potential: 1.15

    Vertex: 0.2

    Scan rate: 20 mV/sec

    Cycles: 10

    For negative controls, the films can be electrodeposited with an EDOT solution lacking phage. After this step, a dark blue film covers the gold electrode, obscuring the original gold color of the electrode. If this color deposition or a cyclic voltammogram as shown in Figure 2-9A is not observed, the process failed to deposit a sufficiently thick film; the process should be repeated following the troubleshooting below.

    The maximum current flowing through the circuit, as monitored by the change in applied potential, increases with every scan. This acts as an indication of increase in the thickness or the surface area of this porous film (i.e., more deposition takes place at the electrode with each scan in Figure 2-9A).

The phage-EDOT solution can be refrigerated and reused. The limiting factor for the phage-EDOT solution is the concentration of phage in the solution. For all procedure optimization experiments, the solution was reused two to four times. For the generation of the calibration curve, a fresh solution was used for each experiment to avoid introducing variation during electrodeposition.

3.3.5 Cyclic Voltammogram

17. The acquired current versus potential data can be exported to any computing software of choice.

    If no parameters are computed from the cyclic voltammogram, the plot merely shows an increase in the maximum current flowing through the circuit. As a result, a graphing program such as MS Excel can be used to plot the trace. Each scan can be manually color-coded.

3.3.6 Electrochemical Impedance Spectroscopy

18. Rinse the film with DI water.
19. Fill a glass jar with ≈50 mL of PBF-Tween buffer.

    The solution is stable and can be reused for up to a week.

20. Rinse the electrode with PBF-Tween, and lower it into the PBF-Tween buffer

from step 19. Also, move the counter and reference electrodes to PBF-Tween after rinsing with DI water.

21. Allow the virus-PEDOT film to equilibrate in PBF-Tween for 10 min.

    The virus-PEDOT film is porous, and the equilibration step is crucial to avoid current disturbances. It was observed that a five min equilibration was sufficient for virus-PEDOT films but a 10 min equilibration was necessary for PEDOT films lacking virus. After 10 min, the electrode can be lifted and placed back in the solution to avoid any concentration gradients forming in the electrode micro-environment.

22. Connect the electrodes to the potentiostat.

23. Acquire 5 consecutive EIS scans: 50 frequency data points spanning 0.1 Hz to 1 MHz with a 10 mV voltage modulation amplitude.

    There should be no significant drift in the resistance or impedance values, and the impedance should be monitored to identify drift. This acquisition provides the native resistance (R_o) of the native film, the virus-PEDOT film with no analyte bound.

3.3.7 Wrapping the Virus-PEDOT Films with Additional Ligands

24. Rinse the electrode and incubate in a 1.5 mL eppendorf tube containing 200 µL of K_{CS}-**1** at a concentration of 0.5 µg/µL. Gently shake at room temperature for 15 min.

*The interaction between K_{CS}-**1** and the virus particles is electrostatic. Since the negative charges on the virus surface are required for incorporation into the PEDOT films and wrapping with K_{CS}-**1**, the virus-PEDOT films were wrapped after the synthesis of the virus-PEDOT films.*

*The electrode remained clamped during this incubation. The K_{CS}-**1** solution is reusable, but a fresh solution was used for each experiment, as described above in step 16.*

25. Rinse the electrode with DI water and then with PBF-Tween.

    *Care should be taken to wipe off any excess wash liquid adhered to the insulator on the electrode, to avoid any changes in concentration especially for the K_{CS}-**1** and PSMA incubation steps.*

26. Optional: check for resistance changes after phage wrapping by acquiring 5 consecutive EIS scans 50 frequency data points spanning 0.1 Hz to 1 MHz with a 10 mV voltage modulation amplitude.

    *In our experiments, the resistance of the films did not undergo any significant change upon phage wrapping with K_{CS}-**1**. However, this aspect should be tested for new peptide wrappers. The dynamic, non-covalent interaction between the K_{CS}-**1** wrappers and the viruses in the films could potentially result in decreased levels of K_{CS}-**1** wrapped on the phage. However, PSMA binding to the film*

*could reduce the possibility of the K_{CS}-**1** wrappers detaching due to its synergistic binding.*

3.3.8 PSMA (Analyte) Binding

27. Incubate the wrapped virus-PEDOT film with a 200 µL solution (of a desired concentration as shown, for example, in Figure 2-12) of PSMA in PBF-Tween buffer for 30 min with shaking.

    Typically higher concentrations are measured first, but random concentrations can also be used.

28. Rinse the electrode, equilibrate and acquire 5 EIS scans as previously described in steps 20 through 23.

    The resistance measurement obtained here is the final resistance of the film (R); this measurement indicates the change in resistance due to PSMA binding.

29. Repeat the above experiment with a different PSMA concentration or an alternative target. Also, perform appropriate negative controls.

3.3.9 Analyze Data

30. Export the data from the 5 scans for both the native film and the film after exposure to PSMA.

    Any computing software capable of doing simple calculations and plotting graphs will suffice for the analysis presented here. MS

Excel was used for our analysis.

31. Calculate the average resistance and standard deviation values across the 5 scans corresponding to each frequency for both the films.

    R = Resistance of the film post PSMA incubation = R_{Re}

    R_o = Resistance of the native film

    Each measurement will provide a set of frequencies, and their corresponding R_{Re} and R_{Im} values, the real and imaginary components of the impedance, respectively.

32. Calculate the change in resistance caused by PSMA binding across all frequencies as:

    $\Delta R = R - R_o$

    This value is found to be proportional to the PSMA concentration.

33. Calculate the corresponding error across all frequencies as:

    $\sigma = \sqrt{(\sigma_i^2 + \sigma_f^2)}$

    where σ_i = standard deviation of the native film

    σ_f = standard deviation of the film post PSMA incubation

    More than one variable is being used to compute the above parameter, and thus, propagation of error is required for the determination of uncertainty.

34. Calculate the relative increase in resistance caused by PSMA binding across all frequencies as $\Delta R/R_o$.

This step is essential to remove the dependence on R_o. For each PSMA measurement, a new film is being synthesized. This leads to a new R_o for each measurement. To eliminate this variable across different films, the increase in resistance is normalized to the native resistance of the film.

35. Next, calculate the relative error as σ/R_o across all frequencies.

    Relative error is required for the calculation in step 34 with interdependent variables.

3.3.10 Plot Data

36. For full impedance scans, plot $\Delta R/R_o$ as a function of frequency.

    *This analysis can be done for any concentration of PSMA. The resultant plot can suggest the optimal frequency range for plotting the calibration curve. Phage-**2**, phage-**2** wrapped with K_{cs}-**1**, and Stop-4 phage targeting PSMA were plotted on the graph in Figure 2-11. Frequencies >100 Hz could provide a conclusive measurement of $\Delta R/R_o$.*

37. For a calibration curve, plot $\Delta R/R_o$ as a function of PSMA concentration.

    For this analysis, a specific frequency of 1000 Hz was selected. The $\Delta R/R_o$ values at 1000 Hz corresponding to each PSMA concentration were plotted. It is essential to run all potential negative controls to test the validity of the data.

3.3.11 Extracting Key Parameters

38. Fit the data from the calibration curve to the Hill equation.

    The equation used is for 'non-linear regression and specific binding with Hill slope.' The parameters computed by the software (GraphPad Prism)[27] include n, K_d and Y_{max}.

39. The parameters obtained, n, K_d *and* Y_{max}, were used to extrapolate the curve to lower concentrations for computing the theoretical LOD.

    The experimentally observed LOD is determined as the PSMA concentration for which the $\Delta R/R_o$ is at least 3-fold over background. The same principle was applied to the extrapolated data, and provides the theoretical LOD.

REAGENTS AND SOLUTIONS

Use Milli-Q water for the preparation of all solutions and buffers unless specified.

Azide- and alkyne-functionalized peptides

The lyophilized peptides can be stored indefinitely at -20 °C. Or dissolve the lyophilized peptides in a solution of acetonitrile and water (HPLC grade) to a final concentration of 200 μM, with the percentage of acetonitrile as needed for solubility. The solutions can also be stored indefinitely at -20 °C.

COMMENTARY

3.4 BACKGROUND INFORMATION

3.4.1 M13 Bacteriophage Viruses

M13 bacteriophage viruses serve as the scaffold for the receptors in the bioaffinity matrix of the biosensor. The viruses have a ssDNA genome, which is encased in a protein coat comprising ≈2700 copies of a single major coat protein (P8), and five copies each of the four minor coat proteins.[24,28] The encapsulated DNA can be modified to display peptides or proteins on the surface of the phage as a fusion to the termini of the coat protein. For phage-**2**, the gene encoding the peptide ligand is fused to the *N*-terminus of the P8 coat protein. Furthermore, the phage propagation protocol could also be modified to simultaneously display two genetically encoded ligands on phage.[29] In each case, the copy number of the displayed peptide ligands on the surface of the phage is much lower in comparison to the total number of P8 coat proteins. Hence, the phage are wrapped with additional chemically synthesized ligands to increase the apparent concentration of ligands in the bioaffinity matrix without increasing the phage concentration. Wrapping phage with additional ligands provides a quick method to increase the affinity and sensitivity of the device due to the enhanced avidity effect.

For the generation of the secondary recognition ligands, the wrappers are synthesized in two parts. The first half consists of an oligolysine (K_{14}) peptide,

which wraps around the phage surface due to electrostatic interactions.[30,31] The residues near the *N*-terminus of the P8 coat protein impart a high negative charge to the phage surface. The K_{14} peptide is coupled to pentynoic acid during the synthesis process, providing an alkyne functionality for the click reaction. The second component of the wrapper is the peptide ligand to PSMA. The peptide ligand is similarly synthesized and functionalized with an azide moiety by coupling to 4-azidobutanoic acid. The two components are subsequently linked together by the click reaction.

3.4.2 Phage Infectivity

A key step in the phage propagation protocol is the infection of the bacterial culture with the helper phage. The helper phage encodes the proteins necessary for propagation, and the assembly of the virus. The phagemids encode an antibiotic resistance gene different from the helper phage. The addition of both antibiotics to the culture ensures the presence of both phagemid and helper phage DNA in each bacterial cell. For further details of phage propagation and design, we refer the reader to various books on this topic.[11,24]

3.4.3 Multiplicity of Infection

The infection of KO7 phage into the bacterial cell proceeds through the F pili, which are the receptors for phage infection. The number of F pili present per bacterial cell are few and limited.[24] Thus, the multiplicity of infection (MOI)

ensures high infection efficiency (equation 1). Additionally, the density of bacterial cell culture at the time of infection is also crucial. Cultures grown past log phase have high cell density, and the expression of pili decreases, which results in lower infection efficiency.

$$MOI\,(m) = \frac{\text{number of virus particles}}{\text{number of bacterial cells}}$$

Equation 1

The number of virus particles actually infecting a cell can be estimated by Poisson distribution as:[32]

$$P(k) = \frac{e^{-m} \cdot m^{k}}{k!}$$

Equation 2

Where,

P(k) = Probability that a cell will be infected by '*k'* virus particles

= Fraction of cells infected by '*k'* virus particles

If $k = 0$, then,

P(0) = fraction of uninfected cells

$= e^{-m}$

For 99% infection efficiency, the fraction of uninfected cells is:

P(0) $= 0.01 = e^{-m}$

Solving for *m*:

m $= 4.6$

Thus, for 99% infection, the ideal MOI is 4.6.

3.4.4 Biosensing Theory

The bioaffinity matrix in the biosensor consists of a composite film of a conductive organic polymer (PEDOT) and viruses deposited on a planar gold electrode. EDOT undergoes electrochemical polymerization in the presence of $LiClO_4$ to form cationic PEDOT units, which associate with perchlorate ions while depositing onto the electrode, Scheme 2-2.[33] Polymerization of EDOT in the presence of phage particles leads to the generation of the virus-PEDOT film due to the incorporation of phage particles as the counter ions during deposition, Scheme 2-2.

Ligand binding interactions are enhanced due to the cooperative effect of the two ligands present on the surface of the phage, one genetically encoded and the other chemically synthesized. This bidentate binding mode combined with the saturation binding effect can be quantified, and its parameters computed using the Hill equation (Equation 3) [34]:

$$Y = \frac{Y_{max} \cdot [L]^n}{K_d{}^n + [L]^n}$$

Equation 3

Where,

$Y = \Delta R/R_o$

L = PSMA concentration

n = Hill coefficient

K_d = Dissociation constant

The Hill coefficient is a measure of cooperativity present in the binding interaction. A value of 1 indicates no cooperative binding interactions. A value >1, as seen in Figure 2-12 indicates positive cooperativity, whereas a value <1, indicates negative cooperativity. The bidentate binding mode of ligands **1** and **2** (arising from the combination of phage-**2** and K_{CS}-**1**) results in a Hill coefficient of 1.5, which demonstrates the synergy of the two ligands in cooperatively binding to PSMA.

3.5 TROUBLESHOOTING

3.5.1 Optimizing the Combination of Ligands

The choice of ligands coating the phage surface might require careful selection to optimize sensitivity of the biosensor. For example, two ligands with negative cooperativity would be a poor choice for biosensor development. Fortunately, phage display selections typically result in large numbers of possible ligands. Various scenarios, their causes, and suggestions for improvement are summarized in a flowchart, Figure 3-1. For non-competing ligands, the identity of the genetically displayed and chemically synthesized ligand could still be a crucial factor due to the inversion of the ligand structure on the phage surface during the synthesis of the wrapper.

3.5.2 Phage Propagation

Acquiring a phage stock free from contamination is very important for obtaining high sensitivity and specificity for analyte detection. During the process of phage propagation, it is essential to meticulously follow all the steps listed above. Possible sources of error and points of concern have been incorporated in the notes for each step in the basic protocol 2. Close attention should also be paid to the yields obtained for phage-displayed peptide. Unforeseen circumstances such as errors with MOI calculations etc., could lead to the propagation and packaging of KO7 phage, but this results in exceptionally high phage yields.

3.5.3 The Cycloaddition Reaction

The choice of azide- and alkyne-functionalized peptides governs the identity of the solvent used for the reaction. If precipitation is observed in the reaction mixture, different temperature conditions (e.g., heating) or solvents could be tried. If the reaction results in low yields, Cu(I) stabilizing ligands such as TBTA could be used.

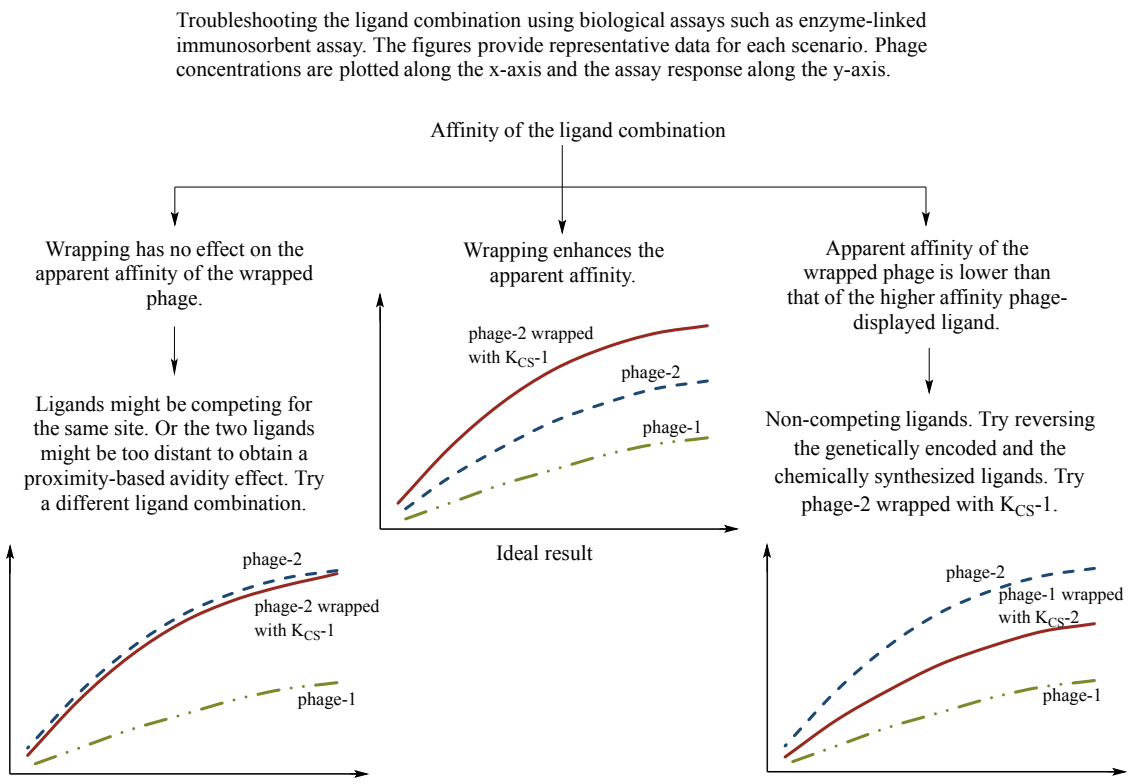

Figure 3-1. Flowchart describing the process of designing and planning a ligand combination for the detection of analyte with increased sensitivity. The commonly observed phenomena are listed here alongside possible solutions, including troubleshooting the ligand combination using biological assays such as enzyme-linked immunosorbent assay. The figures provide representative data for each scenario. Phage concentrations are plotted along the x-axis and the assay response along the y-axis.

3.5.4 Biosensing

A common problem encountered with biosensing is drift observed in the impedance values during EIS. The possible causes leading to drifting values and the corresponding solutions have been summarized as a flowchart in Figure 3-2. Non-specific binding observed during the biosensing experiments could be attributed to impurities in the materials or deteriorated reagent stocks. Phage and peptide purity is essential for low background measurements.

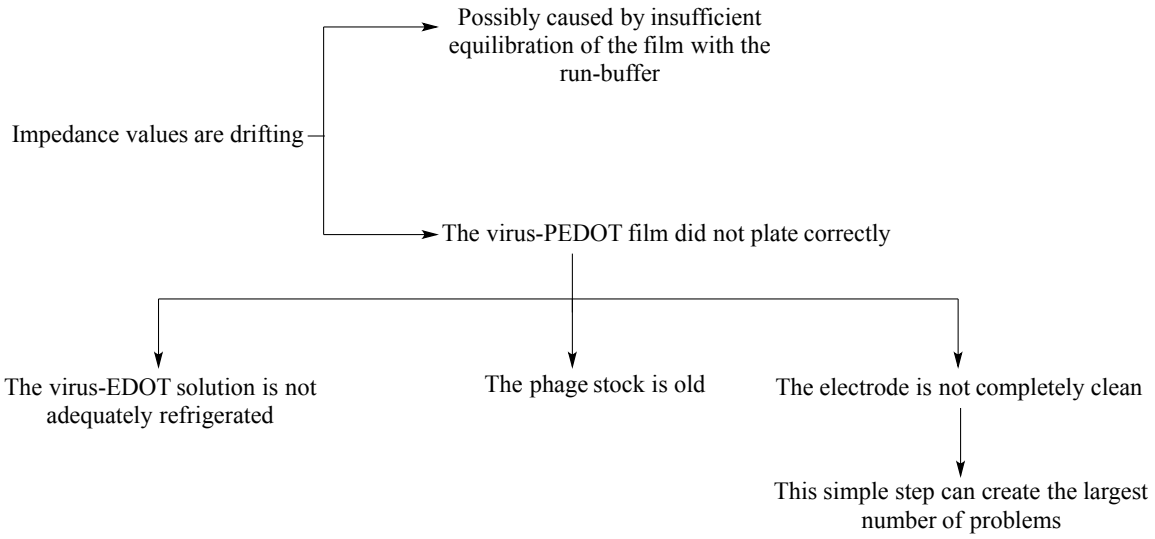

Figure 3-2. Flowchart listing the possible problems, the corresponding sources of errors, and the recommended troubleshooting steps.

ANTICIPATED RESULTS

Basic protocols 1 and 2 provide the materials necessary for the generation of the bioaffinity layer. These materials can then be applied to the detection of the cancer biomarker, as described in basic protocol 3. Once a clinically relevant limit of detection has been obtained for biosensing with virus-PEDOT films, the assay setup can be used for clinical research with biological fluids from cancer patients.

TIME CONSIDERATIONS

Once the purified azide- and alkyne-functionalized peptides have been synthesized and purified, basic protocol 1 can be completed in 3-4 days. Basic protocol 2 takes a total of three days including the transformation step. The majority of the effort required for phage propagation occurs on day 3 with the phage precipitation. For basic protocol 3, each experiment from the cleaning of the electrode to measuring the final resistance upon PSMA incubation takes ≈2.5 hours. With previously prepared, equilibrated and calibrated phage-PEDOT films in device form, five redundant measurements could theoretically be completed in minutes or less.

REFERENCES

(1) Mohan, K.; Donavan, K. C.; Arter, J. A.; Penner, R. M.; Weiss, G. A. Sub-Nanomolar Detection of Prostate-Specific Membrane Antigen in Synthetic Urine by Synergistic, Dual-Ligand Phage. *J. Am. Chem. Soc.* **2013**, *135*, 7761–7767.

(2) Weiss, G. A.; Penner, R. M. The Promise of Phage Display: Customized Affinity and Specificity. *Anal. Chem.* **2008**, *80*, 3082–3089.

(3) Diaz, J. E.; Yang, L.-M. C.; Lamboy, J. A.; Penner, R. M.; Weiss, G. A. Biosensors and Biodetection. *Methods Mol. Biol.* **2008**, *504*, 255–274.

(4) Yang, L.-M. C.; Diaz, J. E.; McIntire, T. M.; Weiss, G. A.; Penner, R. M. Direct Electrical Transduction of Antibody Binding to a Covalent Virus Layer Using Electrochemical Impedance. *Anal. Chem.* **2008**, *80*, 5695–5705.

(5) Yang, L.-M. C.; Tam, P. Y.; Murray, B. J.; McIntire, T. M.; Overstreet, C. M.; Weiss, G. A.; Penner, R. M. Virus Electrodes for Universal Biodetection. *Anal. Chem.* **2006**, *78*, 3265–3270.

(6) Arter, J. A.; Taggart, D. K.; McIntire, T. M.; Penner, R. M.; Weiss, G. A. Virus-PEDOT Nanowires for Biosensing. *Nano Lett.* **2010**, *10*, 4858–4862.

(7) Murphy, G. P.; Kenny, G. M.; Ragde, H.; Wolfert, R. L.; Boynton, A. L.; Holmes, E. H.; Misrock, S. L.; Bartsch, G.; Klocker, H.; Pointner, J.; *et al.* Measurement of Serum Prostate-Specific Membrane Antigen, a New Prognostic Marker for Prostate Cancer. *Urology* **1998**, *51*, 89–97.

(8) Schülke, N.; Varlamova, O. A.; Donovan, G. P.; Ma, D.; Gardner, J. P.; Morrissey, D. M.; Arrigale, R. R.; Zhan, C.; Chodera, A. J.; Surowitz, K. G.; *et al.* The Homodimer of Prostate-Specific Membrane Antigen Is a Functional Target for Cancer Therapy. *Proc. Natl. Acad. Sci. USA* **2003**, *100*, 12590–12595.

(9) Chuang, A.-Y.; DeMarzo, A. M.; Veltri, R. W.; Sharma, R. B.; Bieberich, C. J.; Epstein, J. I. Immunohistochemical Differentiation of High-Grade Prostate Carcinoma from Urothelial Carcinoma. *Am. J. Surg. Pathol.* **2007**, *31*, 1246–1255.

(10) Murase, K.; Morrison, K. L.; Tam, P. Y.; Stafford, R. L.; Jurnak, F.; Weiss, G. A. EF-Tu Binding Peptides Identified, Dissected, and Affinity Optimized by Phage Display. *Chem. Biol.* **2003**, *10*, 161–168.

(11) *Phage Display of Peptides and Proteins*; Kay, B. K.; Winter, J.; McCafferty, J., Eds.; Academic Press, San Diego, 1996.

(12) Brigati, J. R.; Petrenko, V. A. Thermostability of Landscape Phage Probes. *Anal. Bioanal. Chem.* **2005**, *382*, 1346–1350.

(13) Yang, L.-M. C.; Diaz, J. E.; McIntire, T. M.; Weiss, G. A.; Penner, R. M. Covalent Virus Layer for Mass-Based Biosensing. *Anal. Chem.* **2008**, *80*, 933–943.

(14) Nanduri, V.; Sorokulova, I. B.; Samoylov, A. M.; Simonian, A. L.; Petrenko, V. A.; Vodyanoy, V. Phage as a Molecular Recognition Element in Biosensors Immobilized by Physical Adsorption. *Biosens. Bioelectron.* **2007**, *22*, 986–992.

(15) Sokoloff, R. L.; Norton, K. C.; Gasior, C. L.; Marker, K. M.; Grauer, L. S. A Dual-Monoclonal Sandwich Assay for Prostate-Specific Membrane Antigen: Levels in Tissues, Seminal Fluid and Urine. *Prostate* **2000**, *43*, 150–157.

(16) Kehoe, J. W.; Kay, B. K. Filamentous Phage Display in the New Millennium. *Chem. Rev.* **2005**, *105*, 4056–4072.

(17) Levin, A. M.; Weiss, G. A. Optimizing the Affinity and Specificity of Proteins with Molecular Display. *Mol. Biosyst.* **2006**, *2*, 49–57.

(18) Arter, J. A.; Diaz, J. E.; Donavan, K. C.; Yuan, T.; Penner, R. M.; Weiss, G. A. Virus-Polymer Hybrid Nanowires Tailored to Detect Prostate-Specific Membrane Antigen. *Anal. Chem.* **2012**, *84*, 2776–2783.

(19) Rostovtsev, V. V; Green, L. G.; Fokin, V. V; Sharpless, K. B. A Stepwise Huisgen Cycloaddition Process: copper(I)-Catalyzed Regioselective “Ligation” of Azides and Terminal Alkynes. *Angew. Chem., Int. Ed.* **2002**, *41*, 2596–2599.

(20) Cosnier, S. Biomolecule Immobilization on Electrode Surfaces by Entrapment or Attachment to Electrochemically Polymerized Films. A Review. *Biosens. Bioelectron.* **1999**, *14*, 443–456.

(21) Lumiprobe http://www.lumiprobe.com/protocols/click-chemistry-dna-labeling (accessed Sep 7, 2011).

(22) Smith, G. P. Filamentous Fusion Phage: Novel Expression Vectors That Display Cloned Antigens on the Virion Surface. *Science* **1985**, *228*, 1315–1317.

(23) Bacterial transformation https://www.addgene.org/plasmid-protocols/bacterial-transformation/.

(24) Sidhu, S. S.; Weiss, G. A. *Phage Display: A Practical Approach*; Lowman, H. B.; Clackson, T., Eds.; Oxford University Press: New York, 2004.

(25) Donavan, K. C.; Arter, J. A.; Weiss, G. A.; Penner, R. M. Virus-Poly(3,4-Ethylenedioxythiophene) Biocomposite Films. *Langmuir* **2012**, *28*, 12581–12587.

(26) Donavan, K. C.; Arter, J. A.; Pilolli, R.; Cioffi, N.; Weiss, G. A.; Penner, R. M. Virus-poly(3,4-Ethylenedioxythiophene) Composite Films for Impedance-Based Biosensing. *Anal. Chem.* **2011**, *83*, 2420–2424.

(27) Motulsky, H. J. Analyzing Data with GraphPad Prism, GraphPad Software Inc., San Diego CA http://www.graphpad.com.

(28) Welsh, L. C.; Symmons, M. F.; Sturtevant, J. M.; Marvin, D. A.; Perham, R. N. Structure of the Capsid of Pf3 Filamentous Phage Determined from X-Ray Fibre Diffraction Data at 3.1 A Resolution. *J. Mol. Biol.* **1998**, *283*, 155–177.

(29) Mohan, K.; Weiss, G. A. Dual Genetically Encoded Phage-Displayed Ligands. *Anal. Biochem.* **2014**, *453*, 1–3.

(30) Lamboy, J. A.; Tam, P. Y.; Lee, L. S.; Jackson, P. J.; Avrantinis, S. K.; Lee, H. J.; Corn, R. M.; Weiss, G. A. Chemical and Genetic Wrappers for Improved Phage and RNA Display. *ChemBioChem* **2008**, *9*, 2846–2852.

(31) Lamboy, J. A.; Arter, J. A.; Knopp, K. A.; Der, D.; Overstreet, C. M.; Palermo, E. F.; Urakami, H.; Yu, T.-B.; Tezgel, O.; Tew, G. N.; *et al.* Phage Wrapping with Cationic Polymers Eliminates Nonspecific Binding between M13 Phage and High pI Target Proteins. *J. Am. Chem. Soc.* **2009**, *131*, 16454–16460.

(32) Racaniello, V. Multiplicity of Infection http://www.virology.ws/2011/01/13/multiplicity-of-infection.

(33) Sharma, P. S.; Pietrzyk-Le, A.; D'Souza, F.; Kutner, W. Electrochemically Synthesized Polymers in Molecular Imprinting for Chemical Sensing. *Anal. Bioanal. Chem.* **2012**, *402*, 3177–3204.

(34) Hill, A. V. The Possible Effects of the Aggregation of Molecules of Hemoglobin on Its Dissociation Curve. *J. Physiol.* **1910**, *40*, 4–7.

CHAPTER 4

Engineering Chemically Modified Viruses for Prostate Cancer Cell Recognition

ABSTRACT

Specific detection of circulating tumor cells and characterization of their aggressiveness could improve cancer diagnostics and treatment. Metastasis results from such tumor cells, and causes the majority of cancer deaths. Chemically modified viruses could provide an inexpensive and efficient approach to detect tumor cells and quantitate their cell surface biomarkers. However, non-specific adhesion between the cell surface receptors and the virus surface presents a challenge. This report describes wrapping the virus surface with different PEG architectures, including as fusions to oligolysine, linkers, spacers and scaffolded ligands. The reported PEG wrappers can reduce by >75% the non-specific adhesion of phage to cell surfaces. Dynamic light scattering verified the non-covalent attachment by the reported wrappers as increased sizes of the virus particles. Further modifications resulted in specific detection of prostate cancer cells expressing PSMA, a key prostate cancer biomarker. The approach allowed quantification of PSMA levels on the cell surface, and could distinguish more aggressive forms of the disease.

Key reference: Kritika Mohan, Gregory A. Weiss. Engineering chemically modified viruses for prostate cancer cell recognition. *Mol BioSys*, **2015**, 11, 3264-3272.

INTRODUCTION

The migration and dissemination of tumor cells, termed metastasis, causes ≈90% of cancer deaths.[1,2] Metastasis requires loss of apoptotic regulation, and such cells respond poorly to conventional anti-cancer treatments. With a majority of the estimated 27,540 deaths from prostate cancer (PCa) in the US for 2015[3] resulting from metastasis,[2] new methods for efficient detection and characterization of metastatic cells could impact clinical care and patient prognosis. Previously, we reported the sensitive detection of soluble prostate-specific membrane antigen (PSMA), a PCa biomarker, at 100 pM concentrations using viruses incorporated into an electrically conductive polymer.[4] Here, we engineer similar bacteriophage, termed 'phage,' with polymers and ligands for direct binding to PSMA found on the surface of PCa cells.

PSMA, a 750 residue, 90 kD glycoprotein, is overexpressed on the surface of tumor cells as a non-covalent homodimer in both primary and metastatic cancers.[5,6] Differential splicing during tumorigenesis leads to expression of PSMA as a type II integral membrane protein.[7] Elevated PSMA levels have also been observed in seminal fluid and urine of PCa patients.[8] To detect the protein in urine, we reported viruses with both genetically displayed and chemically synthesized ligands for the sensitive detection of PSMA.[4,9] These ligands, selected from phage-displayed peptide libraries had the following amino acid sequences: ligand-**1** (CALCEFLG) and ligand-**2** (SECVEVFQNSCDW).

Genetically encoded, phage-displayed ligand-**2** binds with >100-fold higher affinity to PSMA than ligand-**1**.[4,10]

Used ubiquitously for molecular display applications, the M13 filamentous phage applied here infects *E. coli*, and can be manipulated to present genetically encoded peptides on the phage surface.[11–13] The M13 virus consists of a circular, single-stranded DNA genome surrounded by a protein coat composed of approximately 2700 copies of the major coat protein, P8, an α-helical protein of 50 amino acid residues with an unstructured *N*-terminus. One Glu and two Asp residues near the *N*-terminus of P8 impart a high negative charge to the outer surface of the virus at physiological pH.[14] Selections with phage-displayed libraries of peptides and proteins can target tissue-cultured cells and even organs in living organisms.[15–19] Phage have also been incorporated into nanomedicine platforms for targeted drug delivery[20–24] and imaging.[25,26] Such applications require low background binding by phage to cell surfaces.

Phage typically adhere to cell surfaces with high affinity. Such non-specific adhesion complicates the design of phage-based sensors for the detection of tumor cells; the non-specific background can reduce the signal to noise ratios and the ability to distinguish tumor from non-tumor cells. Francis and co-authors have reported covalently linking the coat proteins of fd phage with both polyethylene glycol (PEG) and imaging agents through a two step reaction.[27] M13 and fd phage are closely homologous with similar sizes, structural features and sequences.[28] An alternative approach described here, applies non-covalent

attachment to the phage surface to access additional architectures for biosensor applications.

Non-covalent attachment offers comparable stability to covalent modification of the virus surface. The high negative charge on the phage surface allows non-covalent wrapping with cationic peptides and polymers.[29,30] Linking these wrappers to recognition ligands opens new routes to greater sensitivity and specificity for target analytes. The peptide ligands can be chemically synthesized and fused to an oligolysine peptide (K_{14}), which wraps around the virus particle through complementary electrostatic interactions. Previously, this strategy allowed maximization of ligand density on the phage surface for sensitive detection of biomarkers in complex biofluids, such as synthetic urine.[4] Here, the overall design incorporates PEG polymers in conjunction with this wrapping strategy to address the problem of non-specific adhesion between phage and cells. Then, we optimize various architectures for the specific detection of PCa cells.

RESULTS AND DISCUSSION

4.1 Non-Specific Adhesion of Viruses to Cells

Among prostate cancer cell lines, LNCaP cells provide the most commonly used *in vitro* model for early stage PCa.[31,32] Derived from the lymph node adenocarcinoma of the human prostate, LNCaP expresses most of the important PCa biomarkers including PSMA, PSA and AR.[33] Attempts to recognize cell surfaces with conventional phage-displayed ligands resulted in unacceptably high, non-specific adhesion by control phage, which lack a displayed peptide. As shown by ELISA, phage-displayed PSMA ligand **2** and control phage produced similar high levels of binding to LNCaP cells, Figure 4-1. In this and essentially all ELISAs reported here, cells are immobilized on microtiter plates; phage are then added before washing away non-binding viruses, and levels of bound phage are quantified spectrophotometrically using an anti-M13 antibody conjugated to horse radish peroxidase (HRP), which catalyzes conversion of its substrate into a colored product. Thus, the high levels of adhesion by both ligand-displayed and control phage are due to non-specific adhesion between phage coat proteins and abundant cell surface receptors, glycans and other molecules. To overcome this non-specific adhesion, we focused on eliminating such interactions by control phage.

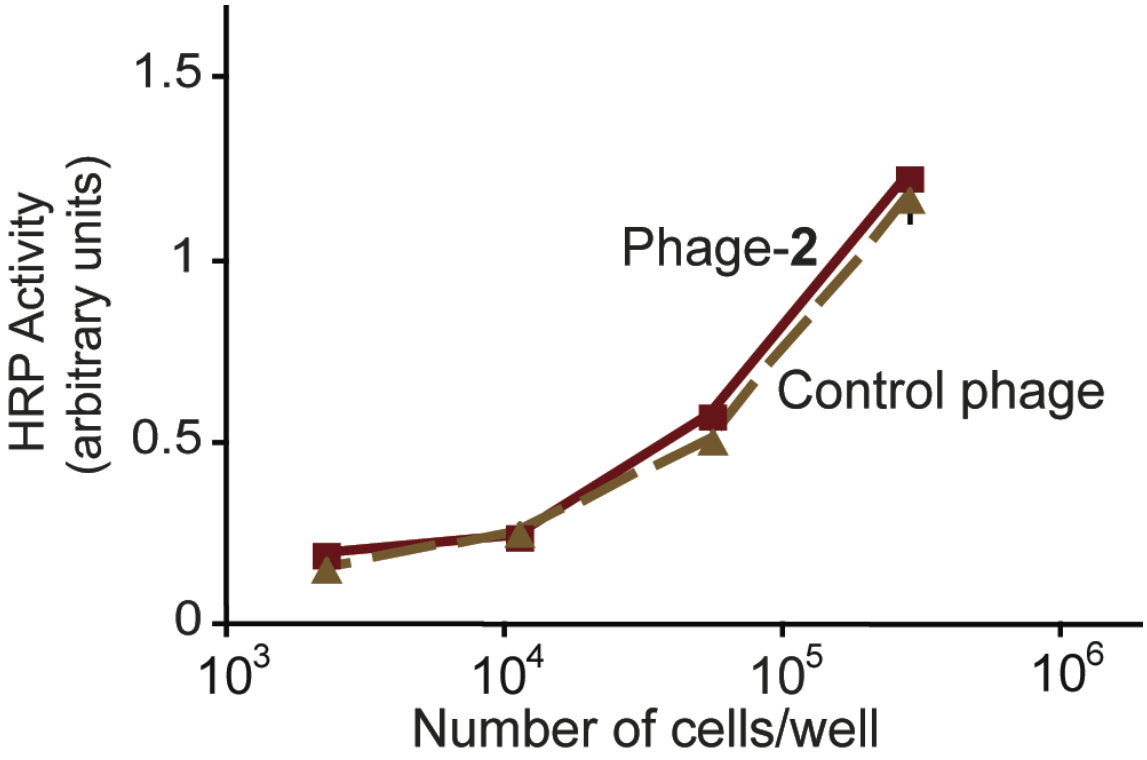

Figure 4-1. Phage-based ELISA demonstrating unacceptably high non-specific adhesion of phage to the surface of LNCaP cells. Phage-**2** display the PSMA ligand **2**. Control phage provides a negative control with no ligand displayed on the phage. Throughout this report, error bars for ELISA data represent standard error (n = 3). All experimental data points include such error bars, though often these are quite small.

4.2 Wrapping Phage with PEG to Prevent Non-Specific Adhesion

The water soluble polymer PEG is commonly bioconjugated to proteins to reduce non-specific adhesion to cells and other surfaces.[34–37] In addition, PEG can increase the solubility of attached therapeutic proteins, prolong circulation times, and decrease proteolysis.[38] Furthermore, the activities of proteins conjugated to PEG typically remain unaffected.[39,40] PEG has been shown to broadly adopt two distinct conformations – descriptively termed 'mushroom' and 'brush.'[34,41,42] The transition from the mushroom conformation, a more random orientation, to the brush conformation is dependent upon the polymer length and packing densities; longer PEG lengths and higher packing densities favor formation of the brush conformation. This transition can result in a significant drop in non-specific adsorption. In many systems, a mole fraction of 0.15 PEG-modified to -unmodified sites yields significantly reduced non-specific adhesion. High packing densities with such mole fractions can force the polymer to adopt a more stretched, and extended brush conformation to more effectively suppress non-specific adhesion.[34] To provide a framework for experimental design and data interpretation, the reported PEG polymers are assumed to form mushroom and brush conformations based on PEG lengths and packing densities, as has been reported previously.[34,41,42]

Initial attempts to block non-specific cell adhesion applied PEG variants with different MWs as phage wrappers. Azide-functionalized, polydispersed PEGs with size distributions centered around 7, 22 or 45 ethylene glycol units (providing average MWs of 300, 1K or 2K, respectively) were conjugated to K_{14}-alkyne using the Cu^{I}-catalyzed cycloaddition ('click') reaction, Figures 4-2 to 4-4. The conjugated peptides were then purified by reverse-phase HPLC and characterized by MALDI-TOF mass spectrometry. The relative adhesion levels of unwrapped and PEG-wrapped phage targeting immobilized LNCaP cells were compared by phage-based ELISA, Figure 4-5. Since the phage lacked a displayed peptide, adhesion could only result from non-specific interactions by the phage coat proteins.

In theory, phage wrapped with PEG should bind to LNCaP cells with much lower affinity due to decreased non-specific adhesion. However, no such reduction was observed for the different MW PEGs used, Figure 4-5. The ineffectiveness of this initial approach likely resulted from interaction between PEG and the K_{14} sidechains used to wrap the phage. A crown ether-like encapsulation can form between the primary amine of the Lys sidechains and ethylene glycols of PEG,[43] thereby could render K_{14} incapable of wrapping the phage surface. Without the PEG wrapping the phage surface, the results merely compare phage in different assay wells, as is evident from the overlapping responses. The lack of wrapping by PEGylated oligolysine was further verified by

dynamic light scattering measurements, which revealed no significant change in the cross-sectional diameter of the treated phage (data not shown).

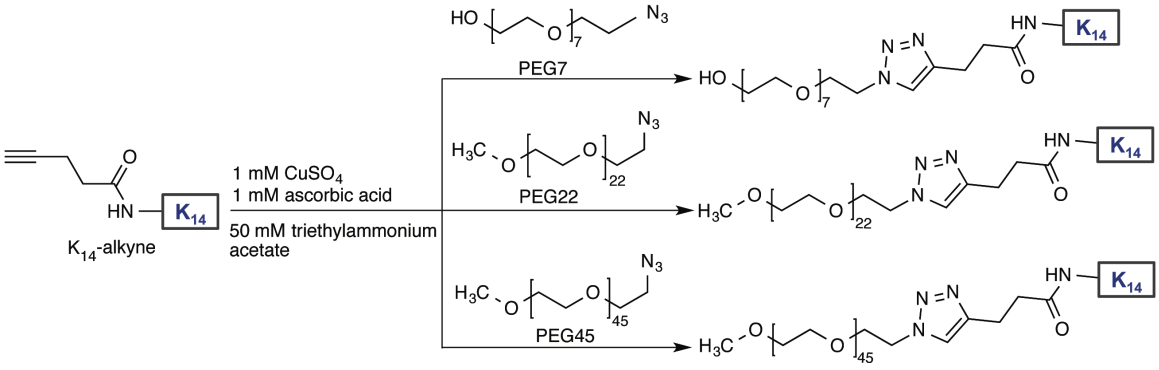

Figure 4-2. Cu^{I}-catalyzed azide-alkyne cycloaddition reaction for the generation of oligolysine-PEG wrappers.

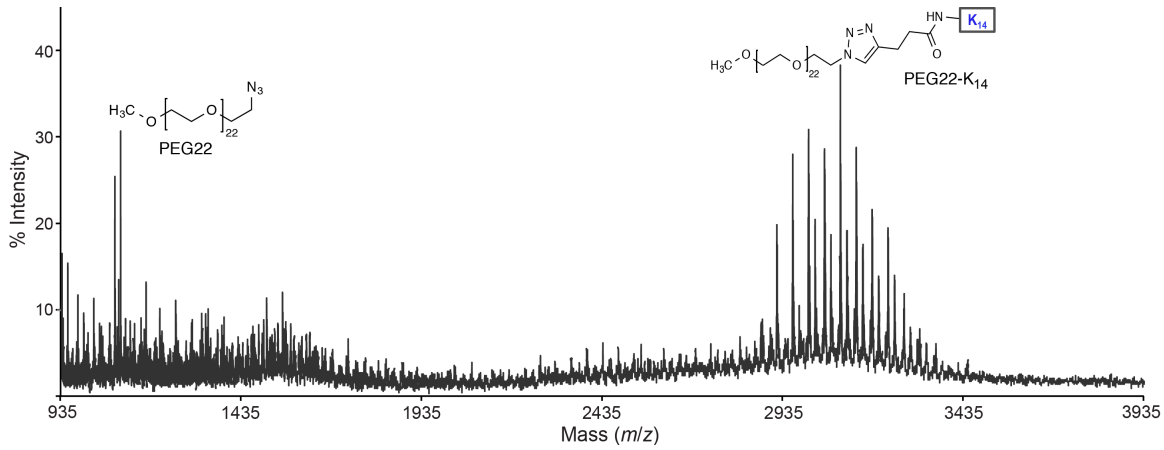

Figure 4-3. MALDI-TOF characterization of K_{14}-alkyne fused to azide-functionalized PEG22. The data obtained for PEGylated oligolysine showed a characteristic shift in the polydispersed PEG spectra by the expected mass of K_{14}-alkyne (1891.57).

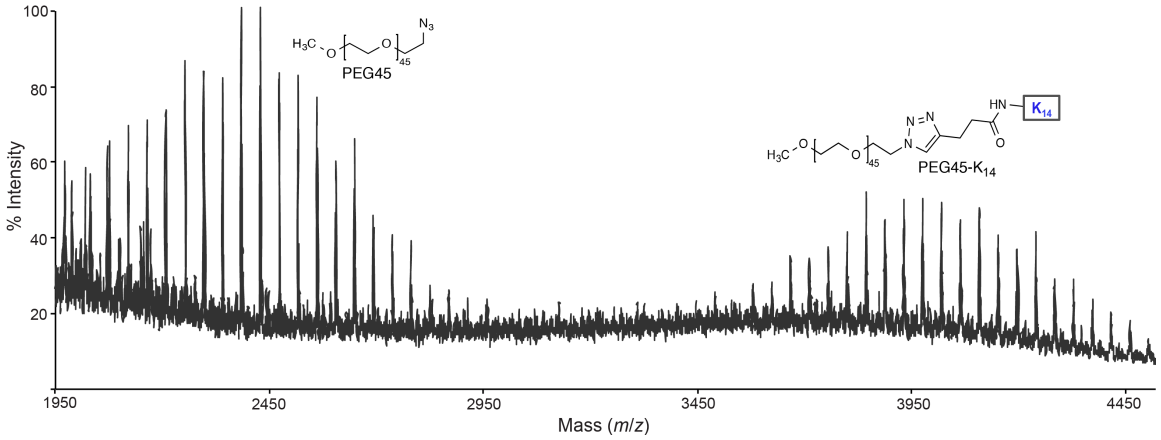

Figure 4-4. MALDI-TOF characterization of K_{14}-alkyne fused to azide-functionalized PEG45. The data obtained for PEGylated oligolysine showed a characteristic shift in the polydispersed PEG spectra by the expected mass of K_{14}-alkyne (1891.57).

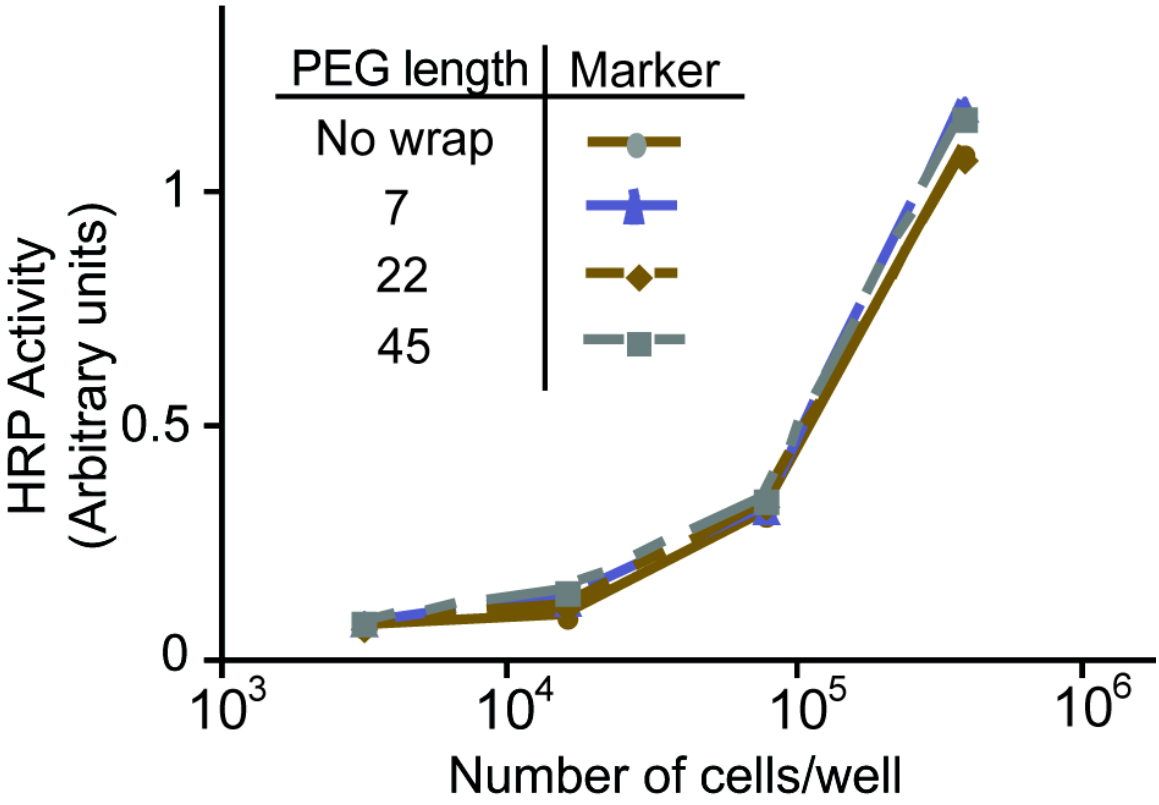

Figure 4-5. Phage-based ELISA demonstrating the ineffectiveness of wrapping phage with PEG polymers due to the encapsulation of oligolysine side chains. In this experiment, phage without wrapper and phage wrapped with PEG7, 22 or 45 at 5 μM concentrations were compared.

4.3 On-phage Cycloaddition Reaction to Generate PEGylated Phage

To overcome K_{14} encapsulation by PEG, phage with PEG wrappers were generated in two steps, Figure 4-6. First, phage were wrapped with K_{14}-alkyne by incubation at room temperature for 15 min. During this step, the K_{14}-alkyne wrap the phage prior to PEG conjugation. Next, PEG azides were added, and the cycloaddition reaction with the K_{14}-alkyne took place on the phage surface for 30 min. Next, the ELISA described for Figure 4-5 was repeated with these PEGylated phage comparing the non-specific adhesion of phage wrapped with different MW PEGs, Figure 4-7; in this experiment negative controls of 'No wrap' and 'No cells' indicate the extremes of high levels of non-specific adhesion to LNCaP cells and non-binding, respectively. Phage wrapped with PEG45 and PEG100 (average MW 2K and 5K, respectively) demonstrate a >75% reduction in non-specific binding to LNCaP cells, as demonstrated by the observed decrease in HRP activity resulting from lower phage binding. The experiment confirms that PEG wrappers can effectively suppress non-specific adhesion, provided the K_{14} wraps around the phage first. The reduction in non-specificity increases with larger MW PEG polymers, and saturates at around 45 ethylene glycol units.

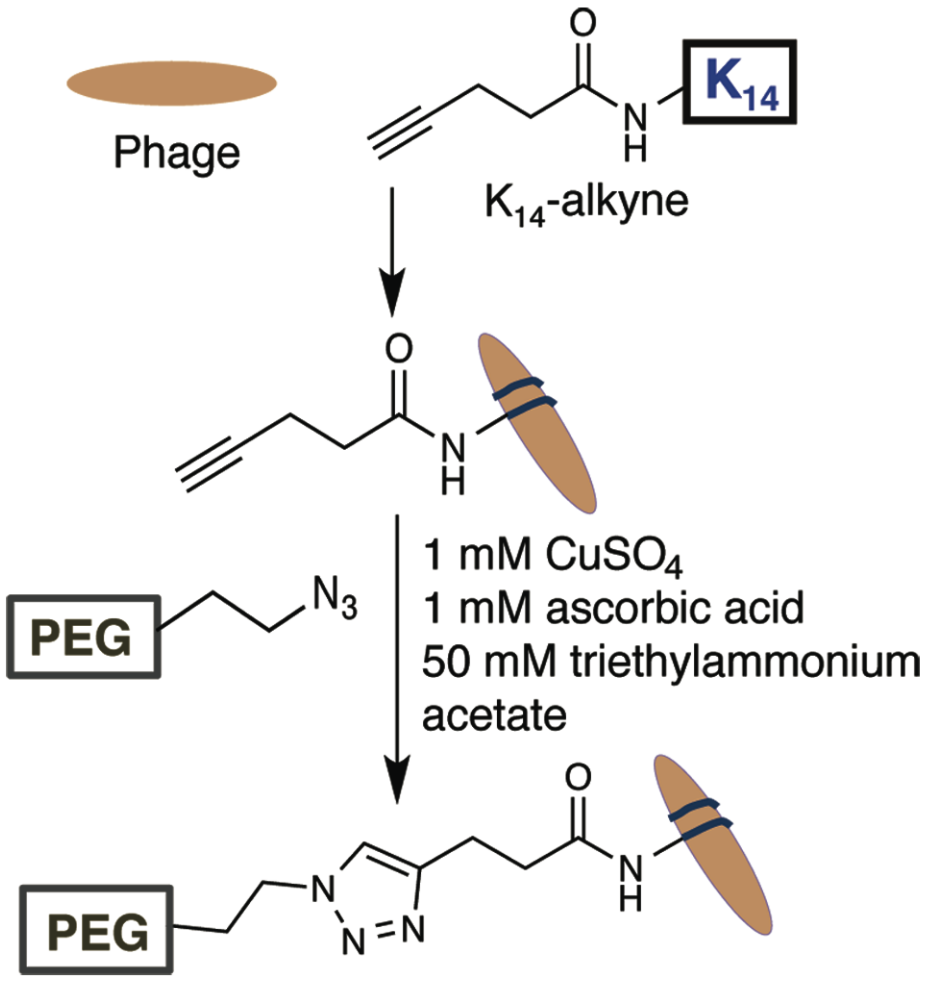

Figure 4-6. Schematic illustration of the on-phage cycloaddition reaction to bioconjugate PEG polymers to the phage surface. Phage are first wrapped with K_{14}-alkyne, and then conjugated to different lengths of azide-functionalized PEG polymers.

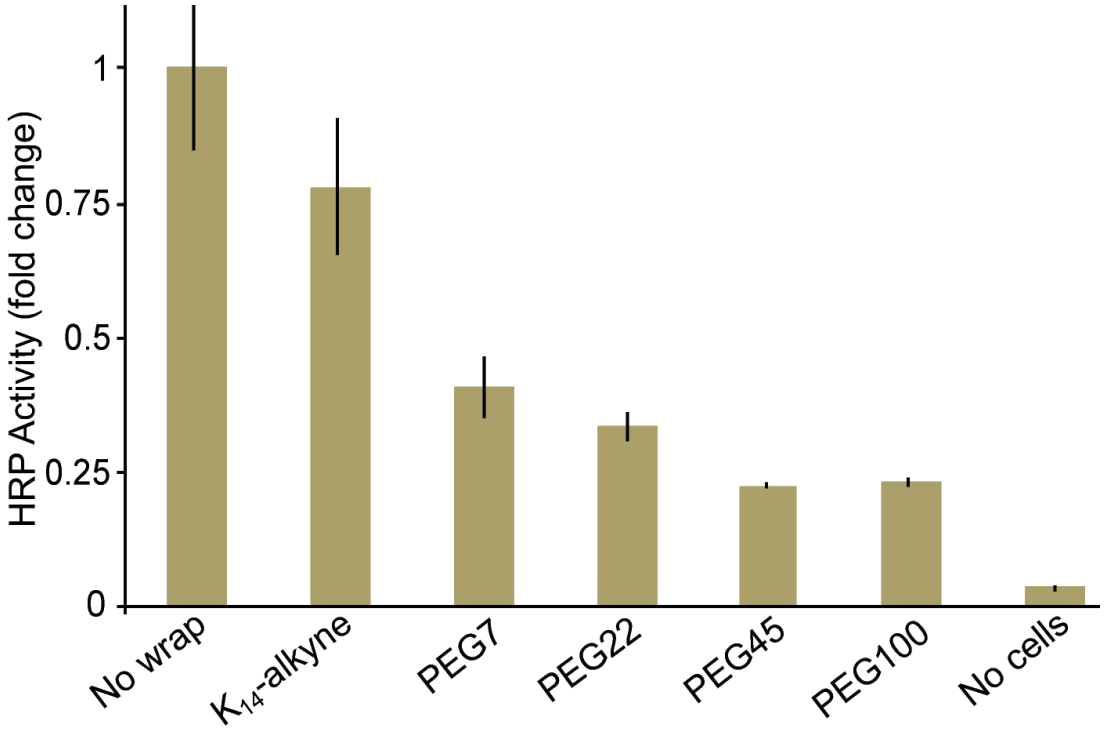

Figure 4-7. Phage-based ELISA demonstrating the effectiveness of wrapping phage by click chemistry with the indicated PEG azides to reduce non-specific adhesion to cellular surfaces. A >75% reduction in non-specific adhesion to LNCaP cells is observed for PEG45 compared to unwrapped phage. A lower HRP signal indicates decreased non-specific adhesion. Throughout this report, LNCaP cells are targeted at 4.5×10^6 cells/mL, and error bars for ELISA data represent standard error (n = 3). All experimental data points include such error bars, though often these are quite small. The p-value is <0.01 for all data reported here.

PEG reduces non-specific binding largely by surrounding the attached surface with a hydration sphere.[44] Direct contact to the phage surface, termed primary adsorption, requires smaller non-specific binding partners to penetrate the PEG layer. Alternatively, the non-specific binding partners could adhere to the outer surface of the PEG layer, termed secondary adsorption. For non-specific adhesion to the larger surfaces of cells, such secondary adsorption is likely a more pronounced effect. To minimize secondary adsorption, the wrappers were applied at 0.15 mole fraction.[34] Here, we estimate the mole fraction as the stoichiometry of PEG molecules added to P8 coat proteins; this analysis is analogous to the calculations for PEG grafted in lipid membranes.[45] Additionally, we assumed that at the concentration used, PEG22, 45 and 100 adopt brush conformations due to their high packing densities,[34,41] which were fixed by maximization of oligolysine wrappers as previously described.[4]

Based on published precedent, PEG7 presumably adopts a mushroom conformation,[34] and fails to suppress non-specific adhesion to the same levels. The brush conformation of the larger PEGs can more efficiently reduce non-specific secondary adsorption due to the hydration sphere extending further from the virus surface. Beyond a certain height of the polymer brush, the effect of secondary adsorption remains constant as shown by the nominal difference obtained between PEG45 and 100 in Figure 6-7. For ligand-based recognition described further below, phage wrapped with PEG45 provided the negative control phage.

4.4 Dynamic Light Scattering (DLS) Analysis of PEGylation

To characterize the PEG-wrapped phage, DLS measurements were conducted, Figure 4-8. The M13 phage used here have dimensions of approximately 6 by 1000 nm.[46] Rayleigh scattering provides an estimated 45.9 nm diameter of the average cross-section; this experiment uses measurement with backscatter mode, having a scattering angle of 173°, for unwrapped and unmodified phage. For comparison, the comparable reported measurement with covalently and genetically modified fd phage yielded a reported average cross-sectional diameter of 70 nm.[47] Due to the filamentous nature of the phage as a long, flexible cylinder, such values can only provide a relative change in size. Furthermore, the forward scatter mode (scattering angle of 13°) provides a 715 nm average size for the M13 phage applied here, which compares well with previously reported 650 nm average size for fd phage.[47] Since the phage length remains roughly unchanged with wrapping, we found negligible difference in the average phage sizes measured by forward scattering, and instead focused on DLS measurement in backscatter mode.

Next, the change in average cross-sectional diameter was measured for different samples from each step of the phage wrapping process, Figure 4-8A. The addition of K_{14}-Cys wrappers on the phage leads to an increase in cross-sectional diameter from 45.9 to 50.0 nm. Upon conjugation of this K_{14}-Cys wrapped phage to maleimide-functionalized PEG100, an approximate 10 nm increase in size is observed. This increase in size matches two independent

reports for size increases after PEG100 bioconjugation to gold nanoparticles.[48,49] Thus, the DLS-based size measurements confirm the formation of the expected phage-wrapped complexes.

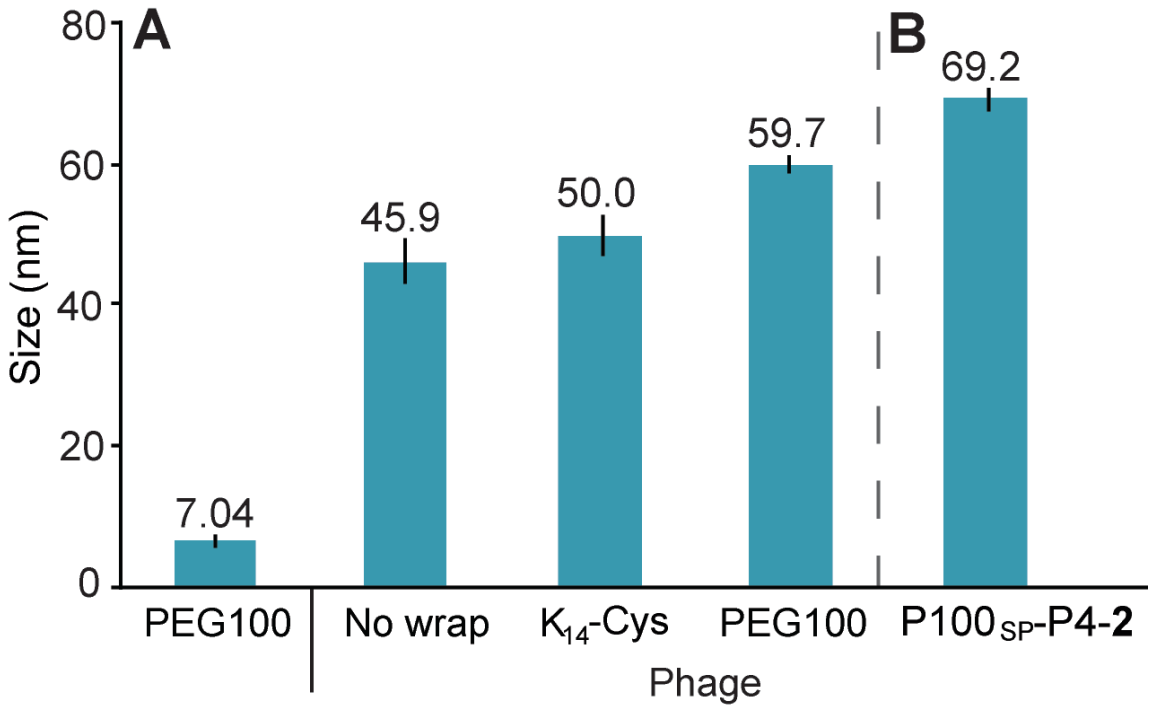

Figure 4-8. Dynamic light scattering measurements indicate the consistent increase in size with the addition of wrappers on phage. Labels indicate the measured average size in nm for each indicated phage. Error bars represent standard error (n=3), with each individual size measurement being the average of ten runs.

4.5 Synthesis of PEGylated Ligands

Towards the goal of specific recognition of a cell surface receptor, different scaffolds for the display of ligands on phage were explored. First, heterobifunctional PEG, Mal-PEG-NH_2, provided reactive groups for selective attachment of oligolysine at the maleimide end and PSMA binding ligands to the amine end, Scheme 4-1. As the scaffold, PEG100 was chosen to provide a longer polymer brush to reduce non-specific secondary adsorption. Azide-functionalized PSMA ligands **1** and **2** were synthesized by conventional solid-phase peptide synthesis (SPPS), and coupled to pentynoic acid via the click reaction. The resultant *N*-terminal carboxylic acid group was then coupled to Mal-PEG100-NH_2 using HBTU as an amide bond forming agent in water. Since this reaction non-specifically couples amine and carboxylate functionalities, the attachment sites could vary as both ligands have sidechain carboxylic acids. The resultant ligand is termed $P100_{NSP}$-**1/2** for 'PEG100, non-specific attachment to ligand **1** or **2.**' as described in Table 4-1.

Subsequently, phage wrapped with K_{14}-Cys were coupled to the maleimide terminus of $P100_{NSP}$-**1/2**, as described above. Preliminary validation of binding to cell surface PSMA by the PEGylated ligand wrappers was performed by phage ELISA as before, Figure 4-9. Compared to the non-specific binding observed in Figure 4-1, a slight improvement in binding affinity resulted from wrapping with the PEGylated ligands. This modest result provided a starting point for further engineering. Phage wrapped with $P100_{NSP}$-**2** displayed a higher affinity

for LNCaP cells compared to $P100_{NSP}$-**1** as expected from its higher binding affinity for PSMA.

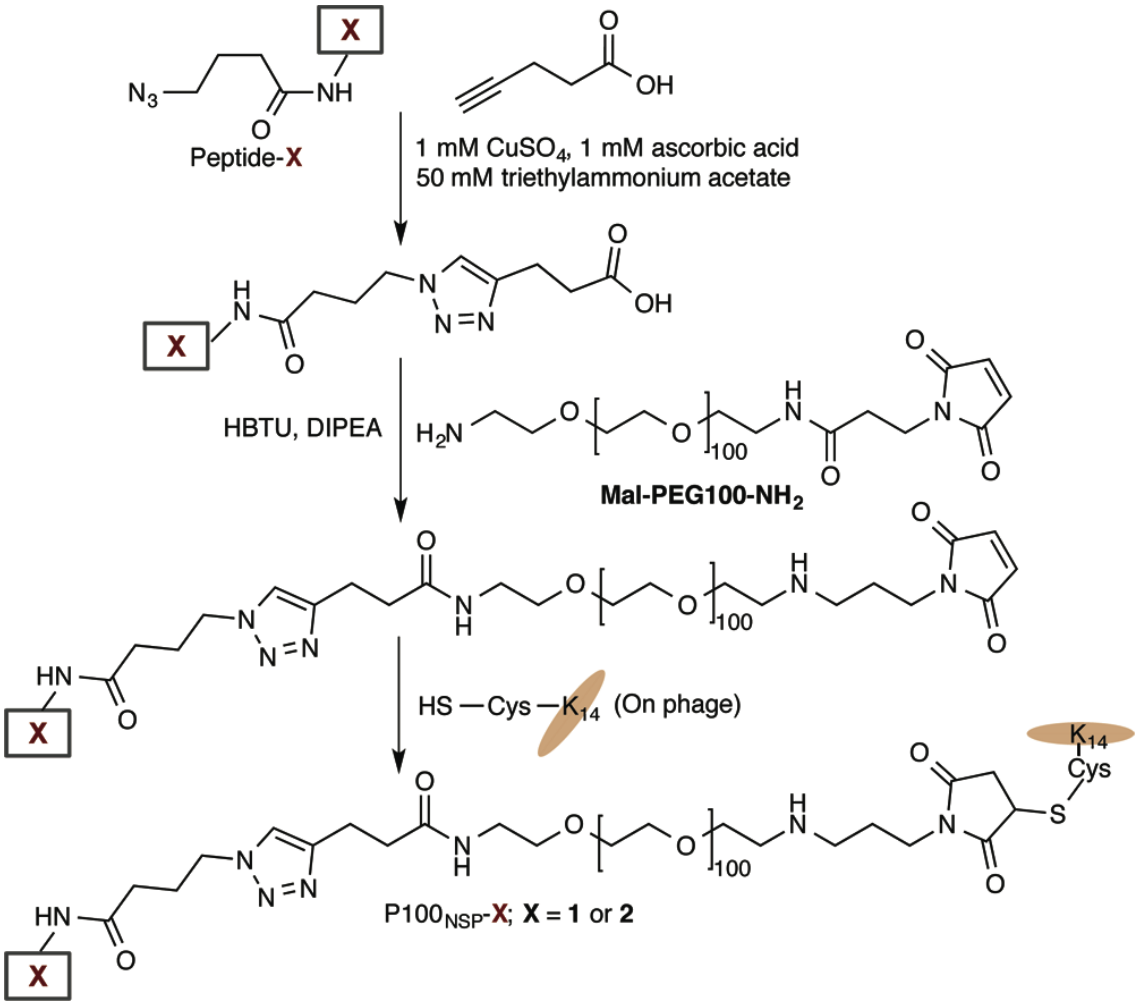

Scheme 4-1. Synthesis scheme for the generation of PEGylated ligands on phage for the selective detection of PSMA on LNCaP cells. **X** indicates the PSMA binding ligands **1** or **2**.

PEG length	Attachment SP:specfic NSP:Non-specific	PEG4 linker	Nomenclature
P100	NSP	—	$P100_{NSP}$-**X**
P100	SP	—	$P100_{SP}$-**X**
P100	NSP	✓	$P100_{NSP}$-P4-**X**
P100	SP	✓	$P100_{SP}$-P4-**X**

X = ligand **1** (CALCEFLG) or **2** (SECVEVFQNSCDW)

Table 4-1. Nomenclature of PEGylated PSMA ligands. All ligands were bioconjugated to phage wrapped with K_{14}-Cys.

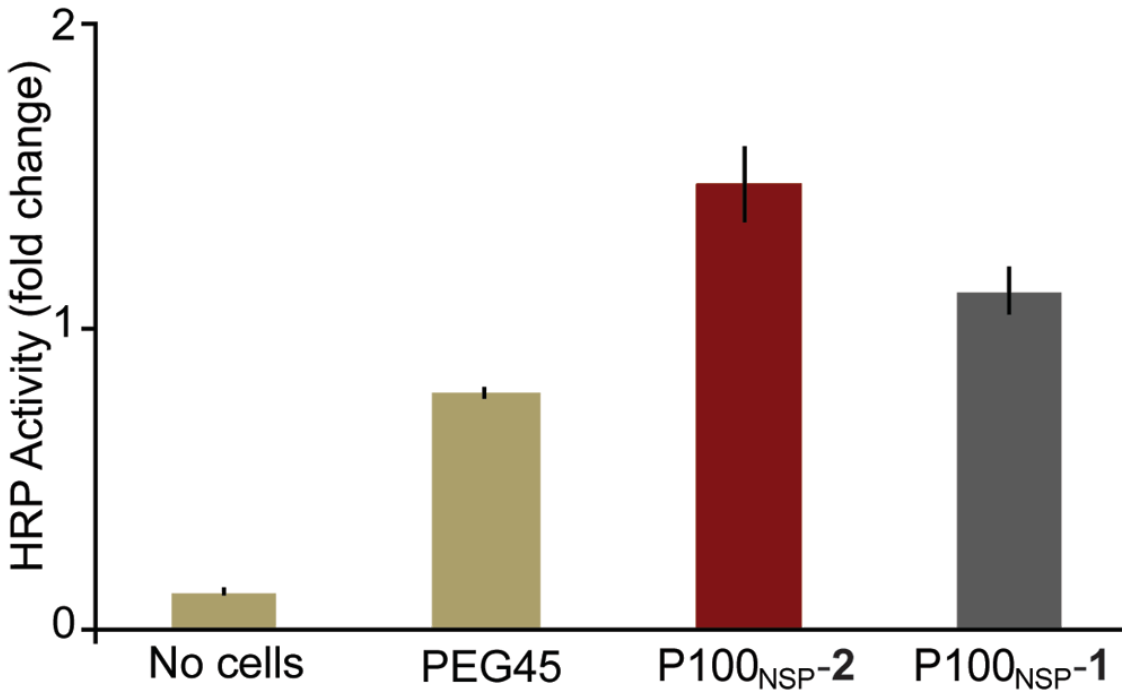

Figure 4-9. Phage-based ELISA illustrates a modest increase in binding affinity using PEGylated ligands on phage targeting LNCaP cells. PEGylated ligands on phage were further engineered for higher affinity recognition.

4.6 Bidentate Binding Mode of PEGylated Ligands

Dual display of ligands **1** and **2** can enable synergistic, high affinity binding to PSMA due to a bidentate binding mode and a velcro-like avidity effect.[4] A phage ELISA targeting LNCaP cells with different ratios of the two PEGylated, phage-wrapped ligands examined relative binding affinities. First, the effectiveness of the bidentate binding mode (red in Figure 4-10) was compared to binding by individual ligands (patterned red bars in Figure 4-10). Having two ligands on the phage surface consistently improved binding affinity. Furthermore, a 2:1 mixture of $P100_{NSP}$-**2** and $P100_{NSP}$-**1** respectively, was found to maximize the recognition of PSMA on LNCaP cells. The improved binding from a 2:1 ratio stems from the higher binding affinity of ligand **2** compared to ligand **1**. Altering this ratio in either direction drops the apparent affinity, likely due to loss of optimal bidentate binding. Hereafter, phage were wrapped with a 2:1 mixture of the PEGylated ligands **2** and **1**, respectively.

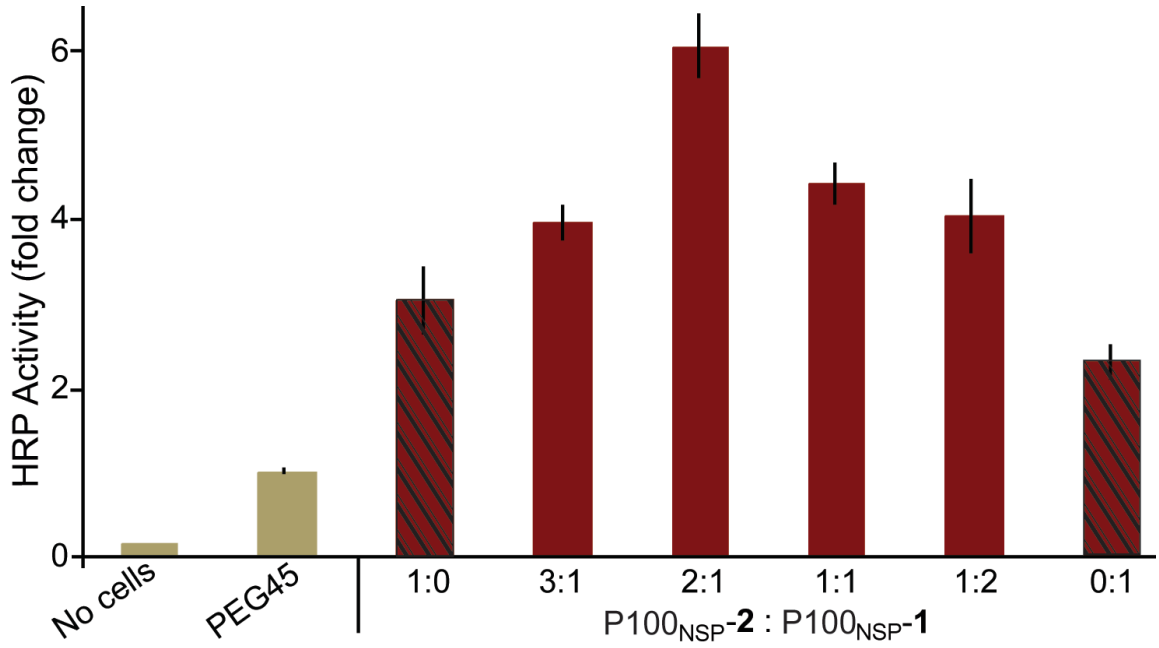

Figure 4-10. Phage-based ELISA demonstrating the effectiveness of the bidentate binding mode for the two PSMA binding ligands on the phage surface. A higher HRP activity indicates stronger binding affinity between the displayed ligands and PSMA on the cell surface. The various ratios of wrapped ligands (red bars) can be compared with wrapping by individual ligands (patterned red bars). A 1:1 ratio of the two ligands indicates the assay of equimolar amounts of each ligand. Negative controls (gold bars) were as previously described. The p-value is <0.01 for all data reported here.

4.7 Optimizing the Attachment Site for PEGylated Ligands

Further optimization explored the size, geometry and attachment site of the ligands fused to the PEG wrapper. Such variables can be crucial to the pharmacokinetic properties of PEGylated drugs, which demonstrates the sensitivity of biological recognition to such factors.[50] For example, the attachment sites of the peptide ligand to PEG100 dictates the ligand orientation and the potential availability of peptide sidechains. An alternative synthesis scheme was designed to control ligand orientation. Mal-PEG100-NH_2 was first coupled to pentynoic acid, Scheme 4-2. The resultant Mal-PEG100-alkyne was then coupled to the azide-functionalized peptide ligands using click chemistry, providing a specific site of attachment to the ligand. The resulting PEGylated ligand is termed $P100_{SP}$-**1/2** for 'PEG100, specific attachment to ligand **1** or **2**,' as described in Table 4-1.

Specific attachment of PEG to the wrapped ligands could improve binding affinity by removing attachment through the ligands' sidechains and also altering their orientation on the phage surface. The significance of ligand orientation is apparent through the higher binding affinity observed for genetically encoded, phage-displayed ligand **2** (dashed red line) relative to phage wrapped with chemically synthesized ligand **2** (solid red line), Figure 4-11. When genetically displayed on the phage, ligand **2** has a free *N*-terminus, but the synthesis of $P100_{SP}$-**2** inverts this orientation, leaving a free *C*-terminus, and an *N*-terminus directly conjugated to the triazole and then PEG100 (as shown in the schematic

flowchart of Fig. S9). As attained by the specific attachment of $P100_{SP}$-**2**, the *N*-terminal Glu residue of ligand **2** requires an unhindered and unmodified carboxylate sidechain, as previously shown by homolog shotgun scanning.[10] The sidechain of Glu2 could be partially modified in $P100_{NSP}$-**2** due to non-specific attachment through the carboxylate sidechain. Subsequent experiments compared bioconjugation to either the *N*-terminal azide or carboxylate sidechain through incorporation of an additional linker.

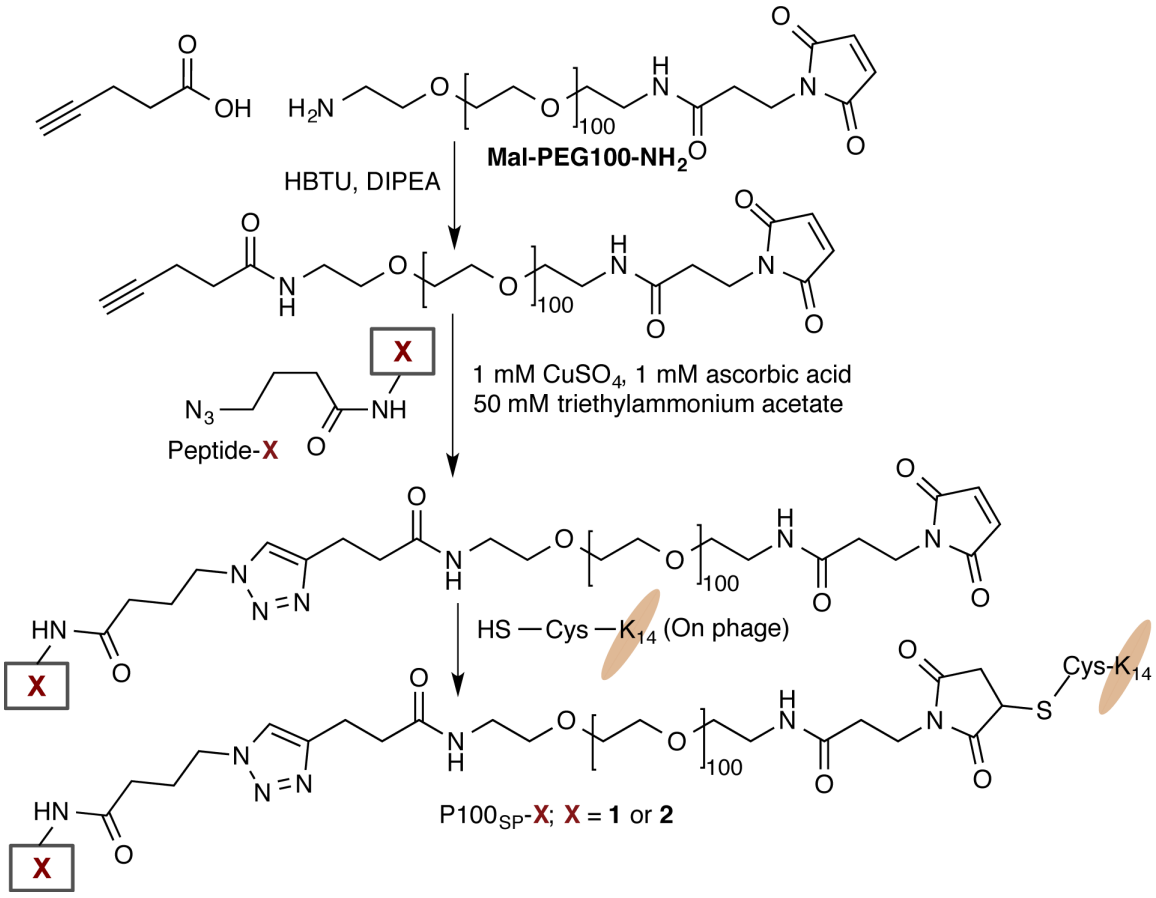

Scheme 4-2. Synthesis scheme for the generation of PEGylated ligands on phage through the specific attachment mode.

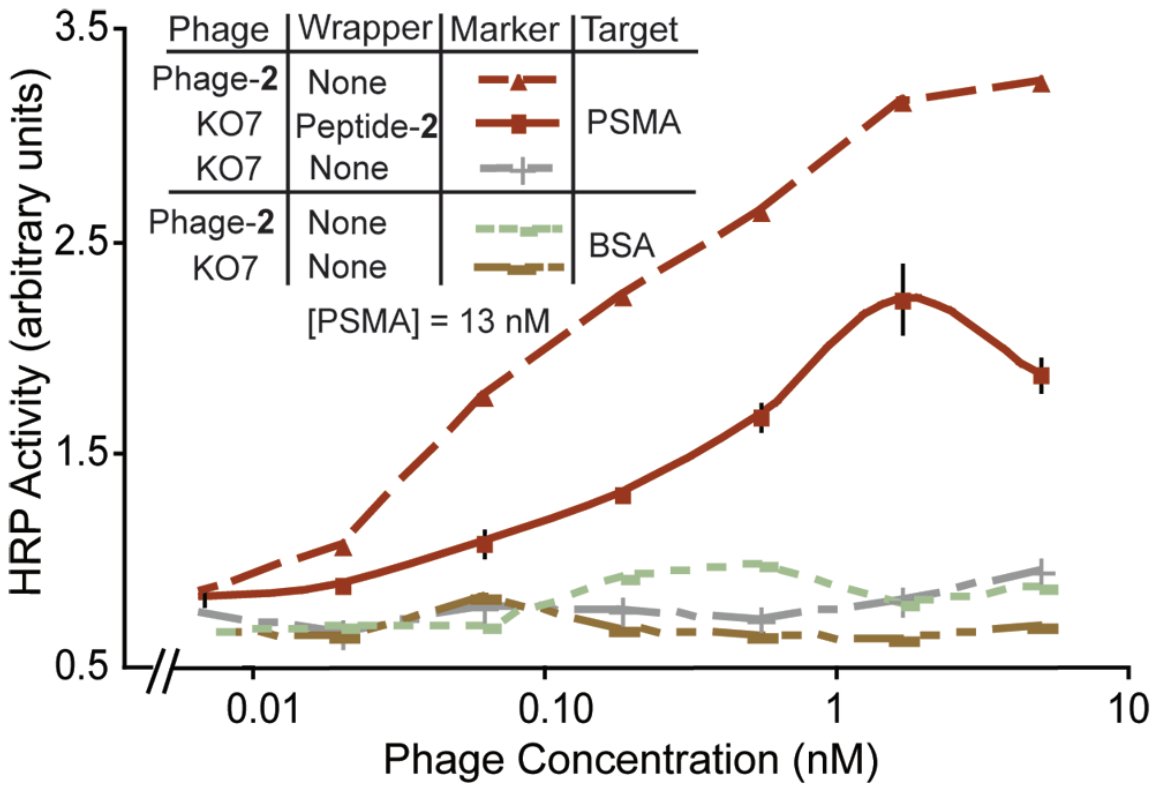

Figure 4-11. Phage-based ELISA demonstrating the significance of the free *N*-terminus of peptide-**2** for PSMA binding as shown by the higher affinity of phage-displayed peptide-**2**. Synthesis and wrapping of oligolysine-peptide-**2** leads to the inversion of geometry providing a free *C*-terminus.

4.8 Insertion of a PEG4 Linker to Reduce Steric Effects on the Attached Ligands

Heterobifunctional linkers between PEG and a molecule of interest can enhance activity through flexible additional spacing.[44] We envisioned the incorporation of an average 175 MW PEG4 linker between the peptide ligand and the triazole generated by the click reaction could enhance the binding affinity of the peptide ligands. With only four ethylene glycol units, this highly flexible linker can disconnect the peptide ligand from any steric constraints dictated by PEG100 or the triazole, Figure 4-12. Thus, the peptide ligands were resynthesized via SPPS, and coupled to azido-PEG4-carboxylic acid (15-Azido-4,7,10,13-tetraoxapentadecanoic acid), thereby inserting a PEG4 linker before the azide functionality. Azido-PEG4-ligands were further linked to PEG100 following the two synthesis routes described above, specific and non-specific addition. The resultant PEGylated ligands are termed $P100_{SP}$-P4-**1/2** and $P100_{NSP}$-P4-**1/2**, P4 to indicate the insertion of the PEG4 linker, Table 4-1.

The $P100_{SP}$-P4-**1** and $P100_{SP}$-P4-**2** conjugated peptides were shown to have the expected sizes by gel permeation chromatography (GPC) and DLS. The commercially purchased, unmodified Mal-PEG100-NH_2 was found to have an average molecular weight of Mn = 3690, and this polymer eluted as a broad peak consistent with its size distribution. The calculated molecular weights for PEGylated-**1** and -**2** with the PEG4 linker, based on the molecular weight of Mal-

PEG100-NH_2, were estimated as 5300 and 5990, respectively. The corresponding molecular weights observed by GPC were 5310 and 6060, respectively. And, a further increase of 10 nm in cross-sectional diameter was observed for the addition of the PEG4-fused ligand by DLS (Figure 4-8).

An ELISA compared the relative binding affinities of the four PEGylated ligand **2** variants – specific (solid) and non-specific (patterned) attachment with and without the PEG4 linker, Figure 4-13A. $P100_{SP}$-**2** demonstrates a higher binding affinity for cell surface PSMA than $P100_{NSP}$-**2**, illustrating the significance of the unmodified Glu sidechain obtained through specific attachment. Furthermore, inclusion of the PEG4 linker further enhances the binding affinity for both $P100_{SP}$-**2** and $P100_{NSP}$-**2**. As a result, the PEGylated ligand $P100_{SP}$-P4-**2** incorporating the PEG4 linker with specific attachment site provided the most effective architecture for the PEGylated ligand to recognize PSMA on the cell surface.

The dual ligand combinations of peptides **1** and **2** were expected to further provide higher affinity through bidentate binding. However, only a modest improvement was observed for the combination of $P100_{NSP}$-**2 +** $P100_{NSP}$-**1** versus the best individual ligand, $P100_{SP}$-P4-**2**, Figure 4-13B. The slightly greater binding affinity can be attributed to the bidentate binding mode of the dual ligand system. Furthermore, the architecture of the PEG4 (P4) linker also required optimization. The geometry of the PEG4 linker clearly affects the availability of the two Lys sidechains in the 8-mer peptide **1**, as shown by the drop in affinity for

$P100_{NSP}$-P4-**2** **+** $P100_{NSP}$-P4-**1**. This reduction in apparent binding affinity could be due to the formation of a crown ether-like cavity by PEG4, which naturally adopts a mushroom-like conformation based on its size.[34] Furthermore, the combination has affinity equivalent to $P100_{NSP}$-P4-**2**, which indicates complete loss of ligand **1** activity by PEG4 masking; this effect renders the dual ligand combination of $P100_{NSP}$-P4-**2** **+** $P100_{NSP}$-P4-**1** equivalent to the individual ligand, $P100_{NSP}$-P4-**2**. Notably, ligand **2** lacks Lys residues, and is therefore not susceptible to such masking effects.

Controlling the geometry of the PEG4 linker could prevent masking of the Lys sidechains of ligand **1**. Sandwiching PEG4 between PEG100 and the peptide ligand through the specific attachment mode, eliminates such debilitating effects, as shown by a significant increase in binding affinity for the dual ligand system $P100_{SP}$-P4-**2** **+** $P100_{SP}$-P4-**1** (Figure 4-12, 4-13B). This specific attachment incorporating the PEG4 linker evidently stretches the PEG4 providing higher apparent affinity from a constitutional isomer with different geometry. Thus, in the next experiments, phage were wrapped with the dual ligand combination of $P100_{SP}$-P4-**2** **+** $P100_{SP}$-P4-**1** in a 2:1 ratio.

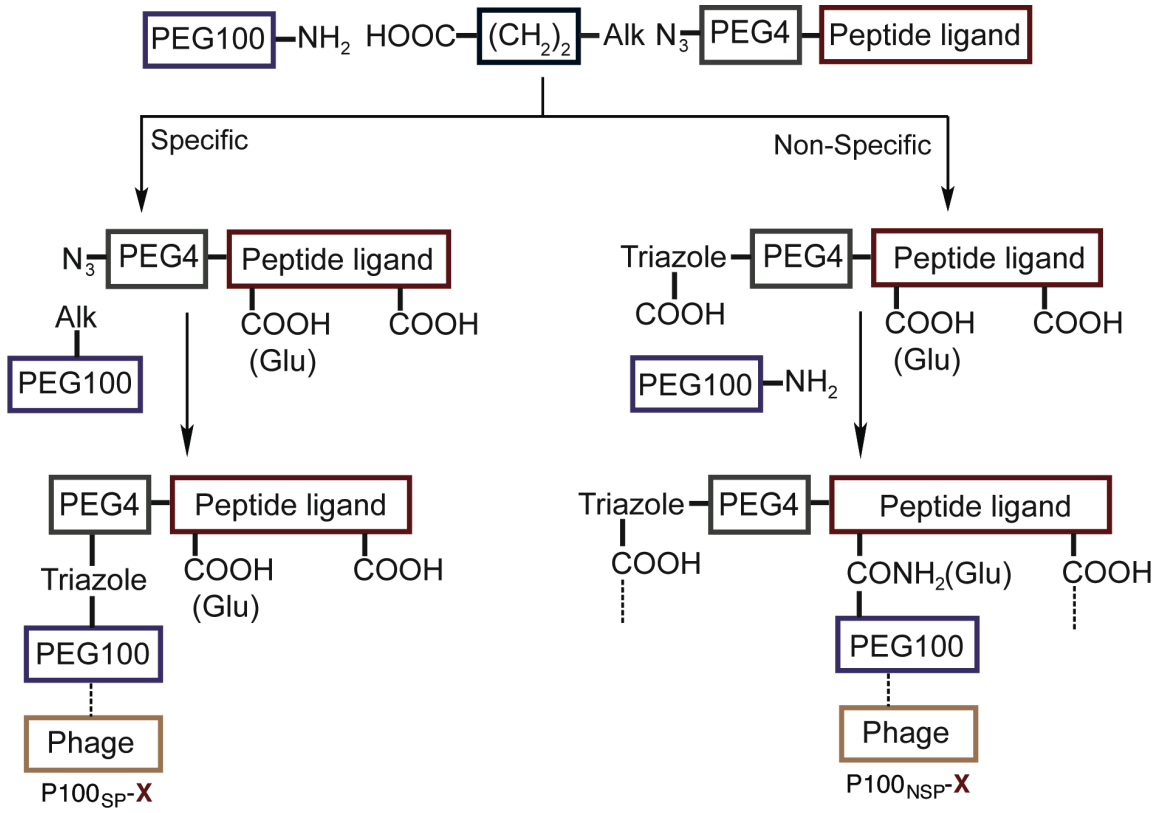

Figure 4-12. Schematic representation of the two constitutional isomers of P100-P4-**X**. The differences between the products obtained through the specific attachment mode (left) and the non-specific attachment mode (right) are illustrated. The non-specific attachment mode leads to partially modified Glu sidechains, along with a flexible PEG4 linker. In contrast, the specific attachment mode provides the free Glu side chain with a sandwiched PEG4 linker. The abbreviation 'Alk' in this schematic represents the alkyne group, whereas the dashed lines indicate possible attachment sites for PEG100-NH_2.

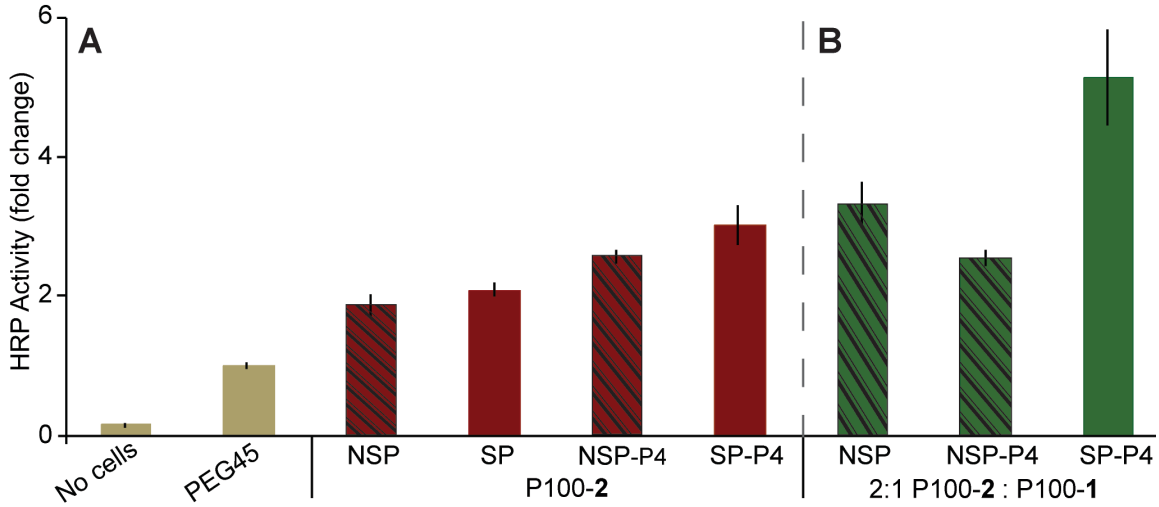

Figure 4-13. (A) Phage-based ELISA comparing the different attachment modes with the incorporation of a PEG4 linker for PEGylated ligand **2** (red bars) targeting PSMA on LNCaP cells. Patterned bars indicate non-specific (NSP) attachment modes. (B) The combination of ligands **1** and **2** (green bars) leads to increased affinity due to the chelate-based avidity effect. The p-value is <0.01 for all data reported here.

4.9 PEG Spacers to Control Relative Ligand Spacing

The relative spacing between ligands governs the synergy of the chelate-based avidity effect. To achieve optimal geometry of the two ligands, the relative spacing was systematically engineered by interspersing long PEGylated ligands with smaller PEG wrappers on the phage surface. The smaller PEG wrappers could provide spacers to push apart the PEG-fused ligands on the phage surface. Generating ligands and spacers required the two wrapping modes described above, click chemistry and cysteine-maleimide reaction, on the same phage. K_{14}-alkyne and K_{14}-Cys were pre-mixed to an estimated mole fraction of 0.19 (as described above), and then used to wrap the phage surface. K_{14}-alkyne was linked to short PEG polymers to provide spacers. Different concentrations of the PEG polymers were explored. The ratio of ligands to spacers was empirically optimized, and a ratio of 1.5:1 provided the best levels of PSMA recognition (data not shown). The concentration of the PEGylated ligands remained unchanged, and a 2:1 molar mixture of the two ligands was reacted with the K_{14}-Cys wrapped on the phage surface. A higher net concentration of wrappers could be accommodated by the phage as the spacers allowed higher packing density.

The dual PSMA ligand combination described above, $P100_{SP}$-P4-**2** + $P100_{SP}$-P4-**1**, without (green) or with spacers (brown) of either PEG 7, 22 or 45, wrapped around the phage were assayed for binding to LNCaP cells, Figure 4-14. All spacers significantly enhanced PSMA recognition by the displayed ligands. However, the PEG7 spacer proved most effective. The much smaller

PEG7 spacer can force the ligands into adopting a more optimal geometry for effective bidentate binding, and the height of this polymer brush does not interfere with ligand binding. Longer spacers failed to boost binding affinity to the same levels. At the mole fraction of PEG used, the PEG polymers can adopt the brush conformation with the height of the polymer brush dependent on the PEG length. Interdigitation of PEG spacers with PEGylated ligands can interfere with the binding affinity of the ligands, as shown with the longer brushes of PEG22 and 45. Also, the addition of K_{14}-alkyne without conjugated PEG spacers has no effect on binding affinity, as expected; thus, the increased packing of oligolysine wrappers is not a contributing factor. Rather, enhanced binding results from the improved geometry through addition of PEG spacers.

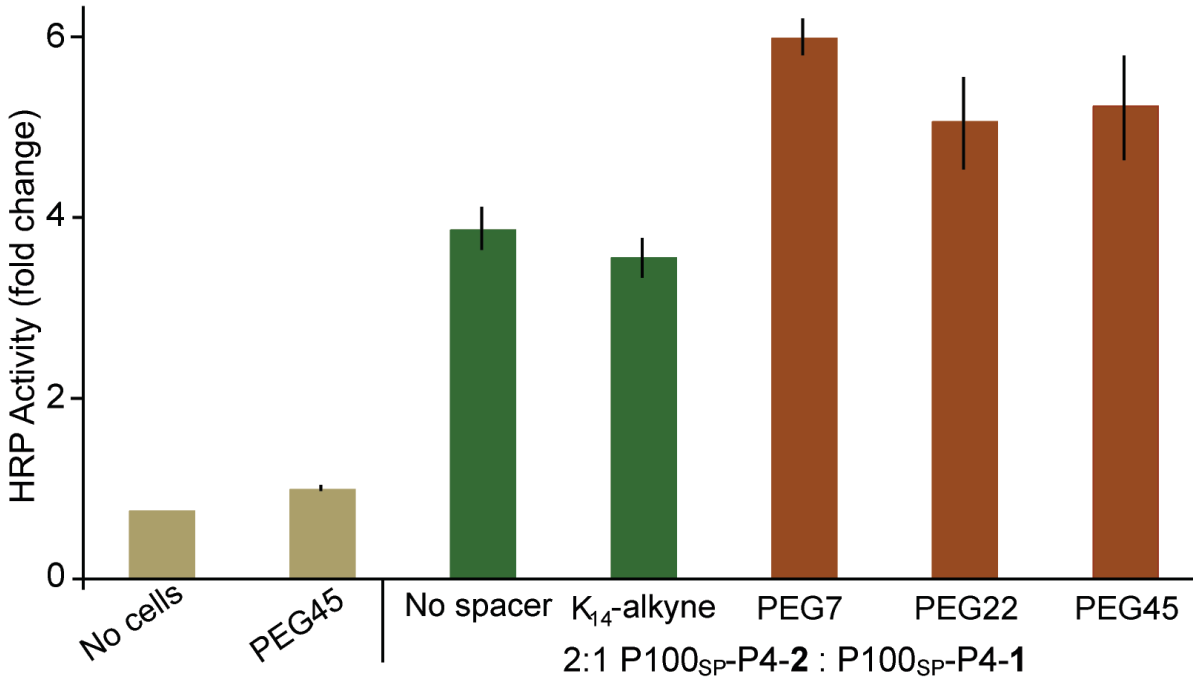

Figure 4-14. Phage-based ELISA demonstrates the effect of smaller PEG polymers applied as spacers to optimize the geometry of the PEGylated dual ligand combination of $P100_{SP}$-P4-**2** + $P100_{SP}$-P4-**1**. The dual ligand combination on phage was assayed with (brown) and without (green) PEG spacers. The p-value is <0.01 for all data reported here.

4.10 Selective Recognition of PSMA Positive Cells

To demonstrate specificity for PCa cells by these chemically modified phage, binding to different prostate cancer cell lines was compared. LNCaP cells can model early or late stage cancer cells, through variation in their culture conditions. The majority of PCa cases gain resistance to therapies based on androgen ablation.[51] The LNCaP cell line, a model for early stage PCa, is androgen sensitive but gradually loses the androgen requirement, providing a model for late stage PCa, which also mimics androgen ablation.[51,52] The latter can be simulated by culturing LNCaP cells in androgen-depleted media, referred to as LNCaP CSS (for charcoal-stripped serum).[53,54] Increased levels of PSMA are associated with androgen independent PCa.[52] Thus, both LNCaP and LNCaP CSS cell lines were assayed. The third cell line, PC3 cells, do not express PSMA, and were used as the negative control.[33,55] The following assays validate the dual ligand system for cell line discrimination and quantification of cell surface receptors.

The optimized dual ligand combination of $P100_{SP}$-P4-**2** + $P100_{SP}$-P4-**1** and the PEG7 spacer was assayed for binding to LNCaP (red), LNCaP CSS (blue), and PC3 cell lines (gold), Figure 4-15. The results demonstrate high specificity for PSMA positive LNCaP cells in a dose-dependent manner with higher apparent affinity to LNCaP CSS cells. This higher sensitivity to LNCaP CSS cells is consistent with the increase in PSMA expression resulting from the

progression of the cancer cells to an androgen independent state in the LNCaP CSS model.[52]

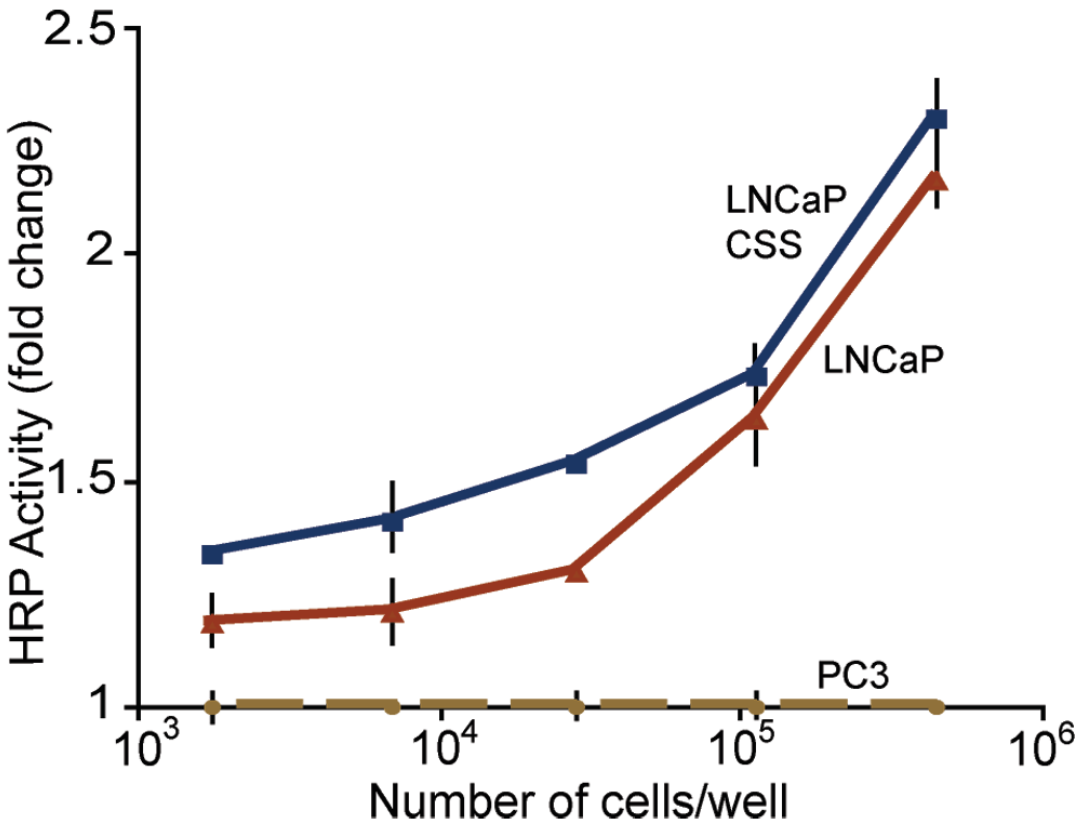

Figure 4-15. A dose response curve demonstrates the specificity of PSMA detection on two types of LNCaP cells relative to the PSMA-negative PC3 cells, as shown by cell-based ELISA. The dual ligand combination of $P100_{SP}$-P4-**2** + $P100_{SP}$-P4-**1** and the PEG7 spacer on phage was used for specific detection of PSMA on the cell surface.

4.11 Detecting PSMA on Suspended Cells and in Culture Media

The tailored phage could also capture cells from solution, which is critical for future analytical applications in circulating tumor cell detection and characterization. In this experiment unlike other ELISAs described here, the phage were immobilized on the microtiter plate before applying a solution of cells, Figure 4-16 and 4-17; levels of bound cells were quantified through application of anti-PSMA primary antibody and HRP-conjugated, anti-mouse, secondary antibody. Again, phage wrapped with the dual ligand combination of $P100_{SP}$-P4-**2** **+** $P100_{SP}$-P4-**1** and the PEG7 spacer were used. In this experiment, the capture of PSMA positive cells is detected by and proportional to cell surface PSMA concentration. PC3 cells, lacking PSMA, do not generate a significant response, as expected.

PSMA levels are elevated in the urine samples of PCa patients, and levels of this biomarker correlate with the aggressiveness of the disease.[8,56] Therefore, cultured PCa cells should release PSMA into their culture media. Thus, PSMA detection was also performed with cell culture supernatant, normalized to the volume and the number of cells (Figure 4-16). The PEGylated dual ligand combination on phage allows sensitive PSMA detection in 100 µL of supernatant from both LNCaP and LNCaP CSS cell cultures. Cell culture media from PC3 cells and fresh culture medias serve as the negative controls. As expected, the negative controls failed to show any significant binding. The effective detection of PSMA shed by LNCaP cells, in androgen sensitive and androgen independent

cells, demonstrates the use of phage wrapped with PEGylated ligands for future development of analytical devices and translation to the clinic.

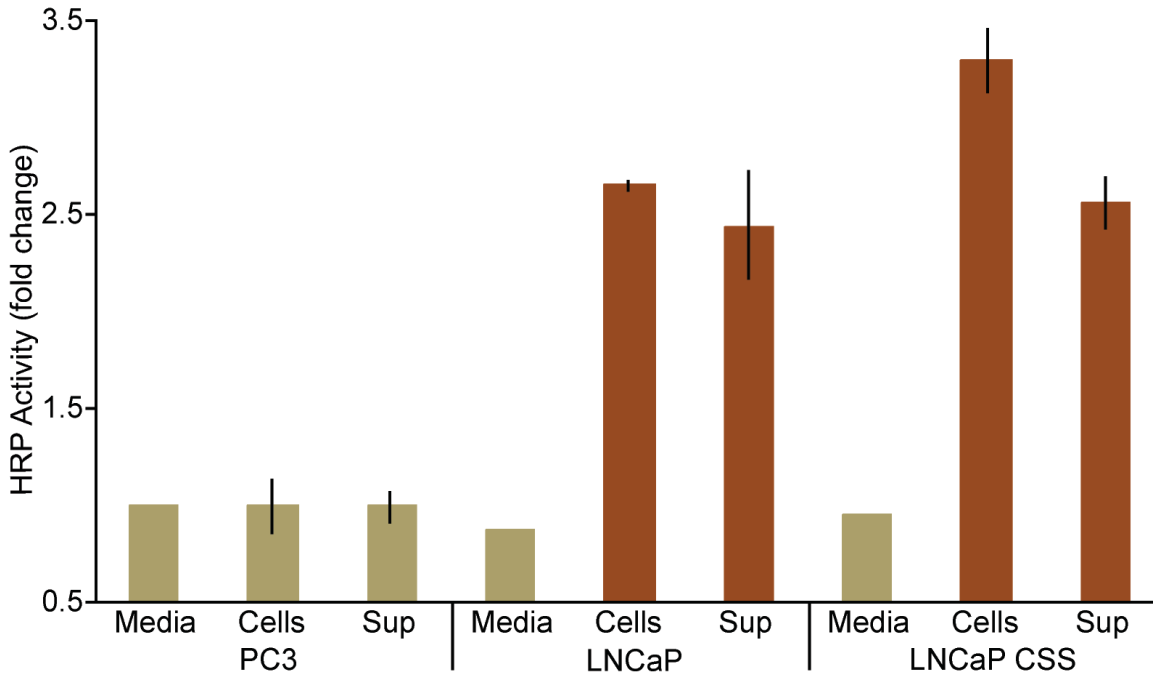

Figure 4-16. A sandwich ELISA demonstrating capture of PSMA positive cells by the dual ligand combination of $P100_{SP}$-P4-**2** + $P100_{SP}$-P4-**1** and the PEG7 spacer on phage, which are immobilized on the microtiter plate. Controls are shown in gold color. 'Media' indicates fresh culture media, whereas 'sup' indicates cell culture supernatant. The p-value is <0.01 for all data reported here.

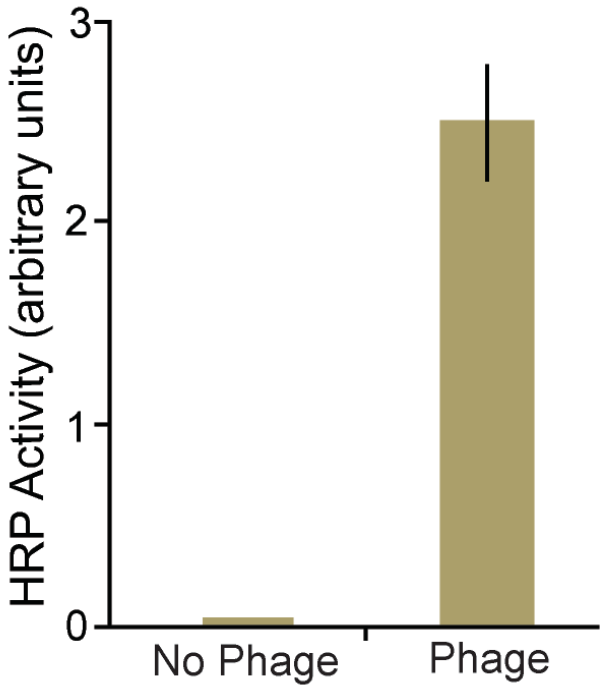

Figure 4-17. Phage-based ELISA demonstrating immobilization of phage in the wells of a microtiter plate, as used in the sandwich ELISA assay (Figure 4-16). The wells were incubated with 100 mL/well of 10 nM phage, and then a BSA blocking solution was used. Levels of bound phage were quantified using a horseradish peroxidase-conjugated anti-M13 antibody. The negative control has identical conditions without the addition of phage.

CONCLUSIONS

In conclusion, this study demonstrates a systematic approach to engineering the phage surface through chemical tailoring. Chemically modifying viruses with PEG addresses a major issue of non-specific adhesion to cellular surfaces, and further engineering allowed specific detection using PEGylated ligands. The reported PEGylated dual ligand combination provides a foundation for applying the phage to cell-based analysis, where highly specific molecular recognition of cells is essential. Optimization of binding affinity required optimization of the PEG length, packing density, point of attachment, linkers and spacers. The versatility of PEG allows such multivariate optimization. This biocompatible polymer is widely available with diverse functionalities for bioconjugation and also has moderately predictable conformations to guide engineering. Furthermore, we demonstrate control over the relative spatial configuration of the ligands using small PEG polymers interdigitated with larger PEG brushes in a general approach applicable to many binding optimization studies. Most importantly, these chemically modified phage could readily distinguish PSMA-positive from PSMA-negative cells, and also identify more aggressive PCa tumor cells. In the future, we will apply such phage to the capture and detection of circulating tumor cells for use in cell-based detectors.

MATERIALS AND METHODS

All chemicals and reagents were purchased from Sigma-Aldrich, and used as received unless otherwise noted. PSMA and the cell lines LNCaP and PC3 were generous gifts from Drs. William Ernst and Gary Fuji (Molecular Express). Maleimide-PEG100-amine and 15-azido-4,7,10,13-tetraoxapentadecanoic acid (azido-PEG4-carboxylic acid) were purchased from Alfa Aesar. N,N-Diisopropylethylamine (DIPEA) and azide-functionalized PEG7, 22 and 45 were purchased from Sigma, and 4-Azidobutanoic acid was purchased from Synthonix. 4-Pentynoic acid (GFS Chemicals, Inc.), O-benzotriazole-N,N,N',N'-tetramethyluronium hexafluorophosphate, HBTU (GL Biochem Ltd.), triethyammonium acetate buffer (Fluka Biochemika) and Tween-20 (EMD Science) were used as received. HPLC-grade water was used for the preparation of solutions.

M13 bacteriophage propagation

Phage propagation and isolation was performed as previously described.[4,57] Briefly, the phagemid DNA was transformed into $CaCl_2$ competent *E. coli* XL-1 Blue cells. The cells were grown at 37 °C in 2 mL 2YT media supplemented with carbenicillin and tetracycline until the culture reached log-phase growth. The culture was then infected with KO7 helper phage with a multiplicity of infection of 4.5:1. The starting culture was then transferred to 75 mL 2YT media supplemented with carbenicillin and kanamycin. The phage culture

was incubated for 16 h at 37 °C with shaking. The phage were isolated from the culture supernatant by centrifugation at 10 krpm after precipitation through addition of 1/5th volume of PEG-NaCl (2.5 M NaCl, 20% PEG-8000). After second precipitation, the phage were resuspended in phosphate-buffered saline (PBS, 135 mM NaCl, 2.50 mM KCl, 8.00 mM Na_2HPO_4, 30.0 mM KH_2PO_4, pH 7.2). Phage concentration was determined by UV absorbance at 268 nm (OD_{268} of 1.0 = 8.31 nM phage).

Solid Phase Peptide Synthesis

The peptides were synthesized by conventional solid-phase peptide synthesis with Fmoc-protected amino acids on Rink-amide resin (Novabiochem), as previously described.[4,58,59] The peptide *N*-terminus was coupled to 4-azido butanoic acid or 4-pentynoic acid to yield the azide- or alkyne-functionalized peptides, respectively. For incorporation of the PEG4 linker, the last coupling step was performed with 15-azido-4,7,10,13-tetraoxapentadecanoic acid. The reported peptides were purified by reverse-phase HPLC purification with a C_{18} column. Fractions containing the purified peptides were combined and concentrated using rotary evaporation, followed by lyophilization and characterization by MALDI-TOF mass spectrometry. The calculated *m*/*z* for peptide-**1** [M^+] 1349.67, found 1349.77. The calculated *m*/*z* for peptide-**2** [M^+] 2040.28, found 2040.23. The calculated *m*/*z* for peptide-**1** fused to the azido-PEG4 linker is [M^+] 1510.80, found 1511.78. The calculated *m*/*z* for peptide-**2**

fused to the azido-PEG4 linker is [M^+] 2201.02, found 2202.06. The calculated *m*/*z* for alkyne-functionalized K_{14} peptide [M+Na]$^+$ 1914.37, found 1914.18. The calculated *m*/*z* for K_{14}-Cys peptide [M^{3+}] 638.79, found 638.79.

Click chemistry reaction for the synthesis of PEGylated oligolysines

The protocol for the synthesis of PEGylated oligolysines was adapted from Lumiprobe Corporation's protocol, as described previously.[4,57,60,61] Briefly, the reaction was performed at a final concentration of 100 µM azide-functionalized PEG. The product obtained was purified using reverse-phase analytical HPLC and characterized by MALDI-TOF mass spectrometry. The calculated *m*/*z* for alkyne-functionalized K_{14} fused to azide-functionalized PEG7 [M^+] 2285.61, found 2286.93. The mass spectrometry data obtained for PEGylated oligolysine showed a shift in the characteristically polydispersed PEG spectra by the expected mass of K_{14}-alkyne, Figure 4-3 and 4-4.

Synthesis of PEGylated ligands – specific attachment mode

The protocol for the synthesis of the PEGylated ligands was adapted from the solid phase peptide synthesis and click chemistry reaction described above, and also described in Figures S7 and S9. In a glass test tube, 40 µL of 1 mM Mal-PEG100-NH_2 (commercially purchased from Alfa Aesar) in water, 12 µL of 10 mM pentynoic acid (in water), 12 µL of 10 mM HBTU (in NMP), 40 µL of DIPEA and 296 µL of HPLC grade water were combined and stirred at room

temperature for 2 h, yielding alkyne-functionalized-PEG100-Mal. To obtain more quantities of the product, multiple reactions at this volume were run in parallel. To remove unreacted starting material and to concentrate the product, the reaction mixtures were diluted with an equal volume HPLC grade water before concentration to 1/5th volume using 2K MWCO concentrators (Sartorius).

For the next step of the synthesis, ≈50 µL of the alkyne-functionalized-PEG100-Mal, obtained as described above, was conjugated to azide-functionalized peptide ligands (final concentration of 40 µM) by click chemistry as before.[4,60] The reaction mixture was stirred overnight at room temperature. Four identical reactions were run in parallel. To remove unreacted starting materials, the four reaction mixtures were then combined and concentrated to 1/4th volume using 3K MWCO concentrators. Next, the resultant solution was diluted with an equal volume of HPLC grade water before concentrating to ≈1/2 volume using 5K MWCO concentrators. The concentrated reaction mixture was purified using reverse-phase analytical HPLC (Figures 4-18 and 4-19) and fractions were identified by MALDI-TOF mass spectrometry. The high polydispersity of the high MW PEG polymer prevents accurate mass determination by this technique, and instead Gel Permeation Chromatography (GPC) was used as described in the next section.

For the non-specific attachment mode described in the text and Figure 4-12, the PEGylated ligands were synthesized in the reverse order. The azide-functionalized peptides were first conjugated to pentynoic acid using click

chemistry. The resultant peptide was then coupled to Mal-PEG100-NH_2 using HBTU and DIPEA as described above.

Gel Permeation Chromatography (GPC)

GPC was used to characterize the MW's of the PEGylated peptides. The molecular weights of the polymers, calibrated with PEG MW standards, were obtained with an Agilent 1100 series GPC system (Agilent Technologies, Santa Clara, CA) using 0.1% (v/v) LiBr/DMF solution (1.0 mL/min) as the eluent.

Dynamic Light Scattering (DLS)

To demonstrate wrapping by PEGylated ligands and other materials on the phage surface, DLS measurements were obtained using Nano ZetaSizer ZS series. For determination of size, 1 mL of each sample was measured at the same concentration as used for the biological assay. Each sample was measured at least three times at 25 °C, with each individual size measurement being the average of 10 runs.

Cell growth

The cell lines were grown as monolayers in media supplemented with 10% fetal bovine serum (Cellgro), 1 mM sodium pyruvate[62] and 1% penicillin-streptomycin-glutamine in a 5% CO_2 and 95% air-humidified atmosphere at 37 °C. LNCaP cells were cultured in RPMI 1640 media. For studies with LNCaP cells cultured in charcoal-stripped serum (LNCaP CSS cells), LNCaP cells were

washed with PBS and then incubated with phenol free RPMI 1640 media supplemented with 10% charcoal-stripped serum (Cellgro) for five minutes. The cells were again washed with PBS, and provided fresh media.[51] PC3 cells were grown in Ham's F-12 media.

Cell-based phage Enzyme-Linked Immunosorbent Assay (ELISA)

Day 1: The cell-based ELISA was performed as previously described by Watanabe et. al. with the following modifications.[63] Cells were detached with Trypsin-EDTA, resuspended in PBS, and then collected by centrifuging at 1200 rpm for 5 min. The cells were further washed with PBS and then concentrated as in the previous step. The concentration of the cells was adjusted to 4.5×10^6 cells/mL in PBS using a hemocytometer, and 100 µL was aliquoted to specific wells of a 96-well microtiter plate (Maxisorp plates from Nunc). The Maxisorp plates used here have a high protein-binding capacity. Thus, the plates can be used to run assays with either the cells or the phage immobilized in the wells. Next, 50 µL of a 0.15% glutaraldehyde in PBS solution was added to the wells at 4 °C, and the solution was gently mixed by pipetting. The ELISA plate was then centrifuged at 1200 rpm for 10 min at 4 °C, followed by overnight incubation at 4 °C.

Day 2: The cell solution was gently removed, and the wells were blocked with 200 µL/well of blocking buffer containing 100 mM glycine, 1% gelatin and

0.1% w/v BSA (bovine serum albumin) in PBS. The plate was incubated overnight (≈20-22 h) at room temperature.

Separately, phage were prepared before attachment to PEG and PEGylated ligands. Phage (10 nM in 100 µL of PBS) and 1 µL of K_{14}-alkyne (525 µM in water) were thoroughly mixed by pipetting ≈25 times. For phage wrapped with PEGylated ligands, phage were mixed with 0.75 µL of K_{14}-Cys (525 µM in water). For mixed wrapping on the phage surface, 0.5 µL of K_{14}-alkyne was pre-mixed with 0.75 µL of K_{14}-Cys, and then mixed with 100 µL of 10 nM phage. The solution was shaken at room temperature for 15 min on an orbital shaker. Next, 2 µL of PEGylated ligand (625 µM in water) was added to the appropriate wells. For the dual ligand combinations, the PEGylated ligands were pre-mixed in the desired ratio (a 2:1 molar ratio for example), and then 2 µL of the mixture was added to the appropriate wells. The solutions were gently mixed by pipetting, and incubated overnight at 4 °C.

Day 3: Next, the click reaction was performed, as previously described, but with the following modifications.[4,57,60] To buffer the pH, triethylammonium acetate was added to a final concentration of 50 mM, followed by the addition of 1.5 µL of 1 mM azide-functionalized PEG. The solutions were mixed by pipetting. Next, ascorbic acid was added to a final concentration of 1 mM and the solutions were mixed by gently pipetting. Then, copper sulfate was added to a final concentration of 1.5 mM, followed by pipetting to mix the solutions. Water was

added to the other wells to maintain consistent phage concentrations. The plate was incubated at room temperature for 30 min.

The wells of the ELISA plate were then incubated with the phage samples. The blocking buffer was removed and the wells were gently washed two times with PBS. Next, the phage solution was added to the respective wells and incubated for 45 min. The phage solution was removed, and the wells were washed three times with 300 µL/well of wash buffer PT (0.05% Tween-20 in PBS), once with PBS, and then incubated with horseradish peroxidase-conjugated anti-M13 antibody (100 µL/well, 1:5000 dilution in PBS) for 40 min. The wells were washed three times with PT and once with PBS. The plate was then developed by incubating with HRP substrate solution (100 µL/well; 1 mg/mL *o*-phenylenediamine dihydrochloride and 0.02% w/v H_2O_2) in citric acid buffer (50 mM citric acid, 50 mM Na_2HPO_4, pH 5.0). The HRP activity was measured spectrophotometrically at 450 nm using a microtiter plate reader (Bio-Tek). The absorbance at 630 nm was subtracted from the absorbance at 450 nm to eliminate background.

Phage-based sandwich ELISA for cell capture.

To demonstrate cell capture by the PEGylated-ligand phage, the phage were coated on the plate, and cells added before quantifying binding. This assay setup inverts other cell-based phage ELISAs reported here. This experiment is a significant step towards establishing the relevance of this phage architecture for

biosensing assays planned in the future. In this assay, the PEGylated phage architecture is immobilized on the plate as demonstrated in Figure 4-17. Next, a cell suspension is added to the wells, and the amount of cells captured are then measured spectrophotometrically as detailed here and in the text. The protocol here focuses on experimental details altered from the above-described ELISA; all other conditions remained unchanged.

Day 1: In this phage capture ELISA, specific wells of a 96-well microtiter plate were coated with 100 µL/well of a solution of 10 nM phage pre-wrapped with oligolysine wrappers, as described above. The plate was incubated for 1 h on a shaker at room temperature. The coating solution was removed, and the wells were blocked with 200 µL/well of 0.2% w/v solution of BSA in PBS for 30 min, and washed two times with PT. Next, 98 µL PBS was added per well, followed by PEGylated ligands and incubated overnight at 4 °C.

Day 2: Azide-functionalized PEG variants were then conjugated as described above. Separately, the cells were collected and the concentration adjusted as described above; the ELISA plate was then incubated with 100 µL/well of the cell solution or media for 1 h. The wells were washed with PBS and incubated with 100 µL/well of the anti-PSMA antibody, YPSMA antibody (Abcam) at 1:1000 dilution. The wells were then washed with PBS, followed by incubation with horseradish-peroxidase-conjugated anti-mouse antibody (Sigma) at a 1:1000 dilution. The levels of phage binding were quantified as described above.

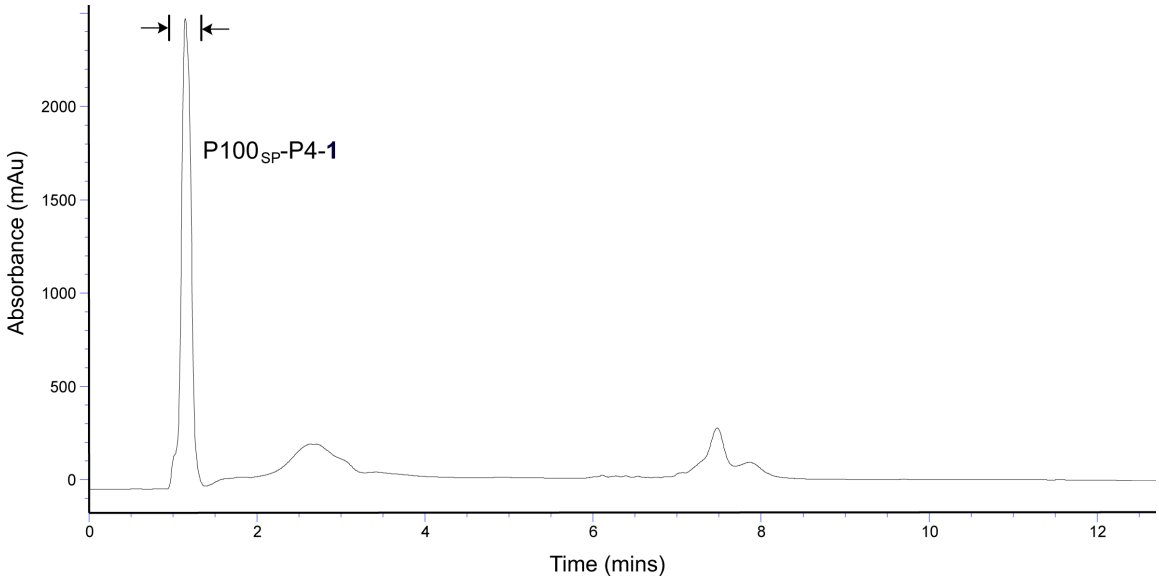

Figure 4-18. Representative reversed-phase HPLC for purification of the concentrated reaction mixture to form $P100_{SP}$-P4-**1**. To obtain pure $P100_{SP}$-P4-**1**, the peak designated in the trace was collected and accurate mass determination was performed using gel permeation chromatography. As shown here, the use of 3K and 5K MW cut off concentrators and extensive washing removed a majority of the unreacted starting materials from the reaction mixture.

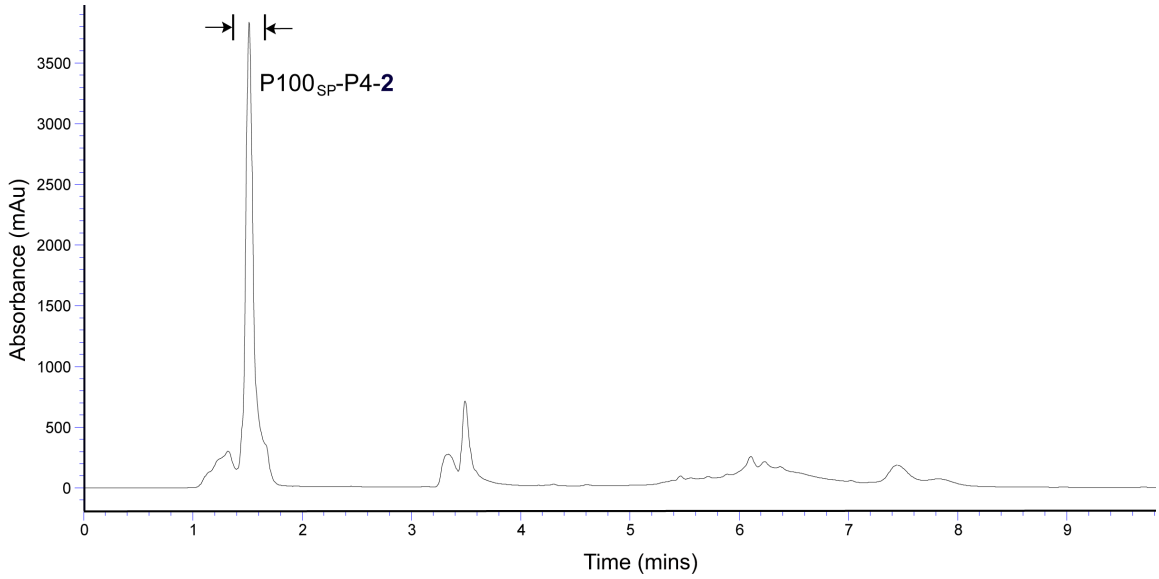

Figure 4-19. Representative reversed-phase HPLC for purification of the concentrated reaction mixture for P100$_{SP}$-P4-**2**. As described above, gel permeation chromatography characterized the mass of this PEGylated ligand. As shown here, the use of 3K and 5K MW cut off concentrators and extensive washing removed a majority of the unreacted starting materials from the reaction mixture.

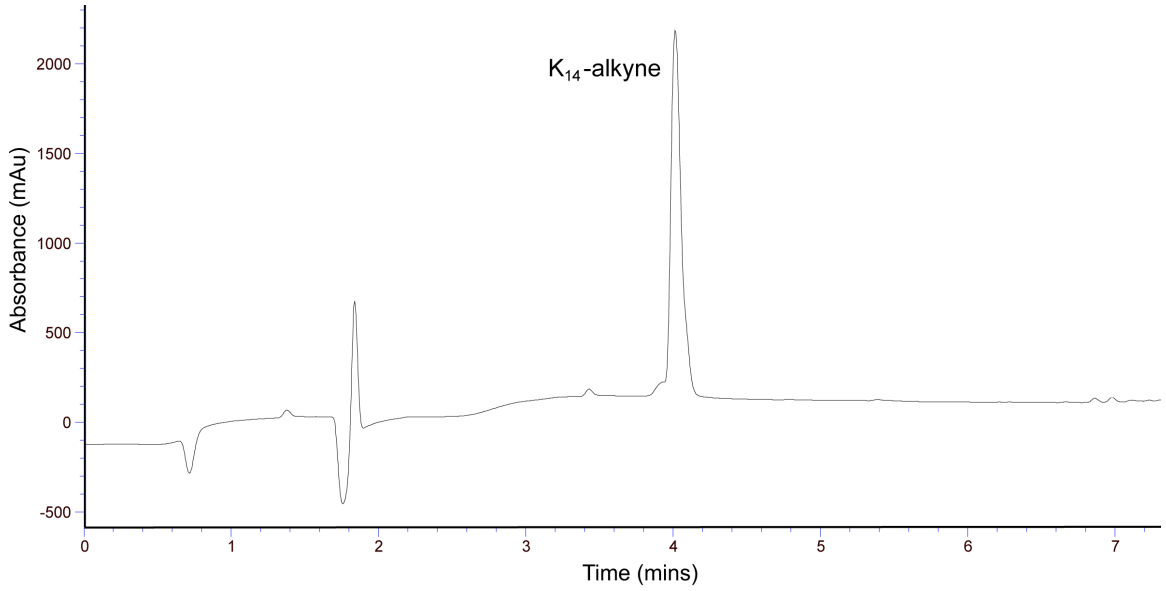

Figure 4-20. Representative reversed-phase HPLC analysis of the purified K_{14}-alkyne. Accurate mass determination was performed using MALDI-TOF mass spectrometry. The features in the HPLC chromatogram before the two minute mark are also observed when only water is injected onto the HPLC column; thus, these features do not reflect the purity of the peptide.

REFERENCES

(1) Joosse, S. A.; Gorges, T. M.; Pantel, K. Biology, Detection, and Clinical Implications of Circulating Tumor Cells. *EMBO Mol. Med.* **2015**, *7*, 1–11.

(2) Mehlen, P.; Puisieux, A. Metastasis: A Question of Life or Death. *Nat. Rev. Cancer* **2006**, *6*, 449–458.

(3) Siegel, R. L.; Miller, K. D.; Jemal, A. Cancer Statistics, 2015. *CA. Cancer J. Clin.* **2015**, *65*, 5–29.

(4) Mohan, K.; Donavan, K. C.; Arter, J. A.; Penner, R. M.; Weiss, G. A. Sub-Nanomolar Detection of Prostate-Specific Membrane Antigen in Synthetic Urine by Synergistic, Dual-Ligand Phage. *J. Am. Chem. Soc.* **2013**, *135*, 7761–7767.

(5) Schülke, N.; Varlamova, O. A.; Donovan, G. P.; Ma, D.; Gardner, J. P.; Morrissey, D. M.; Arrigale, R. R.; Zhan, C.; Chodera, A. J.; Surowitz, K. G.; *et al.* The Homodimer of Prostate-Specific Membrane Antigen Is a Functional Target for Cancer Therapy. *Proc. Natl. Acad. Sci. USA* **2003**, *100*, 12590–12595.

(6) Chuang, A.-Y.; DeMarzo, A. M.; Veltri, R. W.; Sharma, R. B.; Bieberich, C. J.; Epstein, J. I. Immunohistochemical Differentiation of High-Grade Prostate Carcinoma from Urothelial Carcinoma. *Am. J. Surg. Pathol.* **2007**, *31*, 1246–1255.

(7) Kawakami, M.; Nakayama, J. Enhanced Expression of Prostate-Specific Membrane Antigen Gene in Prostate Cancer as Revealed by in Situ Hybridization. *Cancer Res.* **1997**, *57*, 2321–2324.

(8) Sokoloff, R. L.; Norton, K. C.; Gasior, C. L.; Marker, K. M.; Grauer, L. S. A Dual-Monoclonal Sandwich Assay for Prostate-Specific Membrane Antigen: Levels in Tissues, Seminal Fluid and Urine. *Prostate* **2000**, *43*, 150–157.

(9) Mohan, K.; Weiss, G. A. Dual Genetically Encoded Phage-Displayed Ligands. *Anal. Biochem.* **2014**, *453*, 1–3.

(10) Arter, J. A.; Diaz, J. E.; Donavan, K. C.; Yuan, T.; Penner, R. M.; Weiss, G. A. Virus-Polymer Hybrid Nanowires Tailored to Detect Prostate-Specific

Membrane Antigen. *Anal. Chem.* **2012**, *84*, 2776–2783.

(11) Smith, G. P. Filamentous Fusion Phage: Novel Expression Vectors That Display Cloned Antigens on the Virion Surface. *Science* **1985**, *228*, 1315–1317.

(12) Sidhu, S. S.; Weiss, G. A. *Phage Display: A Practical Approach*; Lowman, H. B.; Clackson, T., Eds.; Oxford University Press: New York, 2004.

(13) Scott, J. K.; Smith, G. P. Searching for Peptide Ligands with an Epitope Library. *Science* **1990**, *249*, 386–390.

(14) Welsh, L. C.; Symmons, M. F.; Sturtevant, J. M.; Marvin, D. A.; Perham, R. N. Structure of the Capsid of Pf3 Filamentous Phage Determined from X-Ray Fibre Diffraction Data at 3.1 A Resolution. *J. Mol. Biol.* **1998**, *283*, 155–177.

(15) Trepel, M.; Arap, W.; Pasqualini, R. In Vivo Phage Display and Vascular Heterogeneity: Implications for Targeted Medicine. *Curr. Opin. Chem. Biol.* **2002**, *6*, 399–404.

(16) Abbineni, G.; Modali, S.; Safiejko-Mroczka, B.; Petrenko, V. A.; Mao, C. Evolutionary Selection of New Breast Cancer Cell-Targeting Peptides and Phages with the Cell-Targeting Peptides Fully Displayed on the Major Coat and Their Effects on Actin Dynamics during Cell Internalization. *Mol. Pharm.* **2010**, *7*, 1629–1642.

(17) Arap, W.; Pasqualini, R.; Ruoslahti, E. Cancer Treatment by Targeted Drug Delivery to Tumor Vasculature in a Mouse Model. *Science* **1998**, *279*, 377–380.

(18) Ma, K.; Wang, D.-D.; Lin, Y.; Wang, J.; Petrenko, V.; Mao, C. Synergetic Targeted Delivery of Sleeping-Beauty Transposon System to Mesenchymal Stem Cells Using LPD Nanoparticles Modified with a Phage-Displayed Targeting Peptide. *Adv. Funct. Mater.* **2013**, *23*, 1172–1181.

(19) Wang, Y.; Ju, Z.; Cao, B.; Gao, X.; Zhu, Y.; Qiu, P.; Xu, H.; Pan, P.; Bao, H.; Wang, L.; *et al.* Ultrasensitive Rapid Detection of Human Serum Antibody Biomarkers by Biomarker-Capturing Viral Nanofibers. *ACS Nano* **2015**, *9*, 4475–4483.

(20) Petrenko, V. A.; Jayanna, P. K. Phage Protein-Targeted Cancer

Nanomedicines. *FEBS Lett.* **2014**, *588*, 341–349.

(21) Jayanna, P. K.; Torchilin, V. P.; Petrenko, V. A. Liposomes Targeted by Fusion Phage Proteins. *Nanomedicine.* **2009**, *5*, 83–89.

(22) Wang, T.; Yang, S.; Petrenko, V. A.; Torchilin, V. P. Cytoplasmic Delivery of Liposomes into MCF-7 Breast Cancer Cells Mediated by Cell-Specific Phage Fusion Coat Protein. *Mol. Pharm.* **2010**, *7*, 1149–1158.

(23) Ngweniform, P.; Abbineni, G.; Cao, B.; Mao, C. Self-Assembly of Drug-Loaded Liposomes on Genetically Engineered Target-Recognizing M13 Phage: A Novel Nanocarrier for Targeted Drug Delivery. *Small* **2009**, *5*, 1963–1969.

(24) Kalarical Janardhanan, S.; Narayan, S.; Abbineni, G.; Hayhurst, A.; Mao, C. Architectonics of Phage-Liposome Nanowebs as Optimized Photosensitizer Vehicles for Photodynamic Cancer Therapy. *Mol. Cancer Ther.* **2010**, *9*, 2524–2535.

(25) Ghosh, D.; Lee, Y.; Thomas, S.; Kohli, A. G.; Yun, D. S.; Belcher, A. M.; Kelly, K. A. M13-Templated Magnetic Nanoparticles for Targeted in Vivo Imaging of Prostate Cancer. *Nat. Nanotechnol.* **2012**, *7*, 677–682.

(26) Ghosh, D.; Bagley, A. F.; Na, Y. J.; Birrer, M. J.; Bhatia, S. N.; Belcher, A. M. Deep, Noninvasive Imaging and Surgical Guidance of Submillimeter Tumors Using Targeted M13-Stabilized Single-Walled Carbon Nanotubes. *Proc. Natl. Acad. Sci. U. S. A.* **2014**, *111*, 13948–13953.

(27) Carrico, Z. M.; Farkas, M. E.; Zhou, Y.; Hsiao, S. C.; Marks, J. D.; Chokhawala, H.; Clark, D. S.; Francis, M. B. N-Terminal Labeling of Filamentous Phage to Create Cancer Marker Imaging Agents. *ACS Nano* **2012**, *6*, 6675–6680.

(28) Russel, M.; Lowman, H. B.; Tim, C. *Phage Display: Practical Approach*; Lowman, H. B.; Clackson, T., Eds.; Oxford University Press: New York, 2004.

(29) Lamboy, J. A.; Tam, P. Y.; Lee, L. S.; Jackson, P. J.; Avrantinis, S. K.; Lee, H. J.; Corn, R. M.; Weiss, G. A. Chemical and Genetic Wrappers for Improved Phage and RNA Display. *ChemBioChem* **2008**, *9*, 2846–2852.

(30) Lamboy, J. A.; Arter, J. A.; Knopp, K. A.; Der, D.; Overstreet, C. M.;

Palermo, E. F.; Urakami, H.; Yu, T.-B.; Tezgel, O.; Tew, G. N.; *et al.* Phage Wrapping with Cationic Polymers Eliminates Nonspecific Binding between M13 Phage and High pI Target Proteins. *J. Am. Chem. Soc.* **2009**, *131*, 16454–16460.

(31) Dozmorov, M. G.; Hurst, R. E.; Culkin, D. J.; Kropp, B. P.; Frank, M. B.; Osban, J.; Penning, T. M.; Lin, H.-K. Unique Patterns of Molecular Profiling between Human Prostate Cancer LNCaP and PC-3 Cells. *Prostate* **2009**, *69*, 1077–1079.

(32) Horoszewicz, J. S.; Leong, S. S.; Chu, T. M.; Wajsman, Z. L.; Friedman, M.; Papsidero, L.; Kim, U.; Chai, L. S.; Kakati, S.; Arya, S. K.; *et al.* The LNCaP Cell Line--a New Model for Studies on Human Prostatic Carcinoma. *Prog. Clin. Biol. Res.* **1980**, *37*, 115–132.

(33) Sobel, R. E.; Sadar, M. D. Cell Lines Used in Prostate Cancer Research: A Compendium of Old and New Lines--Part 1. *J. Urol.* **2005**, *173*, 342–359.

(34) Marsh, D.; Bartucci, R.; Sportelli, L. Lipid Membranes with Grafted Polymers: Physicochemical Aspects. *Biochim. Biophys. Acta - Biomembr.* **2003**, *1615*, 33–59.

(35) Crawford, J. Clinical Uses of Pegylated Pharmaceuticals in Oncology. *Cancer Treat. Rev.* **2002**, *28*, 7–11.

(36) Knop, K.; Hoogenboom, R.; Fischer, D.; Schubert, U. S. Poly(ethylene Glycol) in Drug Delivery: Pros and Cons as Well as Potential Alternatives. *Angew. Chem. Int. Ed. Engl.* **2010**, *49*, 6288–6308.

(37) Pai, S. S.; Przybycien, T. M.; Tilton, R. D. Protein PEGylation Attenuates Adsorption and Aggregation on a Negatively Charged and Moderately Hydrophobic Polymer Surface. *Langmuir* **2010**, *26*, 18231–18238.

(38) Fishburn, C. S. The Pharmacology of PEGylation: Balancing PD with PK to Generate Novel Therapeutics. *J. Pharm. Sci.* **2008**, *97*, 4167–4183.

(39) Loo, C.; Lin, A.; Hirsch, L.; Lee, M.-H.; Barton, J.; Halas, N.; West, J.; Drezek, R. Nanoshell-Enabled Photonics-Based Imaging and Therapy of Cancer. *Technol. Cancer Res. Treat.* **2004**, *3*, 33–40.

(40) Loo, C.; Lowery, A.; Halas, N.; West, J.; Drezek, R. Immunotargeted Nanoshells for Integrated Cancer Imaging and Therapy. *Nano Lett.* **2005**,

5, 709–711.

(41) Levin, C. S.; Bishnoi, S. W.; Grady, N. K.; Halas, N. J. Determining the Conformation of Thiolated Poly(ethylene Glycol) on Au Nanoshells by Surface-Enhanced Raman Scattering Spectroscopic Assay. *Anal. Chem.* **2006**, *78*, 3277–3281.

(42) Xia, X.; Yang, M.; Wang, Y.; Zheng, Y.; Li, Q.; Chen, J.; Xia, Y. Quantifying the Coverage Density of Poly(ethylene Glycol) Chains on the Surface of Gold Nanostructures. *ACS Nano* **2012**, *6*, 512–522.

(43) Sarma, M.; Chatterjee, T.; Das, S. K. Ammonium–crown Ether Based Host–guest Systems: N–H···O Hydrogen Bond Directed Guest Inclusion Featuring N–H Donor Functionalities in Angular Geometry. *RSC Adv.* **2012**, *2*, 3920–3926.

(44) Greenwald, R. B.; Choe, Y. H.; McGuire, J.; Conover, C. D. Effective Drug Delivery by PEGylated Drug Conjugates. *Adv. Drug Deliv. Rev.* **2003**, *55*, 217–250.

(45) Montesano, G.; Bartucci, R.; Belsito, S.; Marsh, D.; Sportelli, L. Lipid Membrane Expansion and Micelle Formation by Polymer-Grafted Lipids: Scaling with Polymer Length Studied by Spin-Label Electron Spin Resonance. *Biophys. J.* **2001**, *80*, 1372–13783.

(46) Glucksman, M. J.; Bhattacharjee, S.; Makowski, L. Three-Dimensional Structure of a Cloning Vector. *J. Mol. Biol.* **1992**, *226*, 455–470.

(47) Kim, J.; Korkmaz, N.; Nam, C. H. Phage Assembly Using ATPES-Conjugation of Major Coated p8 Protein for Possible Scaffolds. *IBC* **2012**, *4*, 1–7.

(48) Liu, Y.; Shipton, M. K.; Ryan, J.; Kaufman, E. D.; Franzen, S.; Feldheim, D. L. Synthesis, Stability, and Cellular Internalization of Gold Nanoparticles Containing Mixed Peptide-Poly(ethylene Glycol) Monolayers. *Anal. Chem.* **2007**, *79*, 2221–2229.

(49) Manson, J.; Kumar, D.; Meenan, B. J.; Dixon, D. Polyethylene Glycol Functionalized Gold Nanoparticles: The Influence of Capping Density on Stability in Various Media. *Gold Bull.* **2011**, *44*, 99–105.

(50) Harris, J. M.; Martin, N. E.; Modi, M. Pegylation: A Novel Process for

Modifying Pharmacokinetics. *Clin. Pharmacokinet.* **2001**, *40*, 539–551.

(51) Tovar, C.; Higgins, B.; Kolinsky, K.; Xia, M.; Packman, K.; Heimbrook, D. C.; Vassilev, L. T. MDM2 Antagonists Boost Antitumor Effect of Androgen Withdrawal: Implications for Therapy of Prostate Cancer. *Mol. Cancer* **2011**, *10*, 49–59.

(52) Denmeade, S. R.; Sokoll, L. J.; Dalrymple, S.; Rosen, D. M.; Gady, A. M.; Bruzek, D.; Ricklis, R. M.; Isaacs, J. T. Dissociation between Androgen Responsiveness for Malignant Growth vs. Expression of Prostate Specific Differentiation Markers PSA, hK2, and PSMA in Human Prostate Cancer Models. *Prostate* **2003**, *54*, 249–257.

(53) Culig, Z.; Hoffmann, J.; Erdel, M.; Eder, I. E.; Hobisch, A.; Hittmair, A.; Bartsch, G.; Utermann, G.; Schneider, M. R.; Parczyk, K.; *et al.* Switch from Antagonist to Agonist of the Androgen Receptor Bicalutamide Is Associated with Prostate Tumour Progression in a New Model System. *Br. J. Cancer* **1999**, *81*, 242–251.

(54) Iwasa, Y.; Mizokami, A.; Miwa, S.; Koshida, K.; Namiki, M. Establishment and Characterization of Androgen-Independent Human Prostate Cancer Cell Lines, LN-REC4 and LNCaP-SF, from LNCaP. *Int. J. Urol.* **2007**, *14*, 233–239.

(55) Ghosh, A.; Wang, X.; Klein, E.; Heston, W. D. W. Novel Role of Prostate-Specific Membrane Antigen in Suppressing Prostate Cancer Invasiveness. *Cancer Res.* **2005**, *65*, 727–731.

(56) Su, S. L.; Huang, I. P.; Fair, W. R.; Powell, C. T.; Heston, W. D. Alternatively Spliced Variants of Prostate-Specific Membrane Antigen RNA: Ratio of Expression as a Potential Measurement of Progression. *Cancer Res.* **1995**, *55*, 1441–1443.

(57) Mohan, K.; Penner, R. M.; Weiss, G. A. Biosensing with Virus Electrode Hybrids. *Curr. Protoc. Chem. Biol.* **2015**, *7*, 53–72.

(58) Merrifield, R. B. Solid Phase Peptide Synthesis. I. The Synthesis of a Tetrapeptide. *J. Am. Chem. Soc.* **1963**, *85*, 2149–2154.

(59) Amblard, M.; Fehrentz, J.-A.; Martinez, J.; Subra, G. Methods and Protocols of Modern Solid Phase Peptide Synthesis. *Mol. Biotechnol.* **2006**, *33*, 239–254.

(60) Lumiprobe http://www.lumiprobe.com/protocols/click-chemistry-dna-labeling (accessed Sep 7, 2011).

(61) Rostovtsev, V. V; Green, L. G.; Fokin, V. V; Sharpless, K. B. A Stepwise Huisgen Cycloaddition Process: Copper(I)-Catalyzed Regioselective Ligation of Azides and Terminal Alkynes. *Angew. Chem., Int. Ed.* **2002**, *41*, 2596–2599.

(62) Kularatne, S. A.; Wang, K.; Santhapuram, H. R.; Low, P. S. Prostate-Specific Membrane Antigen Targeted Imaging and Therapy of Prostate Cancer Using a PSMA Inhibitor as a Homing Ligand. *Mol. Pharm.* **2009**, *6*, 780–789.

(63) Watanabe, K.; Joh, T.; Seno, K.; Sasaki, M.; Todoroki, I.; Miyashita, M.; Tochikubo, K.; Itoh, M. Development and Clinical Application of an Immunoassay Using Intact Helicobacter Pylori Attached to a Solid Phase as an Antigen. *Clin. Biochem.* **2001**, *34*, 291–295.

CHAPTER 5

Dual Genetically-Encoded Phage-Displayed Ligands

ABSTRACT

M13 bacteriophage display presents polypeptides as fusions to phage coat proteins. Such phage-displayed ligands offer useful reagents for biosensors. Here, we report a modified phage propagation protocol for the consistent and robust display of two different, genetically encoded ligands on the major coat protein, P8. The results demonstrate that the phage surface reaches a saturation point for maximum peptide display.

Key reference: Kritika Mohan, Gregory A. Weiss. Dual genetically encoded phage-displayed ligands. *Anal Biochem*, **2014**, 453, 1-3.

INTRODUCTION

M13 bacteriophage or “phage” have a readily customizable protein coat allowing the display of peptide or protein ligands on their surfaces. Such molecular display links the phenotype of the displayed ligand with its encoding DNA encapsulated by the phage. The display of one peptide in single or multiple copies on the phage surface, termed individual-display here, is extensively used for therapeutic and ligand discovery.[1,2] However, some experiments require two different ligands displayed on the same phage surface, termed dual-display. For example, we previously attached to the phage surface two different ligands – one chemically synthesized and one genetically encoded. Such viruses with two ligands presented were then incorporated into a bioaffinity matrix for the sensitive detection of prostate-specific membrane antigen (PSMA).[3,4]

M13 viruses infect only bacteria, and consist of a single-stranded DNA genome encapsulated by a protein coat. Approximately 2700 copies of the major coat protein (P8) appear along the length of the virus, and five copies each of the four minor coat proteins cap the ends of the virus.[5–8] Manipulating the viral genome allows the display of individual ligands as fusions to the phage coat proteins. Multi-copy ligand display can increase the affinity for the target due to avidity effects. Here, we report a method to simultaneously introduce two genetically encoded, different ligands on the phage surface. Fusion of each ligand to P8 can best allow the two different ligands to simultaneously bind to the target, as both binding sites appear along the length of the virus.

RESULTS AND DISCUSSION

5.1 Double Infection into *E. coli* Cells

Double transformations can result from bacteria having two plasmids simultaneously or consecutively inserted. To achieve such double transformations, bacteria can be infected by two phage; however, infection of the same *E. coli* cell by two phage is generally an inefficient process.[9] Despite this caveat, double infection remains a staple procedure in phage display, as helper phage typically infect phage-infected cells after each round of selection. As an additional caveat, the growth advantages of one plasmid can result in the loss of the other plasmid after double transformation.[10] As reported here, the phage propagation protocol can be modified to provide a consistent combination of two peptides presented on the phage surface. Furthermore, the modified procedure prevents loss of the slower propagating plasmid, as confirmed by ELISA (enzyme-linked immunosorbent assay) and other assays described below.

5.2 Generation of Dual Genetically Encoded Phage

Two previously reported peptide ligands specific for PSMA (provided by Molecular Express), binding ligands **1** – LDCVEVFQNSCDW and **2** – SECVEVFQNSCDW,[11] were simultaneously displayed using a modified phage propagation protocol. First, *E. coli* were transformed with the phagemid DNA encoding the first ligand. Next, the bacterial cell cultures were infected with bacteriophage

displaying the second ligand. The resultant phage were designated either phage-**12** or phage-**21**. This nomenclature identifies the ligand introduced through genetic transformation as the first number; the second number indicates the second ligand introduced by super-infection. Reversing the order of ligands used during the two steps generates two combinations of the dual-ligand system. The phage resulting from each combination could have potentially the same or different copy numbers of each ligand.

5.3 Propagation of Dual Genetically Encoded Phage

Phage propagation was performed as reported earlier.[12] Chemicals and reagents were purchased from Sigma-Aldrich and used as received, unless otherwise noted. Phage-**1** consistently propagates 20% more efficiently than phage-**2** (yields of 412 and 342 pmol per 150 mL culture, respectively). Briefly, the M13 phage display vectors (phagemids) with an ORF encoding either peptide **1** or **2** fused to P8 were used to transform $CaCl_2$ competent *E. coli* XL-1 Blue cells, before plating onto LB agar plates supplemented with carbenicillin. For example, phage-**12** resulted from a single colony of cells transformed with phagemid-**1**, and then grown at 37 °C in 2 mL 2YT media supplemented with carbenicillin and tetracycline until the culture reached log-phase growth. The culture was then infected with phage-**2** at an MOI (multiplicity of infection) of 200:1 and shaken at 250 rpm for 45 min at 37 °C. Next, M13-KO7 (GE Healthcare) phage (MOI of 3:1) was added. The starting culture was then transferred to 75 mL of 2YT media, and grown overnight. Phage were isolated from the cells by PEG-NaCl

precipitation. Phage concentration was determined by UV absorbance at 268 nm (OD_{268} = 8.31 nM).

5.4 Packaging of Either Phagemid

Packaging of both phagemids was confirmed by PCR, followed by sequencing (Genewiz, Inc.), Figure 5-1. This procedure can verify propagation of both phagemids, but does not confirm dual-display. The forward primers were specific for ligands **1** or **2**, whereas each PCR used the same reverse primer:

Primer-**1**: CAGCCATATGGCCTATGCATTGGACT

Primer-**2**: CAGCCATATGGCCAGCGCGTCG

Reverse Primer: CAGGAAACAGCTATGACGACAACAACCATCGCCC

PCR was performed with Iproof DNA polymerase. When subjected to PCR and sequencing, phage-**12** and -**21** confirmed the presence of both individual phagemids in each of the dual-displayed phage samples. Each dual-displayed phage sample, phage-**12** and -**21**, includes both phagemid-**1** and -**2**. Phage-**1** amplified with primer-**1**, and phage-**2** amplified with primer-**2** serve as the positive controls for priming and amplification. Phage-**1** amplified with primer-**2**, and vice-versa, were used as negative controls to test for non-specific annealing of the primers.

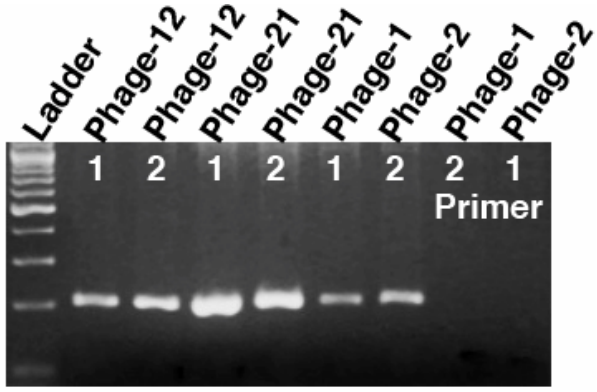

Figure 5-1. Agarose (1%) gel electrophoresis confirms the presence of both phagemids from dual display phage samples. Phage-**1** amplified with primer-**2**, and phage-**2** amplified with primer-**1** serve as the negative controls to dismiss any non-specific annealing of the primers.

5.5 Binding Affinities of Dual-Displayed Phage with Similar Sequences

A previously reported phage-based ELISA was next used to examine binding to PSMA.[12] Briefly, specific wells of a 96-well microtiter plate (Nunc Maxisorp) were coated with a 5.6 nM PSMA solution, followed by blocking with BSA (bovine serum albumin). The wells were then incubated with serially diluted, phage-displayed ligands. Levels of bound phage were quantified using a horseradish-peroxidase-conjugated anti-M13 antibody. The negative controls included phage-displayed ligands targeting BSA and Stop-4 phage replacing the phage-displayed ligands. Stop-4 phage consists of a phagemid with the wild type phage coat, four stop codons in the ORF encoding the display sequence, and, thus, no peptide displayed on the phage surface.

An ELISA compared binding by dual- and individual-displayed phage. This experiment also examined possible differences in affinity resulting from the new propagation protocols, compared to conventional practices (phage-**1** and phage-**2**). Phage-**12** and -**21** produced an overlapping response upon binding to PSMA, Figure 5-2. In comparison, the individual-displayed phage-**1** and -**2** revealed the expected extremes of weak and strong binding, respectively. Phage-**2** binds with >100-fold higher affinity to PSMA than phage-**1**. Strikingly, the binding affinity of the dual-displayed phage falls between the binding affinities of each individual-displayed ligand.

The intermediate binding observed for the dual-displayed phage suggests that the number of displayed peptides per phage particle remains narrowly constant. Thus,

the apparent binding failed to result from the simple addition of binding affinities of phage-**1** and -**2** which would result in a much higher apparent binding affinity by the dual-displayed phage. In addition, the overlapping responses for both phage-**12** and -**21** demonstrates that the inherent growth advantage for phagemid-**1** does not eliminate phagemid-**2** during propagation of dual-displayed phage. Thus, the two distinct modes of propagating phage-**12** or -**21** results in the same display levels. Comparing this result with binding by the mixture of phage-**1** and phage-**2** (inset Figure 5-2) suggests that the dual-displayed phage present a mixture of peptides on their surfaces. This experiment rules out the possibility of phage-**12** or -**21** consisting of a mixture of individual-displayed phage resulting from each propagation condition; such a mixture would be expected to have different phage levels and altered apparent affinities from the two modes of propagation with two phage experiencing unequal growth conditions.

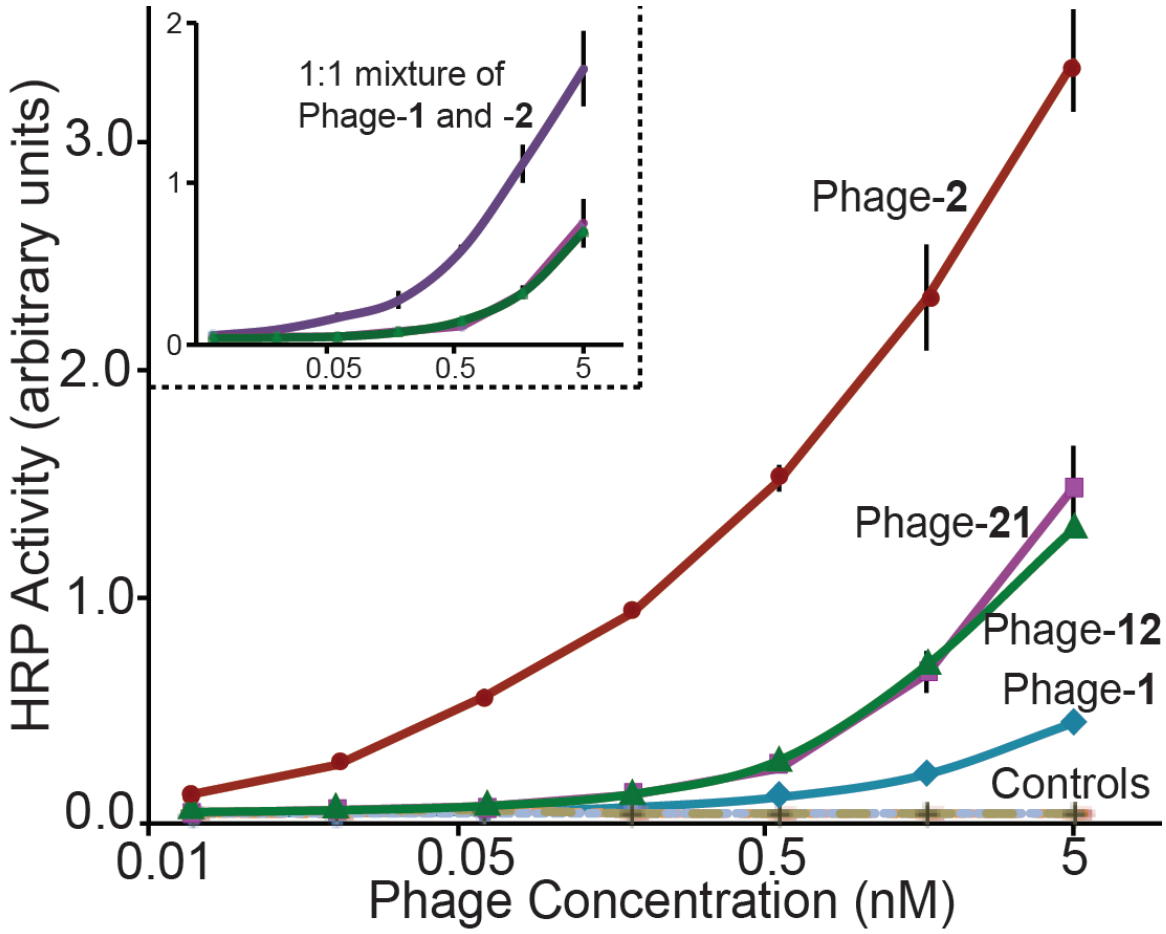

Figure 5-2. Phage-based ELISAs demonstrating the binding affinity of dual-displayed phage generated with similar ligand sequences targeting PSMA. The inset compares a 1:1 mixture of phage-**1** and -**2**, to phage-**12** and -**21**. Phage-displayed ligands targeting BSA, and Stop-4, helper phage packaging the phagemid DNA targeting PSMA, serve as the negative control. Throughout this report, error bars indicate standard error (n=3).

5.6 Binding Affinities of Dual-Displayed Phage with Dissimilar Sequences

To further investigate the generality of the method, dual-displayed phage were prepared with two PSMA binding ligands having dissimilar sequences, ligands **1** and **3** – CALCEFLG;[11] ligands **1** and **2** differ in only two residues, but ligands **1** and **3** differ in every position. As shown above, similar binding affinities of dual-displayed phage result from a different order of propagation, and, thus, only phage-**23** was produced. The propagation protocol and negative controls used for this experiment were as described above. The binding affinity of phage-**23** falls between the binding affinities of phage-**2** and -**3**, as expected, Figure 5-3. This experiment demonstrates that the generation of dual-displayed phage is independent of the ligands' sequence homology.

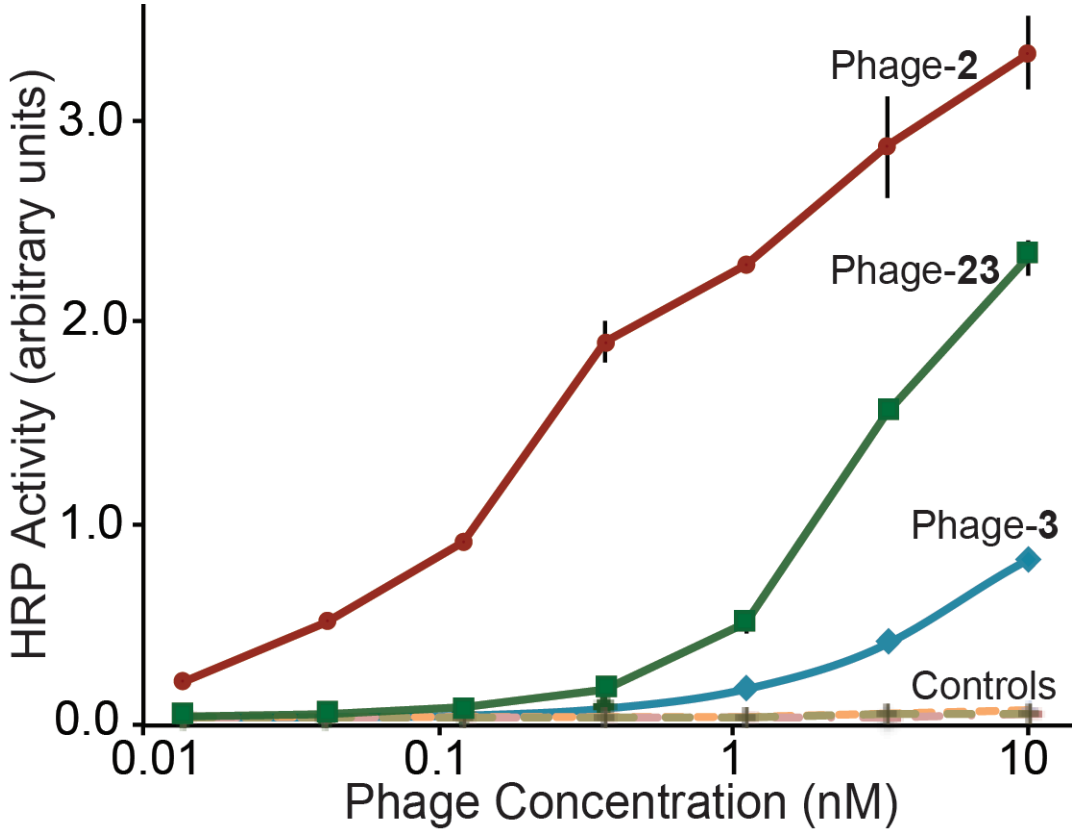

Figure 5-3. Phage-based ELISAs demonstrating the binding affinity of dual-displayed phage generated with dissimilar ligand sequences targeting PSMA. Phage-displayed ligands targeting BSA, and Stop-4 phage targeting PSMA, serve as the negative control.

5.7 Dual-displayed Phage with Ligands to Different Targets

To further demonstrate, dual display of two different peptides on the surface of the phage, a sandwich ELISA was designed for simultaneous detection of two ligands displayed on the phage surface. In this experiment, dual-displayed phage were prepared with PSMA binding ligand **2** and BSA binding ligand **4** – SSQDVCELGRWLSEECELYM. The binding affinity of phage-**24** towards BSA and PSMA confirms the presence of both ligands on phage, Figure 5-4. The ELISA protocol was modified as follows. Briefly, specific wells were coated with a 5.6 nM BSA solution, followed by blocking with SuperBlock (Thermo scientific). The wells were then incubated with phage-displayed ligands, followed by incubation with PSMA (16.8 nM). Levels of bound PSMA were quantified using anti-PSMA (YPSMA-1) antibody (Abcam) at a 1:1000 dilution, followed by horseradish-peroxidase-conjugated anti-mouse antibody (Sigma) at a 1:1000 dilution. The negative controls included phage-displayed ligands and Stop-4 phage replacing phage-**24** in the sandwich ELISA setup. Packaging of both phagemids for phage-**23** and -**24** was verified by PCR as described above.

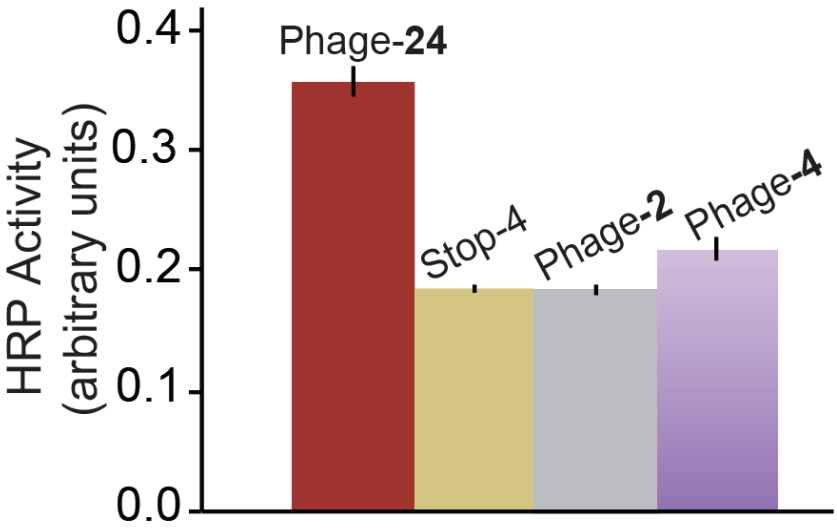

Figure 5-4. Phage-based ELISA demonstrating simultaneous binding to both BSA and PSMA. Stop-4 phage and individual-displayed phage ligands replacing phage-**24** in the sandwich ELISA setup, serve as the negative controls.

CONCLUSIONS

As reported here, the technique of super-infection provides a method for consistently generating *E. coli* cells with two different phagemids. The approach allows for the display of two genetically encoded ligands fused to P8. Such dual-displayed phage particles could potentially be used for targeting different markers, and thus be enormously useful for biosensing.

REFERENCES

(1) Kehoe, J. W.; Kay, B. K. Filamentous Phage Display in the New Millennium. *Chem. Rev.* **2005**, *105*, 4056–4072.

(2) Levin, A. M.; Weiss, G. A. Optimizing the Affinity and Specificity of Proteins with Molecular Display. *Mol. Biosyst.* **2006**, *2*, 49–57.

(3) Lamboy, J. A.; Tam, P. Y.; Lee, L. S.; Jackson, P. J.; Avrantinis, S. K.; Lee, H. J.; Corn, R. M.; Weiss, G. A. Chemical and Genetic Wrappers for Improved Phage and RNA Display. *ChemBioChem* **2008**, *9*, 2846–2852.

(4) Lamboy, J. A.; Arter, J. A.; Knopp, K. A.; Der, D.; Overstreet, C. M.; Palermo, E. F.; Urakami, H.; Yu, T.-B.; Tezgel, O.; Tew, G. N.; *et al.* Phage Wrapping with Cationic Polymers Eliminates Nonspecific Binding between M13 Phage and High pI Target Proteins. *J. Am. Chem. Soc.* **2009**, *131*, 16454–16460.

(5) Smith, G. P. Filamentous Fusion Phage: Novel Expression Vectors That Display Cloned Antigens on the Virion Surface. *Science* **1985**, *228*, 1315–1317.

(6) Sidhu, S. S. Engineering M13 for Phage Display. *Biomol. Eng.* **2001**, *18*, 57–63.

(7) Sidhu, S. S.; Weiss, G. A. *Phage Display: A Practical Approach*; Lowman, H. B.; Clackson, T., Eds.; Oxford University Press: New York, 2004.

(8) Smith, G. P.; Scott, J. K. Libraries of Peptides and Proteins Displayed on Filamentous Phage. *Methods Enzym.* **1993**, *217*, 228–257.

(9) Goldsmith, M.; Kiss, C.; Bradbury, A. R. M.; Tawfik, D. S. Avoiding and Controlling Double Transformation Artifacts. *Protein Eng. Des. Sel.* **2007**, *20*, 315–318.

(10) Sblattero, D.; Bradbury, A. Exploiting Recombination in Single Bacteria to Make Large Phage Antibody Libraries. *Nat. Biotechnol.* **2000**, *18*, 75–80.

(11) Arter, J. A.; Diaz, J. E.; Donavan, K. C.; Yuan, T.; Penner, R. M.; Weiss, G. A. Virus-Polymer Hybrid Nanowires Tailored to Detect Prostate-Specific Membrane Antigen. *Anal. Chem.* **2012**, *84*, 2776–2783.

(12) Mohan, K.; Donavan, K. C.; Arter, J. A.; Penner, R. M.; Weiss, G. A. Sub-Nanomolar Detection of Prostate-Specific Membrane Antigen in Synthetic Urine by Synergistic, Dual-Ligand Phage. *J. Am. Chem. Soc.* **2013**, *135*, 7761–7767.

CHAPTER 6

PEGylated, Extended-Linker Phage Library for Selections against Cell Surfaces

INTRODUCTION

Specific binding to diseased cells such as cancer cells is crucial for both diagnostic and therapeutic purposes. For example, efficient and specific detection of metastatic cells could improve prognosis for the >90% of deaths resulting from metastatic causes.[1] Additionally, side effects to drugs are observed due to the non-specific delivery to non-target sites. Non-specific delivery, in addition, leads to reduced effective dose at the target site, thereby requiring increase in the drug dosage with concomitant increased site effects. Furthermore, the delivery of hydrophobic drugs such as doxorubicin and paclitaxel is affected by heightened non-specific delivery due to adhesion to the hydrophobic lipid membranes of cells.[2–4] Thus, we engineer phage to provide a specific capture or delivery platform with improved sensitivity and selectivity based on not just one target protein, but the whole cell surface.

Phage-display is a well-established technique for molecular display and affinity selection.[5,6] M13 bacteriophage or 'phage,' are rod-shaped filamentous viruses that infect bacterial cells. The dimensions of the virion are approximately 1 μm by 6 nm, and it packages a single-stranded circular DNA genome or a 'phagemid' plasmid. The majority of the virus capsid comprises of a single coat

protein P8, which constitutes the length of the capsid. Five copies each of P3 and P6 are found at one end, whereas P7 and P9 are found at the other end. Additionally, P8 proteins are oriented such that the *C*-terminus interacts with the packaged DNA, whereas the *N*-terminus is exposed to the environment. Hence, the gene of interest is fused to the *N*-terminus of P8 gene, and leads to the display of the peptide or protein of interest as a fusion to the coat protein. [7–9] A phagemid display system provides less than 10% coverage of the displayed protein on the virus surface, to avoid damage to the capsid structure.[10] Furthermore, the phage surface presents a high negative charge due to the presence of three carboxylate bearing Asp and Glu residues in the *N*-terminal region of P8.[11]

Sensitive and specific detection of biopolymers and small molecules can be achieved through utilization of the phage surface. To maximize the density of ligands present on the surface, we previously established the concept of 'phage wrapping.' An oligolysine peptide (Lys_{14}) wraps around the surface of the phage due to electrostatic interactions. Furthermore, the oligolysine peptide was functionalized with an alkyne or thiol group for conjugation to azide-functionalized PEG or peptide ligands, or maleimide-functionalized PEGylated ligands, respectively. The approach allowed the sensitive detection of prostate-specific membrane antigen (PSMA),[12–14] a prostate cancer biomarker, at 100 pM limit of detection. Two PSMA binding peptide ligands were used: ligand-**1** (CALCEFLG) and ligand-**2** (SECVEVFQNSCDW). Also, phage-displayed peptide-**2**

demonstrates a >100-fold higher affinity for PSMA than peptide-**1**.[15,16] In a subsequent study, the wrapping concept along with the PSMA binding ligands was utilized to specifically capture PSMA expressing, prostate cancer LNCaP cell line.[17] PSMA is present on LNCaP cells as an integral membrane protein.[18–20]

A cell surface presents a multitude of receptors on its surface. The presence of these receptors in conjunction with the hydrophobic lipid membrane renders the surface prone to non-specific adhesion. As previously reported, phage surface shows high non-specific adhesion to cells. To eliminate this non-specificity, we previously used polyethylene glycol (PEG) conjugated wrappers on phage, which reduced such adhesion by ≈80%. PEG is commonly employed in a myriad of biomedical applications to reduce non-specific adhesion, among other benefits.[21] Additionally, longer PEGylated ligands with ≈100 PEG units, wrapped on phage allowed selective capture of target cells.[17] Here, we envisioned replacing the non genetically-encoded PEG linker with a genetically-encoded Gly-Ser linker to improve the properties of the entire system, retaning the displayed ligand. In addition, the use of a genetically encoded linker would allow the generation of a peptide library on phage for selections against cell surfaces. The non-specific adhesion will be reduced with the use of PEGylated wrappers.

RESULTS AND DISCUSSION

6.1 Design of Genetically-Encoded Linkers

Linkers act as a connector between two different protein domains, which can be functionally independent or cooperative. Linkers assist binding affinity and other properties by creating a covalent link between the two domains. The key variables for linker design are length and composition. The most commonly used amino acids for the design of linkers in nature are Gly, Ser, Thr, and Ala.[22] The absence of a β-carbon allows Gly to adopt conformations, which are unachievable by other amino acids.[23] This property programs Gly with flexibility, which is especially relevant for designing linkers and forming loops that interconnect independent domains.[24,25] Though poly-Gly linkers provide the maximum levels of flexibility, they affect the stability, solubility or oligomeric state of the fused protein.[26] Thus, Gly-rich linkers are preferred to poly-Gly linkers, and obtained through the insertion of Ser residues. Ser is preferred over Ala due to the hydrophilic nature of the amino acid. Ser predominately improves linkers by slowing the rate of unfolding of the attached protein, thus, providing more stability to the conjugate.[27] For optimal stability and flexibility, >60% Gly composition is considered favorable.[26]

Codon optimization of the Gly-Ser linker is essential for enhanced expression. Gly is encoded by GGN, where N indicates the base A, T, G or C in IUB code, whereas Ser is encoded by codons such as AGC, TCA or TCC. A

>60% Gly composition could lead to long repeats of G. Thus, a careful design of the linker is required for insertion into the phagemid through Kunkel mutagenesis-based approach.[28] Furthermore, codon pairs that are over-represented are known to translate slower than the under-represented ones. The over-represented pairs act as ribosomal pause sites, thereby leading to slower incorporation. Additionally, such pairs can pause translation to assist in the proper folding of the nascent protein. For example, the codon is GGA GGC is extremely slow, whereas is GGT GGC a faster incorporating pair.[29,30] Furthermore, a complete array of Gly-Ser linker patterns is seen in the literature with specific patterns such as $(GGGGS)_n$ or $(GGS)_n$, to completely random linkers with no obvious pattern.[26] In addition, the specific positions of Gly and Ser in the linker are known to be unimportant, though the overall composition is relevant.[27] Thus, a random mixture of Gly and Ser residues, with >60% Gly composition was used to design the linkers discussed in this chapter. Gly codons were mixed, and interspersed with Ser codons, to avoid long stretches of G. The linkers also incorporated a mixture of slow and fast incorporating codon pairs.

6.2 Generation of Phagemid-2 with Different Linker Lengths

Phage-displayed peptide-**2** was genetically modified to insert linkers of different lengths. The Gly-Ser linkers were inserted between the displayed peptide and P8 through extension of kunkel mutagenesis. Briefly, the Gly-Ser linker was designed as a primer with flanking regions overlapping the displayed peptide and the *N*-terminus of the P8 coat protein. Next, uracil containing phagemid DNA was prepared, and the primer annealed, extended and ligated to provide a non-uracil containing genome with the linker inserted. The hybrid DNA was then transformed into *E. coli* cells carrying dUTPase and uracil deglycosidase, which can degrade the uracil containing parental DNA. The result is the phagemid DNA containing the inserted linker. Despite the necessary precautions taken during the design of the Gly-Ser linker primers, full incorporation of the desired linkers was not achieved. For example, mutagenesis to insert a 30-mer Gly-Ser linker lead to the incorporation of only 20 Gly-Ser residues, probably due to non-specific annealing of the primers. Finally, three different scaffolds were generated with 15, 35 and 51-mer Gly-Ser linkers, termed 'phage-$GS_{15/35/51}$-**2**,' where the subscript indicates the linker length.

The sequences of the obtained linkers are as follows:

General format: SECVEVFQNSCDW-$(Gly\text{-}Ser)_n$- AEGD

Phage-GS_{15}-**2:** GGGSGSSSGGGSGGG

Phage-GS_{35}-**2:** GGGSGSSSGGGGSSGGGSGGGSGGSGGSSSGSGGG

Phage-GS_{51}-**2:** GGGSGSSSGGGGSSGGGSGGGSGGSGGGSGGSGGGSGSS SGGGSGGSSGGG

SECVEVFQNSCDW is the sequence for PSMA ligand **2**, AEGD is the beginning of the P8 coat protein sequence, and $(Gly\text{-}Ser)_n$ indicates a combination of Gly and Ser as the linker.

6.3 PSMA Binding Affinities of Phage with Extended Gly-Ser Linkers

The relative binding affinities of the phage-displayed ligands with the extended Gly-Ser linkers (phage-$GS_{15/35/51}$-**2**) targeting PSMA were first compared by ELISA, Figure 6-1. In this assay, PSMA protein was immobilized on microtiter plates, followed by the addition of phage-$GS_{15/35/51}$-**2**. The levels of bound phage were quantified using HRP-conjugated anti-M13 antibody, which generates a colored product upon substrate addition. The color change can be

measured spectrophotometrically. The ELISA illustrates that peptide-**2** with any of the three linker lengths is still effective at targeting PSMA, with high but different affinities. A very slight decrease in the binding affinity of phage-GS_{35}-**2** is observed, compared to phage-GS_{15}-**2**. Whereas, an almost 35% reduction in affinity is observed for phage-GS_{51}-**2** compared to phage-GS_{15}-**2**. The decrease in affinity could be attributed to the lower copy number of the phage-displayed ligands with increase in linker length, which causes the combined size of the displayed moiety to increase. Thus, the longer 51-mer Gly-Ser linker could lead to fewer displayed peptides on the phage surface compared to the 15-mer linker. The larger size of the displayed protein can interfere with the capsid formation. As a result, the drop in affinity for phage-GS_{51}-**2** could be a consequence of the increased size of the displayed peptide. Phage targeting bovine serum albumin (BSA), and Stop-4 phage (control phage with no ligands displayed on the surface) targeting PSMA provided the negative controls for the assay.

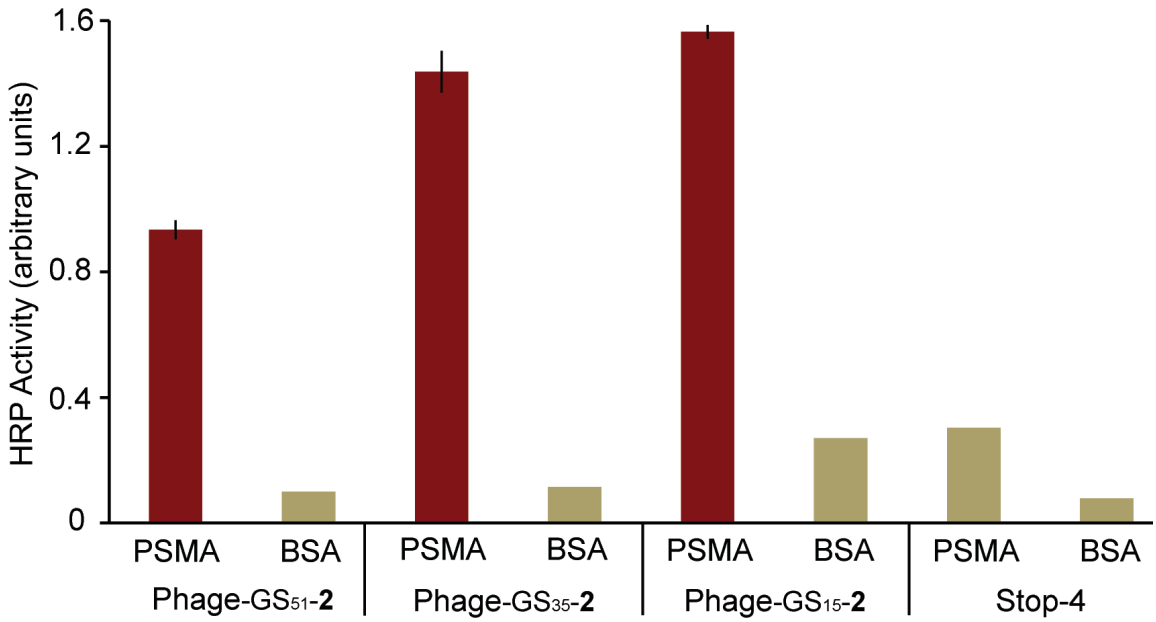

Figure 6-1. Phage-based ELISA comparing the relative binding affinities of phage-displayed peptide-**2** (red bars) with 15, 35 or 51-mer Gly-Ser linker targeting PSMA. A higher HRP acitivity indicates stronger binding between the ligands and the target. Phage-**2** targeting BSA, and Stop-4 phage (control phage with no displayed ligands) targeting both BSA and PSMA provide negative controls (gold bars) for the assay. Error bars represent standard error, n = 3. All experimental data points with the exception of the negative controls (n = 1) include such error bars.

6.4 Pegylated Wrappers on Phage with Extended Gly-Ser Linkers

Wrapping the extended-linker phage-displayed ligands with PEG would be required for cell targeting assays. Thus, it is necessary to evaluate the affinity of phage-displayed ligands upon PEG wrapping. As previously described, azide-functionalized PEG with 7, 22 or 45 ethylene glycol units (average molecular weights of 300, 1K or 2K, respectively) were used. Three different lengths of PEG were previously compared as differences in PEG units leads to different conformations of the polymer. Smaller PEG length such as PEG 7 presumably adopts a mushroom conformation, whereas PEG 22 or 45 adopt the brush conformation with the height of the brush increasing with increase in the number of PEG units. The brush conformation is more efficient at reducing non-specific adhesion due to the extended hydration sphere leading to lower secondary adsorption, which is defined as adhesion occuring at the outer surface of the PEG layer. Additionally, as previously described, the wrappers were applied at 0.15 mole fraction to minimize secondary non-specific adhesion.[17]

The binding affinities of proteins conjugated to PEG normally remain unaffected.[31,32] But, the affinities of the phage-displayed ligands could be affected if the PEG layer completely or partially encapsulates the displayed ligands. An ELISA compared the binding affinities of phage-$GS_{15/35/51}$-**2** wrapped with PEG 45, Figure 6-2. The wrappers were applied at an estimated concentration of 500/

phage, as previously reported.[17] All the extended-linker phage-displayed peptides wrapped with PEG bound to PSMA, although with decreased affinities compared to the unwrapped phage. A 30% decrease in affinity is observed for wrapped phage-GS_{15}-**2**, compared to unwrapped phage, whereas a 45% decrease is observed for phage-GS_{35}-**2**. In theory, a much larger decrease in affinity should have been observed for the 15-mer Gly-Ser linker compared to the 35-mer linker, as the shorter linker might lead to the displayed peptides being more susceptible to encapsulation by PEG. The reversal in trend could be attributed to the high copy number of the shorter linker-peptide, providing a saturation in assay response. As expected, the long 51-mer linker allows the peptide ligands to be most spatially free and unencumbered by the PEG layer, thereby providing the lowest drop in affinity, and will be used as the scaffold for the remainder of the experiments.

To further confirm the hypothesis that the decrease in binding affinity of wrapped phage-displayed ligands resulted from PEG encapsulation or hindrance, different PEG lengths were assayed. An ELISA compared the binding affinities of phage-$GS_{15/35/51}$-**2** wrapped with PEG 7/22/45, Figure 6-3. As expected, the decrease in affinity increases with longer lengths of the PEG polymer. The trend is consistent across different lengths of Gly-Ser linkers, thereby confirming the initial hypothesis. But, as the drop in affinity is not as significant between PEG 7 and PEG 45, PEG 45 will be used with phage-GS_{51}-**2** for future experiments to

reduce non-specific adhesion, as this length of PEG has previously been shown to be the most effective.[17]

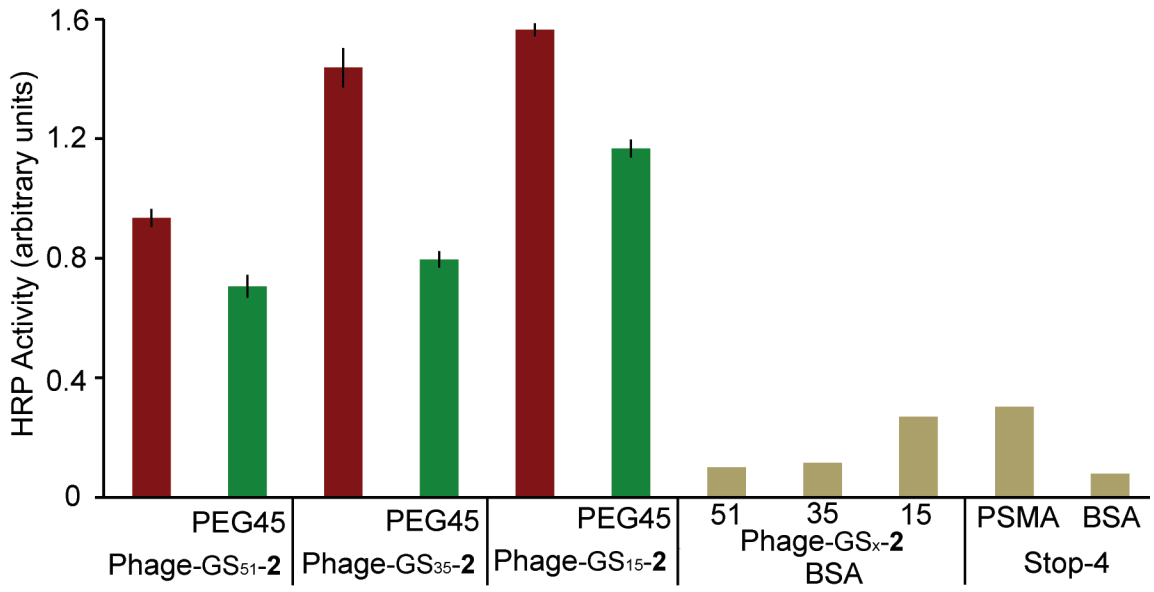

Figure 6-2. Phage-based ELISA illustrating the effect of PEG 45 wrapping on phage-GS$_{15/35/51}$-**2** (red bars) targeting PSMA. Green bars indicate phage wrapped with PEG 45. The negative controls (gold bars) were as described above. The wrappers were applied at an estimated concentration of 500/phage.

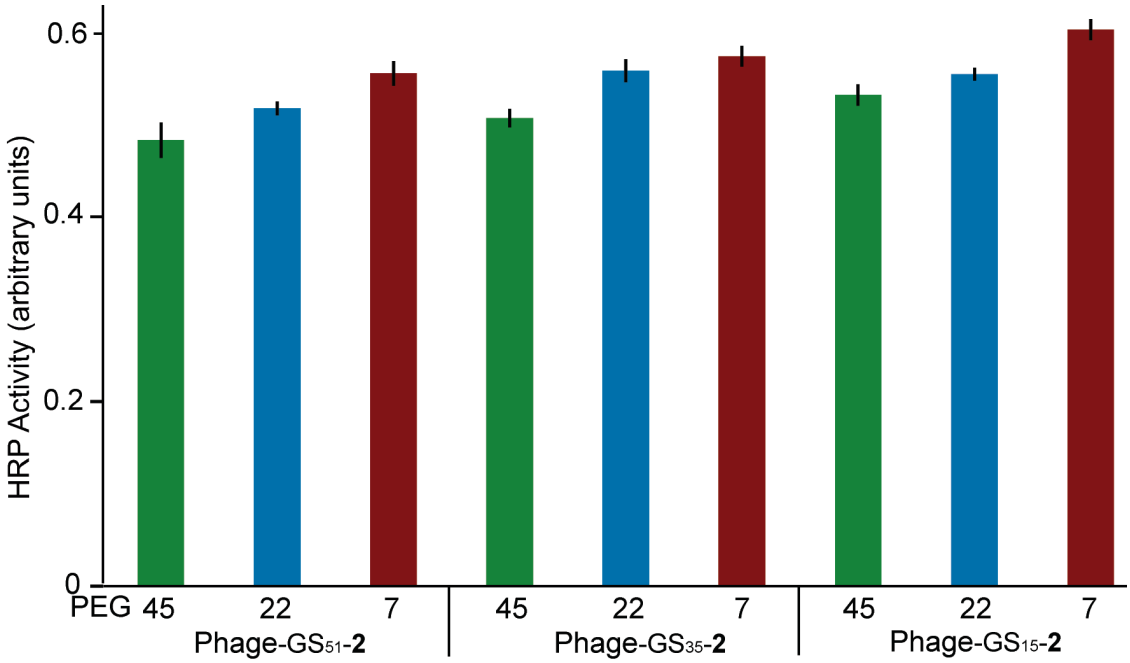

Figure 6-3. Phage-based ELISA comparing the effects of different lengths of PEGylated wrappers on Gly-Ser extended-linker phage targeting PSMA. The colors indicate the length of the PEG wrapper used; green bars correspond to PEG 45, blue bars correspond to PEG 22, and red bars correspond to PEG 7. A similar trend is observed for all three Gly-Ser linkers; a decrease in PSMA-binding affinity results from increasing the length of the PEGylated wrapper.

6.5 Library Generation with 51-mer Gly-Ser Linker

To obtain cell targeting peptides, a phage-displayed library was constructed. As a proof of concept study, the phage-GS_{51}-**2** was used as the template for this library. The sequence of peptide-**2,** SECVEVFQNSCDW could be represented as $X_2CX_7CX_2$, where X could be any amino acid. Thus, $X_2CX_7CX_2$ was used as one of the scaffolds for library generation with some modifications. The two Cys residues were retained to provide conformational rigidity. Furthermore, in the phagemid, the *C*-terminal end of the ligand is followed by the Gly-Ser linker. The high Gly composition implies multiple G bases, which could lead to non-specific annealing during mutagenesis, which is used for library generation, as explained below. Thus, the last two *C*-terminal residues Asp and Trp were retained for specific annealing providing X_2CX_7CDW as the library scaffold. An increase in the X7 variable region of the library would further enhance the library diversity, while also providing a longer construct capable of different binding modes. Therefore, a $X_2CX_{11}CDW$ library scaffold was also designed.

The libraries were constructed using an oligonucleotide-directed mutagenesis protocol.[9,28] As described above, uracil-containing phage-GS_{51}-**2** DNA was generated. Next, the oligonucleotides were annealed, extended and ligated to the uracil-containing template DNA. Transformation into *E. coli* cells provided the desired phage libraries. Both the libraries were generated separately, and then mixed in equimolar amounts. The theoretical diversity of

X_2CX_7CDW would be 5.1×10^{11}, and the $X_2CX_{11}CDW$ library includes 8.2×10^{16} different peptides for complete representation. The experimental diversity of the combined library was calculated to be 1.8×10^7, whereas phage propagation and amplification provided 9×10^{14}, indicating the presence of multiple copies of each individual clone obtained above.

6.6 Cell-Targeting Selections

The synthesized libraries were next used to target LNCaP cells, and extract high affinity ligands through cell-based selections. To increase the specificity of selections, a negative selection round was first performed with prostate cancer PC3 cells. This could increase the specificity of ligands obtained for LNCaP cells. The selection assays were modified from previous cell-based ELISAs.[17] Briefly, the cells were cultured in 24-well plates, to ≈80-90% confluency, and fixed with glutaraldehyde. The phage library at a concentration of 15 nM was first wrapped with PEG 45, and then incubated with PC3 cells. Next, the depleted library was transferred to LNCaP cells. After incubation and washing away the non-binders, the bound phage were eluted with hydrochloric acid, and propagated in *E. coli* cells. Unfortunately, this initial attempt did not yield the desired result. The phage titers obtained indicated negligible amounts of eluted phage, which was suspected during the elution step with hydrochloric acid, as the immobilized layer seemed highly stable under the microscope. The

glutaraldehyde used for cross-linking could have cross-linked phage to the cells, and, thus, rendered them incapable of elution.

CONCLUSIONS AND FUTURE DIRECTIONS

Selections towards whole cell surfaces offer an advantageous approach for specific cell targeting, for capture and delivery purposes. A novel phage-displayed peptide library was designed with an extended, genetically-encoded Gly-Ser linker. A 51-mer Gly-Ser linker incorporated into the library allowed phage wrapping with PEG 45 without hindering the displayed ligands. Wrapping phage with PEG 45 prevents non-specific adhesion to the cell surfaces. The library scaffolds designed were X_2CX_7CDW and $X_2CX_{11}CDW$.

This chapter provides the phage scaffold, the PEGylated extended-linker libraries for performing cell-based selections. The cell-targeting approach presented in this chapter requires optimization. For example, the fixation step could either be avoided or performed with methanol. Alternatively, microtiter plates could be tried as a replacement for 24-well plates. Additionally, an initial negative selection round could be avoided to prevent excessive depletion of the library. And, the phage elution step with hydrochloric acid requires an in-depth analysis. Furthermore, additional library scaffolds could also be designed. For example, Ala residue, which increases linker stability by accelerating folding,[27] could be incorporated. We hope that careful optimization and planning would provide a suitable approach for performing cell-based selections.

MATERIALS AND METHODS

All chemicals and reagents were purchased from Sigma-Aldrich, and used as received unless otherwise noted. PSMA and the cell lines LNCaP and PC3 were generous gifts from Drs. William Ernst and Gary Fuji (Molecular Express). N,N-Diisopropylethylamine (DIPEA) and azide-functionalized PEG7, 22 and 45 were purchased from Sigma, and 4-Azidobutanoic acid was purchased from Synthonix. 4-Pentynoic acid (GFS Chemicals, Inc.), O-benzotriazole-N,N,N',N'-tetramethyluronium hexafluorophosphate, HBTU (GL Biochem Ltd.), triethyammonium acetate buffer (Fluka Biochemika) and Tween-20 (EMD Science) were used as received. Library DNA oligonucleotides were purchased from Integrated DNA Technologies, Inc. HPLC-grade water was used for the preparation of solutions.

M13 bacteriophage propagation

Phage propagation and isolation were performed as previously described.[15–17] Briefly, phagemid DNA encoding for the desired peptide was transformed into $CaCl_2$ competent *E. coli* XL-1 Blue cells. The cells were grown in a 2 mL 2YT media culture supplemented with carbenicillin and tetracycline antibiotics, at 37 °C. Next, the culture at log-phase growth was infected with KO7 helper phage with a 4.6 multiplicity of infection. This starting culture was then transferred to a 75 mL 2YT media culture supplemented with carbenicillin, and kanamycin. The phage culture was incubated for 19 h at 37 °C with shaking. The

phage were isolated using PEG-NaCl (2.5 M NaCl, 20% PEG-8000) precipitation. The phage precipitation step was repeated to obtain a phage solution of higher purity. After the second precipitation, the phage were resuspended in phosphate-buffered saline (PBS, 135 mM NaCl, 2.50 mM KCl, 8.00 mM Na_2HPO_4, 30.0 mM KH_2PO_4, pH 7.2). The phage concentration was determined by UV absorbance at 268 nm (OD_{268} of 1.0 = 8.31 nM phage).

For the propagation of uracil-containing phage, the phagemid was transformed into *E. coli* CJ236 cells. The overnight 75 mL culture was supplemented with 0.5 μg/mL uracil, in addition to the antibiotics. Subsequently, the uracil containing phagemid DNA was isolated using Qiagen QIAprep M13 spin kit.

Solid-phase peptide synthesis

The oligolysine peptide was synthesized by conventional solid-phase peptide synthesis with Fmoc-protected amino acids on Rink-amide resin (Novabiochem), as previously described.[15,33,34] The final coupling step with 4-pentynoic acid provided an alkyne functionality at the *N*-terminus. The peptide was purified by reverse-phase HPLC, and characterized by MALDI-TOF mass spectrometry. The calculated *m*/*z* for alkyne-functionalized K_{14} peptide $[M+Na]^+$ 1914.37, found 1914.18.

Oligonucleotide design for Gly-Ser linker generation

To generate phage-GS_{35}-**2**:

5' - GGA TCC GGA GGA GGC GGT GGG AGC GGT GGC GGA GGC TCA AGC GGA GGG GGT TCC GGA GGT GGC AGC GGG GGC AGC GGG GGA TCC AGC TCA GGG AGC GGG GGA GGT GCC GAG GGT GAC GAT - 3'

To generate phage-GS_{51}-**2**:

5'-GGG AGC GGG GGA GGT TCA GGA TCC GGA AGC GGC GGC TCC GGT GGG AGC GGT GGA GGC TCA GGT TCC TCA AGC GGA GGT GGG TCC GGC GGA AGC TCA GGT GGA GGG GCC GAG GGT GAC GAT C - 3'

To generate X_2CX_7CDW library scaffold:

5' - G TTT AGC GCC AGC GCG NNS NNS TGC NNS NNS NNS NNS NNS NNS NNS TGC GAC TGG GGT GGC - 3'

To generate $X_2CX_{11}CDW$ library scaffold:

5' - G TTT AGC GCC AGC GCG NNS NNS TGC NNS NNS NNS NNS NNS NNS NNS NNS NNS NNS NNS TGC GAC TGG GGT GGC - 3'

The underlining denotes the overlapping region, flanking the insert. And, N = A/T/G/C, and S = G or C.

Oligonucleotide-directed mutagenesis

Library generation: The oligonucleotides for library generation were first phosphorylated at the 5' terminus in a 22 µL reaction, as follows. In a thin walled tube, 2 µL of 10x TM buffer, 2 µL of 10 mM ATP, 1 µL of 100 mM DTT, and 2 µL of T4 polynucleotide kinase were added. Next, oligonucleotide was added to a

final concentration of 2 μM. The volume was completed to 22 μL using DEPC-treated water, and the reaction was incubated at 37 °C for 2h.

Next, the phosphorylated oligonucleotides were annealed to the uracil-containing DNA template at 20 μg scale. The DNA template was added to the phosphorylated reaction mixture, followed by addition of 25 μL of 10x TM buffer. The volume was completed to 250 μL using DEPC-treated water. The reaction mixture was given a pulse spin followed by incubation at 90 °C for 2 min, 50 °C for 3 min, and 20 °C for 5 min. The reaction mixture was then place on ice for 5 min. Next, 10 μL of 10 mM ATP, 10 μL of 25 mM dNTPs, 15 μL of 10 mM DTT, and 3 μL of T7 DNA polymerase were added, and the reaction mixture was allowed to incubate at room temperature for 1 h. Then, 1 μL of T4 Ligase was added and the reaction mixture was incubated overnight at room temperature. The product of the reaction was analyzed using gel electrophoresis. The hybrid hetero-DNA was then electroporated into SS320 electrocompetent cells. Next, the cells were transferred to a 2YT media culture, and phage propagation and purification was performed, as described above, to isolate the extended-linker Gly-Ser phage-displayed peptide libraries.

For the insertion of Gly-Ser linkers, a smaller scale of the same procedure was followed. The reaction product was analyzed using gel electrophoresis, and the band containing the circular, covalently closed DNA was extracted. Next, the DNA was transformed into *E. coli* XL-1 cells, and plated on agar. The colonies obtained were analyzed by polymerase chain reaction for the insertion of the Gly-

Ser linker. The insertion of the Gly-Ser linkers was confirm through sequencing, Figures 6-4, 6-5 and 6-6.

PSMA Targeting Enzyme-Linked Immunosorbent Assay (ELISA)

The phage-based ELISAs were performed as previously described.[15] Briefly, specific wells of a 96-well microtiter plate (Nunc Maxisorp) were coated with 11 nM, 100 µL/well PSMA solution for 1 h on a shaker at room temperature. Next, the wells were blocked with a 0.2% w/v solution of bovine serum albumin (BSA) in PBS for 30 min. The wells on the ELISA plate were then incubated with the phage samples (100 µL/well, 10 nM) for 1 h. The levels of bound phage were quantified using horseradish-peroxidase-conjugated anti-M13 antibody (100 µL/well, 1:5000 dilution in PBS) for 30 min. Next, HRP substrate *o*-phenylenediamine dihydrochloride was added in conjunction with hydrogen peroxide, a redox mediator. The enzyme activity was measured spectrophotometrically at 450 nm using a microtiter plate reader (Bio-Tek).

***Phage wrapping*:** Phage (10 nM in 100 µL) was wrapped with 1 µL of K_{14}-alkyne (525 µM), as previously described.[17] Next, the azide-alkyne copper-catalyzed cycloaddition 'click' reaction was performed, but with the following modifications.[15,16,35] Triethylammonium acetate was added to a final concentration of 50 mM, followed by the addition of 1.5 µL of 1 mM azide-

functionalized PEG. Next, ascorbic acid was added to a final concentration of 1 mM, followed by the addition of copper sulfate to a final concentration of 1.5 mM.

Cell growth

The cell lines were grown as monolayers in media supplemented with 10% fetal bovine serum (Cellgro), 1 mM sodium pyruvate[36] and 1% penicillin-streptomycin-glutamine in 5% CO_2 and 95% air-humidified atmosphere at 37 °C. LNCaP cells were cultured in RPMI 1640 media. PC3 cells were grown in Ham's F-12 media.

Cell-based Selections

LNCaP and PC3 cells were grown to ≈80-90% confluency in 24-well plates. The cells were washed twice with 500 µL PBS/well. Next, 400 µL of a 0.05% glutaraldehyde in PBS solution was added to the wells, and allowed to incubate at room temperature for 15 min. The solution was removed, and the wells were washed twice with 700 µL PBS/well. Next, the wells were blocked with 400 µL/well of blocking buffer containing 1% w/v BSA in PBS. The plate was incubated for 45 min at room temperature. The solution was removed, and the wells were washed twice with 700 µL PBS/well.

Separately, phage libraries were prepared before wrapping with PEG. Phage (15 nM in 100 µL of PBS) were wrapped with K_{14}-alkyne (1.5 µL of 525 µM in water) by thoroughly mixing and incubating at room temperature for 15

min. PEGylated phage were then generated through an on-phage click reaction, as previously described.[15,16,35] Briefly, triethylammonium acetate buffer was added to a final concentration of 50 mM. Next, 2.25 µL of 1 mM azide-functionalized PEG was added. Ascorbic acid was added to a final concentration of 1 mM, and copper sulfate was added to a final concentration of 1.5 mM. The solutions were gently mixed by pipetting at each step, and incubated for 30 min at room temperature.

The wells of the 24-well plate containing the PC3 cells were first incubated with 400 µL/well of PEG-wrapped phage for 30 min. Next, the phage solution was gently aspirated and transferred to the wells containing LNCaP cells, and incubated for 1 h at room temperature with shaking at 50 rpm. The solution was removed, and the wells were washed three times with 700 µL/well of PBS. Next, 400 µL/well of 0.1 M hydrochloric acid was added, and the plate was sonicated for 10 min at room temperature. The solution was neutralized with 1/3rd volume of Tris(hydroxymethyl) aminomethane buffer (pH 8). A 10 mL *E. coli* XL-1 cell culture was infected with the eluted- and neutralized-phage solution for 45 min at 37 °C. Next, the cells were infected with KO7 helper phage at 4.6 multiplicity of infection for 1 h at 37 °C. The solution was then transferred to 150 mL 2YT media supplemented with carbenicillin and kanamycin. Phage propagation was continued as described above.

```
  1 GCCAGCGCGTCGGAGTGCGTCGAGGTCTTCCAAAACTCGTGCGACTGGGGTGGCGGCAGC 60
  1  A   S   A   S   E   C   V   E   V   F   Q   N   S   C   D   W   G   G   G   S  20

 61 GGCAGCTCCAGCGGTGGAGGATCCGGAGGAGGCGCCGAGGGTGACGATCCCGCAAAAGCG 120
 21  G   S   S   S   G   G   G   S   G   G   G   A   E   G   D   D   P   A   K   A  40

121 GCCTTTAACTCCCTGCAAGCCTCAGCGACCGAATATATCGGTTATGCGTGGGCGATGGTT 180
 41  A   F   N   S   L   Q   A   S   A   T   E   Y   I   G   Y   A   W   A   M   V  60

181 GTTGTCATTGTCGGCGCAACTATCGGTATCAAGCTGTTTAAGAAATTCACCTCGAAAGCA 240
 61  V   V   I   V   G   A   T   I   G   I   K   L   F   K   K   F   T   S   K   A  80

241 AGCTGATAA 249
 81  S   *   *  83
```

Figure 6-4. Sequence of phage-GS_{15}-**2** confirming the insertion of a 15-mer Gly-Ser linker. ASA corresponds to the end of the DsbA Signal sequence. SECVEVFQNSCDW corresponds to the sequence of peptide-**2**, followed by the Gly-Ser linker. AEGD corresponds to the beginning of the P8 coat protein, and the sequence ends with the stop codon.

```
  1 GCCAGCGCGTCGGAGTGCGTCGAGGTCTTCCAAAACTCGTGCGACTGGGGTGGCGGCAGC 60
  1  A  S  A  S  E  C  V  E  V  F  Q  N  S  C  D  W  G  G  G  S  20

 61 GGCAGCTCCAGCGGTGGCGGAGGCTCAAGCGGAGGGGGTTCCGGAGGTGGCAGCGGGGGC 120
 21  G  S  S  S  G  G  G  G  S  S  G  G  G  S  G  G  G  S  G  G  40

121 AGCGGGGGATCCAGCTCAGGGAGCGGGGGAGGTGCCGAGGGTGACGATCCCGCAAAAGCG 180
 41  S  G  G  S  S  S  G  S  G  G  G  A  E  G  D  D  P  A  K  A  60

181 GCCTTTAACTCCCTGCAAGCCTCAGCGACCGAATATATCGGTTATGCGTGGGCGATGGTT 240
 61  A  F  N  S  L  Q  A  S  A  T  E  Y  I  G  Y  A  W  A  M  V  80

241 GTTGTCATTGTCGGCGCAACTATCGGTATCAAGCTGTTTAAGAAATTCACCTCGAAAGCA 300
 81  V  V  I  V  G  A  T  I  G  I  K  L  F  K  K  F  T  S  K  A  100

301 AGCTGATAA 309
101  S  *  *  103
```

Figure 6-5. Sequence of phage-GS_{35}-**2** confirming the insertion of a 35-mer Gly-Ser linker. ASA corresponds to the end of the DsbA Signal sequence. SECVEVFQNSCDW corresponds to the sequence of peptide-**2**, followed by the Gly-Ser linker. AEGD corresponds to the beginning of the P8 coat protein, and the sequence ends with the stop codon.

```
  1 GCCAGCGCGTCGGAGTGCGTCGAGGTCTTCCAAAACTCGTGCGACTGGGGTGGCGGCAGC 60
  1  A  S  A  S  E  C  V  E  V  F  Q  N  S  C  D  W  G  G  G  S  20

 61 GGCAGCTCCAGCGGTGGCGGAGGCTCAAGCGGAGGGGGTTCCGGAGGTGGCAGCGGGGGG 120
 21  G  S  S  S  G  G  G  G  S  S  G  G  G  S  G  G  G  S  G  G  40

121 AGCGGGGGAGGAAGCGGCGGGAGCGGTGGAGGCTCAGGTTCCTCAAGCGGAGGTGGGTCC 180
 41  S  G  G  G  S  G  G  S  G  G  G  S  G  S  S  S  G  G  G  S  60

181 GGCGGAAGCTCAGGTGGAGGGGCCGAGGGTGACGATCCCGCAAAAGCGGCCTTTAACTCC 240
 61  G  G  S  S  G  G  G  A  E  G  D  D  P  A  K  A  A  F  N  S  80

241 CTGCAAGCCTCAGCGACCGAATATATCGGTTATGCGTGGGCGATGGTTGTTGTCATTGTC 300
 81  L  Q  A  S  A  T  E  Y  I  G  Y  A  W  A  M  V  V  V  I  V  100

301 GGCGCAACTATCGGTATCAAGCTGTTTAAGAAATTCACCTCGAAAGCAAGCTGATAA 357
101  G  A  T  I  G  I  K  L  F  K  K  F  T  S  K  A  S  *  *  119
```

Figure 6-6. Sequence of phage-GS_{51}-**2** confirming the insertion of a 51-mer Gly-Ser linker. ASA corresponds to the end of the DsbA Signal sequence. SECVEVFQNSCDW corresponds to the sequence of peptide-**2**, followed by the Gly-Ser linker. AEGD corresponds to the beginning of the P8 coat protein, and the sequence ends with the stop codon.

REFERENCES

(1) Mehlen, P.; Puisieux, A. Metastasis: A Question of Life or Death. *Nat. Rev. Cancer* **2006**, *6*, 449–458.

(2) Ghosh, D.; Kohli, A. G.; Moser, F.; Endy, D.; Belcher, A. M. Refactored M13 Bacteriophage as a Platform for Tumor Cell Imaging and Drug Delivery. *ACS Synth. Biol.* **2012**, *1*, 576–582.

(3) Wang, T.; Petrenko, V. A.; Torchilin, V. P. Paclitaxel-Loaded Polymeric Micelles Modified with MCF-7 Cell-Specific Phage Protein: Enhanced Binding to Target Cancer Cells and Increased Cytotoxicity. *Mol. Pharm.* **2010**, *7*, 1007–1014.

(4) Wang, T.; Petrenko, V. A.; Torchilin, V. P. Optimization of Landscape Phage Fusion Protein-Modified Polymeric PEG-PE Micelles for Improved Breast Cancer Cell Targeting. *J. Nanomed. Nanotechnol.* **2012**, *Suppl 4*, 008.

(5) Kehoe, J. W.; Kay, B. K. Filamentous Phage Display in the New Millennium. *Chem. Rev.* **2005**, *105*, 4056–4072.

(6) Levin, A. M.; Weiss, G. A. Optimizing the Affinity and Specificity of Proteins with Molecular Display. *Mol. Biosyst.* **2006**, *2*, 49–57.

(7) Smith, G. P. Filamentous Fusion Phage: Novel Expression Vectors That Display Cloned Antigens on the Virion Surface. *Science* **1985**, *228*, 1315–1317.

(8) Russel, M.; Lowman, H. B.; Tim, C. *Phage Display: Practical Approach*; Lowman, H. B.; Clackson, T., Eds.; Oxford University Press: New York, 2004.

(9) Sidhu, S. S.; Weiss, G. A. *Phage Display: A Practical Approach*; Lowman, H. B.; Clackson, T., Eds.; Oxford University Press: New York, 2004.

(10) Sidhu, S. S.; Weiss, G. A.; Wells, J. A. High Copy Display of Large Proteins on Phage for Functional Selections. *J. Mol. Biol.* **2000**, *296*, 487–495.

(11) Welsh, L. C.; Symmons, M. F.; Sturtevant, J. M.; Marvin, D. A.; Perham, R.

N. Structure of the Capsid of Pf3 Filamentous Phage Determined from X-Ray Fibre Diffraction Data at 3.1 A Resolution. *J. Mol. Biol.* **1998**, *283*, 155–177.

(12) Horoszewicz, J. S.; Kawinski, E.; Murphy, G. P. Monoclonal Antibodies to a New Antigenic Marker in Epithelial Prostatic Cells and Serum of Prostatic Cancer Patients. *Anticancer Res.* **1987**, *7*, 927–935.

(13) Schülke, N.; Varlamova, O. A.; Donovan, G. P.; Ma, D.; Gardner, J. P.; Morrissey, D. M.; Arrigale, R. R.; Zhan, C.; Chodera, A. J.; Surowitz, K. G.; *et al.* The Homodimer of Prostate-Specific Membrane Antigen Is a Functional Target for Cancer Therapy. *Proc. Natl. Acad. Sci. USA* **2003**, *100*, 12590–12595.

(14) Chuang, A.-Y.; DeMarzo, A. M.; Veltri, R. W.; Sharma, R. B.; Bieberich, C. J.; Epstein, J. I. Immunohistochemical Differentiation of High-Grade Prostate Carcinoma from Urothelial Carcinoma. *Am. J. Surg. Pathol.* **2007**, *31*, 1246–1255.

(15) Mohan, K.; Donavan, K. C.; Arter, J. A.; Penner, R. M.; Weiss, G. A. Sub-Nanomolar Detection of Prostate-Specific Membrane Antigen in Synthetic Urine by Synergistic, Dual-Ligand Phage. *J. Am. Chem. Soc.* **2013**, *135*, 7761–7767.

(16) Mohan, K.; Penner, R. M.; Weiss, G. A. Biosensing with Virus Electrode Hybrids. *Curr. Protoc. Chem. Biol.* **2015**, *7*, 53–72.

(17) Mohan, K.; Weiss, G. A. Engineering Chemically Modified Viruses for Prostate Cancer Cell Recognition. *Mol. Biosyst.* **2015**, *11*, 3264–3272.

(18) Kawakami, M.; Nakayama, J. Enhanced Expression of Prostate-Specific Membrane Antigen Gene in Prostate Cancer as Revealed by in Situ Hybridization. *Cancer Res.* **1997**, *57*, 2321–2324.

(19) Dozmorov, M. G.; Hurst, R. E.; Culkin, D. J.; Kropp, B. P.; Frank, M. B.; Osban, J.; Penning, T. M.; Lin, H.-K. Unique Patterns of Molecular Profiling between Human Prostate Cancer LNCaP and PC-3 Cells. *Prostate* **2009**, *69*, 1077–1079.

(20) Horoszewicz, J. S.; Leong, S. S.; Chu, T. M.; Wajsman, Z. L.; Friedman, M.; Papsidero, L.; Kim, U.; Chai, L. S.; Kakati, S.; Arya, S. K.; *et al.* The LNCaP Cell Line--a New Model for Studies on Human Prostatic Carcinoma.

Prog. Clin. Biol. Res. **1980**, *37*, 115–132.

(21) Marsh, D.; Bartucci, R.; Sportelli, L. Lipid Membranes with Grafted Polymers: Physicochemical Aspects. *Biochim. Biophys. Acta - Biomembr.* **2003**, *1615*, 33–59.

(22) Argos, P. An Investigation of Oligopeptides Linking Domains in Protein Tertiary Structures and Possible Candidates for General Gene Fusion. *J. Mol. Biol.* **1990**, *211*, 943–958.

(23) Ramachandran, G. N.; Sasisekharan, V. Conformation of Polypeptides and Proteins. *Advan. Prot. Chem.* **1968**, *23*, 283–437.

(24) Steinert, P. M.; Mack, J. W.; Korge, B. P.; Gan, S. Q.; Haynes, S. R.; Steven, A. C. Glycine Loops in Proteins: Their Occurrence in Certain Intermediate Filament Chains, Loricrins and Single-Stranded RNA Binding Proteins. *Int. J. Biol. Macromol.* **1991**, *13*, 130–139.

(25) Lubkowski, J.; Hennecke, F.; Plückthun, A.; Wlodawer, A. Filamentous Phage Infection: Crystal Structure of g3p in Complex with Its Coreceptor, the C-Terminal Domain of TolA. *Structure* **1999**, *7*, 711–722.

(26) Reddy Chichili, V. P.; Kumar, V.; Sivaraman, J. Linkers in the Structural Biology of Protein-Protein Interactions. *Protein Sci.* **2013**, *22*, 153–167.

(27) Robinson, C. R.; Sauer, R. T. Optimizing the Stability of Single-Chain Proteins by Linker Length and Composition Mutagenesis. *Proc. Natl. Acad. Sci. USA* **1998**, *95*, 5929–5934.

(28) Kunkel, T. A.; Roberts, J. D.; Zakour, R. A. Rapid and Efficient Site-Specific Mutagenesis without Phenotypic Selection. *Methods Enzymol.* **1987**, *154*, 367–382.

(29) Trinh, R.; Gurbaxani, B.; Morrison, S. L.; Seyfzadeh, M. Optimization of Codon Pair Use within the $(GGGGS)_3$ Linker Sequence Results in Enhanced Protein Expression. *Mol. Immunol.* **2004**, *40*, 717–722.

(30) Irwin, B.; Heck, J. D.; Hatfield, G. W. Codon Pair Utilization Biases Influence Translational Elongation Step Times. *J. Biol. Chem.* **1995**, *270*, 22801–22806.

(31) Loo, C.; Lin, A.; Hirsch, L.; Lee, M.-H.; Barton, J.; Halas, N.; West, J.;

Drezek, R. Nanoshell-Enabled Photonics-Based Imaging and Therapy of Cancer. *Technol. Cancer Res. Treat.* **2004**, *3*, 33–40.

(32) Loo, C.; Lowery, A.; Halas, N.; West, J.; Drezek, R. Immunotargeted Nanoshells for Integrated Cancer Imaging and Therapy. *Nano Lett.* **2005**, *5*, 709–711.

(33) Merrifield, R. B. Solid Phase Peptide Synthesis. I. The Synthesis of a Tetrapeptide. *J. Am. Chem. Soc.* **1963**, *85*, 2149–2154.

(34) Amblard, M.; Fehrentz, J.-A.; Martinez, J.; Subra, G. Methods and Protocols of Modern Solid Phase Peptide Synthesis. *Mol. Biotechnol.* **2006**, *33*, 239–254.

(35) Lumiprobe http://www.lumiprobe.com/protocols/click-chemistry-dna-labeling (accessed Sep 7, 2011).

(36) Kularatne, S. A.; Wang, K.; Santhapuram, H. R.; Low, P. S. Prostate-Specific Membrane Antigen Targeted Imaging and Therapy of Prostate Cancer Using a PSMA Inhibitor as a Homing Ligand. *Mol. Pharm.* **2009**, *6*, 780–789.

CHAPTER 7

Conclusions and Future Directions

Chemical modifications of the M13 virus have allowed its incorporation into many systems with multifarious applications. Here, we exploited the inherent negative charge present on the surface of the phage coat protein to further expand the repertoire of phage-based applications. The concept of 'phage wrapping' was developed to enhance the binding affinity, while simultaneously reducing the non-specific adhesion.[1,2] The concept utilizes the electrostatic interactions between the negatively charged phage surface and the positively charged oligolysine peptide. Furthermore, one end of the oligolysine peptide is pre-modified to impart additional and orthogonal functionalities to the phage surface such as an alkyne or a thiol group. These functional groups allow the placement of a second ligand, in addition to the genetically displayed one, or the attachment of moieties such as polyethylene glycol (PEG). In addition, another approach was applied to generate dual-modified phage through double-infections into *E. coli* cells during phage propagation. The method allowed the generation of dual genetically modified phage; two sets of ligands present on the same phage particle but targeting two different proteins.[3]

In a major application of phage wrapping, highly sensitive and specific detection of a prostate cancer biomarker, prostate-specific membrane antigen, PSMA, was achieved.[4] An electrochemical biosensor was designed to

incorporate such wrapped viruses. The bioaffinity matrix utilized a polymeric film composed of a conducting organic polymer, PEDOT, incorporating viruses again through electrostatic interactions.[5] The binding of the target biomarker, PSMA, provided a quantifiable change in resistance, which was found to be proportional to the PSMA concentration. Furthermore, the placement of additional ligands on the phage surface through phage wrapping provided an increase in the apparent affinity through maximization of ligand density, and a bidentate binding mode of the two ligands. Such avidity effects allowed the highly sensitive electrochemical detection of PSMA at 100 pm levels in synthetic urine, which is relevant for early diagnosis of prostate cancer.[1,6,7] This study was further advanced to detect PSMA in human urine samples in an ELISA format. The ability to detect PSMA in barely 100 μL of urine samples from 2006-08 signifies the strength of the protein as a clinically relevant biomarker. In the future, biosensing measurements with wrapped phage will be utilized to study a full array of urine samples for comprehensive analysis of this method. This study holds the potential towards the development of a point-of-care device for early prostate cancer detection.

The concept of phage wrapping was also applied towards the detection of whole cell surfaces to develop a method for the early detection of metastasis. The phage surface though highly applicative, suffers from the limitation of high non-specific adhesion to cell surfaces. This major challenge was solved by the combination of phage wrappers and PEG. The oligolysine wrappers functionalized with alkynes allowed the placement of azide-functionalized PEG

through on-phage cycloaddition. Furthermore, the phage surface was simultaneously modified with PEGylated PSMA-binding ligands through a thiol-maleimide wrapping system. This unique wrapping system with two orthogonal reactions allowed the placement of two different wrappers, and thus, two different moieties on the same phage surface in the desired ratios. The PEG polymers reduced the non-specific adhesion to cell surfaces by ~80%, whereas the ligands allowed the capture of PSMA-positive LNCaP cells from a solution.[2]

The ability of PEGylated phage to selectively target cells was next utilized towards the development of phage-based libraries for performing whole cell-based selections. The infrastructure of PEGylated phage, though, was devoid of a genetic link between the phage genome and the attached ligand, thereby limiting its capabilities for selections. As a result, the chemically applied ligand-PEG-oligolysine wrappers were replaced with an extended, genetically encoded Gly-Ser linker. Furthermore, the framework allowed the genetic display of ligands and libraries, and only a marginal drop in affinity was observed in the presence of PEG wrappers. In the future, these novel extended-linker libraries will be used for selections towards whole cell surfaces. Additionally, the viruses wrapped with PEG and ligands will be incorporated into the bioaffinity matrix for efficient and selective capture of whole cells for metastasis detection and other applications.

In addition to the above mentioned research, a foundation was laid for the following projects. The binding and attachment to the cell-surface PSMA leads to internalization of the bound moeity.[8,9] This concept, in conjunction with the

orthogonal wrappers could be utilized to develop a highly specific imaging and delivery platform, with suitably functionalized payloads. On the biosensing front, the exact mechanism behind the change in resistance of the virus-PEDOT films obtained on PSMA binding, is still unknown. Additionally, PSMA binding could also affect the dielectric constant of the film leading to similar outcomes. To further investigate this cause, variants of Lysozyme protein carrying neutral, positive or negative charge at pH 7, could be designed through controlled acetylation of the Lysine amines.[10] Biosensing measurements with these charged variants could further shed light on the mechanism, and allow the development of a universal sensing platform.

A significant advantage of the biosensor is the easy adaptation of the device towards the detection of other diseases with markers present in the biological fluids, through alteration of the ligands in the bioaffinity matrix. Current preliminary diagnostics for pancreatic cancer utilizes the levels of expression of the biomarker, Carbohydrate Antigen, CA-19-9.[11] A biosensor based detection of CA-19-9 in conjunction with TIMP1 (tissue inhibitor of metalloproteinase) and IGFBP4 (insulin like growth factor binding protein) could improve diagnostic specificity.[12–14] Diseases other than cancers, such as urinary tract infection with *E. coli* being the primary causative agent could also be readily detected as phage inherently target F^+ bacterial cells.[15] The biosensing platform could provide an efficient alternative to the time-consuming current detection method involving urine cultures. The key goal would be the generation of modified phage for the

specific detection of individual *E. coli* strains responsible for the infection. The preliminary steps towards each of these goals were undertaken, with initial success. I wish, in the future, the research presented here will provide the platform necessary to further the interdisciplinary area of chemically modified viruses and prostate cancer.

REFERENCES

(1) Mohan, K.; Donavan, K. C.; Arter, J. A.; Penner, R. M.; Weiss, G. A. Sub-Nanomolar Detection of Prostate-Specific Membrane Antigen in Synthetic Urine by Synergistic, Dual-Ligand Phage. *J. Am. Chem. Soc.* **2013**, *135*, 7761–7767.

(2) Mohan, K.; Weiss, G. A. Engineering Chemically Modified Viruses for Prostate Cancer Cell Recognition. *Mol. Biosyst.* **2015**, *11*, 3264–3272.

(3) Mohan, K.; Weiss, G. A. Dual Genetically Encoded Phage-Displayed Ligands. *Anal. Biochem.* **2014**, *453*, 1–3.

(4) Murphy, G. P.; Kenny, G. M.; Ragde, H.; Wolfert, R. L.; Boynton, A. L.; Holmes, E. H.; Misrock, S. L.; Bartsch, G.; Klocker, H.; Pointner, J.; *et al.* Measurement of Serum Prostate-Specific Membrane Antigen, a New Prognostic Marker for Prostate Cancer. *Urology* **1998**, *51*, 89–97.

(5) Donavan, K. C.; Arter, J. A.; Pilolli, R.; Cioffi, N.; Weiss, G. A.; Penner, R. M. Virus-poly(3,4-Ethylenedioxythiophene) Composite Films for Impedance-Based Biosensing. *Anal. Chem.* **2011**, *83*, 2420–2424.

(6) Sokoloff, R. L.; Norton, K. C.; Gasior, C. L.; Marker, K. M.; Grauer, L. S. A Dual-Monoclonal Sandwich Assay for Prostate-Specific Membrane Antigen: Levels in Tissues, Seminal Fluid and Urine. *Prostate* **2000**, *43*, 150–157.

(7) Xiao, Z.; Adam, B.-L.; Cazares, L. H.; Clements, M. A.; Davis, J. W.; Schellhammer, P. F.; Dalmasso, E. A.; Wright, G. L. Quantitation of Serum Prostate-Specific Membrane Antigen by a Novel Protein Biochip

Immunoassay Discriminates Benign from Malignant Prostate Disease. *Cancer Res.* **2001**, *61*, 6029–6033.

(8) Kularatne, S. A.; Wang, K.; Santhapuram, H. R.; Low, P. S. Prostate-Specific Membrane Antigen Targeted Imaging and Therapy of Prostate Cancer Using a PSMA Inhibitor as a Homing Ligand. *Mol. Pharm.* **2009**, *6*, 780–789.

(9) Ghosh, A.; Heston, W. D. W. Tumor Target Prostate Specific Membrane Antigen (PSMA) and Its Regulation in Prostate Cancer. *J. Cell. Biochem.* **2004**, *91*, 528–539.

(10) Shaw, B. F.; Schneider, G. F.; Bilgiçer, B.; Kaufman, G. K.; Neveu, J. M.; Lane, W. S.; Whitelegge, J. P.; Whitesides, G. M. Lysine Acetylation Can Generate Highly Charged Enzymes with Increased Resistance toward Irreversible Inactivation. *Protein Sci.* **2008**, *17*, 1446–1455.

(11) Chen, R.; Pan, S.; Brentnall, T. A.; Aebersold, R. Proteomic Profiling of Pancreatic Cancer for Biomarker Discovery. *Mol. Cell. Proteomics* **2005**, *4*, 523–533.

(12) Faca, V. M.; Song, K. S.; Wang, H.; Zhang, Q.; Krasnoselsky, A. L.; Newcomb, L. F.; Plentz, R. R.; Gurumurthy, S.; Redston, M. S.; Pitteri, S. J.; *et al.* A Mouse to Human Search for Plasma Proteome Changes Associated with Pancreatic Tumor Development. *PLoS Med.* **2008**, *5*, e123.

(13) Kleine, T.; Bartsch, S.; Bläser, J.; Schnierer, S.; Triebel, S.; Valentin, M.; Gote, T.; Tschesche, H. Preparation of Active Recombinant TIMP-1 from Escherichia Coli Inclusion Bodies and Complex Formation with the Recombinant Catalytic Domain of PMNL-Collagenase. *Biochemistry* **1993**, *32*, 14125–14131.

(14) Gomis-Rüth, F. X.; Maskos, K.; Betz, M.; Bergner, A.; Huber, R.; Suzuki, K.; Yoshida, N.; Nagase, H.; Brew, K.; Bourenkov, G. P.; *et al.* Mechanism of Inhibition of the Human Matrix Metalloproteinase Stromelysin-1 by TIMP-1. *Nature* **1997**, *389*, 77–81.

(15) Bardhan, N. M.; Ghosh, D.; Belcher, A. M. M13 Virus Based Detection of Bacterial Infections in Living Hosts. *J. Biophotonics* **2014**, *7*, 617–623.